

New approaches to the therapy of glioblastoma:
investigations on RNA interference, kinesin Eg5 and
ABCB1/ABCG2 inhibition

Dissertation

zur Erlangung des Doktorgrades der Naturwissenschaften (Dr. rer. nat.)
der Naturwissenschaftlichen Fakultät IV – Chemie und Pharmazie –
der Universität Regensburg



vorgelegt von
Christine Müller
aus Bühl (Baden)

2007

Die vorliegende Arbeit entstand in der Zeit von Mai 2003 bis Mai 2007 unter der Leitung von Herrn Prof. Dr. A. Buschauer und Herrn Prof. Dr. G. Bernhardt am Institut für Pharmazie der Naturwissenschaftlichen Fakultät IV – Chemie und Pharmazie – der Universität Regensburg.

Das Promotionsgesuch wurde eingereicht am 31. Mai 2007.

Tag der mündlichen Prüfung: 22. Juni 2007

Prüfungsausschuss:

Prof. Dr. S. Elz	(Vorsitzender)
Prof. Dr. A. Buschauer	(Erstgutachter)
Prof. Dr. G. Bernhardt	(Zweitgutachter)
Prof. Dr. A. Göpferich	(Prüfer)

Für Mama

Der Gipfel unseres Lebens ist dort, wo uns die Liebe Berge gibt.

© *Ernst Ferstl, (*1955), österreichischer Lehrer, Dichter und Aphoristiker*
Quelle : »einfach kompliziert einfach«

Danksagungen

An dieser Stelle möchte ich mich bedanken bei:

Herrn Prof. Dr. Armin Buschauer für die Möglichkeit an diesem interessanten Projekt arbeiten zu dürfen sowie für seine wissenschaftlichen Anregungen und seine konstruktive Kritik bei der Durchsicht der Arbeit.

Herrn Prof. Dr. Günther Bernhardt für seine wissenschaftliche Anleitung und umfassende Betreuung, seine stetige Unterstützung beim Lösen experimenteller Probleme, sein Interesse am Fortgang der Experimente und für die kritische Durchsicht dieser Arbeit.

Herrn Dr. Thilo Spruß für die Betreuung und Unterstützung bei der Durchführung der Tierversuche und der histologischen Untersuchungen.

Herrn Franz Wiesenmayer und Herrn Oskar Baumann für die Unterstützung bei der Durchführung der Tierversuche. Frau Petra Pistor für die Erstellung der histologischen Schnittserien.

Herrn Dr. Gerald Böhm und Frau Dr. Claudia Immisch der Firma ACGT ProGenomics (Halle) für die Kooperation und die Bereitstellung des TmHU Proteins und der EGFP-siRNA.

Herrn Prof. Dr. Otto Wolfbeis und Herrn Dr. Axel Dürkop für die Bereitstellung des Fluorimeters sowie die wissenschaftliche Betreuung.

Herrn Prof. Dr. Athanassios Giannis (Universität Leipzig) für die Bereitstellung der Kinesin Eg5 Inhibitoren.

Herrn Prof. Burkhard König, Herrn Michael Egger und Frau Xuqin Li für die Synthese der Tariquidar Derivate und die hervorragende Zusammenarbeit.

Herrn Dr. Gero Brockhoff für die Möglichkeit die Zellzyklusanalyse Daten mit der Software "MultiCycle for Windows" auswerten zu können und die Einweisung in das Programm.

Frau Susanne Bollwein, Frau Elvira Schreiber und Frau Renate Liebl für die fachliche Unterstützung bei den Arbeiten mit der Zellkultur.

Frau Martina Luginger und Frau Sylvia Heinrich für ihre Unterstützung bei allen organisatorischen Fragen.

Herrn Peter Richthammer für seine Hilfsbereitschaft bei technischen Problemen, seine gute Laune und die unterhaltsamen Gespräche beim Frühstück.

meinen Kollegen Dietmar Gross, Peter Jarzyna, und Ralf Ziemek für die Einweisung und Unterstützung beim Erlernen der verschiedenen Methoden besonders zu Beginn meiner Arbeit.

meinen Laborkolleginnen Edith Hofinger und Lydia Schneider für ihre Hilfsbereitschaft und die heitere Atmosphäre im Raum CH 13.1.34.

meinen studentischen Hilfskräften und Freunden Susanne Rutzinger und Alexander Kratzer für ihre engagierte und zuverlässige Mitarbeit im Labor.

meinen Kollegen und Freunden Edith Hofinger, Erich Schneider, Hendrik Preuß, Johannes Mosandl, Martina Hubensack, Martin Göttle, Matthias Kühnle, Max Keller, Patrick Igel, Peter Höcherl, Ralf Ziemek und Stephan Braun für viele anregende Diskussionen, aber auch für eine schöne und unvergessliche Zeit in Regensburg,

sowie allen Mitgliedern des Lehrstuhls für ihre Kollegialität, ihre Hilfsbereitschaft und die angenehme Arbeitsatmosphäre.

Des Weiteren möchte ich danken:

meinem Chemielehrer Herrn Jochen Hoerth für seinen tollen Unterricht und dafür, dass er mich zum Pharmaziestudium ermutigt hat.

meinen Freundinnen Nicole Braxmeier, Esther Droll und Nadja Fischer für unsere besondere Freundschaft und ihre moralische Unterstützung.

meiner wunderbaren Familie, vor allem meiner Mutter Ursula, die mich immer in meinen Vorhaben und Plänen unterstützt. Herta und Winfried Ertelt für all ihre großzügige Unterstützung. Frau Waltraud Ertelt, die durch ihre Vertretung ermöglicht hat, dass ich mehr Zeit mit Johannes verbringen konnte.

meinem Freund Johannes für seine Liebe, Geduld und Verständnis in vier wunderschönen und spannenden Jahren.

Abstracts and Publications

Prior to submission of this thesis, results were in part published or presented as posters or short lectures:

Publications:

Müller, C., Gross, D., Sarli, V., Gartner, M., Giannis, A., Bernhardt, G. and Buschauer, A. (2007) Inhibitors of kinesin Eg5: antiproliferative activity of monastrol analogues against human glioblastoma cells. *Cancer Chemother. Pharmacol.* V59(2):157-164.

Egger, M., Li, X., Müller, C., Bernhardt, G., Buschauer, A., König, B. (2007) Tariquidar Analogues: Synthesis by Cu^I-Catalysed N/O-Aryl Coupling and Inhibitory Activity against the ABCB1 transporter. *Europ. J. Org. Chem.*, DOI: 10.1002/ejoc.200700142.

Hubensack, M., Müller, C., Höcherl, P., Fellner, S., Spruss, T., Bernhardt, G., Buschauer, A. (2007) Effect of the ABCB1 modulators elacridar and tariquidar on the distribution of paclitaxel in nude mice. *J. Cancer Res. Clin. Oncol.*, submitted for publication.

Poster Presentations and Short Lectures:

2004:

Annual Meeting of the German Pharmaceutical Society (DPhG) in Regensburg, October 6-8:
Müller, C., Bernhardt, G., Immisch, C., Weidensdorfer, D., Böhm, G., Buschauer, A.
“Quantification of siRNA effects *in vitro* and *in vivo*”, Poster Contribution

2005:

Annual Meeting of the German Pharmaceutical Society (DPhG) in Mainz, October 5-8:
Müller, C. B., Sarli, V., Gartner, M., Bernhardt, G., Giannis, A., Buschauer, A.
“Cytostatic effects of specific kinesin Eg5 inhibitors against human glioblastoma cells *in vitro*”, Poster Contribution

2006:

3rd Summer School Medicinal Chemistry, Regensburg, September 25-27:
Müller, C. B., Egger, M., Bernhardt, G., König, B., Buschauer, A.
“Inhibition of the drug efflux transporters ABCB1 and ABCG2 by tariquidar analogs”,
Poster Contribution

2007:

BHS 2007 Treffen der Blut-Hirn Schranke-Experten und Caco-2 Anwender in Bad Herrenalb,
May 21-23:
„Neue Tariquidar Derivate als ABCB1 und ABCG2 Inhibitoren“, Short Lecture

Contents

Chapter 1

1	General introduction.....	1
1.1	Primary malignant brain tumors.....	2
1.1.1	Classification.....	3
1.1.2	Prognosis	3
1.1.3	Diagnosis and characteristics of astrocytomas.....	4
1.2	Standard therapy.....	6
1.2.1	Tumor resection.....	6
1.2.2	Radiation treatment	6
1.2.3	Chemotherapy	7
1.2.4	Temozolomide.....	9
1.3	New approaches to the treatment of gliomas	10
1.3.1	Down-regulation of oncogenes in tumor cells by RNA interference.....	10
1.3.2	Inhibition of mitotic kinesin Eg5 by specific inhibitors.....	11
1.3.3	Overcoming the blood-brain barrier.....	12
	References	13

Chapter 2

2	TmHU as siRNA transfection reagent.....	19
2.1	Introduction	20
2.1.1	RNA interference	20
2.1.1.1	Mechanism of RNAi	20
2.1.1.2	Silencing by small interfering RNA (siRNA)	22
2.1.1.3	siRNA design	22
2.1.2	Transient transfection of siRNA.....	23
2.1.2.1	Electroporation	23
2.1.2.2	Lipofection	24
2.1.2.3	Polyfection.....	27
2.1.3	Problems of transfection in vivo	30
2.1.4	The TmHU protein	31
2.1.4.1	The TmHU protein family.....	31

2.1.4.2	TmHU, the histone-like protein from <i>Thermotoga maritime</i>	32
2.1.4.3	TmHU as gene transfer reagent.....	33
2.2	Objective	36
2.3	Materials and methods.....	38
2.3.1	Chemicals and drugs	38
2.3.2	Amplification and purification of plasmid DNA	38
2.3.2.1	The pEGFP-N1, pcDNA3EGFP and pDsRed2-C1 vectors	38
2.3.2.2	Plasmid DNA maxi-preparation and determination of DNA concentration	39
2.3.2.3	Restriction enzyme digest	40
2.3.2.4	Agarose gel electrophoresis.....	40
2.3.3	Cell culture	41
2.3.4	Stable transfection of human glioblastoma cell lines.....	41
2.3.4.1	Fluorescence microscopy	42
2.3.4.2	Flow cytometry and cell sorting.....	42
2.3.5	Chemosensitivity assay	42
2.3.6	Fluorescence detection	43
2.3.7	Transfection of double-stranded siRNA.....	43
2.3.7.1	Nonsilencing siRNA and specific EGFP-siRNA	43
2.3.7.2	Procedure.....	43
2.3.8	In vivo experiments	44
2.3.9	Histology	44
2.3.9.1	Preparation of paraffin sections.....	44
2.3.9.2	Conventional fluorescence microscopy and confocal laser scanning microscopy	45
2.3.10	In vivo imaging	46
2.3.11	Micro-osmotic pumps.....	47
2.3.11.1	Preparation of micro-osmotic pumps	47
2.3.11.2	Performance of the in vitro delivery study	47
2.3.11.3	Subcutaneous application of micro-osmotic pumps in nude mice	48
2.4	Results	49
2.4.1	EGFP and DsRed2 expressing human glioblastoma cells.....	49
2.4.1.1	Stable transfection	49
2.4.1.2	Cell sorting by flow cytometry.....	50
2.4.1.3	Chemosensitivity of the transfectants.....	52

2.4.2	Fluorescence assay by means of micorplate reader for the quantitation of siRNA effects in vitro.....	55
2.4.2.1	Establishment of an assay for the quantification of EGFP expression.....	55
2.4.2.2	Establishment of an assay for DsRed2 expressing cells.....	59
2.4.3	Cytotoxicity of the TmHU protein	63
2.4.4	siRNA transfection with TmHU.....	64
2.4.5	In vivo growth characteristics, selection and expansion of subcutaneous tumors	65
2.4.5.1	Subcutaneous U-87 MG EGFP tumors	66
2.4.5.2	Subcutaneous U-118 MG EGFP tumors	67
2.4.5.3	Subcutaneous U-373 MG EGFP tumors	69
2.4.5.4	Subcutaneous DsRed2 expressing glioblastoma	70
2.4.6	Quantitation of EGFP in paraffin sections of subcutaneous tumors	70
2.4.7	In vivo imaging of subcutaneous U-373 MG EGFP tumors in nude mice	71
2.4.8	Investigations on micro-osmotic pumps.....	73
2.4.8.1	Verification of the delivery in vitro.....	73
2.4.8.2	Verification of the delivery in vivo	75
2.5	Summary	78
References	80

Chapter 3

3	Inhibitors of kinesin Eg5: antiproliferative activity of monastrol analogs against human glioblastoma cells	91
3.1	Introduction	92
3.1.1	The mitotic spindle as a target in cancer chemotherapy	92
3.1.1.1	The role of microtubules in the mitotic spindle	93
3.1.1.2	Microtubule interfering agents	95
3.1.2	Mitotic spindle assembly.....	98
3.1.3	Microtubule-based motor proteins	99
3.1.4	Mitotic arrest through Eg5 kinesin inhibition	102
3.1.5	Eg5 kinesin inhibitors.....	104
3.2	Objective	106
3.3	Materials and methods.....	107
3.3.1	Kinesin Eg5 inhibitors.....	107
3.3.2	Cell lines and culture conditions	107

3.3.3	Chemosensitivity assay	109
3.3.4	Flow cytometric calcein-AM efflux assay	110
3.3.5	Confocal laser-scanning microscopy.....	110
3.3.5.1	Treatment of the cells	111
3.3.5.2	Fixation and permeabilization of the glioblastoma cells.....	111
3.3.5.3	Staining and immunofluorescence	111
3.3.5.4	Image processing.....	111
3.4	Results	112
3.4.1	Drug exposure and chemosensitivity	112
3.4.2	Incubation of glioblastoma cells after pre-incubation of new Eg5 inhibitors in culture medium.....	117
3.4.3	Effect of new Eg5 inhibitors after incubation times of 1, 3 and 6 h	119
3.4.4	Effect of new monastrol analogs on quiescent cells.....	120
3.4.5	Flow cytometric calcein-AM efflux assay (ABCB1 assay)	121
3.4.6	Effect of the new monastrol analogs on the spindle apparatus and on the cytoskeleton of resting cells	122
3.5	Discussion	124
References	126

Chapter 4

4	Tariquidar analogs as ABCB1 and ABCG2 inhibitors	133
4.1	Introduction	134
4.2	Objective	137
4.3	Materials and methods.....	138
4.3.1	Drugs and chemicals	138
4.3.2	Tariquidar analogs.....	138
4.3.3	Cell lines and culture conditions	142
4.3.4	Flow cytometric calcein-AM efflux assay	142
4.3.5	Flow cytometric mitoxantrone efflux assay	143
4.3.6	Chemosensitivity assay	144
4.3.7	Cell cycle analysis	145
4.4	Results	146
4.4.1	Inhibitors activity and selectivity	146

4.4.2	Effect of tariquidar analogs on the chemosensitivity of Kb-V1 cells against topotecan	152
4.4.3	Effect of tariquidar analogs on the chemosensitivity of MCF-7/Topo cells against topotecan	155
4.4.4	Effect of tariquidar analogs on proliferating U-373 MG cells	160
4.4.5	Effect of tariquidar analogs on quiescent U-373 MG cells	164
4.4.6	Cell cycle analysis of tariquidar analogs	166
4.5	Discussion	168
References	170
Chapter 5		
5	Summary	173

Abbreviations

ABCB1	Member 1 of the <u>A</u> TP <u>b</u> inding <u>c</u> assette transporter B subfamily
ABCG2	Member 2 of the <u>A</u> TP <u>b</u> inding <u>c</u> assette transporter G subfamily
AM	acetoxymethylester
APC	anaphase promoting complex
ATCC	American Type Culture Collection
ATP	adenosine triphosphate
BBB	blood-brain barrier
BCNU	carmustine
BCRP	Breast Cancer Resistance Protein (=ABCG2)
BCSFB	blood-cerebrospinal fluid barrier
Bub	budding uninhibited by benzimidazole
CCNU	lomustine
CNS	central nervous system
CT	chemotherapy
Da	dalton
DMEM	Dulbecco's modified Eagle medium
DMSO	dimethylsulfoxide
DNA	desoxyribonucleic acid
EGFP	enhanced green fluorescent protein
EGFR	epidermal growth factor receptor
EMEM	Eagles minimum essential medium
FCS	fetal calf serum
G418	geneticin
GTP	guanosine triphosphate
IC ₅₀	concentration of inhibitor required to give a 50% inhibition of activity
LOH	loss of heterozygosity
MAD	mitosis arrest deficient
MDM2	murine double minute 2
MGMT	O ⁶ -methylguanine-DNA methyltransferase
mRNA	messenger RNA
O6BG	O ⁶ -benzylguanine

p14arf	tumor suppressor protein
p16/BK4A	tumor suppressor protein
p16/NK4a	tumor suppressor gene
PBS	phosphate buffered saline
PDGF	platelet-derived growth factor
PDGFR	PDGF receptor
PFA	paraformaldehyde
PFS	progression-free survival
p-gp	p-glycoprotein 170 (=ABCB1)
pH	negative logarithm of the hydrogen ion concentration
PSC 833	valspodar
PTEN	phosphate and tensin homolog
RNA	ribonucleic acid
RT	Radiotherapy
siRNA	small interfering RNA
SRS	stereotactic radiosurgery
Topo	topotecan
TP53	tumor protein p53
VEGF	vascular endothelial growth factor
WHO	World Health Organization
XKCM1	<i>Xenopus</i> kinesin central motor 1

Chapter 1

General introduction

1.1 Primary malignant brain tumors

Brain tumors represent a heterogeneous group of central nervous system (CNS) neoplasms. The World Health Organization (WHO) recognizes approximately 100 different types of brain tumors classified according to pathological diagnosis. In general, these tumors can be classified into either primary or secondary tumors, depending on whether they originate from the brain or spread to the CNS from elsewhere. Primary tumors often spread into other sites in the central nervous system, such as the spinal cord, but rarely metastasize to other parts of the body. These tumors show a high biological diversity, and can be named and classified according to the normal brain tissue from which they have derived. A major part of all primary brain tumors are collectively known as gliomas. The term “glioma” specifies a group of cancers that includes astrocytomas, oligodendrogliomas, ependymomas and oligoastrocytomas. They are malignant forms of glial cells, which primarily constitute the connective and supportive tissue in the central nervous system. Several glial cell types are known from which gliomas can derive:

- Astrocytomas are primary brain tumors derived from astrocytes, which serve supportive functions for nerve cells, and their foot processes encapsulate the brain capillaries.
- Oligodendrogliomas originate from oligodendrocytes, which surround nerve cells and thereby provide a protective coating. Pure oligodendrogliomas however are rare, and in most cases malignant oligodendroglioma cells occur in mixed gliomas.
- Ependymomas are derived from ependymal cells. These cells line the brain ventricles and the central canal of the spinal cord.
- Mixed gliomas consist of a mixture of different malignant glioma cells, mostly malignant oligodendrocytes and astrocytes.

Of these gliomas, the astrocytomas have the highest incidence of 5 to 10 per 100,000 persons (Legler, 1999; Wrensch, 2002). In adults astrocytomas amount to about 75% of all primary malignant brain tumors.

1.1.1 Classification

Approximately half of all primary brain tumors are glial cell neoplasms, and more than three quarters of all glial tumors are astrocytomas. Astrocytomas differ in their pathological behavior: some astrocytomas are classified as low-grade tumors, meaning they are growing slowly, whereas glioblastoma multiforme represent the most aggressive type. Based on their histological appearance the World Health Organization classifies astrocytomas into four grades. Pilocytic astrocytomas (WHO grade I) are relatively benign tumors that generally occur in children and young adults. Low-grade or diffuse astrocytomas (WHO grade II) are tumors of well-differentiated cells that grow slowly, but diffusely infiltrate normal brain structures. Malignant or high-grade gliomas include anaplastic astrocytomas or anaplastic oligodendrogliomas (WHO grade III) and glioblastomas (WHO grade IV). The characteristic histopathology of these gliomas is defined by the presence of mitosis, cellular and nuclear atopia, and in glioblastomas by microvascular proliferation, necrosis and pseudopallisading (Burger, 1985).

1.1.2 Prognosis

The prognosis for patients with malignant gliomas remains very dismal: the median survival of patients with anaplastic astrocytomas is two to three years, and that of patients with glioblastoma multiforme is ten to twelve months. Thus, glioblastoma multiforme is one of the most lethal and treatment-resistant human tumors. Among the therapeutic triad of surgery, radiation therapy, and chemotherapy, only radiation therapy has been shown to improve survival (Salazar, 1979). Despite more than 30 years of intensive efforts to find an effective chemotherapy regimen for glioblastoma multiforme, the median survival of 12 to 15 months has not changed appreciably since the introduction of radiation therapy. Furthermore, the improvements in surgery, radiation and chemotherapy failed to result in long-term survival for most patients with malignant gliomas. Malignant gliomas recur most commonly within 2 cm of the primary tumor location (Wallner et al., 1989), and only a minority of patients achieves long-term survival (Senger et al., 2003). However, the results of combined temozolomide and radiation in the randomized study by Stupp et al. in patients with glioblastoma are encouraging (see Chapter 1.2.4).

1.1.3 Diagnosis and characteristics of astrocytomas

Due to the distinct ability of astrocytomas to invade normal brain tissue, extensive resections are unlikely to eradicate all malignant cells. The great variability in the geometry, extent, and character of the peripheral infiltrating margin of glioblastomas displays a diagnostic problem (Burger et al., 1988). The regional histological heterogeneity within each tumor hampers tumor sampling. Particularly a small biopsy may result in the incorrect diagnosis of a lower grade tumor. In many cases the first diagnosis from the biopsy has to be changed when the tumors have been removed by resection (Jackson, 2001). Furthermore, when a low-grade glioma is diagnosed, transformation to a higher malignant grade is very probable. This may be ascribed to a progressive genetic instability recently linked to the loss of chromosome 10 in the tumor cells (Nigro et al., 2005).

Currently evaluated gene expression arrays allow detailed genetic profiling of tumors with a highly specific molecular classification of tumor type and grade (Mischel, 2003). This approach may also provide the basis for a more accurate and histology independent classification system in the future (Nutt et al., 2003; Freije et al., 2004). Figure 1.1 shows the most frequent genetic abnormalities in astocytomas, reviewed by Gonzalez and Gilbert (Gonzalez and Gilbert, 2005). The genetic profiling and molecular analysis of tumors is suggested to allow optimized individual treatment. Especially the O^6 -methylguanine-DNA methyltransferase (MGMT) represents the most important and clinically relevant resistance mechanism. Since temozolomide produces cytotoxicity by methylation of DNA (O^6 -methylation of guanine), the activity of DNA repair mechanisms has been suggested to stand against temozolomide efficacy, and may cause poor response to temozolomide treatment. Friedman et al. found a significant negative correlation between MGMT expression in newly diagnosed glioblastoma and the response to temozolomide treatment (Friedman, 1998).

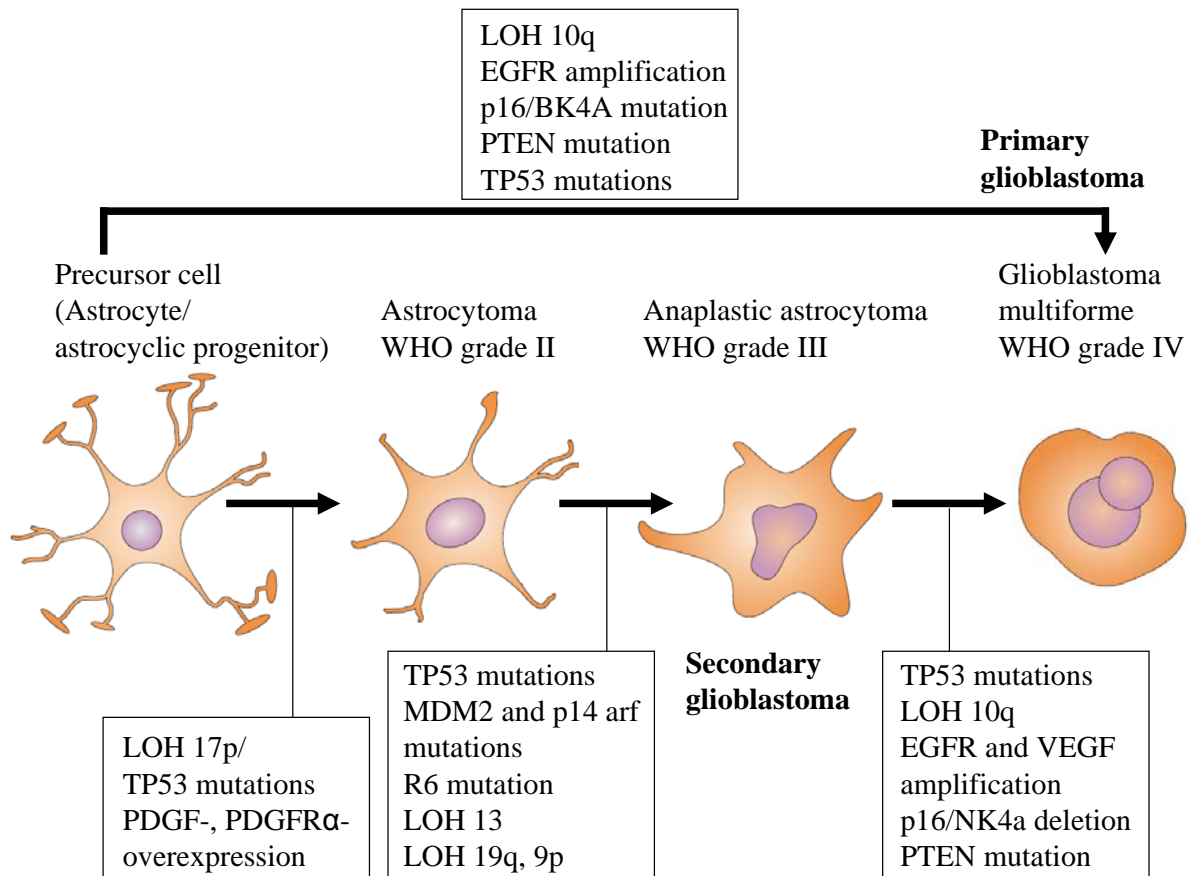


Figure 1.1: Pathways from normal precursor cells to gliomas. Several genetic abnormalities have been associated with the development of glioblastoma via different WHO grades, or by direct transformation into WHO grade IV (Lesniak and Brem, 2004; Gonzalez and Gilbert, 2005).

1.2 Standard therapy

1.2.1 Tumor resection

Surgical resection can achieve rapid symptom control, which is of primary relevancy for patients with large tumors, causing life-threatening situations. Moreover, resection provides tissue for histological diagnosis. Even though a complete eradication of the tumor is rather unlikely, extensive tumor resection has an impact on survival. As reported by Lacroix et al., a significant advantage in patients' survival was associated with the resection of 98 % or more of the tumor volume (median survival of 13 months) compared to resections of less than 98 % (median survival of 8.8 months) (Lacroix et al., 2002). However, in many cases surgical removal to this extent is not possible due to the highly invasive growth of the tumor.

1.2.2 Radiation treatment

Radiation represents one of the most effective forms of treatment for gliomas. Nearly all treatment regimens for newly diagnosed tumors include radiation treatment. Several studies showed that it is best to use radiotherapy in the post-surgical treatment of malignant glioma, e.g. for anaplastic astrocytoma (Walker, 1978) and for glioblastoma multiforme patients (Deutsch, 1989). The current standard of the radiation therapy specifies the use of a total dose of 60 Gy in 30 fractions. With higher radiation doses no additional benefit was observed (Nelson, 1988). Hyper-fractionation of the dose does not improve the outcome significantly, as shown in patients suffering from WHO grade III and IV tumors (Ludgate et al., 1988).

Another technique in radiotherapy involves the use of radiosensitizers, chemotherapeutic agents, which are supposed to increase the sensitivity of the tumors against radiation. Several compounds have been evaluated for this therapeutic purpose, e.g. misonidazole (Huncharek, 1998; Prados et al., 1999), carmustin (BCNU), lomustine (CCNU), and vincristine, with or without bromdesoxyuridine (Prados et al., 1999). To date, no clear clinical benefit compared to the standard radiation regimen has been demonstrated. Stereotactic radiosurgery (SRS) also has been considered as a promising treatment approach, but SRS followed by conventional radiation therapy in combination with BCNU showed no improved outcome in the treated patients with glioblastoma multiforme (Souhami et al., 2004). Finally, the interstitial brachytherapy of glioma with stereotactic radiation implants has been evaluated, also with no decisive success (Laperriere et al., 1998).

1.2.3 Chemotherapy

The combination of radiotherapy and chemotherapy in the treatment of malignant gliomas has been studied for several decades, but all trials failed to demonstrate a significant increase in survival (Walker et al., 1980). A large individual patient data based meta-analysis including over 3000 patients showed that adjuvant (after radiation treatment) chemotherapy may improve the 2-year survival by only 5 %, from 15 % to 20 % (Table 1.1) (Glioma Meta-analysis Trialists (GMT) Group, 2002). Unfortunately, no curative chemotherapy for malignant gliomas exists so far. The choice of applicable chemotherapeutic agents for the therapy of malignant brain tumors is limited to a few compounds, because of the poor penetration from the blood to the brain after systemic administration. Amongst them are the alkylating nitrosoureas carmustine (BCNU), lomustine (CCNU) as well as procarbazine, and temozolomide (Figure 1.2).

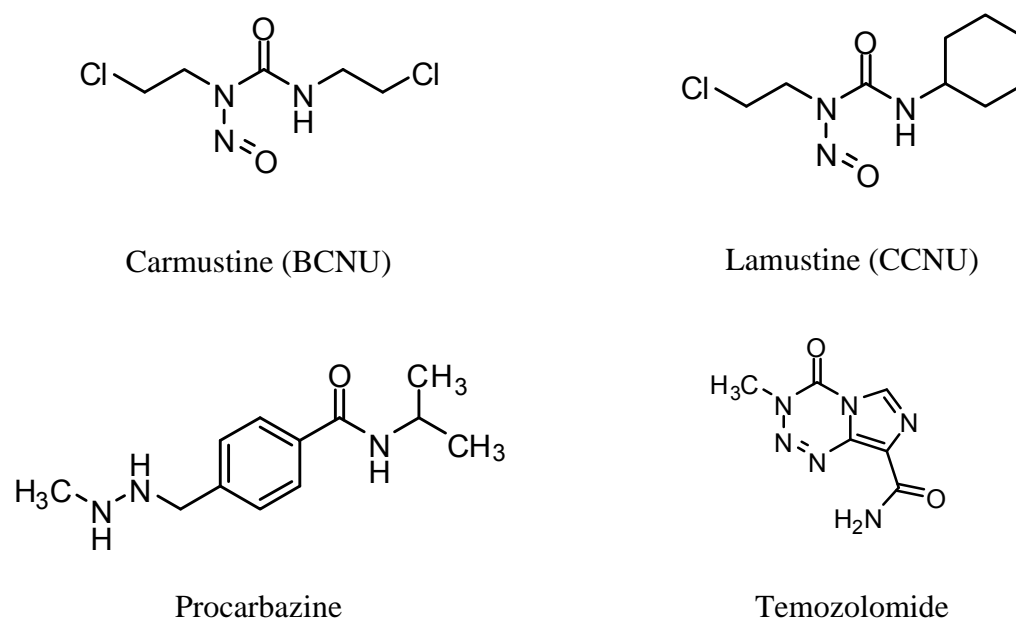


Figure 1.2: Structures of carmustine, lamustine, procarbazine and temozolomide.

Most of the present chemotherapy regimens are involved in adjuvant therapy after tumor resection or irradiation therapy. Several randomized trials have been conducted on the combined radiotherapy and chemotherapy. Some studies failed to demonstrate a significant increase in survival when chemotherapy was added to radiation treatment (Walker, 1978; Walker et al., 1980; Medical Research Council Brain Tumor Working party, 2001). However, meta-analysis of several randomized clinical trials demonstrated some benefit for the adjuvant

chemotherapy. Fine et al. used the results from 16 randomized clinical trials and reported on an absolute increase in patient survival of 10.1 % at 1 year and 8.6 % at 2 years after treatment with combined radiation and chemotherapy (Fine et al., 1993). Another meta-analysis with the data from 12 randomized controlled trials was performed by Stewart (Stewart, 2002). The results showed a significant increase of 6 % in the 1-year survival, and an increase of two months in the median survival. Despite the positive results from the meta-analysis, individual trials failed to provide a significant therapeutic advantage. As mentioned in a review on the treatment of astrocytomas by Gonzalez and Gilbert (Gonzalez and Gilbert, 2005), much of the controversy on the administration of adjuvant chemotherapy was the concern about toxic side effects associated with the use of nitrosoureas in classical adjuvant chemotherapy.

Table 1.1: Median 1- and 2-year survival of patients with high-grade glioma after various postoperative adjuvant treatments (van den Bent et al., 2006).

Reference	Treatment	Median survival	% 1-year survival	% 2-year survival
Walker et al. 1978	Supportive care	3 months	3	0
	BCNU	4 months	12	0
	RT	8 months	24	1
	RT + BCNU	8 months	32	5
Glioma Meta-analysis Trialists group 2002	RT		40	15
	RT + CT		46	20
EORTC 26981	RT	12 months	51	10
Stupp et al. 2005	RT + temozolomide	15 months	61	27

RT: radiotherapy; CT: chemotherapy; BCNU: carmustine

1.2.4 Temozolomide

Temozolomide (Temodal[®]) is an alkylating agent with an almost 100 % oral bioavailability. It penetrates into all body tissues including the central nervous system due to its ability to pass the blood-brain barrier (BBB). Spontaneous conversion into the active metabolite MTIC is postulated as the mechanism of activation (Ostermann et al., 2004). The activity of temozolomide was first demonstrated in patients with recurrent high-grade glioma. Three phase II trials were conducted with patients suffering from glioblastoma multiforme and anaplastic astrocytoma at first relapse (Yung et al., 1999; Yung et al., 2000; Brada et al., 2001). Low objective response rates in glioblastoma multiforme of 5 % to 7 % were disappointing, but an interesting response rate of 35 % in the anaplastic astrocytoma study was observed. These studies suggested an increase in the fraction of patients being progression-free at 6 months compared to a historical database. In the study of Yung et al. a significantly improved progression-free survival (PFS) rate at 6 months was observed for temozolomide (21 % versus 8 % with procarbazine treatment). Moreover the median PFS was increased (12.4 versus 8.3 weeks), and a higher 6-month survival rate was observed (60 % versus 44 %) (Yung et al., 2000). Temozolomide has largely replaced the nitrosoureas in the treatment of primary malignant brain tumors, and is considered as the mainstay of chemotherapy of high-grade gliomas. A recent study showed that the combined irradiation and temozolomide treatment in newly diagnosed glioblastoma multiforme patients improved median survival by 3 months, compared to radiotherapy alone, with acceptable levels of severe side effects (Stupp et al., 2005). Recent developments in the use of temozolomide in the chemotherapy of brain tumors has been reviewed by van den Bent et al. (van den Bent et al., 2006).

1.3 New approaches to the treatment of gliomas

Taken together, after more than 30 years of intensive research efforts the median survival of 12 to 15 months in glioma patients has not markedly changed since the introduction of radiation therapy. For glioblastoma multiforme no effective chemotherapy regimen exists so far. Only modest therapy improvements were achieved by advances in surgery, irradiation treatment, and some advances in chemotherapy. However, no improved long-term survival for most patients with malignant glioma was accomplished. Only the combined therapy of temozolomide and radiation treatment yielded encouraging results in long term survival of patients suffering from malignant glioma. Moreover, genetic profiling provides the specific classification of tumor type and grade with a more accurate prognosis. Thus, it may allow the development of a more effective and individualized treatment of patients in the future. However, there is still a great need to develop new approaches for the treatment of brain tumors.

1.3.1 Down-regulation of oncogenes in tumor cells by RNA interference

A modern and promising technology is cancer gene therapy aiming at effective and selective killing of malignant cells. This modern treatment option is based on the efforts that have been made in identification, cloning, sequencing and functional analysis of oncogenes during the last three decades. In the 1980s activated oncogenes in human tumor cells, especially ras genes (*H-ras*, *K-ras* and *N-ras*) were identified. With its central role in cell signaling, ras is one of the most mutated oncogenes in human malignancies, accounting for about 30 %-50 % of human cancers (Bos, 1989). Not only one mutated oncogene but also several genetic abnormalities are responsible for the development of tumors. Almost all human cancers have accumulated multiple genetic lesions including oncogenes and it is often unknown whether an oncogene is continuously required for tumorigenesis. Furthermore, it is very difficult to target an essential oncogene with drugs without affecting the corresponding non-mutated protooncogene or related factors (Heidenreich, 2004), for example in the case of a sequence-specific anti-ras therapy. The wild-type ras and its oncogenic form differ very slightly with regard to their DNA sequence (one point mutation) but enormously in their biochemical consequences. The recent discovery of RNA interference provides now tools to examine the role of oncogenes in tumorigenesis and it could be shown that the application of small double-

stranded RNA molecules (small interfering RNA, siRNA) silenced gene expression in mammalian cell culture (Elbashir et al., 2001). Moreover, oncogene specific siRNAs may become promising candidates for more cancer-specific therapeutic approaches (Brummelkamp et al., 2002). Brummelkamp et al. showed that the expression of mutated K-ras^{V12} was inhibited by RNA interference while other ras isoforms were unaffected.

However, the main challenge to any gene therapy must also be overcome with RNA interference: the double-stranded RNA or the expression vector encoding siRNA molecules have to reach the tumor cells efficiently, which displays a special problem in the case of brain tumors. The neutralization by the immune system may be a barrier for the small interfering RNAs to reach their destination. Due to the extreme sequence specificity of RNAi cancer cells may circumvent the siRNA-mediated attack, because a single point mutation in the targeted region prevents mRNA degradation and may cause RNAi-resistance in tumors (Borkhardt, 2002). The available technologies, e.g. the potency of therapeutic genes and efficacy of gene delivery systems, are far from optimal to achieve the desired clinical benefits in the field of solid tumors (Rubanyi, 2001). A proof for the in vivo efficacy of systemically delivered siRNAs is still missing and the investigations of the pharmacokinetics of siRNAs are in their beginnings with no therapeutically acceptable delivery method (Heidenreich, 2004). Therefore, a non-toxic transfection reagent with promising properties for in vivo application was examined for its efficacy of siRNA transfection. For details see Chapter 2.

1.3.2 Inhibition of mitotic kinesin Eg5 by specific inhibitors

Another strategy for the therapy of brain tumors is the evaluation of new potential pharmacological targets, and new classes of pharmacologically active compounds, capable of penetrating into the brain after standard drug administration. The mitotic kinesins are potential pharmacological targets in tumor therapy, because they are exclusively involved in the formation and function of the mitotic spindle, and some kinesins are only expressed in proliferating cells. The mitotic kinesin Eg5 mediates centrosome separation and the formation of the bipolar spindle. Inhibition of Eg5 leads to cell cycle arrest during mitosis, giving rise to cells with monopolar spindles, so-called monoasters (Blangy et al., 1995). In contrast to classical mitotic inhibitors (vinca alkaloids, taxanes), Eg5 inhibitors do not interfere with other microtubule-dependent processes (Wood et al., 2001), being the main reason for neurotoxicity (Quasthoff and Hartung, 2002). Thus, these compounds are supposed to be less neurotoxic anticancer drugs. Monastrol was the first specific small-molecule inhibitor of Eg5

(Mayer et al., 1999), however with a low inhibitory potency. As the inhibition of the mitotic kinesin Eg5 is an attractive new approach to cancer treatment (Wood et al., 2001), new monastrol analogs were synthesized (Gartner et al., 2005; Sarli et al., 2005; Tarby et al., 2006) and investigated for their antiproliferative activity against human glioblastoma cells. For details see Chapter 3.

1.3.3 Overcoming the blood-brain barrier

The brain is one of the least accessible organs for the delivery of pharmacological compounds (Scherrmann, 2002). There are two physiological barriers separating the brain from the systemic blood circulation. These are the blood-brain barrier (BBB) and the blood-cerebrospinal fluid barrier (BCSFB) controlling the entry and exit of endogenous and exogenous compounds. The regulation of drug concentrations in the brain via the BCSFB is considered to be negligibly small (Rautio and Chikhale, 2004), because the surface area of the BBB is estimated to be 5000 times greater than that of the BCSFB (Pardridge, 1995).

The BBB is defined by the brain capillaries which consist of a monolayer of polarized endothelial cells connected by tight junctions (Brightman, 1977). The tight junctions forming a continuous lipid layer effectively restrict the influx of molecules from the blood into the brain. Consequently, only small, electrically neutral, lipid soluble molecules can penetrate the BBB, and most chemotherapeutic agents do not fall in this category (Lesniak and Brem, 2004). Moreover, drug efflux transporters on the luminal membrane of the cerebral endothelium, e.g. the ABCB1 transporter (p-glycoprotein 170) actively remove a broad variety of drugs before they can enter the CNS. Thus, the treatment of brain tumors often fails due to very low concentrations of drugs within the CNS. By blocking the ABCB1 mediated efflux it is possible to increase the concentration of ABCB1 substrates, e. g. paclitaxel, in the brain (Scherrmann, 2002; Begley, 2004; Fromm, 2004; Bauer et al., 2005; Loescher and Potschka, 2005). The ABCB1 mediated transport is inhibited by certain substances, the so-called ABCB1 modulators (Fricker and Miller, 2004; Breedveld, 2006). Co-administration of paclitaxel and valspodar, a 2nd generation modulator of ABCB1, led to increased paclitaxel levels in the brain (Fellner et al., 2002). Hence, modulators of drug efflux transporters are very promising drugs for the treatment of primary and secondary brain tumors in combination with cytostatic agents. The development of other potent modulators of the ABC transporters is of particular interest in order to enlarge the variety of applicable anticancer drugs in the treatment of malignant brain tumors. For details see Chapter 4.

References

- Bauer, B., Hartz, A. M. S., Fricker, G. and Miller, D. S. (2005) Modulation of p-Glycoprotein Transport Function at the Blood-Brain Barrier. *Exp. Biol. Med.* 230(2):118-127.
- Begley, D. J. (2004) Delivery of therapeutic agents to the central nervous system: the problems and the possibilities. *Pharmacol. Ther.* 104(1):29-45.
- Blangy, A., Lane, H. A., d'Herin, P., Harper, M., Kress, M. and Nigg, E. A. (1995) Phosphorylation by p34cdc2 regulates spindle association of human Eg5, a kinesin-related motor essential for bipolar spindle formation in vivo. *Cell* 83(7):1159-1169.
- Borkhardt, A. (2002) Blocking oncogenes in malignant cells by RNA interference--New hope for a highly specific cancer treatment? *Cancer Cell* 2(3):167-168.
- Bos, J. L. (1989) ras Oncogenes in Human Cancer: A Review. *Cancer Res.* 49(17):4682-4689.
- Brada, M., Hoang-Xuan, K., Rampling, R., Dietrich, P.-Y., Dirix, L. Y., Macdonald, D., Heimans, J. J., Zonnenberg, B. A., Bravo-Marques, J. M., Henriksson, R., Stupp, R., Yue, N., Bruner, J., Dugan, M., Rao, S. and Zaknoen, S. (2001) Multicenter phase II trial of temozolomide in patients with glioblastoma multiforme at first relapse. *Ann. Oncol.* 12(2):259-266.
- Breedveld, P. B., Jos H.; Schellens, Jan H. M. (2006) Use of P-glycoprotein and BCRP inhibitors to improve oral bioavailability and CNS penetration of anticancer drugs. *Trends Pharmacol. Sci.* 27(1):17-24.
- Brightman, M. W. (1977) Morphology of blood-brain interfaces. *Exp. Eye Res.* 25(Suppl):1-25.
- Brummelkamp, T. R., Bernards, R. and Agami, R. (2002) Stable suppression of tumorigenicity by virus-mediated RNA interference. *Cancer Cell* 2(3):243-247.
- Burger, P. C., Heinz, E. R., Shibata, T. and Kleihues, P. (1988) Topographic anatomy and CT correlations in the untreated glioblastoma multiforme. *J. Neurosurg.* 68(5):698-704.
- Burger, P. C. V., F S; Green, S B; Strike, T A (1985) Glioblastoma multiforme and anaplastic astrocytoma. Pathologic criteria and prognostic implications. *Cancer* 56(5):1106-1111.
- Deutsch, M. G., S B; Strike, T A; Burger, P C; Robertson, J T; Selker, R G; Shapiro, W R; Mealey, J Jr; Ransohoff, J 2nd; Paoletti, P and et al. (1989) Results of a randomized trial comparing BCNU plus radiotherapy, streptozotocin plus radiotherapy, BCNU plus hyperfractionated radiotherapy, and BCNU following misonidazole plus radiotherapy in the postoperative treatment of malignant glioma. *Int. J. Radiat. Oncol. Biol. Phys.* 16(6):1389-1396.
- Elbashir, S. M., Harborth, J., Lendeckel, W., Yalcin, A., Weber, K. and Tuschl, T. (2001) Duplexes of 21-nucleotide RNAs mediate RNA interference in cultured mammalian cells. *Genes Dev.* 15(18):1054-1062.

- Fellner, S., Bauer, B., Miller, D. S., Schaffrik, M., Fankhänel, M., Spruss, T., Bernhardt, G., Gräff, C., Färber, L., Gschaidmeier, H., Buschauer, A. and Fricker, G. (2002) Transport of paclitaxel (Taxol) across the blood-brain barrier in vitro and in vivo. *J. Clin. Invest.* 110(9):1309-1318.
- Fine, H. A., Dear, K. B. G., Löffler, J. S., McBlack, P. L. and Canellos, G. P. (1993) Meta-analysis of radiation therapy with and without adjuvant chemotherapy for malignant gliomas in adults. *Cancer* 71(8):2585-2597.
- Freije, W. A., Castro-Vargas, F. E., Fang, Z., Horvath, S., Cloughesy, T., Liao, L. M., Mischel, P. S. and Nelson, S. F. (2004) Gene Expression Profiling of Gliomas Strongly Predicts Survival. *Cancer Res.* 64(18):6503-6510.
- Fricker, G. and Miller, D. S. (2004) Modulation of Drug Transporters at the Blood-Brain Barrier. *Pharmacology* 70(4):169-176.
- Friedman, H. M., RE; Kerby, T; Dugan, M; Bigner, SH; Henry, AJ; Ashley, DM; Krischer, J; Lovell, S; Rasheed, K; Marchev, F; Seman, AJ; Cokgor, I; Rich, J; Stewart, E; Colvin, OM; Provenzale, JM; Bigner, DD; Haglund, MM; Friedman, AH; Modrich, PL (1998) DNA mismatch repair and O6-alkylguanine-DNA alkyltransferase analysis and response to Temodal in newly diagnosed malignant glioma. *J. Clin. Oncol.* 16(12):3851-3857.
- Fromm, M. F. (2004) Importance of P-glycoprotein at blood-tissue barriers. *Trends Pharmacol. Sci.* 25(8):423-429.
- Gartner, M., Sunder-Plassmann, N., Seiler, J., Utz, M., Vernos, I., Surrey, T. and Giannis, A. (2005) Development and Biological Evaluation of Potent and Specific Inhibitors of Mitotic Kinesin Eg5. *ChemBioChem* 6(7):1173-1177.
- Glioma Meta-analysis Trialists (GMT) Group (2002) Chemotherapy in adult high-grade glioma: a systematic review and meta-analysis of individual patient data from 12 randomised trials. *Lancet* 359(9311):1011-1018.
- Gonzalez, J. and Gilbert, M. R. (2005) Treatment of astrocytomas. *Curr. Opin. Neurol.* 18(6):632-638.
- Heidenreich, O. (2004) Oncogene suppression by small interfering RNAs. *Curr. Pharm. Biotechnol.* 5(4):349-354.
- Huncharek, M. (1998) Meta-analytic re-evaluation of misonidazole in the treatment of high grade astrocytoma. *Anticancer Res.* 18(3B):1935-1939.
- Jackson, R. J. F., G N; Abi-Said, D; Lang, F F; Gokaslan, Z L; Shi, W M; Wildrick, D M; Sawaya, R (2001) Limitations of stereotactic biopsy in the initial management of gliomas. *Neuro-oncology* 3(3):193-200.
- Lacroix, M., Abi-Said, D., Fourney, D. R., Gokaslan, Z. L., Shi, W., DeMonte, F., Lang, F. F., McCutcheon, I. E., Hassenbusch, S. J., Holland, E., Hess, K., Michael, C., Miller, D. and Sawaya, R. (2002) A multivariate analysis of 416 patients with glioblastoma multiforme: prognosis, extent of resection, and survival. *J. Neurosurg.* 95(2):190-198.

- Laperriere, N. J., Leung, P. M. K., McKenzie, S., Milosevic, M., Wong, S., Glen, J., Pintilie, M. and Bernstein, M. (1998) Randomized study of brachytherapy in the initial management of patients with malignant astrocytoma. *Int. J. Radiat. Oncol. Biol. Phys.* 41(5):1005-1011.
- Legler, J. M. R., L A; Smith, M A; Warren, J L; Heineman E F; Kaplan, R S; Linet, M S (1999) Cancer surveillance series [corrected]: brain and other central nervous system cancers: recent trends in incidence and mortality. *J. Natl. Cancer Inst.* 91(23):2050-2051.
- Lesniak, M. S. and Brem, H. (2004) Targeted therapy for brain tumours. *Nat. Rev. Drug Discov.* 3(6):499-508.
- Loescher, W. and Potschka, H. (2005) Drug resistance in brain diseases and the role of drug efflux transporters. *Nature Reviews Neuroscience* 6(8):591-602.
- Ludgate, C. M., Douglas, B. G., Dixon, P. F., Steinbok, P., Jackson, S. M. and Goodman, G. B. (1988) Superfractionated radiotherapy in grade III, IV intracranial gliomas. *Int. J. Radiat. Oncol. Biol. Phys.* 15(5):1091-1095.
- Mayer, T. U., Kapoor, T. M., Haggarty, S. J., King, R. W., Schreiber, S. L. and Mitchison, T. J. (1999) Small molecule inhibitor of mitotic spindle bipolarity identified in a phenotype-based screen. *Science* 286(5441):971-974.
- Medical Research Council Brain Tumor Working party (2001) Randomized Trial of Procarbazine, Lomustine, and Vincristine in the Adjuvant Treatment of High-Grade Astrocytoma: A Medical Research Council Trial. *J. Clin. Oncol.* 19(2):509-518.
- Mischel, P. S. S., Ruty; Shi, Tao; Horvath, Steve; Lu, Kan V.; Choe, Gheeyoung; Seligson, David; Kremen, Thomas J.; Palotie, Aarno; Liao, Linda M.; Cloughesy, Timothy F.; Nelson, Stanley F. (2003) Identification of molecular subtypes of glioblastoma by gene expression profiling. *Oncogene* 22(15):2361-2373.
- Nelson, D. F. D.-W., M; Horton, J; Chang, C H; Schoenfeld, D; Nelson, J S (1988) Combined modality approach to treatment of malignant gliomas--re-evaluation of RTOG 7401/ECOG 1374 with long-term follow-up: a joint study of the Radiation Therapy Oncology Group and the Eastern Cooperative Oncology Group. *NCI Monogr.* 6(1):279-284.
- Nigro, J. M., Misra, A., Zhang, L., Smirnov, I., Colman, H., Griffin, C., Ozburn, N., Chen, M., Pan, E., Koul, D., Yung, W. K. A., Feuerstein, B. G. and Aldape, K. D. (2005) Integrated Array-Comparative Genomic Hybridization and Expression Array Profiles Identify Clinically Relevant Molecular Subtypes of Glioblastoma. *Cancer Res.* 65(5):1678-1686.
- Nutt, C. L., Mani, D. R. and Betensky, R. A. (2003) Gene expression-based classification of malignant gliomas correlates better with survival than histological classification. *Cancer Res.* 63(1):1602-1607.
- Ostermann, S., Csajka, C., Buclin, T., Leyvraz, S., Lejeune, F., Decosterd, L. A. and Stupp, R. (2004) Plasma and Cerebrospinal Fluid Population Pharmacokinetics of Temozolomide in Malignant Glioma Patients. *Clin. Cancer Res.* 10(11):3728-3736.

- Pardridge, W. M. (1995) Transport of small molecules through the blood-brain barrier: biology and methodology. *Adv. Drug Deliv. Rev.* 15(1-3):5-36.
- Prados, M. D., Scott, C., Sandler, H., Buckner, J. C., Phillips, T., Schultz, C., Urtasun, R., Davis, R., Gutin, P. and Cascino, T. L. (1999) A phase 3 randomized study of radiotherapy plus procarbazine, CCNU, and vincristine (PCV) with or without BUdR for the treatment of anaplastic astrocytoma: a preliminary report of RTOG 9404. *Int. J. Radiat. Oncol. Biol. Phys.* 45(5):1109-1115.
- Quasthoff, S. and Hartung, H. P. (2002) Chemotherapy-induced peripheral neuropathy. *J. Neurol.* 249(1):9-17.
- Rautio, J. and Chikhale, P. J. (2004) Drug delivery systems for brain tumor therapy. *Curr. Pharm. Des.* 10(12):1341-1353.
- Rubanyi, G. M. (2001) The future of human gene therapy. *Mol. Aspects Med.* 22(3):113-142.
- Salazar, O. M. R., P; Feldstein, M L; Pizzutiello, R (1979) High dose radiation therapy in the treatment of malignant gliomas: final report. *Int. J. Radiat. Oncol. Biol. Phys.* 5(10):1733-1740.
- Sarli, V., Hümmer, S., Sunder-Plassmann, N., Mayer, T. and Giannis, A. (2005) Synthesis and Biological Evaluation of Novel Eg5 Inhibitors. *ChemBioChem* 6(11):2005-2013.
- Scherrmann, J.-M. (2002) Drug delivery to brain via the blood-brain barrier. *Vascul. Pharmacol.* 38(6):349-354.
- Senger, D., Cairncross, J. G. and Forsyth, P. A. (2003) Long-term survivors of glioblastoma: statistical aberration or important unrecognized molecular subtype? *Cancer J.* 9(1):214-221.
- Souhami, L., Seiferheld, W., Brachman, D., Podgorsak, E. B., Werner-Wasik, M., Lustig, R., Schultz, C. J., Sause, W., Okunieff, P. and Buckner, J. (2004) Randomized comparison of stereotactic radiosurgery followed by conventional radiotherapy with carmustine to conventional radiotherapy with carmustine for patients with glioblastoma multiforme: Report of Radiation Therapy Oncology Group 93-05 protocol. *Int. J. Radiat. Oncol. Biol. Phys.* 60(3):853-860.
- Stewart, L. A. (2002) Chemotherapy in adult high-grade glioma: a systematic review and meta-analysis of individual patient data from 12 randomized trials. *Lancet* 359(9311):1011-1018.
- Stupp, R., Mason, W. P., van den Bent, M. J., Weller, M., Fisher, B., Taphoorn, M. J. B., Belanger, K., Brandes, A. A., Marosi, C., Bogdahn, U., Curschmann, J., Janzer, R. C., Ludwin, S. K., Gorlia, T., Allgeier, A., Lacombe, D., Cairncross, J. G., Eisenhauer, E., Mirimanoff, R. O. and Group, t. E. O. f. R. a. T. o. C. B. T. a. R. G. t. N. C. I. o. C. C. T. (2005) Radiotherapy plus Concomitant and Adjuvant Temozolomide for Glioblastoma. *N. Engl. J. Med.* 352(10):987-996.

- Tarby, C. M., Kaltenbach, R. F., Huynh, T., Pudzianowski, A., Shen, H., Ortega-Nanos, M., Sheriff, S., Newitt, J. A., McDonnell, P. A., Burford, N., Fairchild, C. R., Vaccaro, W., Chen, Z., Borzilleri, R. M., Naglich, J., Lombardo, L. J., Gottardis, M., Trainor, G. L. and Roussel, D. L. (2006) Inhibitors of human mitotic kinesin Eg5: Characterization of the 4-phenyl-tetrahydroisoquinoline lead series. *Bioorg. Med. Chem. Lett.* 16(8):2095-2100.
- van den Bent, M. J., Hegi, M. E. and Stupp, R. (2006) Recent developments in the use of chemotherapy in brain tumours. *Eur. J. Cancer* 42(5):582-588.
- Walker, M., Green, S., Byar, D., Alexander, E., Batzdorf, U., Brooks, W., Hunt, W., MacCarty, C., Mahaley, M., Mealey, J., Owens, G., Ransohoff, J., Robertson, J., Shapiro, W., Smith, K., Wilson, C. and Strike, T. (1980) Randomized comparisons of radiotherapy and nitrosoureas for the treatment of malignant glioma after surgery. *N. Engl. J. Med.* 303(23):1323-1329.
- Walker, M. D. A., E Jr; Hunt, W E; MacCarty, C S; Mahaley, M S Jr; Mealey, J Jr; Norrell, H A; Owens, G; Ransohoff, J; Wilson, C B; Gehan, E A; Strike, T A (1978) Evaluation of BCNU and/or radiotherapy in the treatment of anaplastic gliomas. A cooperative clinical trial. *J. Neurosurg.* 49(3):333-343.
- Wallner, K. E., Galicich, J. H., Krol, G., Arbit, E. and Malkin, M. G. (1989) Patterns of failure following treatment for glioblastoma multiforme and anaplastic astrocytoma. *Int. J. Radiat. Oncol. Biol. Phys.* 16(1405-1409).
- Wood, K. W., Cornwell, W. D. and Jackson, J. R. (2001) Past and future of the mitotic spindle as an oncology target. *Curr. Opin. Pharmacol.* 1(4):370-377.
- Wrensch, M. M., Yuriko; Chew, Terri; Bondy, Melissa; Berger, Mitchel S (2002) Epidemiology of primary brain tumors: current concepts and review of the literature. *Neuro-oncology* 4(4):278-299.
- Yung, W. K. A., Prados, M. D., Yaya-Tur, R., Rosenfeld, S. S., Brada, M., Friedman, H. S., Albright, R., Olson, J., Chang, S. M., O'Neill, A. M., Friedman, A. H., Bruner, J., Yue, N., Dugan, M., Zaknoen, S. and Levin, V. A. (1999) Multicenter Phase II Trial of Temozolomide in Patients With Anaplastic Astrocytoma or Anaplastic Oligoastrocytoma at First Relapse. *J. Clin. Oncol.* 17(9):2762-2771.
- Yung, W. K. A., Albright, R. E., Olson, J., Fredericks, R., Fink, K., Prados, M. D., Brada, M., Spence, A., Hohl, R. J., Shapiro, W., Glantz, M., Greenberg, H., Selker, R. G., Vick, N. A., Rampling, R., Friedman, H., Phillips, P., Bruner, J., Yue, N., Osoba, D., Zaknoen, S. and Levin, V. A. (2000) A phase II study of temozolomide vs. procarbazine in patients with glioblastoma multiforme at first relapse. *Br. J. Cancer* 83(5):588-593.

Chapter 2

TmHU as siRNA transfection reagent

2.1 Introduction

2.1.1 RNA interference

During the past decade it has been elucidated how RNA molecules can act as regulators of gene expression. Long double-stranded RNAs induce post-transcriptional and gene-specific silencing in many different organisms by presenting various short or small interfering RNA (siRNA) sequences to the target mRNA. The underlying regulatory pathway is the ancient and conserved RNA interference (RNAi) pathway utilizing small duplex RNAs (Carmichael, 2005).

2.1.1.1 Mechanism of RNAi

RNAi mediated by the introduction of long dsRNA has been used as a method to investigate gene function in various organisms including plants (Baulcombe, 1999), *Planaria* (Alvarado and Newmark, 1999), Hydras (Lohmann et al., 1999), Trypanosomes (Ngô et al., 1998), *Drosophila* (Misquitta and M., 1999), mosquitoes (Caplen et al., 2002) and mouse oocytes (Svoboda et al., 2000; Wianny and Zernicka-Goetz, 2000). RNAi is carried out in two steps, and several studies have shown that this process is restricted to the cytoplasm (Zeng and Cullen, 2002; Kawasaki and Taira, 2003). In the first step, small or short interfering RNAs (siRNAs) are generated from the long double-stranded RNA via digestion by the RNase Dicer in an ATP-dependent reaction (Novina et al., 2002). SiRNAs are 21–23-nt dsRNA duplexes with symmetric 2–3-nt 3' overhangs and 5'-phosphate and 3'-hydroxyl groups (Elbashir et al., 2001b). This structure is characteristic of an RNase III-like enzymatic cleavage pattern, which led to the identification of the highly conserved Dicer family of RNase III enzymes as the mediators of the dsRNA cleavage (Bernstein et al., 2001; Ketting et al., 2001).

In the second step, the siRNAs are incorporated into a multi-component nuclease, the RNA-inducing silencing complex (RISC) that recognizes and destroys target mRNAs. There is a strict requirement for the siRNA to be 5' phosphorylated to enter into RISC (Nykänen et al., 2001; Schwarz et al., 2002), and siRNAs that lack a 5' phosphate are rapidly phosphorylated by an endogenous kinase (Schwarz et al., 2002). Recent reports suggest that RISC must be activated from a latent form, containing a double-stranded siRNA to an active form, RISC* (Nykänen et al., 2001). By the ATP-dependent unwinding of the siRNA the non-complementary strand is discarded. Then RISC* uses the unwound single-stranded siRNA as

a guide to substrate selection by the specific binding of the antisense strand to its complementary target mRNA through Watson-Crick base-pairing (Hammond et al., 2000; Martinez et al., 2002). The target mRNA is cleaved at a single site in the centre of the duplex region between the guide siRNA and the target mRNA, 10 nt from the 5' end of the siRNA (Elbashir et al., 2001b). This endonucleolytic cleavage leads to subsequent degradation of the target mRNA by cellular nucleases thereby preventing unwanted protein expression. The liberated RISC* complex is catalytic as it can turn over several times and cleave multiple targets resulting in very efficient and long-term destruction of unwanted target mRNAs (Haley and Zamore, 2004).

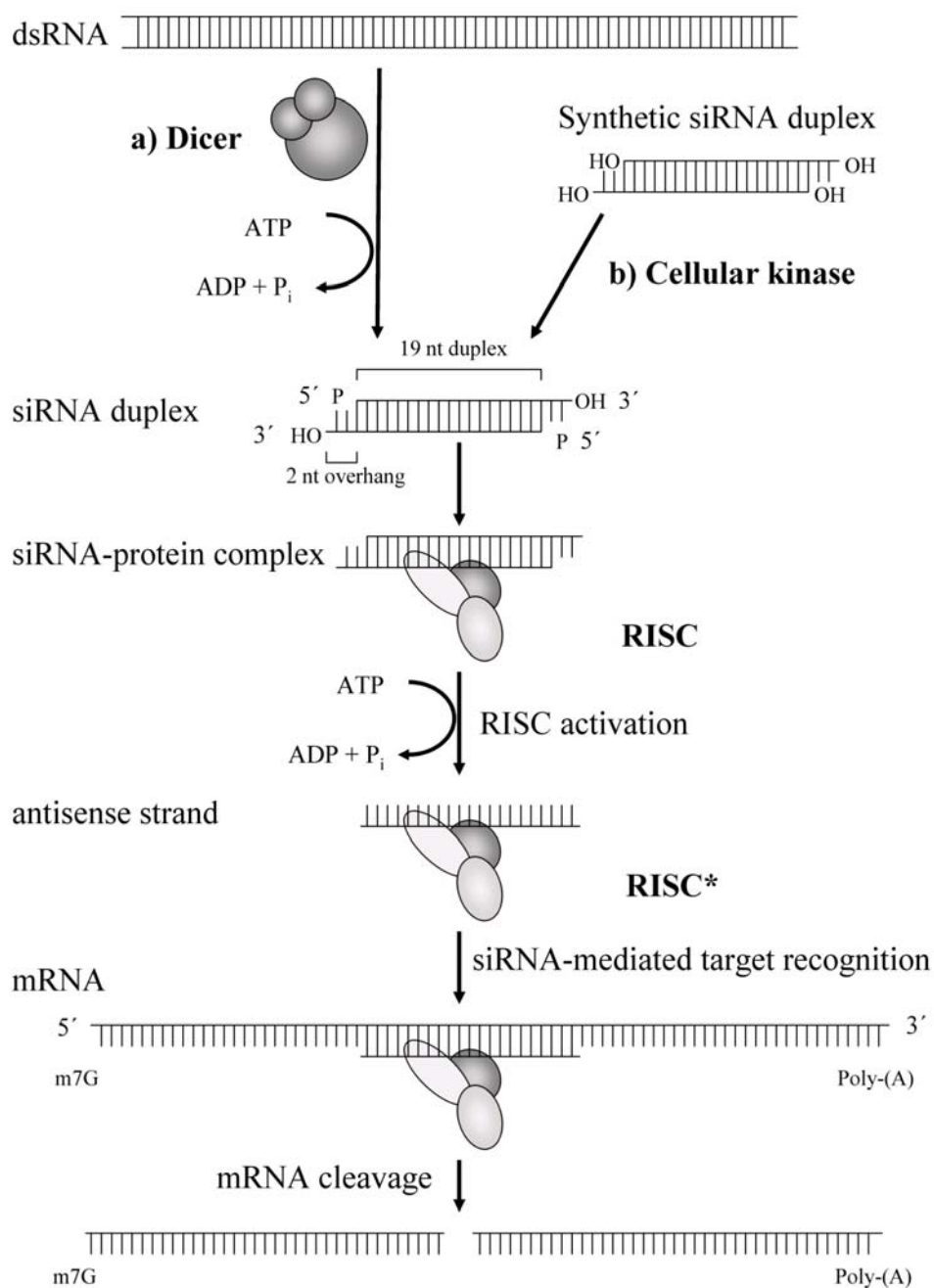


Figure 2.1: The RNA interference pathway. a) Long double-stranded RNA (dsRNA) is cleaved by the RNase III family member, Dicer, into siRNAs in an ATP-dependent reaction. b) After the transduction of synthetic siRNAs the siRNAs are phosphorylated by a cellular kinase. These siRNAs from step a) or b), respectively, are then incorporated into the RNA-inducing silencing complex (RISC). Although the uptake of siRNAs by RISC is independent of ATP, the unwinding of the siRNA duplex requires ATP. Once unwound, the single-stranded antisense strand guides RISC to messenger RNA that has a complementary sequence, which results in the endonucleolytic cleavage of the target mRNA (modified from Dykxhoorn et al., 2003).

2.1.1.2 Silencing by small interfering RNA (siRNA)

The applicability of long double-stranded RNAs is limited in mammals because the introduction of dsRNA longer than 30 nt induces a sequence-nonspecific interferon response (Elbashir et al., 2001a). Interferon triggers the degradation of mRNA by inducing 2'-5' oligoadenylate synthase, which in turn activates RNase L. In addition, interferon activates the protein kinase R, which phosphorylates the translation initiation factor eIF2 α leading to a global inhibition of mRNA translation (Stark et al., 1998). To test, whether siRNAs could mediate effective silencing of gene expression without inducing the interferon response, Tuschl and colleagues (Elbashir et al., 2001a) introduced chemically synthesized siRNA into mammalian cells. They showed that the synthetic siRNAs were functional in vivo and the siRNA transfection resulted in the sequence-specific silencing of the targeted protein in several cell lines without activating nonspecific effects. These findings led to the widespread use of this technology to study gene function, including the targeted disruption of clinically relevant genes (Dykxhoorn et al., 2003). Since siRNAs are too short to induce an interferon response, and since all other RISC components necessary for genes suppression are present in mammals, transfection of mammalian cells with preformed siRNAs may result in a profound and sequence-specific inhibition of gene expression (Caplen et al., 2001; Elbashir et al., 2001a). Consequently, this RNAi-based technology permits not only target validation but is also considered as a potential therapeutic application (Heidenreich, 2004).

2.1.1.3 siRNA design

To promote efficient gene silencing using a siRNA to a single site in the target mRNA, consideration of the siRNA sequence is crucial (Dykxhoorn et al., 2003). It is known that siRNAs, which target different regions of the same gene, vary markedly in their effectiveness (Holen et al., 2002; Miyagishi and Taira, 2002; Hemann et al., 2003; Vickers et al., 2003). As the rules that govern efficient siRNA-directed silencing still remain undefined, the selection

of the right siRNAs is an empirical process. On the basis of the analysis of a small number of target genes, several groups have proposed a set of guidelines that seek to narrow the choices of siRNA that could potentially silence gene expression (Elbashir et al., 2002; Paddison and Hannon, 2002). There exist many protocols and web-based tools for siRNA design with most following the guidelines outlined by Tuschl and colleagues (Tuschl et al., 1999; Elbashir et al., 2001a; Elbashir et al., 2001b; Elbashir et al., 2001c). Several siRNA sequences in different locations along the gene of interest can be selected and tested. Key parameters to consider include the length of 19 to 21 nt, the format AAN₁₉TT is preferable and the GC content of 30 to 50 %. To ensure that the chosen siRNA sequence targets a single gene, a BLAST search of the selected sequence should be carried out against sequence databases such as EST or Unigene libraries using the National Center of Biotechnology Information (NCBI) website. A query against the small nucleotide polymorphism database will confirm that there are no sequence polymorphisms. A single point mutation in certain locations of the paired region of a siRNA duplex is sufficient to abolish target mRNA degradation (Elbashir et al., 2001a) Helpful web-based tools are for example provided by Qiagen using the GeneGlobe web portal (<http://www.qiagen.com>).

2.1.2 Transient transfection of siRNA

Transient transfection of siRNA duplexes into mammalian cells can be performed by conventional liposomal methods using various commercial reagents or through electroporation. Recent evidence showed that the effectiveness of siRNAs may depend on the method of transfection (Walters and Jelinek, 2002).

2.1.2.1 Electroporation

Electroporation as a simple physical method of transferring genes into eucaryotic cells was first described in 1982 (Wong and Neumann, 1982). Electroporation designates the use of short (5-10 μ s) high-voltage (5-10 kV/cm) pulses to overcome the barrier of the cell membrane. By applying an external electric field, which just surpasses the capacitance of the cell membrane, transient and reversible breakdown of the membrane can be induced. This transient, permeabilized state can be used to load cells with a variety of different molecules, either through simple diffusion in the case of small molecules, or through electrophoretically driven processes allowing passage through the destabilized membrane - as is the case for

nucleic acid transfer (Shigekawa and Dower, 1988; Tupin et al., 2003). The transfection rates depend on the amplitude and the period of the electric pulses as well as the concentration and quantity of the nucleic acids. Electroporation has proven useful both *in vitro*, *in vivo* and in patients, where drug delivery to malignant tumors has been performed (Gehl, 2003). Electroporation *in vivo* is carried out directly after the injection of naked DNA by an electrode which is localized in the targeted tissue. Successful transfections *in vivo* by means of electroporation were observed in muscles (Rambabu et al., 2005), brain (Luo and Redies, 2004), skin (Pavselj and Preat, 2005), liver (Thanaketaipaisarn et al., 2005) and tumors (Mitrus et al., 2005).

2.1.2.2 Lipofection

The binding of nucleic acids to lipids results in organized structures like liposomes or micelles are formed. Liposomes are vesicles that consist of a phospholipid bilayer surrounding an aqueous compartment (Agrawal et al., 1997; Petersen et al., 2002). Liposomes have become the vehicles of choice for transfer of nucleic acids such as plasmids and oligodeoxynucleotides to cells in culture and in principle *in vivo* (Dass, 2002). Although generally not as efficient as viral vectors, nonviral systems such as lipidic vectors have the potential advantages of being less toxic, nonrestrictive in cargo DNA size, potentially targetable, and easy to produce in relatively large amounts. More important, lipidic vectors generally lack immunogenicity, allowing repeated *in vivo* transfection using the same vector. Different types of lipidic gene transfer vectors are described: 1) DNA/cationic liposome complexes, 2) DNA encapsulated in neutral or anionic liposomes, and 3) liposome-entrapped, polycation-condensed DNA (Lee and Huang, 1997). In principle, these delivery systems are also suitable for the transfection of siRNA. Therefore, several *in vitro* and *in vivo* studies were carried out to develop optimal liposomal-based siRNA transfection reagents (Hassani et al., 2005; Santel et al., 2006a; Santel et al., 2006b; Tagami et al., 2007). Many optimized lipid formulations for siRNA are already commercially available, for example Lipofectamine™ 2000 (Invitrogen Inc., Karlsruhe, Germany), GeneSilencer® (PeqLab), GeneEraser™ (Stratagene) and HiPerFect® (Qiagen), but only applicable *in vitro* so far.

Cationic lipids and helper lipids

Cationic lipid–DNA complexes, also called lipoplexes, are formed by the interaction of anionic nucleic acids binding to the surface of cationic lipids eventually forming multilamellar lipid–nucleic acid complexes. The negatively-charged nucleic acids are

attracted to the surface of the positively-charged vesicles, initially forming complexes with nucleic acid molecules docked onto the surface of the cationic vesicles (Dass, 2002) (Figure 2.2). In the case of double-stranded DNA, the nucleic acid molecules persist glued to lipidic molecules with a lipid bilayer surrounding the compacted nucleolipidic particles in one of several different moieties (Choi et al., 2001).

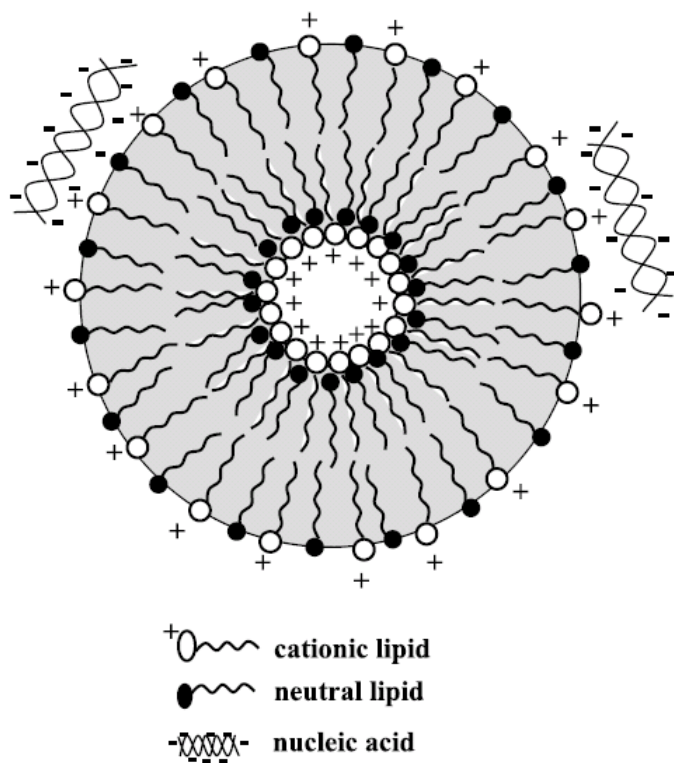


Figure 2.2: Formation of lipoplexes. Anionic nucleic acid molecules are attracted to the surface cationic charge of the liposomes (made from a cationic and a neutral lipid mixture) forming complexes that eventually form compact nucleolipidic particles of various morphologies and sizes (Dass, 2002).

Most of the cationic lipid reagents in use today are formulated as liposomes containing two lipid species, a cationic amphiphile and a neutral phospholipid (Felgner et al., 1994; Hofland et al., 1996; Godbey and Mikos, 2001). Commonly used cationic lipids are 1,2-dioleoyl-3-trimethyl ammonium propane (DOTAP) (Lasic, 1997), *N*-[1-(2,3-dioleoyloxy)-propyl-*N,N,N*-trimethyl ammonium chloride (DOTMA) (Felgner et al., 1987), 2,3-dioleoyloxy-*N*-[2-(spermincarboxamido)ethyl]-*N,N*-dimethyl-1-propanaminium (DOSPA) (Lasic, 1997), dioctadecylamidoglycylspermine (DOGS, Transfectam[®]) (Behr et al., 1989) and 3 β -[*N*-[2-(*N,N*-dimethylamino)ethyl]carbonyl]cholesterol (DC-Chol) (Zhdanov et al., 2002). The cationic lipids form complexes with the polyanionic nucleic acids leading to DNA condensation and the formation of the lipoplexes that protects the DNA from degradation by intracellular nucleases. The positively charged lipoplexes adhere onto the negatively charged

cellular surface, whereby the internalization is facilitated. The neutral lipids, also called helper or fusogenic lipids, support permeation and fusion of the lipoplexes with the cell membrane. Dioleoyl phosphatidylethanolamine (DOPE) is mostly used as a helper lipid for formation of liposomes from cationic lipids (Felgner et al., 1994). In many cases, for example Lipofectin[®], the equimolar mixture of a cationic lipid and DOPE ensures optimally efficient transfection (Felgner et al., 1987). The major disadvantage of cationic liposomes as a gene delivery system is their much lower transfection efficiency compared to viral vector systems. The limitations of cationic liposome usage for transfection purposes (as a gene therapy tool) are closely connected to a short lifetime of the complexes, as well as to their inactivation by serum proteins (Zhdanov et al., 2002) and the cytotoxicity of cationic lipids at high concentrations in vitro (Lappalainen et al., 1994; Patil et al., 2004) and in vivo (Filion and Phillips, 1997; Dokka et al., 2000).

Anionic and neutral lipids

Anionic and neutral lipids for the construction of synthetic vectors as alternative for cationic lipids have also been used (Patil and Rhodes, 2000; Fillion et al., 2001; Lakkaraju et al., 2001; Patil et al., 2004). But their transfection efficiency is very low and has to be improved. One major problem is the packaging of the negatively charged DNA into the liposomes enabled by cations like Na⁺, K⁺ (Fillion et al., 2001), Ca²⁺ (Patil et al., 2005b) and polycations (Lee and Huang, 1997; Guo et al., 2002) which saturate the negative charge of the nucleic acids. Disadvantages of anionic liposomes as delivery vectors are the poor DNA encapsulation (Zelphati and Szoka, 1996) and the lack of toxicity data (Fillion et al., 2001). Nevertheless, neutral and anionic liposomes have been developed for gene therapy in vivo (Gaucheron et al., 2001).

pH-sensitive liposomes

They are designed in order to release their contents in response to acidic pH within the endosomal system while remaining stable at neutral pH in plasma thus improving the cytoplasmic delivery of various polar materials and macromolecules (Venugopalan et al., 2002). pH-sensitive liposomes have been used to deliver anticancer drugs, antibiotics, antisense oligonucleotides, ribozymes, plasmids, proteins and peptides to cells in culture or in vivo (Simoes et al., 2004).

Immunoliposomes

Immunoliposomes are generated by the modification of the lipid bilayer membrane integrating antibodies or antibody-fragments (Kontermann, 2006). These antibodies are targeted at defined receptors on the surface of the targeted cells. Thus, immunoliposomes can be designed for specific recognition of a target antigen followed by receptor-mediated endocytosis. In principle, the therapeutic index can be increased by targeting liposomes and their contents directly into tumor cells, and this may be useful for resistant cancers (Mamot et al., 2003).

Stealth liposomes

Stealth liposomes are sterically stabilized liposomal formulations containing polyethylenglycol (PEG) conjugated lipids. PEG prevents the recognition of the liposomes by the reticuloendothelial system and thus their degradation. Pegylated liposomes were called "stealth liposomes" because of their ability to evade interception by the immune system, by analogy as a stealth bomber evades radar. They are characterized by a very long-circulation half-life, favorable pharmacokinetic behavior and specific accumulation in tumor tissues (Cattel et al., 2003).

2.1.2.3 Polyfection

One non-viral gene delivery strategy involves the use of polycationic polymers as a DNA complexing agent. Generally cationic polymers are preferred due to their ability to form positively charged complexes with anionic nucleic acids (Hwang and Davis, 2001). These Polymer/DNA complexes, termed polyplexes, interact with the negatively charged cell surface and are taken up by a variety of cells via endocytosis (Luo and Saltzman, 2000).

Polymers display striking advantages as vectors for gene delivery. They can be specifically tailored for the proposed application by choosing appropriate molecular weights, coupling of cell or tissue specific targeting moieties and/or performing other modifications that confer upon them specific physiological or physicochemical properties (Merdan et al., 2002). Among the variety of different non-viral vectors, the use of polymers confers several advantages, due to their ease of preparation, purification and chemical modification as well as their enormous stability (Lungwitz et al., 2005). Commonly used polymers are polyethylenimine (PEI) (Lemkine and Demeneix, 2001), poly-L-lysine (PLL) (Lollo et al., 2002), chitosan (Borchard, 2001) and dendrimers (Merdan et al., 2002).

PEI/DNA polyplexes are internalized by a large variety of cells via endocytosis delivering polymer/DNA complexes to the endolysosomal compartment. They are finally released due to their buffer capacity via the so-called ‘proton sponge mechanism’. The proton-sponge hypothesis (Behr, 1994) asserts that polymers containing a large number of unprotonated basic groups (typically amines) may prevent acidification of endocytic vesicles by sequestering protons actively transported into the compartment by the endolysosomal ATPase proton pump. Furthermore, because of the buffering by the polymer, the enzyme continues to transport protons into the vesicle, the concentration of negative counter ions and the osmotic pressure increase, and the vesicles ultimately rupture (Forrest and Pack, 2002).

Despite the relatively low transfection efficiency compared to viral transfection systems, as well as the cytotoxicity, the polyamine PEI has gained some prominence compared to other non-viral gene delivery systems. The implementation of strategies for their optimization yielded higher transfection efficiencies and lower cytotoxicity. Different polyethylenimine forms like branched (BPEI) and linear (LPEI) morphological isomers (Zou et al., 2000; Wightman et al., 2001; Wiseman et al., 2003; Breunig et al., 2005) as well as per-N-methylated PEIs (Breunig et al., 2004) were synthesized and appropriate transfection conditions were determined.

The efficacy of PEI-derived non-viral vectors and their cytotoxic effects depend on various parameters: 1) material characteristics such as the molecular weight, the degree of branching, the cationic charge density and buffer capacity (Fischer et al., 1999; von Harpe et al., 2000; Kunath et al., 2003); 2) the polyplex properties, such as the DNA content, particle size, the N/P ratio (quotient of the nitrogen atoms of PEI to DNA phosphates) and with it the zeta potential dramatically influences the transfection efficacy and the cytotoxicity; 3) experimental conditions e. g. the polyplex concentration, the presence or absence of serum during transfection, the incubation time and the transfection model chosen for the gene delivery experiment (Lungwitz et al., 2005). In order to gain more insight into LPEI-mediated gene transfer and to explore conceptual aspects for further optimization various steps during the transfection process were investigated and the results suggest that the endocytosis seems not to be a decisive parameter that determines the efficacy of a polymer in the transfection process (Breunig et al., 2007). But the intracellular release of the nucleic acid from the non-viral carrier system may be a relevant criterion for the high transfection efficiency of certain polymers. Therefore, fluorescence resonance energy transfer (FRET) in combination with confocal laser scanning microscopy or flow cytometry was evaluated as a tool to determine the intracellular disintegration of LPEI/DNA-polyplexes (Breunig et al., 2006).

In vivo the specific delivery of highly charged particles to the desired cells fails, due to the non-specific interaction with blood components and extracellular matrix as well as non-targeted cells and tissues (Lungwitz et al., 2005). To suppress non-specific interactions, the cationic surface charge has been shielded by the covalent or non-covalent attachment of a hydrophilic polymer layer, using polyethyleneglycol (PEG), pluronic® (Nguyen et al., 2000; Ochietti et al., 2002), polyacrylic acid (Trubetskoy et al., 2003), poly-*N*-(2-hydroxypropyl)methacrylamide derived copolymers (Oupicky et al., 2002; Carlisle et al., 2004), dextran (Tseng and Jong, 2003) or dextran sulfate (Tiyaboonchai et al., 2003), as well as plasma proteins like transferrin (Kircheis et al., 1999; Kircheis et al., 2001) or human serum albumin (Rhaese et al., 2003).

Moreover, polyplexes between siRNA and polyethyleneimine derivatives are promising nonviral carriers for siRNA. The polyplex stability is of critical importance for efficient siRNA delivery to the cytoplasm. First studies on the evaluation of the efficacy of different polyethylenimine structures for siRNA delivery and the determination of the biophysical and structural characteristics of PEIs for siRNA delivery were successful. SiRNA delivery was observed within a very narrow window of conditions, and only with the 25,000 branched PEI at an N:P ratio of 6:1 and 8:1 and with very high siRNA concentrations (200 nM) (Grayson et al., 2006). Mao et al. investigated the effect of PEGylation at a constant ratio (~50 %) on the biophysical properties of the polyplexes (Mao et al., 2006). It was shown that both the chain length and graft density of PEG strongly influence siRNA condensation and stability and hence affect the knockdown efficiency of PEI-PEG/siRNA polyplexes.

2.1.3 Problems of transfection in vivo

In order to study the function of genes associated with human disease, in particular with oncogenesis, it has been shown that gene silencing by siRNA is a very successful and promising tool (Cheng et al., 2003). This technology permits not only target validation but may, at least in theory, provide oncogene-specific siRNAs for the development of cancer-specific therapeutic approaches (Heidenreich, 2004). Finding the oncogene-specific siRNA is not the major challenge. For in vivo application, the greatest difficulty still is the efficient delivery of siRNA or plasmid DNA, respectively, into the targeted cells.

The advantage of viral delivery systems is their extremely high transfection efficiency in a variety of human tissues, but due to the toxicity of the viruses and the potential of generating a strong immune response this transfection method is not acceptable in vivo (Patil et al., 2005a).

Non-viral delivery systems can circumvent some of the problems associated with viral vectors and are emerging as favorable alternatives to viral vectors. The greatest advantages of non-viral gene vectors are lack of immune response and ease of formulation and assembly (Merdan et al., 2002). But, besides the toxicity, the major disadvantage of non-viral transfection reagents and the reason for the failure of their successful application in vivo is the very low transfection efficiency. In order to solve this problem numerous efforts on the improvement of transfection methods and on the development of efficient non-viral transfection reagents have been made, but failed so far. Thus, there is still a great need to find a non-viral, efficient and non-toxic transfection reagent which can be applied repeatedly in vivo.

2.1.4 The TmHU protein

2.1.4.1 The HU protein family

HU proteins belong to a group of small basic proteins abundant in all prokaryotes capable of interacting with DNA and inducing DNA condensation. They are termed as histone-like or HU proteins because their biochemical properties are similar to eukaryotic histones (Drlica and Rouviere-Yaniv, 1987; Bonnefoy and Rouviere-Yaniv, 1991; Oberto and Rouviere-Yaniv, 1996). The term HU is derived from the DNA-binding and DNA-condensing protein *Heat Unstable Nucleotide Protein* from *E. coli*. The HU proteins are highly homologous to each other and consist of about 90 amino acid residues with a monomeric molecular mass of 9-10 kDa. The amino acid sequence is highly conserved (Drlica and Rouviere-Yaniv, 1987) resulting in the analogous supra-secondary structures of the HU proteins. In solution, they form either homodimers or heterodimers (Bonnefoy and Rouviere-Yaniv, 1991; Oberto and Rouviere-Yaniv, 1996). HU proteins are essentially involved in the formation of supra-molecular nucleo-protein-complexes and play an important role in different DNA metabolizing processes, such as replication, transcription and transposition (Hwang and Kornberg, 1992; Lavoie and Chaconas, 1994). They are able to repair DNA (Murphy and Zimmerman, 1994; Kamashev and Rouviere-Yaniv, 2000) and to increase the “melting temperature” (T_m) of DNA (Esser et al., 1999). By interaction with the genome the HU proteins can influence gene expression, the growth and the vitality of microorganisms.

HU proteins bind DNA mainly in a non-sequence-specific manner (Boubrik et al., 1991) with relatively low affinity to linear DNA, whereas kinked DNA forms tight complexes (Shimizu et al., 1995). On the one hand HU proteins bend double-stranded DNA, thereby condensing it into compact higher-ordered nucleosome-like structures (Murphy and Zimmerman, 1994), and, on the other hand, HU proteins promote DNA flexibility (Paull et al., 1993). More information on the mechanism of DNA binding was obtained with the determination of the HU protein structure from the thermophilic bacterium *Bacillus stearothermophilus*, BstHU, by X-ray crystallography (White et al., 1989) and NMR spectroscopy (Vis et al., 1995). BstHU is a homodimer, which consists of an α -helical part involved in dimerization, and of a β -sheet region responsible for DNA binding. Two long β -hairpin arms extending from the protein core are suggested to bind tightly into the minor groove of DNA (Haerd et al., 1989; Goshima et al., 1992).

2.1.4.2 TmHU, the histone-like protein from *Thermotoga maritima*

Due to their enormous stability, especially against thermal denaturation, proteins from hyperthermophilic organisms are of major interest for the biotechnological industry (Jaenicke et al., 1996). Normally, they are recombinantly expressed without difficulty (Jaenicke and Böhm, 1998; Christodoulou and Vorgias, 2002), and due to their high thermo-stability the first step in the purification of the proteins from crude cell lysate is performed by cheap and effective heat precipitation. Moreover, the handling, storage and cooling during and after the purification of thermo-stable proteins is unproblematic.

TmHU is the HU protein from the marine hyperthermophilic eubacterium *Thermotoga maritima*. The native protein represents a stable homodimer. The monomer consists of 90 amino acids with highly conserved regions in the sequence compared to other HU proteins. Esser et al. demonstrated by CD spectroscopical studies with secondary structure analysis and comparative modeling that the dimeric TmHU has a tertiary structure similar to homologous HU proteins (Esser et al., 1999). The model 3D structure of TmHU is shown in Figure 2.3.

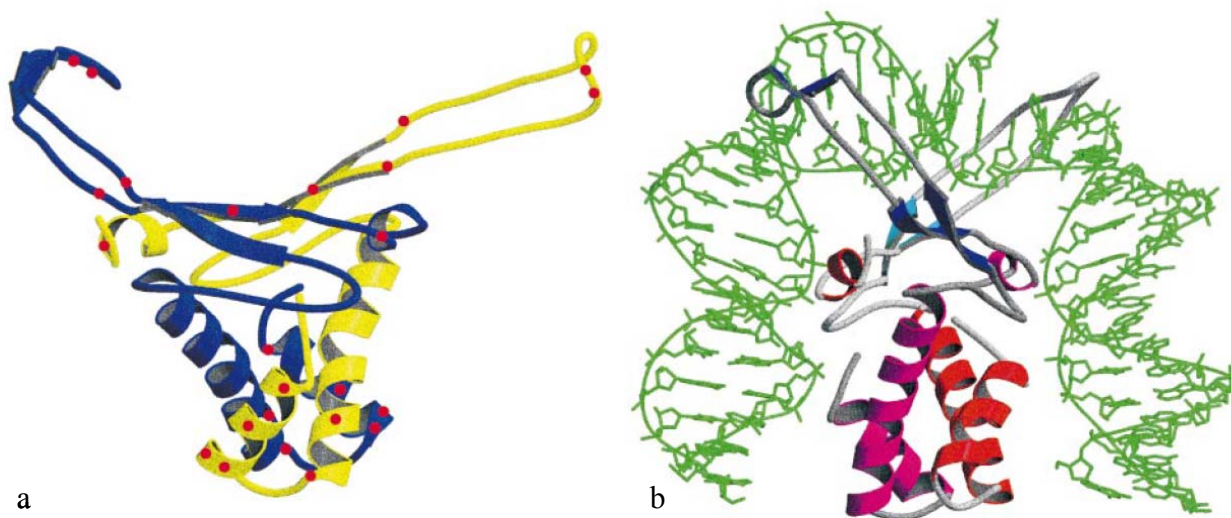


Figure 2.3: Model structure of TmHU. (a) Schematic representation of the dimer; the model is based on the NMR structure of the HU protein from *B. stearothermophilus*. The positions of additional positively charged residues in TmHU compared to BstHU are indicated by red circles, demonstrating their clustering at the bottom and at the DNA-binding interface of the protein. (b) Model of the DNA interaction between TmHU and a kinked 35 bp DNA fragment based on the coordinates of the IHF (integration host factor) structure from *E. coli*, which recognizes specific DNA sequences (Boubrik et al., 1991; Ellenberger and Landy, 1997). The protein interacts with the central part of the bended DNA, using minor groove contacts and contacts to the phosphodiester backbone, and induces a bend of more than 160 °, thereby reversing the direction of the DNA (Esser et al., 1999).

The “melting temperature” (T_m) of the protein was determined to be 96 °C, and thermal unfolding is almost completely reversible (Esser et al., 1999). Compared to other HU proteins TmHU possess a large number of basic amino acids, and therefore, a higher isoelectric point ($pI = 10.36$). Due to its positive charge TmHU is able to interact with DNA. The protein binds to DNA in a highly cooperative manner, with a K_D of 73 nM and a Hill coefficient of 7.6 for a 56 bp DNA fragment. TmHU is capable of increasing the “melting temperature” of a synthetic, double-stranded DNA by 47 °C, thus suggesting that DNA stabilization may be a major function of this protein in hyperthermophiles (Esser et al., 1999).

2.1.4.3 TmHU as gene transfer reagent

After recombinant expression in *E. coli*, purification and physicochemical characterization of the extremely hyperthermophilic DNA-binding TmHU protein (Esser et al., 1999), a biotechnologically feasible and economical approach for gene delivery using the TmHU protein as an efficient gene transfer reagent was carried out (Esser et al., 2000).

Esser et al. established a protocol for TmHU-mediated transient transfection in vitro, transfecting the *E. coli lacZ* gene into NIH 3T3 cells. The protocol was optimized for several critical parameters, such as the TmHU:DNA ratio and the conditions of pre-incubation. The optimal TmHU:DNA ratio was 12.5:1 (wt/wt), corresponding to a 5- to 6-fold net positive charge excess at physiological pH. Upon heating the reaction mixture (95 °C for 40 min) and adding calcium to a final concentration of 2 mM, a dense, compact precipitate formed, accompanied by a 100-fold increase in transfection efficiency and a higher reproducibility. In the absence of calcium, the observed aggregates were larger, had a lower density, and floated in the medium. The optimized system routinely yielded about $1 \cdot 10^4$ X-gal positive cells/mg DNA, the number of transfected cells being roughly proportional to the amount of reaction mixture used. A control experiment without TmHU yielded only 3 X-gal positive cells/mg DNA, demonstrating that the transfection was not due to DNA–calcium phosphate co-precipitation. The DEAE-dextran method (Stratagene, La Jolla, CA) and lipofection using the cationic lipid Tfx-50 (Promega) yielded about $3 \cdot 10^2$ and $3.3 \cdot 10^3$ X-gal positive cells/mg DNA, respectively. Transfecting several cell lines with TmHU, compared with DEAE-dextran mediated transfection efficiencies were increased (33 fold (NIH 3T3), 120-fold (U251), and 6-fold (A431)). 293T cells could not be transfected with DEAE-dextran (the cells detached) but were very efficiently transfected with TmHU.

Addition of endosomolytical agents (e.g., chloroquine) under several conditions did not improve transfection by TmHU but in fact was often detrimental. Esser et al. neither observed

a decrease in transfection efficiency when cells grew confluent nor inhibition of transfection by serum. All transient transfections with TmHU were therefore performed with confluent cultures in the presence of serum.

Since these features point towards the feasibility of an *in vivo* application, Esser et al. tested this potential, injecting TmHU–DNA complexes into the thigh muscles of female BALB/c mice. The transient expression of the luciferase reporter gene increased by an average of 8-fold compared to the injection of naked DNA. However, the conditions for efficient transfection *in vivo* differed considerably from those determined *in vitro*, with precipitate formation seemingly decreasing efficiency, probably because of impaired diffusion. The optimal TmHU:DNA ratio for *in vivo* transfection was determined to be 1.2:1 (wt/wt).

In order to evaluate toxicity, Esser et al. monitored the number of viable 293T cells after 24 h incubation with various concentrations of either TmHU or the cationic lipid Lipofectin[®] (GIBCO BRL). Whereas incubation with even low amounts of Lipofectin[®] (0.05 mg/ml) caused considerable cell death, an effect of TmHU was observed only at very high concentrations (1 mg/ml TmHU). Considering that only 1.2 mg TmHU were used to transfect 1 mg DNA *in vivo*, but usually a 3- to 4-fold mass excess of Lipofectin over DNA was used, the authors concluded that TmHU is at least two orders of magnitude less toxic.

The protocol optimized for transient transfection was also successfully applied to stably transfect NIH 3T3 cells with the neomycin resistance gene *in vitro*. TmHU-mediated gene transfer in presence or absence of calcium yielded colonies of stable transfectants after selection with G418. The yields were comparable to those of the standard calcium phosphate precipitation method.

It was further investigated, whether the prior formation of TmHU–DNA complexes could enhance the efficiency of lipofection. Different experiments were set up using 1 mg of plasmid DNA and varying amounts of TmHU and of the cationic lipid Tfx-50. The optimal condition for lipofection in the absence of TmHU was a charge ratio of 2:1, resulting in $3.3 \cdot 10^3$ X-gal positive cells/mg DNA. Pre-incubation with TmHU increased the transfection efficiency significantly, yielding up to $1.6 \cdot 10^4$ X-gal positive cells/mg DNA (3:1 charge ratio, 6.25 mg TmHU). This yield was significantly higher than the sum of yields obtained using either TmHU or cationic lipid alone, indicating a synergistic effect. Unlike the optimized protocol for TmHU-mediated transfection, heating the TmHU–DNA mixture before adding it to the cationic lipid decreased the transfection efficiency to about 30%.

Taken together, TmHU can mediate transfection of eukaryotic cells with high efficiency because it is a polycation, like many transfection reagents. It binds DNA nonspecifically and

protects it efficiently from DNase digestion. At a high TmHU:DNA ratio, the surplus positive charges facilitate binding of the TmHU–DNA complex to the negatively charged cell membrane. Furthermore, considering that some cationic amphiphilic peptides are known to cause endosomal disruption (Wyman et al., 1997), a fraction of TmHU molecules or partially denatured molecules may destabilize the endosomal membrane, inducing uptake into the cytosol. The presence of calcium might further enhance endosomolysis, as has been postulated earlier (Zaitsev et al., 1997). TmHU is an efficient carrier of heterologous DNA into various eukaryotic cells and an enhancer of another transfection method (lipofection). Moreover, large amounts of the protein can be produced easily and efficiently to provide sufficient material for large-scale in vitro or in vivo transfections.

In preliminary toxicity studies, TmHU proved to be significantly less toxic than Lipofectin, and no adverse effects have been observed in the in vivo experiments. One important point is the potential immunogenicity of TmHU; the bacterial origin of the protein might elicit an immune response that could be detrimental for repeated injections. Relevant studies will have to be performed to investigate these potential hazards. In addition, the formation of large aggregates that is inherent to this technique may not always be favorable and may sometimes even pose a potential danger in vivo (e.g., in intravenous applications).

2.2 Objective

Synthetic small interfering RNA (siRNA) has been shown to be a selective and potent inhibitor of gene expression in mammalian cells (Elbashir et al., 2001a). Since the specific down-regulation of oncogene expression is predicted to be an efficient procedure for the selective killing of tumor cells, siRNAs are considered as promising agents for cancer treatment (Dorsett and Tuschl, 2004). However, efficient transfection of the cancer cells is a prerequisite for this new concept, and reliable *in vitro* and *in vivo* models are indispensable for the proof of principle. Moreover, the *in vivo* application of siRNA is very critical and difficult. Non-toxic and safe transfection reagents suitable for *in vivo* application are not available, so far. Possibly, the discovery of the non-toxic TmHU protein as DNA transfection reagent may provide a new alternative for siRNA transfection *in vivo*. It has already been shown that HU proteins can bind to RNA. The bacterial histone-like protein EcoHu from *Escherichia coli* specifically recognizes similar structures not only in DNA but also in double-stranded RNA and in hybrids of DNA and RNA (Balandina et al., 2002). Another example for the interaction of HU proteins with RNA is HBSu from *Bacillus subtilis*, which binds the Alu domain of small cytoplasmatic RNA (Nakamura et al., 1999).

The objective of this work was to explore the suitability of TmHU as siRNA transfection reagent *in vitro* and *in vivo* in order to obtain new therapy options in the treatment of tumors. For the development of appropriate assays three human glioblastoma cell lines had to be stably transfected with the gene encoding the enhanced green fluorescent protein (EGFP) and the gene encoding the red fluorescent protein (DsRed2), respectively. After the selection of the transfectants with the antibiotic G418, the fluorescent cells were enriched by cell sorting with the flow cytometer. The chemosensitivity of the wild type and the transfected cell lines had to be investigated to assure the similarity of the cell lines and the comparability of the test results.

For the *in vitro* assay the extent of EGFP or DsRed2 expression had to be quantified with respect to total cell number using a Tecan GENiosPro fluorescence plate reader. A crucial procedure was the validation of this method with different transfection reagents, specific and nonspecific siRNA. The application of the siRNA-transfection reagent complexes should be carried out by subcutaneous implantation of micro-osmotic pumps to achieve a continuous release of the transfection mixture.

Furthermore, this project was intended to comprise the development of a practicable method for in vivo studies on siRNA effects. Therefore, solid subcutaneous tumors had to be established after subcutaneous injection of EGFP and DsRed2 expressing glioblastoma cells into nude mice. The quantitation of the fluorescence intensity should be accomplished in histological sections by conventional fluorescence microscopy and confocal laser scanning microscopy. This morphometric procedure is based on serial sections, very complex and extremely time-consuming. Moreover, the animals have to be killed and therefore only an end point measurement is possible. Due to this difficulty it was also planned to quantify the fluorescence intensity of the tumors by an in vivo imaging system, an innovative, non-invasive method.

2.3 Materials and methods

2.3.1 Chemicals and drugs

Water was purified by a Milli-Q system (Millipore, Eschborn, Germany). If not mentioned otherwise chemicals were of analytical grade and were obtained from Merck (Darmstadt, Germany). The following selection antibiotics were used: ampicillin sodium (Amp, 50 µg/µl, Sigma, Deisenhofen, Germany), kanamycin sulfate (Kan, 50 µg/µl, Sigma) and geneticin disulfate (G418, neomycin, 400 µg/µl, PAA Laboratories, Cölbe, Germany). All antibiotics were kept as aliquoted stock solutions in millipore water at -20 °C. Phosphate buffered saline (PBS) was made of 8.0 g/l NaCl, 1.0 g/l Na₂HPO₄·2H₂O, 0.2 g/l KCl, 0.2 g/l KH₂PO₄ and 0.15 g/l NaH₂PO₄·H₂O and adjusted to pH 7.4 with NaOH or HCl. DAPI (4',6'-diamidino-2-phenylindole, Sigma) was a gift from the Institute of Pathology (University of Regensburg) and was kept as stock solutions with a concentration of 2 mg/ml in DMSO. SYTO 60 (Molecular Probes, Eugene, USA) kept as 5 mM stock solution in DMSO and was aliquoted in sterile PBS to 50 µM. The DNA (300 mg/l) solution was made of deoxyribonucleic acid sodium salt from calf thymus (Sigma) diluted in CS buffer (sodium citrate 0.01 M, NaCl 0.15 M, pH 7.0).

2.3.2 Amplification and purification of plasmid DNA

2.3.2.1 The pEGFP-N1, pcDNA3EGFP and pDsRed2-C1 vectors

The glycerol stock culture of the pEGFP-N1 vector (BD biosciences Clontech, Heidelberg, Germany) was kindly provided by Prof. Göpferich (Institute of Pharmacy) from the University of Regensburg (Figure 2.4). The pcDNA3EGFP vector was generated by the isolation of the EGFP encoding fragment from the pEGFP-N1 vector and the subsequent insertion into the *HindIII/NotI* cassette of the pcDNA3 vector (Ziemek, 2006). The purified plasmid DNA of pDsRed2-C1 (BD biosciences Clontech) was a gift from ACGT ProGenomics (Halle a. d. Saale, Germany) (Figure 2.5).

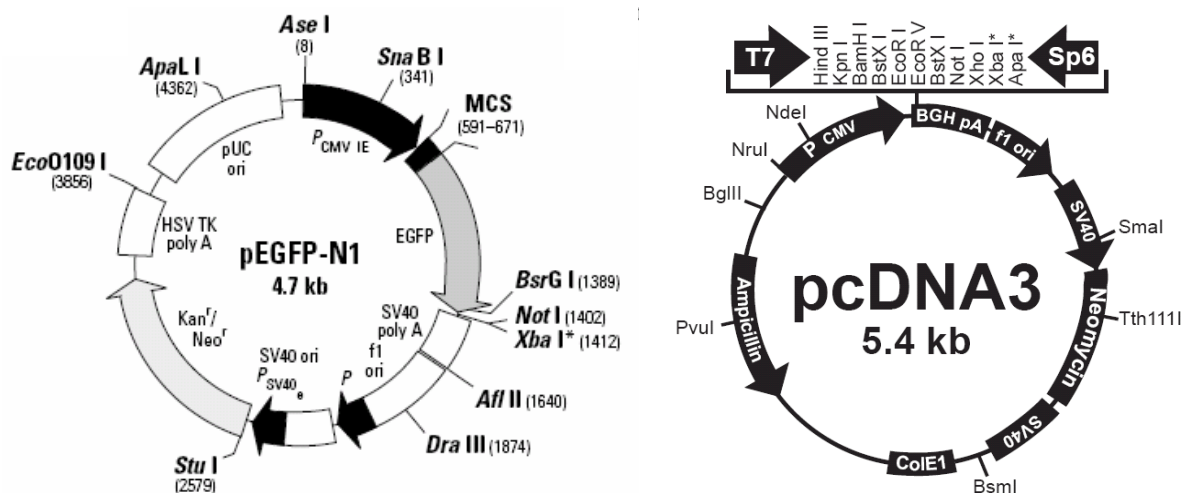


Figure 2.4: Vector maps of pEGFP-N1 and pcDNA3.

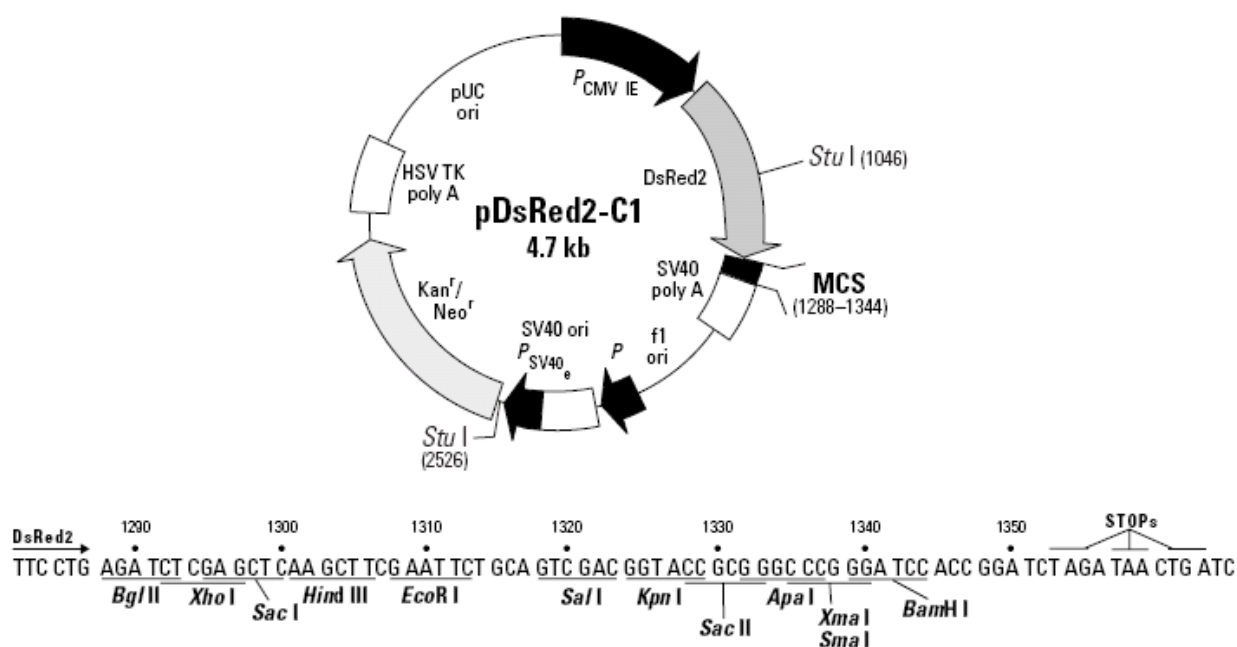


Figure 2.5: Vector map of pDsRed2-C1.

2.3.2.2 Plasmid DNA maxi-preparation and determination of DNA concentration

The plasmid DNA was isolated from *E. coli* (strain K12-XL-blue). For the plasmid DNA maxi-preparation of pEGFP-N1 and pcDNA3EGFP 110 ml of LB medium, supplemented with the appropriate selection antibiotic (Kan 30 µg/ml, Amp 100 µg/ml), were inoculated with a sample from the glycerol stock culture (800 µl of bacterial suspension, 200 µl 85 % glycerol), which was stored at -80 °C. The culture was grown overnight at 37 °C (shaker, 300

rpm). Next day, the DNA was isolated using the Qiagen Plasmid Purification Kit (Qiagen, Hilden, Germany) with the Qiagen-tip 500 column according to the manufacturer instructions. A 1:50 dilution of a Maxi-Prep DNA was prepared, and the DNA concentration was determined photometrically according to the following equation:

$$c (\mu\text{g/ml}) = 70 A_{260} - 40 A_{280}.$$

The identification of the plasmid DNA was carried out by the determination of the molecular weight with agarose gel electrophoresis.

2.3.2.3 Restriction enzyme digest

For the restriction analysis of plasmid DNA the enzymes *Hind*III (10 U/ μ l, Roche Diagnostics, Mannheim, Germany) and *Not*I (10 U/ μ l, MBI Fermentas, St. Leon-Rot, Germany) were used. Normally, 1 μ l of the enzyme stock solution was mixed with 2 μ l of the 10x NEBuffer 3 (New England BioLabs, Frankfurt am Main, Germany) including 10% of BSA solution (10 mg/ml, Serva, Heidelberg, Germany). After addition of 0.5 μ g of DNA the samples were diluted to a final volume of 25 μ l with millipore water. The reaction was carried out for 60 min at 37 °C in an Eppendorf reaction vessel, and enzymes were heat-inactivated for 15 min at 65 °C. The samples were cooled to room temperature and for agarose gel electrophoresis 5 μ l of 6x gel loading buffer (Peqlab, Erlangen, Germany) were added to each sample.

2.3.2.4 Agarose gel electrophoresis

5x TBE buffer contained 445 mM tris-base (USB, Cleveland, USA), 445 mM boric acid and 10 mM EDTA (Titriplex III). The 5x TBE buffer stock was diluted by 1:5 with Millipore water to obtain 1x TBE for preparation of agarose gels. 0.5 g of agarose (peqGOLD Universal-Agarose; Peqlab, Erlangen, Germany) were dissolved in 50 ml of 1x TBE buffer under heating on a magnetic stirrer, then 2 μ l of ethidium bromide solution (10 mg/ml H₂O, Janssen Chimica, Beerse, Belgium) were added. The mixture was allowed to cool for an appropriate period of time and poured into the gel chamber. The solidified gel was covered with 1x TBE buffer up to the denoted fill line.

Prior to electrophoresis, TBE buffer was filled into the gadget and 25 μ l of each sample were pipetted per pocket. As reference, the peqGOLD DNA (Peqlab) ladder mix was prepared according to the manufacturers instructions.

Electrophoresis was performed for 60 – 90 minutes at 90 V until tracking dye had migrated 2/3 of the gel length. After electrophoresis, the gels were inspected in a gel analysis and

documentation system (Gel-Doc 2000, Bio-Rad Laboratories, München, Germany) with UV excitation of 254 nm. The acquired data were analyzed with the Quantity One software (Bio-Rad).

2.3.3 Cell culture

The human U-87 MG (HTB 14), the U-118 MG (HTB 15) and the U-373 MG (HTB-17) glioblastoma/astrocytoma cells (Beckman et al., 1971) were obtained from the American Type Culture Collection (ATCC). Cell banking and quality control were performed according to the "seed stock concept" (Hay, 1988). Wild type and stably transfected U-87 MG and U-373 MG cells were grown in Eagle's minimum essential medium (EMEM, Sigma) containing L-glutamine, 2.2 g/l NaHCO₃, 110 mg/l sodium pyruvate, and 5 % fetal calf serum (FCS, Biochrom, Berlin, Germany), whereas the U-118 MG cells were maintained in Dulbecco's minimum essential medium (DMEM, Sigma), which was also supplemented with 5 % FCS. The transfected cells were cultured in the appropriate culture medium containing 400 µg/ml of G418. All cells were cultured in a water-saturated atmosphere of 95% air and 5% carbon dioxide at 37 °C in 75-cm² culture flasks (Nunc, Wiesbaden, Germany) and were serially passaged following trypsinization using trypsin (0.05 %)/EDTA (0.02 %) (Roche Diagnostics, Mannheim, Germany). Culture media without phenol red were used to prevent interferences with the fluorescence measurements.

2.3.4 Stable transfection of human glioblastoma cell lines

U-87 MG and U-118 MG wild type cells were transfected with pEGFP-N1 in passage 182 and 532, respectively, whereas the U-373 MG cell line was transfected with pcDNA3EGFP in passage 226. The transfection of the U-87 MG, U-118 MG and U-373 MG cells with pDsRed2-C1 was carried out in passages 221, 560 and 277, respectively. One day before transfection, wild-type cells were seeded into 6-well plates (Greiner, Frickenhausen, Germany) in the appropriate culture medium. The cell density was adjusted to 50-70% confluency on the day of transfection. The cells were transfected with the respective plasmid DNA, using the FuGene[®] 6 transfection reagent (Roche, Mannheim, Germany). For each well 1 µg of plasmid DNA was used. The DNA/FuGene[®]-complex was prepared prior to transfection, according to the manufacturers instructions. Briefly, DNA and transfection

reagent were pre-incubated in serum-free medium for 15 min at RT. This mixture was added dropwise to the cells, and after 12 h of incubation in the incubator the medium was replaced with fresh culture medium. 48 hours after transfection, the culture medium was exchanged by medium containing 400 µg/ml of the selection antibiotic G418 (Geneticin, PAA Laboratories). After the first passage cells were maintained in 25-cm² culture flasks (Nunc, Wiesbaden, Germany). The cells were analyzed by fluorescence microscopy and flow cytometry.

2.3.4.1 Fluorescence microscopy

Living cells were analyzed under a LEICA DM IRB inverse microscope equipped with a PL FLUOTAR 10x/0.30 Ph1 objective and a FITC fluorescence filter. Images were made with a Nikon Coolpix 4500 digital camera.

2.3.4.2 Flow cytometry and cell sorting

The sorting of the fluorescent cells was performed with a FACSCaliburTM flow cytometer (BD Biosciences, Heidelberg, Germany) in the single cell modus according to the manufacturer's instructions.

2.3.5 Chemosensitivity assay

The assays were performed according to Bernhardt et al. (Bernhardt et al., 1992). In brief: tumor cell suspensions (100 µl/well) were seeded into 96-well flat-bottomed microtitration plates (Greiner, Frickenhausen, Germany) at a density of ca. 15 cells/microscopic field (magnification 320x). After 2 days the culture medium was removed by suction and replaced by fresh medium (200 µl/well) containing varying drug concentrations or vehicle, respectively. On every plate 16 wells served as controls and 16 wells were used per drug concentration. After various times of incubation the cells were fixed with glutardialdehyde (Merck, Darmstadt, Germany) and stored at 4 °C. At the end of the experiment all plates were stained with crystal violet (Serva, Heidelberg, Germany) simultaneously. Absorbance was measured at 578 nm using a Biotek 309 Autoreader (Tecnomara, Fernwald, Germany). Growth curves were created using SigmaPlot analysis software (Systat Software GmbH, Erkrath, Germany).

2.3.6 Fluorescence detection

The detection of the fluorescence spectra was performed with an SLM-AMINCO Bowman Series 2 Luminescence Spectrometer (AMINCO-Bowman, Urbana, USA).

The fluorescence based assays were performed with the microplate reader GENios Pro (Tecan Deutschland GmbH, Crailsheim, Germany). The following filter sets were used for the detection of the blue, green and the red fluorescence, respectively: BP 485 \pm 20 nm/ BP 535 \pm 25 nm and BP 612 \pm 10 nm/ BP 670 \pm 25 nm.

2.3.7 Transfection of double-stranded siRNA

2.3.7.1 Nonsilencing siRNA and specific EGFP-siRNA

The chemically synthesized double stranded negative control siRNA with the non-silencing target sequence 5'-AAT TCT CCG AAC GTG TCA CGT-3' was purchased from Qiagen (Hilden, Germany). The specific double-stranded EGFP-siRNA (MWG Biotech, Ebersberg, Germany) with the antisense sequence 3'-UUC GUC GUG UCG AAG AAG UUC-5' targeting the EGFP coding region 237-258 relative to the first nt of the start codon 5'-AAG CAG CAC GAC UUC UUC AAG-3' was a gift from Dr. Böhm (ACGT ProGenomics AG, Halle (Saale), Germany).

2.3.7.2 Procedure

One day before transfection 5,000 cells per well were seeded in a 96-well plate (Greiner). 20 pmol siRNA per well were incubated with 0.3 μ l of Lipofectamine 2000, 100 pmol TmHU protein, 25 μ l CaCl₂ solution (8 mM) and 100 pmol of TmHU protein plus 25 μ l CaCl₂ solution (8 mM), respectively. Culture medium without serum was added to a final volume of 200 μ l per well, to adjust a final CaCl₂ concentration of 1 mM. Cells were washed with PBS, and the mixture of siRNA and transfection reagent was added. 4 hours after incubation the medium was removed and culture medium containing 5% FCS was added. 72 hours after transfection total cell number was determined at $\lambda_{\text{ex}} = 612$ and $\lambda_{\text{em}} = 670$ nm after staining of the living cells with the nucleic acid stain SYTO 60 (Molecular Probes), whereas EGFP expression was measured simultaneously at $\lambda_{\text{ex}} = 485$ and $\lambda_{\text{em}} = 535$ nm.

2.3.8 In vivo experiments

For the characterization of the in vivo growth of the human glioblastomas NMRI(nu/nu) nude mice obtained from the nude mouse laboratory of the department were used. The mice were allowed to take autoclaved water and food, a combined breed and maintenance diet especially for nude mice (Ssniff, Soest, Germany), ad libitum. The animals were housed under specified pathogen-free conditions at a 12 h light/dark cycle at a temperature of 25 °C and a relative humidity of 70 %. At an age of 6 weeks the mice were used for the studies. For subcutaneous injection suspensions of the respective cells were prepared in vitro. Cells were detached from the culture flask with trypsin/ EDTA and FCS-free medium and washed twice with FCS-free medium. To adjust the appropriate cell number ($4 \cdot 10^6$ cells/100 μ l) cells were resuspended in FCS free medium. Under aseptic conditions 100 μ l of the cell suspensions were injected under the thoracic dermis. To maintain the subcutaneous tumors in the mice a solid tumor was excised when the tumor growth reached an area of about 150 mm². For serial transplantation solid tumors were cut into pieces of 2 mm³ in sterile PBS and transplanted for several passages.

Tumor growth kinetics was recorded by measuring tumor diameters with an electronic caliper weekly. Tumor areas were calculated as the product of two perpendicular diameters, of which one represents the largest diameter of the tumor. As measure for a potential detracting of the animals by the tumor growth the weight of the animals was measured once a week. Tracking of the tumors was performed by labeling the mice with earmarks or tattoos.

2.3.9 Histology

2.3.9.1 Preparation of paraffin sections

The production of the paraffin sections was performed with modifications according to the procedure described by Walter et al. (Walter et al., 2000).

After dissection, tumors were fixed in 4 % buffered paraformaldehyde (Fluka, St. Gallen, Switzerland), pH 7.4, for at least 6 h at room temperature. Then the specimens were washed three times with PBS for 10 min followed by dehydration in an ascending ethanol series at room temperature. Ethanol was removed and xylene was added for 3 x 2 h at room temperature. Xylene was replaced with the paraffin Paraplast X-tra[®] (Sherwood Medical, Roth GmbH, Karlsruhe, Germany) and left for 4 x 4 h at 50-54 °C. The final embedding step was performed with Paraplast[®] at 55 °C. The blocks were stored at room temperature over

night and kept in the fridge until sectioning. 6 µm-thick sections were cut and mounted on glass slides pretreated with poly-L-lysine (Sigma). Sections were deparaffinized in xylene, rehydrated in a descending series of ethanol and mounted in VECTASHIELD® Hard+Set™ Mounting Medium containing DAPI.

Table 2.1: Embedding procedure with times, embedding solvents and temperature.

Time	Solvent	Temperature
1 h	70% ethanol	RT
1 h	96% ethanol	RT
1 h	96% ethanol	RT
1 h	96% ethanol	RT
1 h	100% ethanol	RT
2 h	Xylene	RT
2 h	Xylene	RT
2 h	Xylene	RT
4 h	Paraplast X-tra	50 - 54 °C
4 h	Paraplast X-tra	50 - 54 °C
4 h	Paraplast X-tra	50 - 54 °C
4 h	Paraplast X-tra	50 - 54 °C
Embedding	Paraplast	55 °C

2.3.9.2 Conventional fluorescence microscopy and confocal laser scanning microscopy

Sections were evaluated using conventional fluorescence microscopy and with a confocal laser scanning microscope. The nuclei were stained with DAPI and examined with excitation-filter BP360/51 and emission-filter BP460/10. EGFP expression was detected by laser scanning (Ar-Laser 488 nm, BP-filter 505-525 nm). Autofluorescence of the wild type tumors was detected with the same settings. The relative fluorescence intensity was quantified by the software tool “histo” of the Zeiss LSM Image Browser.

2.3.10 In vivo imaging

The subcutaneous human U-373 MG EGFP tumors were investigated three months after the injection of the cell suspension. A 3:1 (v/v) mixture of Ketamin 10 % (WDT, Garbsen, Germany) and Xylazin 2 % (cp pharma, Burgdorf, Germany) was prepared and 0.01 – 0.015 ml per 10 g body weight were injected intraperitoneally. After the narcotization, the mice were placed on the thermostated sample stage in the darkbox. The excitation of the green fluorescence in the solid tumor was performed with the excitation filter HQ 470/40. The fluorescence emission was detected by the CCD camera with the emission filter HQ 545/90. The computer based Hamamatsu Imaging System DSCN consisting of a darkbox and an air cooled 16 bit CCD camera ORCA II-BT-512 (Typ: C4742-MG-26LA) was used for the in vivo imaging studies. The composition of this in vivo imaging system is shown schematically in Figure 2.6.

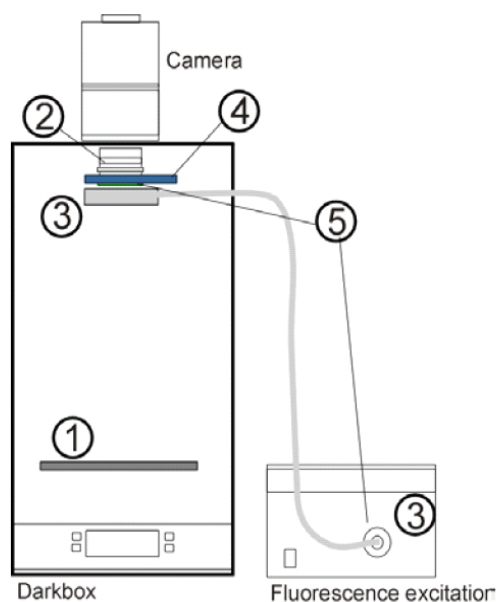


Figure 2.6: Schematic illustration of the essential components for in vivo fluorescence imaging. 1: flexible and heatable sample stage; 2: fluorescence imaging lenses with high numerical aperture; 3: light source connected to a ring light via a fiber cable and with excitation filter; 4: emission filter; 5: fluorescence filter sets.

2.3.11 Micro-osmotic pumps

2.3.11.1 Preparation of micro-osmotic pumps

Osmotic pumps (ALZET[®], Charles River, Sulzfeld, Germany) were used to ensure a continuous and controlled release of the substances. For the application in nude mice the smallest size of osmotic pumps with a volume of $88 \pm 3 \mu\text{l}$ (model 1003D) was chosen. The flow rate was $1.06 \mu\text{l/h}$ ($\pm 0.05 \mu\text{l/h}$) and the entire delivery period was 72 h.

The required length of the polyethylene infusion catheter PE 60 (ALZET[®]) was calculated with the following parameters: the volume that should be released was around $100 \mu\text{l}$ and the inner diameter of the PE catheter was 0.75 mm. With the formula for cylinders the length was determined to be 226 mm ($\approx 23 \text{ cm}$).

The 23 cm long catheters were deformed spirally to wrap them around the pumps as tightly as possible. Therefore, the catheters were wound around a 1-ml syringe, dipped into boiling water for 1 min and subsequently cooled in ice water. Afterwards, the catheters were sterilized in a 10% H_2O_2 solution.

ALZET pumps have a start-up gradient during which the pumps soak up fluid and come to temperature. This start up period was accomplished by “priming” the pumps in vitro prior to implantation in vivo. The empty pumps, together with the appropriate flow moderator, were weighed separately. Afterwards, the pumps were filled without air bubbles using a 1-ml syringe and a 27G canula according to the manufacturer’s instructions. The filling volume was controlled by weighing the pumps. Then, the catheters were filled with a 0.01% Evans Blue solution and attached to the flow moderator. After inserting the flow moderator into the pump, the pumps were weighed again. For the in vivo experiment the pre-filled pumps were placed in sterile 0.9% saline at 37°C over night.

2.3.11.2 Performance of the in vitro delivery study

After filling, the pumps were placed in one well of a 6-well-plate (Greiner[®]) each containing 5 ml of PBS. The end of the catheter was put in a second well filled with 2.0 ml of PBS (Figure 2.41). After equilibration („priming“) over night the first samples were taken from the wells, where the end of the catheters were put in. $1000 \mu\text{l}$ were removed and measured photometrically at 600 nm. Subsequently, the $1000 \mu\text{l}$ in the cuvette were transferred back to the corresponding well quantitatively.

2.3.11.3 Subcutaneous application of micro-osmotic pumps in nude mice

The subcutaneous implantation of the prepared pumps into four nude mice was performed under anesthesia with a mixture of Ketamin and Xylazin. The end of the catheters was placed nearby the implanted tumors to assure a direct delivery on the tumor. The pumps were implanted in dorsal position, two pumps pointing towards the cranium (Figure 2.44a) and two pumps pointing towards the tail (Figure 2.44b).

2.4 Results

2.4.1 EGFP and DsRed2 expressing human glioblastoma cells

2.4.1.1 Stable transfection

In order to investigate siRNA effects on EGFP expression levels in vitro and in vivo three human glioblastoma variants were stably transfected with the gene encoding the enhanced green fluorescent protein (EGFP) and the gene encoding the red fluorescent protein (DsRed2), respectively. The generated cells, expressing the green fluorescent protein were named U-87 MG EGFP, U-118 MG EGFP and U-373 MG EGFP. They are shown in Figure 2.7.

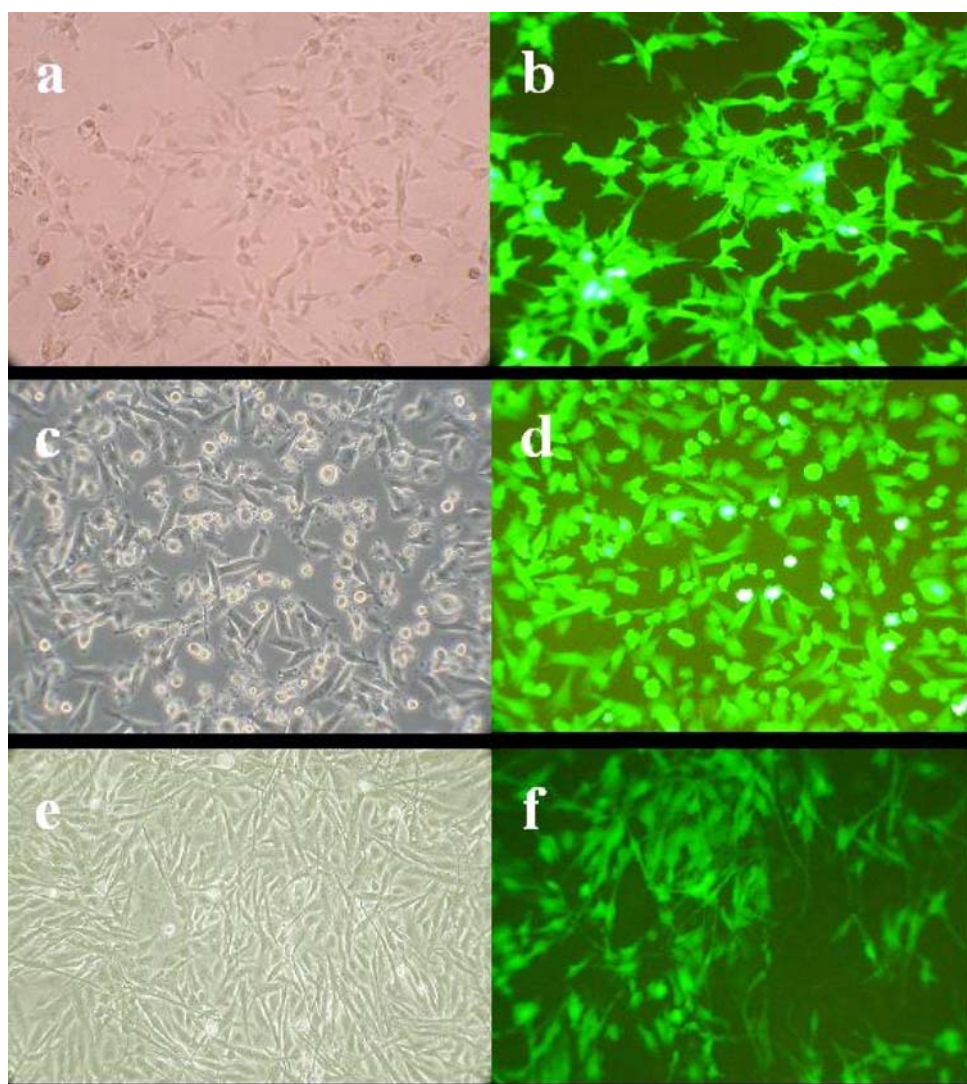


Figure 2.7: Conventional fluorescence microscopic images of EGFP expressing human glioblastoma cell lines U-87 MG EGFP (a, b), U-118 MG EGFP (c, d) and U-373 MG EGFP (e, f); on the left site cells in transmission mode.

The DsRed2 expressing transfectants were designated U-87 MG DsRed2, U-118 MG DsRed2 and U-373 MG DsRed2. A confocal laser scanning image of a U-373 MG DsRed2 cell is shown in Figure 2.8.

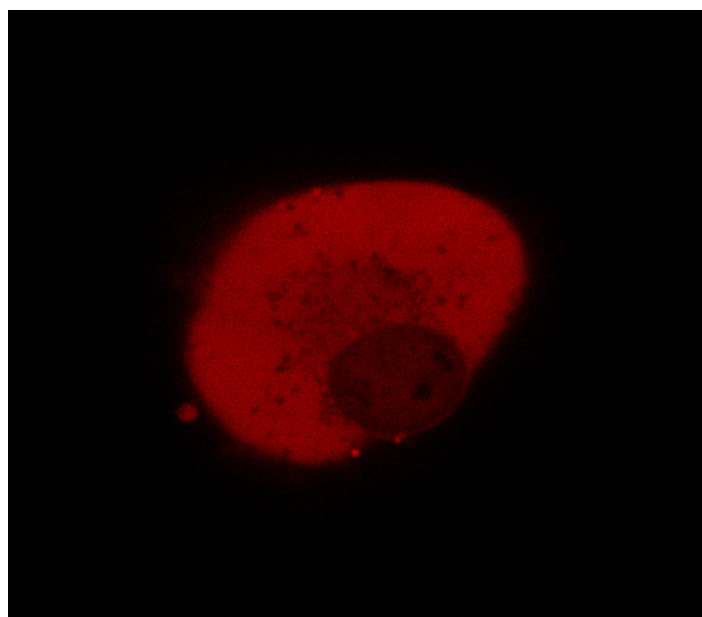


Figure 2.8: Confocal laser scanning image of a U-373 MG DsRed2 cell (HeNe Laser 543 nm, LP-filter 560 nm)

2.4.1.2 Cell sorting by flow cytometry

After the transfection of the cell lines and the selection with the antibiotic G418 only a small fraction of around 30% of the cells expressed EGFP. To obtain cell populations with a predominant EGFP expression, the fluorescent cells were collected with the FACSCaliburTM flow cytometer. As an example the results of the U-87 MG EGFP cell line are shown in Figure 2.9 and Figure 2.10.

After cell sorting, 80% of the cells stably expressed EGFP. After numerous passages the ratio of fluorescent cells did not markedly decrease. Moreover, additional cell sorting did not increase the fraction of EGFP expressing cells.

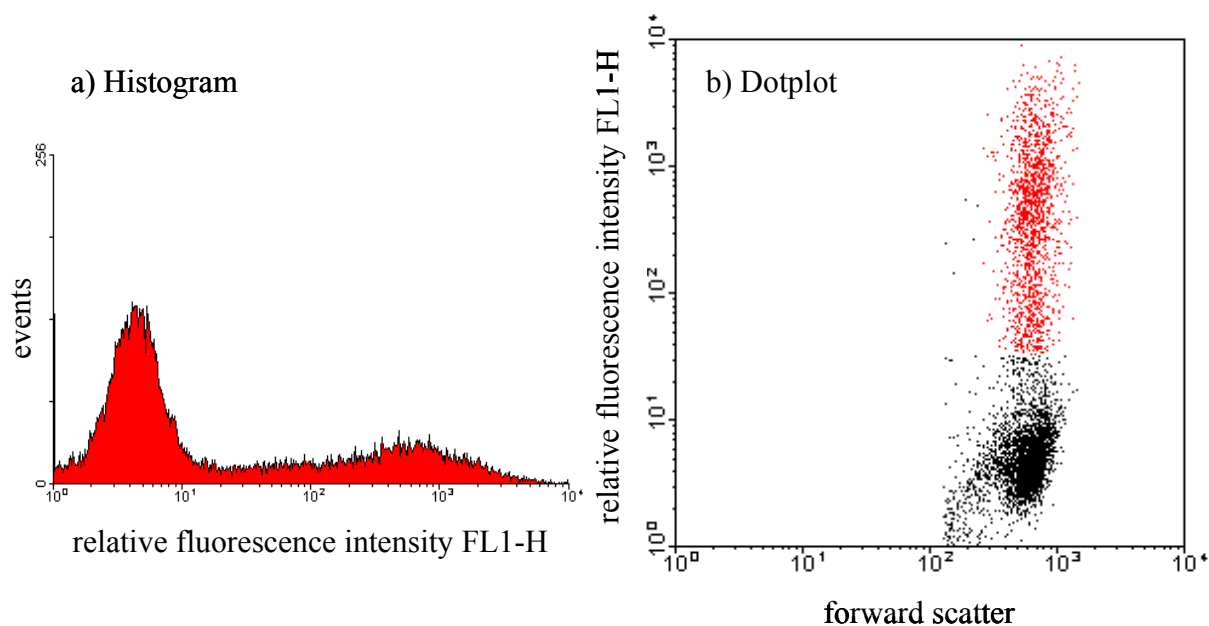


Figure 2.9: U-87 MG EGFP (passage 188) cell population before sorting with the FACSCalibur™ flow cytometer. a) The histogram displays the number of cells with the corresponding fluorescence intensity. b) The DotPlot shows the living cells with a distinct size and the corresponding fluorescence intensity. Cells with a relative fluorescence intensity higher than 30 (~ 32%) were defined as EGFP expressing cells (marked in red) and were collected.

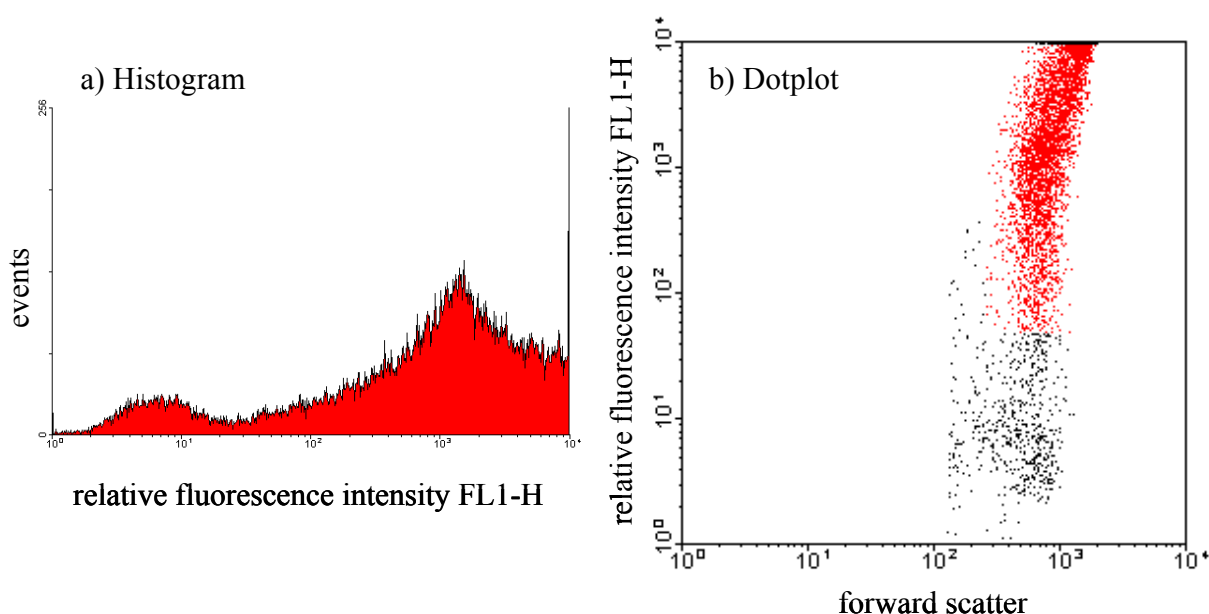


Figure 2.10: U-87 MG EGFP (passage 190) cell population after sorting with the FACSCalibur™ flow cytometer. a) The histogram displays the number of cells with the corresponding fluorescence intensity. b) The DotPlot shows the living cells with a distinct size and the corresponding fluorescence intensity. Cells with a relative fluorescence intensity higher than 30 were defined as EGFP expressing cells (marked in red) and were collected.

2.4.1.3 Chemosensitivity of the transfectants

Aiming at the exploitation of siRNA effects for the down-regulation of oncogenes in tumor cells it is very important to assure that the behavior of the transfectants is similar to the wild type cells. Therefore, the growth of the wild type cells was compared with that of the EGFP transfected cells in culture medium with and without the selection antibiotic G418. The results are shown in Figure 2.11, Figure 2.12 and Figure 2.13.

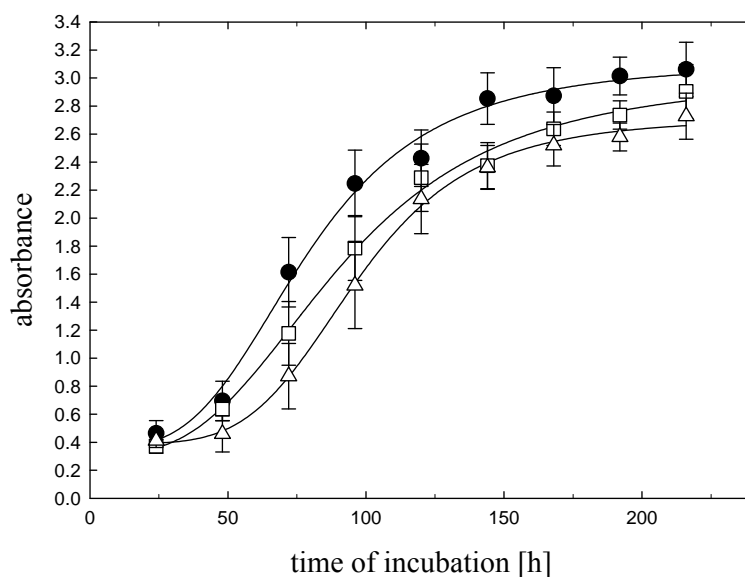


Figure 2.11: Comparison of the cell growth of U-87 MG cells (*filled circle*) and U-87 MG EGFP cells incubated without (*open square*) and with 400 µg/ml G418 (*open triangle*), respectively.

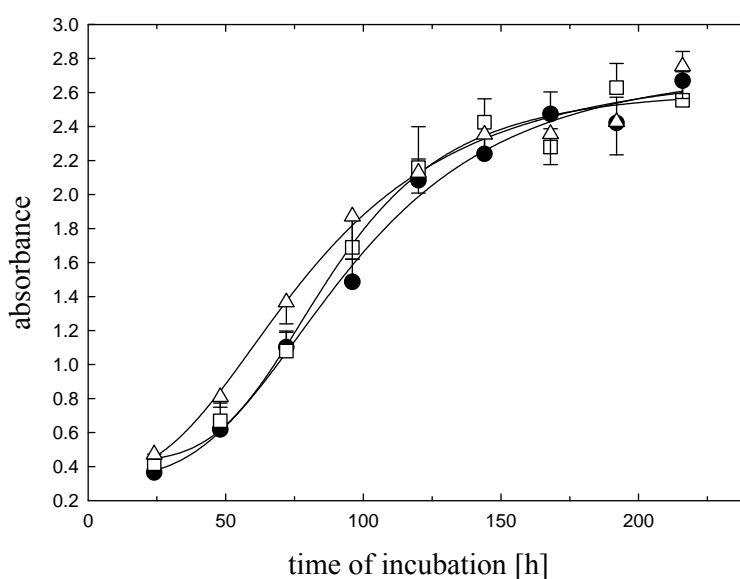


Figure 2.12: Comparison of the cell growth of U-373 MG cells (*filled circle*) and U-373 MG EGFP cells incubated without (*open square*) and with 400 µg/ml G418 (*open triangle*), respectively.

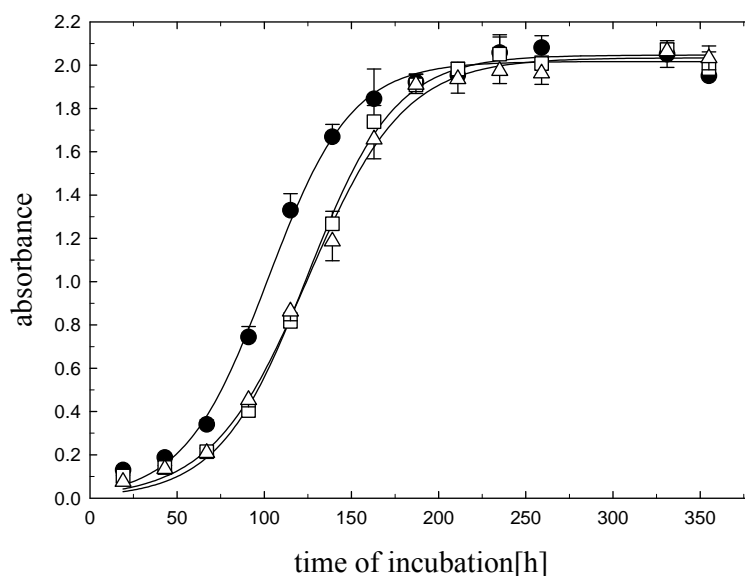


Figure 2.13: Comparison of the cell growth of U-373 MG cells (*filled circle*) and U-373 MG EGFP cells incubated without (*open square*) and with 400 $\mu\text{g/ml}$ G418 (*open triangle*), respectively.

The transfection of human glioblastoma variants with the gene encoding EGFP did not significantly influence the growth kinetics of the cells. No difference between the cells maintained in culture medium with or without the selection antibiotic G418 was observed.

Furthermore, the chemosensitivity of all wild type and transfected cells against the cytostatic doxorubicin was comparable. The results are shown for the U-373 MG cells as an example in Figure 2.14.

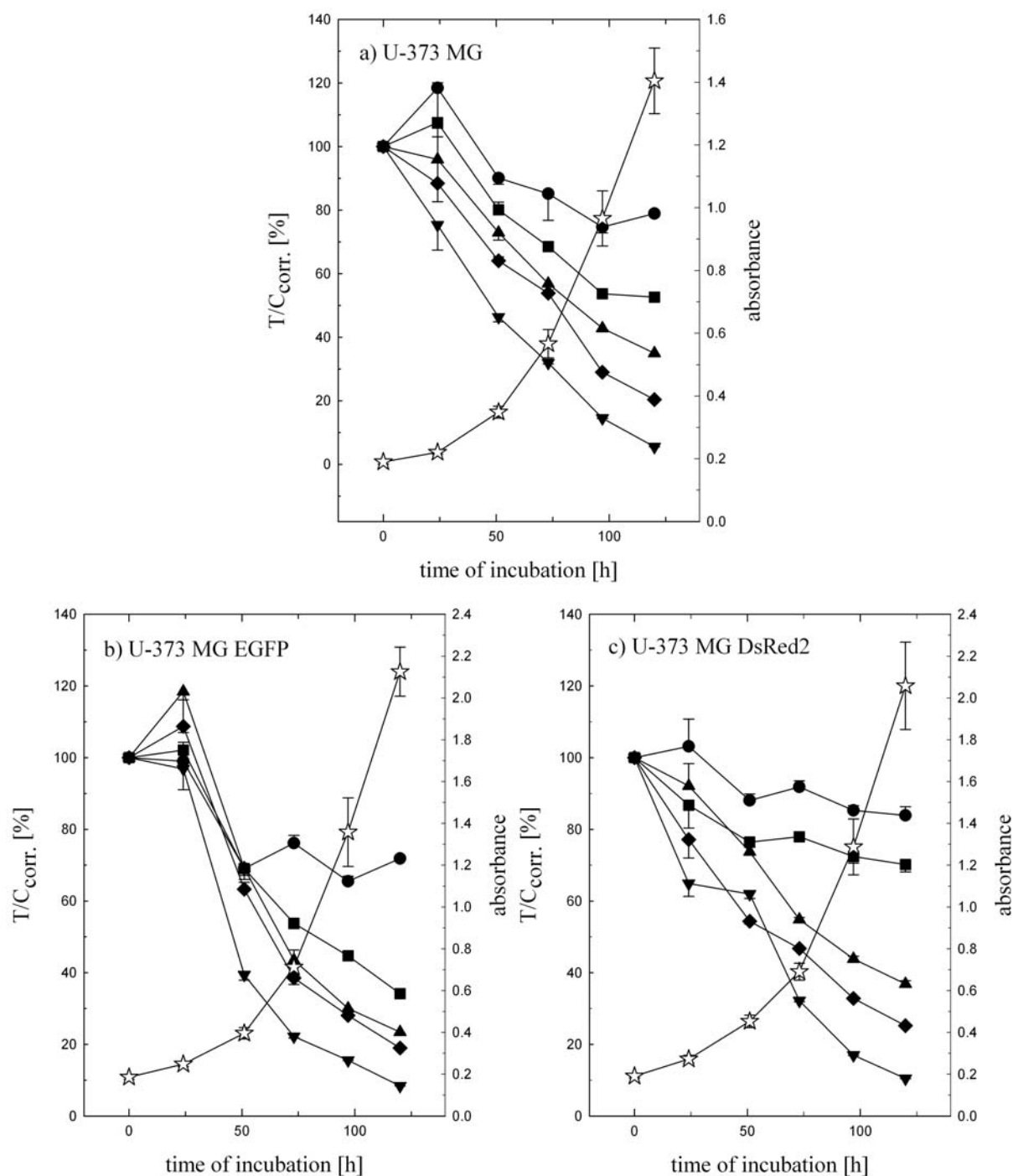


Figure 2.14: Incubation of a) U-373 MG wild type cells and the corresponding transfected cells b) U-373 MG EGFP and c) U-373 MG DsRed2 cells with various concentrations of doxorubicin: 2.5 nM (*filled circle*), 5.0 nM (*filled square*), 7.5 nM (*filled triangle*), 10 nM (*filled diamond*), 15 nM (*filled inverted triangle*) and vehicle EtOH 70% (*open star*).

2.4.2 Fluorescence assay by means of a microplate reader for the quantitation of siRNA effects in vitro

Most of the commercially available siRNA transfection reagents, for example Lipofectamine[®] 2000 are cytotoxic. Therefore, it is possible that large fractions of the incubated cells die during the experiment. In order to exclude incorrect results caused by this effect, in this assay the extent of EGFP or DsRed2 expression was quantified with respect to total cell number.

2.4.2.1 Establishment of an assay for the quantification of EGFP expression

Varying numbers of wild type cells and EGFP expressing cells were seeded in 96-well plates. The next day, the cells were stained with the nucleic acid stain SYTO 60 at a concentration of 500 nM and incubated for two hours at 37 °C in an atmosphere of 5% CO₂ (Figure 2.15). Afterwards, the cells were washed twice with sterile PBS, and culture medium without phenol red was added.

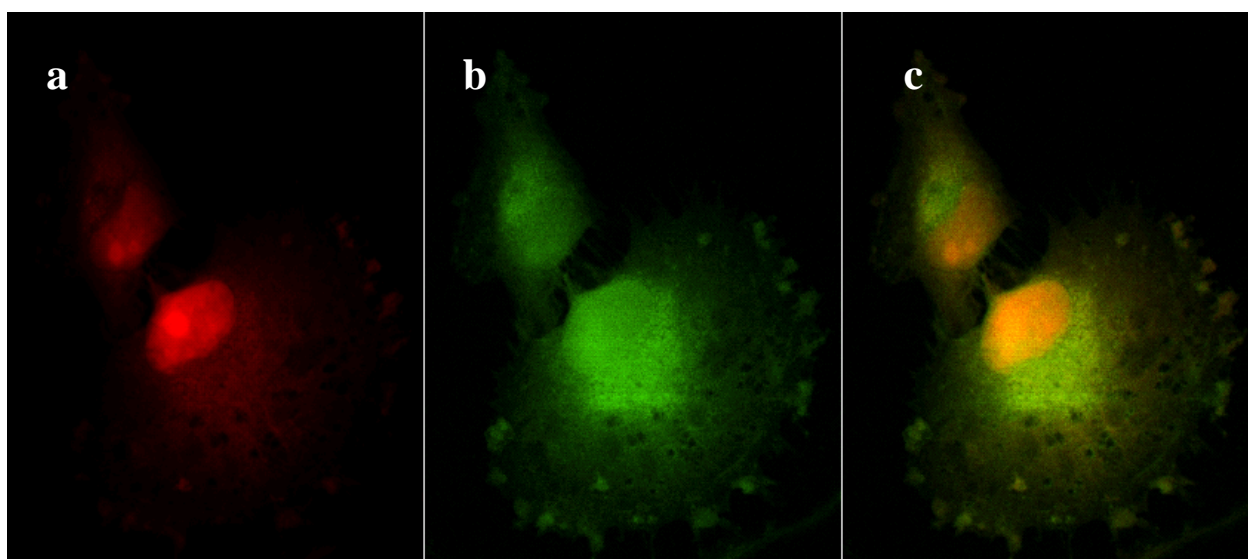


Figure 2.15: LSM images of living U-87 MG cells expressing EGFP stained with the nucleic acid stain SYTO 60. a: SYTO 60 (HeNe-Laser 633 nm, LP-filter 650 nm), b: EGFP (Ar-Laser 488 nm, BP-filter 505-525 nm), c: Overlay

The extent of EGFP expression was quantified with respect to total cell number using a Tecan GENiosPro fluorescence plate reader. For the investigations on EGFP expressing cells the cell number was determined by staining the cells with the red fluorescent nucleic acid stain SYTO 60 (Molecular Probes). Total cell number was determined at $\lambda_{\text{ex}} = 612$ and $\lambda_{\text{em}} = 670$ nm

(compare Figure 2.16), whereas EGFP expression was measured simultaneously at $\lambda_{\text{ex}} = 485$ and $\lambda_{\text{em}} = 535$ nm (compare Figure 2.17).

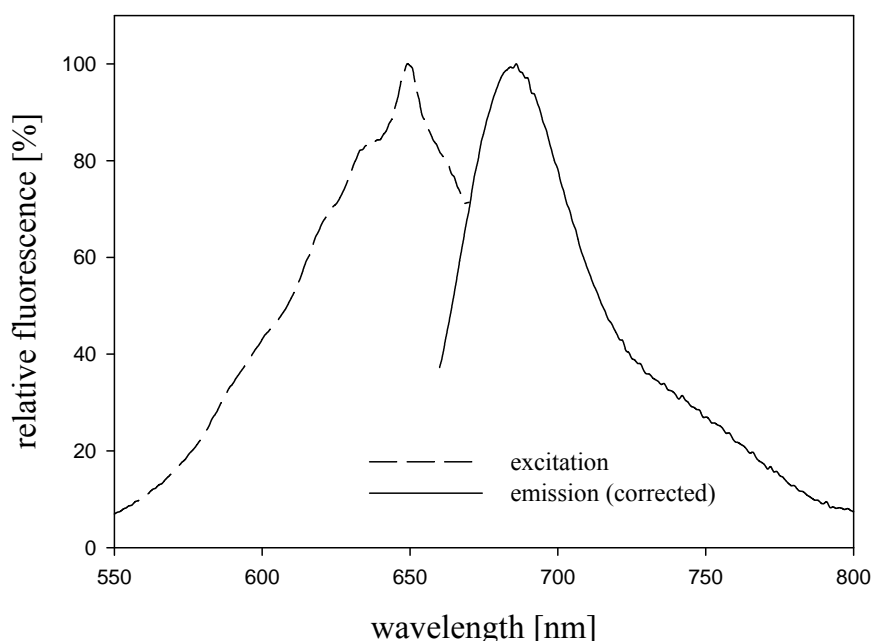


Figure 2.16: Fluorescence excitation and emission spectra of the nucleic acid stain SYTO 60 (5 μM) bound to DNA (300 mg/l) with excitation and emission maxima at 650 nm and 681 nm, respectively; excitation spectra: $\lambda_{\text{em}} = 675$ nm and emission spectra: $\lambda_{\text{ex}} = 599$ nm; excitation and emission slits: 5 nm.

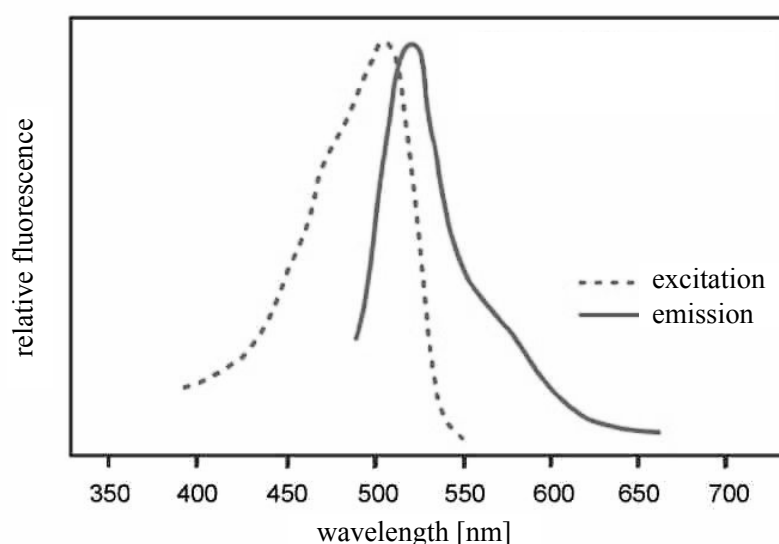


Figure 2.17: Fluorescence excitation and emission spectra of the enhanced green fluorescent protein EGFP (from the National Cancer Institute NCI, modified, <http://home.ncifcrf.gov/ccr/flowcore/spectra/GFPspec.htm>).

Measuring the green fluorescence of a dilution series of EGFP expressing cells revealed a linear increase in fluorescence intensity with increasing cell numbers. Wild type cells always yielded the same fluorescence intensity independent of the cell number (Figure 2.18). Therefore, the green fluorescence of the EGFP expressing cells can be corrected by subtraction of the constant auto-fluorescence (Figure 2.19), determined for the wild type cells. Detection of the red fluorescence due to nucleic acid stain SYTO 60 showed a linear dependency of the intensity from the cell number (Figure 2.20).

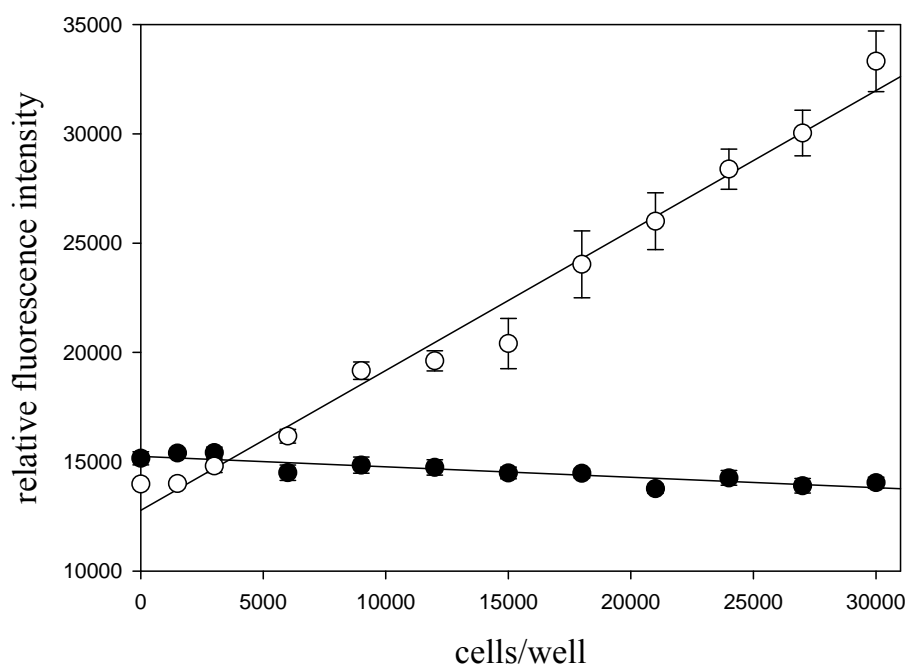


Figure 2.18: Comparison of the green fluorescence ($\lambda_{\text{ex}} = 485 \text{ nm}$, $\lambda_{\text{em}} = 535 \text{ nm}$) of U-87 MG wild type cells (*filled circle*) and EGFP expressing U-87 MG EGFP cells (*open circle*) as a function of the cell number.

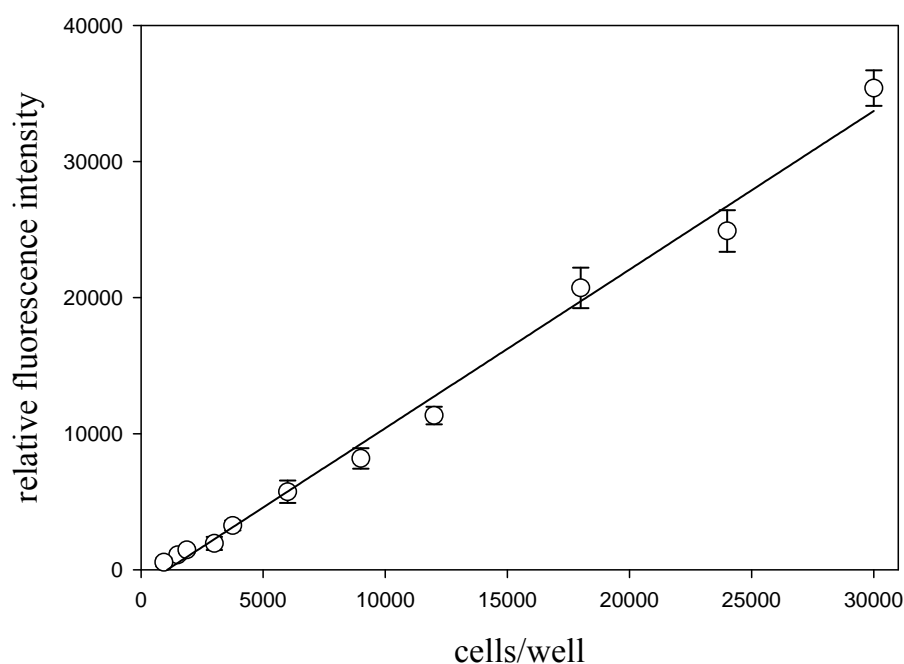


Figure 2.19: Green fluorescence ($\lambda_{\text{ex}} = 485 \text{ nm}$, $\lambda_{\text{em}} = 535 \text{ nm}$) of the EGFP expressing U-87 MG EGFP cells (*open circle*) corrected for the auto-fluorescence of the wild type U-87 MG cells as a function of cell number.

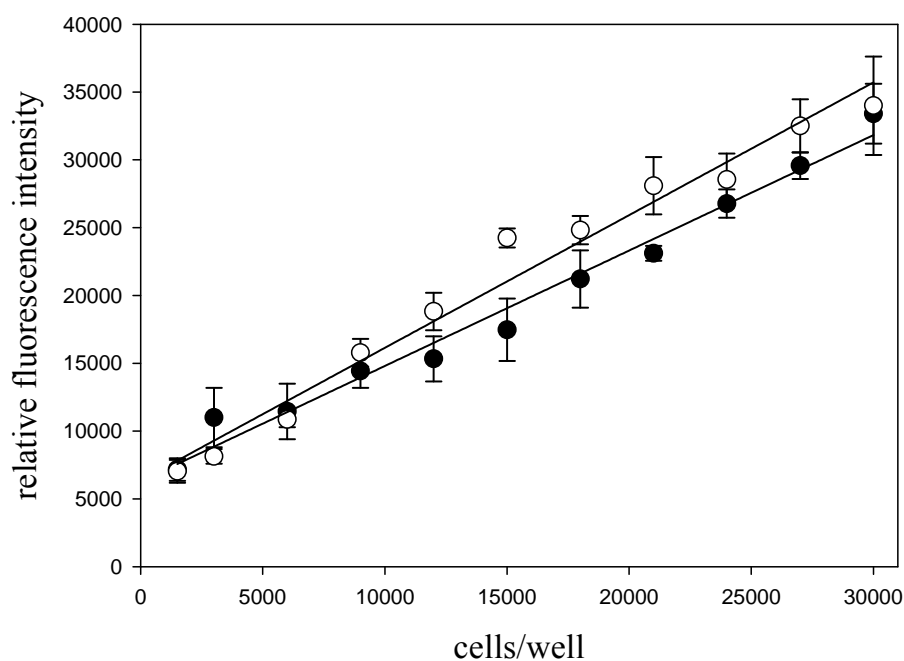


Figure 2.20: Red fluorescence ($\lambda_{\text{ex}} = 612 \text{ nm}$, $\lambda_{\text{em}} = 670 \text{ nm}$) of wild type U-87 MG cells (*filled circle*) and EGFP expressing U-87 MG EGFP cells (*open circle*) due to the nucleic acid stain SYTO 60 as a function of cell number.

The fraction of EGFP expressing cells (F_{EGFP}) was calculated according to the following equations:

$$F_{\text{EGFP}} [\%] = \left(\frac{\text{emT}_{535, \text{corrected}}}{\text{const.} \cdot \text{emT}_{670}} \right) \cdot 100 \quad (\text{eq. 2.1}),$$

with emT_{670} representing the emission of the test population at 670 nm after nucleic acid staining with SYTO 60. The emission of the test population at 535 nm without the autofluorescence of the wild type cells ($\text{emT}_{535, \text{corrected}}$) was evaluated according to equation 3.2:

$$\text{emT}_{535, \text{corrected}} = \text{emT}_{535} - \text{emC}_{535, \text{wild type}} \quad (\text{eq. 2.2})$$

A constant (const.) indicating the value of the green fluorescence compared to the red fluorescence was determined. This constant was defined by means of the control in all tests according to equation 3.3.

$$\text{const.} = \frac{\text{emC}_{535, \text{corrected}}}{\text{emC}_{670}} \quad (\text{eq. 2.3})$$

The abbreviation for the emission at 670 nm of the control after nucleic acid staining with SYTO 60 is emC_{670} .

The fluorescence emission at 535 nm of the control without the autofluorescence of the wild type cells ($\text{emC}_{535, \text{corrected}}$) was determined according to equation 3.4:

$$\text{emC}_{535, \text{corrected}} = \text{emC}_{535} - \text{emC}_{535, \text{wild type}} \quad (\text{eq. 2.4})$$

with emC_{535} and $\text{emC}_{535, \text{wild type}}$ representing the emission at 535 nm of the EGFP expressing cells and of the wild type cells, respectively.

2.4.2.2 Establishment of an assay for DsRed2 expressing cells

Different quantities of wild type cells and DsRed2 expressing cells were seeded in 96-well plates. The next day, the cells were stained with the nucleic acid stain DAPI at a concentration of 1 μM and incubated two hours at 37 °C and 5% CO_2 (Figure 2.21). Afterwards, the cells were washed twice with sterile PBS buffer and culture medium without phenol red added.

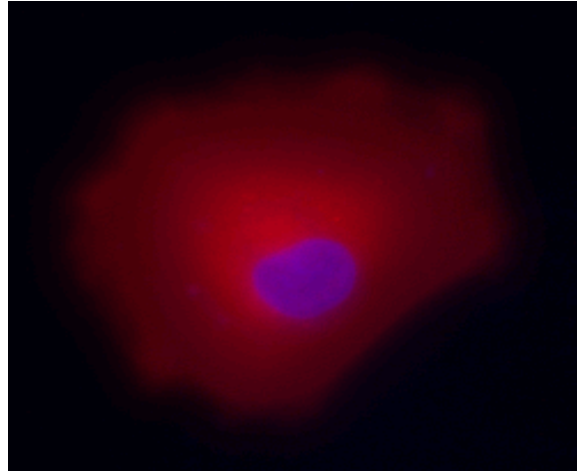


Figure 2.21: Conventional fluorescence microscopic image of the DsRed2 expressing human U-373 MG DsRed2 glioblastoma cells stained with the nucleic acid stain DAPI. The excitation and emission wavelength were $\lambda_{\text{ex}} = 340 \text{ nm}$, $\lambda_{\text{em}} = 460 \text{ nm}$ for DAPI and $\lambda_{\text{ex}} = 560 \text{ nm}$, $\lambda_{\text{em}} = 600 \text{ nm}$ for DsRed2.

In case of DsRed2 expression the cell number was quantified by staining the nuclei with the blue fluorescent stain DAPI. Total cell number was determined at $\lambda_{\text{ex}} = 340 \text{ nm}$ and $\lambda_{\text{em}} = 485 \text{ nm}$ (compare Figure 2.22), whereas DsRed2 expression was measured simultaneously at $\lambda_{\text{ex}} = 535 \text{ nm}$ and $\lambda_{\text{em}} = 612 \text{ nm}$. The red fluorescent protein DsRed2 shows excitation and emission maxima at 560 nm and 570 nm (spectra not shown).

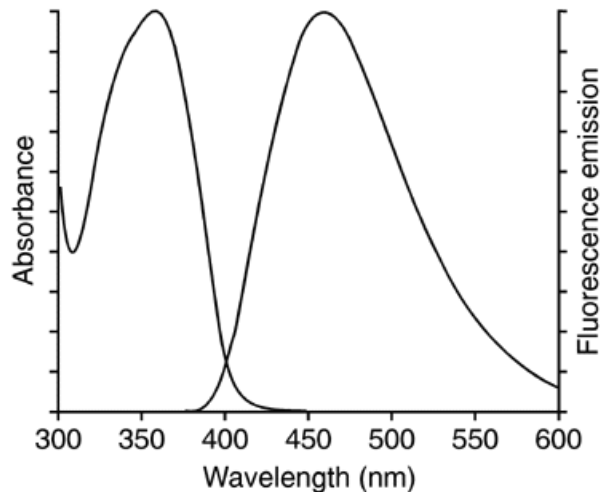


Figure 2.22: Fluorescence excitation and emission spectra of DAPI with excitation and emission maxima at 359 nm and 461 nm, respectively (from the Institute for stem cell research, ISCR, University of Edinburgh, UK).

Measuring the red fluorescence of a dilution series of DsRed2 expressing cells revealed a linear increase in fluorescence intensity with increasing cell numbers (Figure 2.23). Due to the low signal to noise ratio of the red fluorescence compared to the green fluorescence, the autofluorescence of the wild type cells was disregarded. Detection of the blue fluorescence due to nucleic acid stain DAPI showed a linear dependency of the intensity from the cell number (Figure 2.24).

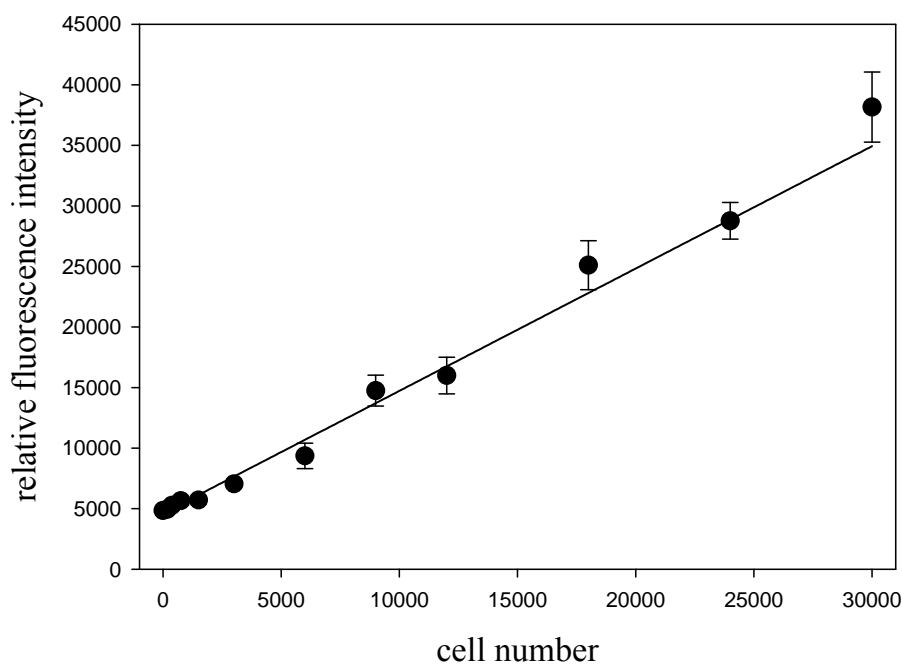


Figure 2.23: Red fluorescence ($\lambda_{\text{ex}} = 535 \text{ nm}$, $\lambda_{\text{em}} = 612 \text{ nm}$) of the DsRed2 expressing U-87 MG DsRed2 cells (*filled circle*) as a function of cell number.

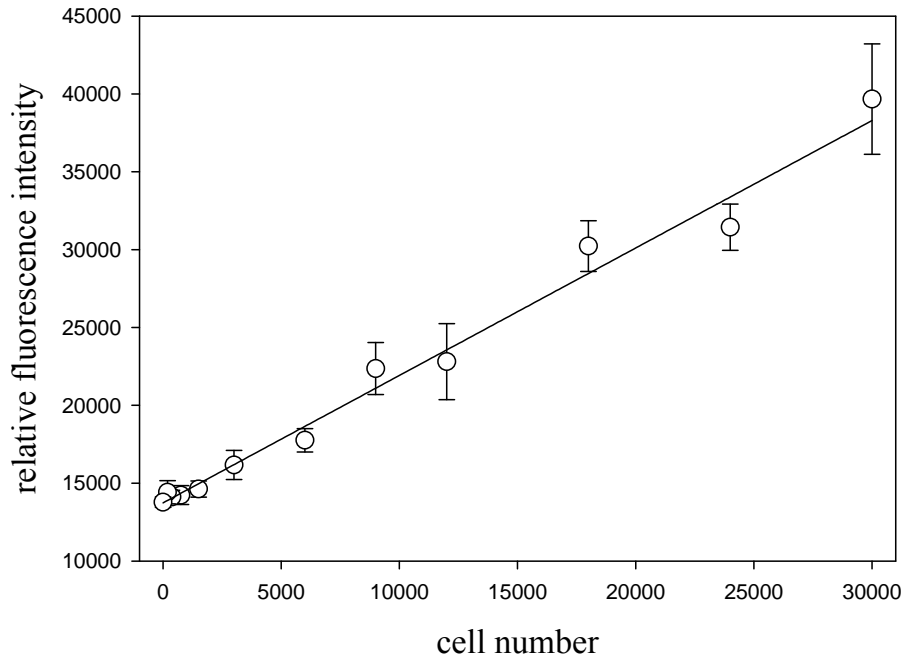


Figure 2.24: Blue fluorescence ($\lambda_{\text{ex}} = 340 \text{ nm}$, $\lambda_{\text{em}} = 485 \text{ nm}$) of U-87 MG DsRed2 cells (*open circle*) due to the nucleic acid stain DAPI as a function of cell number.

The fraction of DsRed2 expressing cells (F_{DsRed2}) was calculated according to the following equations:

$$F_{\text{DsRed2}} [\%] = \left(\frac{\text{emT}_{612}}{\text{const.} \cdot \text{emT}_{485}} \right) \cdot 100 \quad (\text{eq. 2.5}),$$

with emT_{485} representing the emission of the test population at 485 nm after nucleic acid staining with DAPI. The emission of the test population at 612 nm is defined by the abbreviation emT_{612} .

A constant (const.) indicating the value of the red fluorescence compared to the blue fluorescence was determined. This constant was defined by means of the control in all tests according to equation 3.6.

$$\text{const.} = \frac{\text{emC}_{612}}{\text{emC}_{485}} \quad (\text{eq. 2.6})$$

with emC_{612} representing the emission at 612 nm of the DsRed2 expressing cells. The abbreviation for the emission at 485 nm of the control after nucleic acid staining with DAPI is emC_{485} .

2.4.3 Cytotoxicity of the TmHU protein

As a prerequisite for its application as reagent for *in vivo* transfection the potential cytotoxicity of TmHU was determined against the three human glioblastoma cell variants U-87 MG, U-118 MG and U-373 MG. As an example the results are shown in Figure 2.25 for the U-87 MG cell line. As expected the TmHU protein exhibited no cytotoxic effect even at very high concentrations.

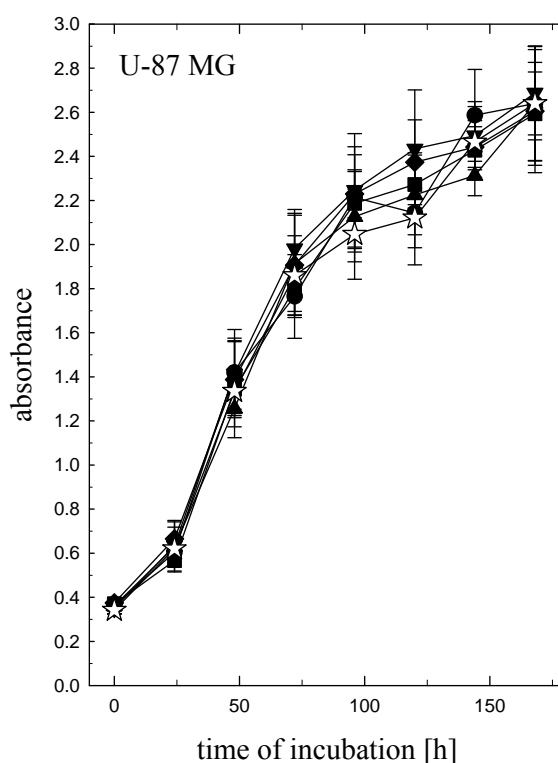


Figure 2.25: Proliferation of U-87 MG cells incubated with different concentrations of the TmHU protein: 0.5 μ M (*filled circle*), 1.25 μ M (*filled square*), 2.5 μ M (*filled triangle*), 3.75 μ M (*filled diamond*), 5 μ M (*filled inverted triangle*) and PBS as vehicle (*open star*).

2.4.4 siRNA transfection with TmHU

The method was validated with EGFP specific and nonspecific siRNAs and different transfection reagents: Lipofectamine[®] 2000 as positive control, TmHU protein, CaCl₂ and TmHU protein in combination with CaCl₂. The results of three independent assays are summarized in Figure 2.26.

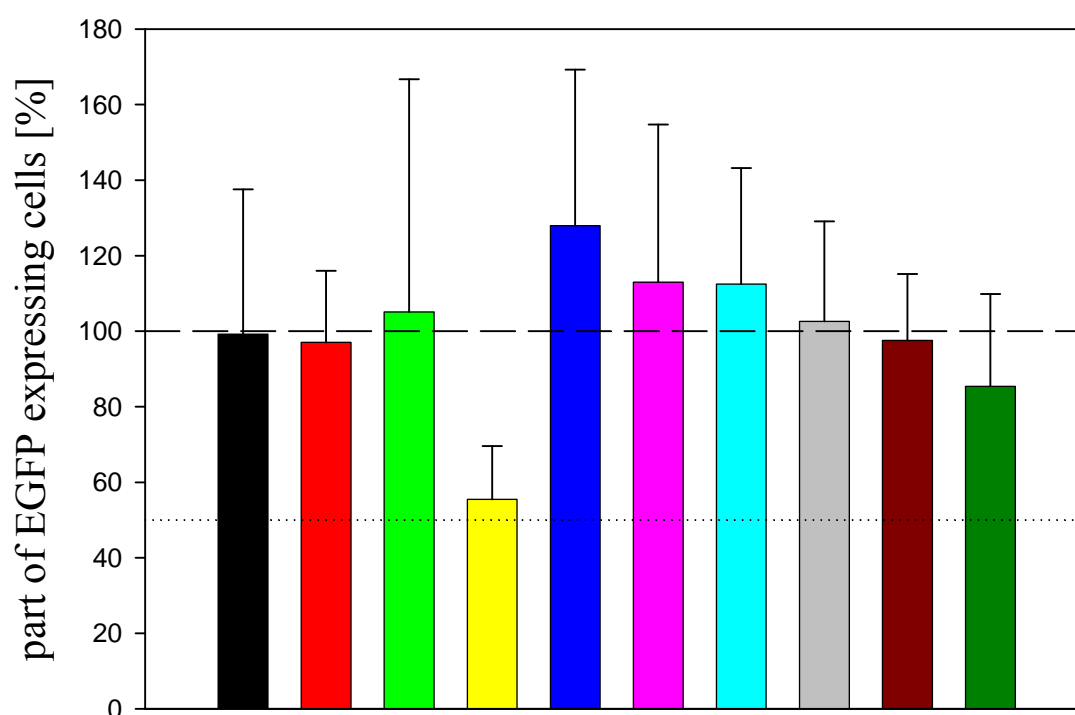


Figure 2.26: Fraction of EGFP expressing U-87 MG EGFP cells 72 hours after the addition of the substances. Culture medium (black bar) and EGFP-siRNA (red bar) served as controls. The nonsilencing nonspecific siRNA was incubated together with Lipofectamine[®] 2000 (green bar), with TmHU (blue bar), with CaCl₂ (cyan bar) and with TmHU plus CaCl₂ (brown bar). The silencing EGFP-siRNA was incubated together with Lipofectamine[®] 2000 (yellow bar), with TmHU (pink bar), with CaCl₂ (gray bar) and with TmHU plus CaCl₂ (dark green bar).

Only Lipofectamine[®] 2000 together with the specific EGFP-siRNA showed a down-regulating effect on the EGFP expression. Numerous variations in the performance of the assay concerning the concentration ratios of transfection reagent and siRNA and the incubation time of the transfection mixture did not improve the effects.

2.4.5 In vivo growth characteristics, selection and expansion of subcutaneous tumors

As tumor model for the in vivo investigations of siRNA effects, subcutaneous tumors of EGFP and DsRed2 expressing cells were established. It was shown that the tumors retain their ability to stably express the fluorescent proteins without selection pressure by the antibiotic G418. After several passages the fluorescence intensity was retained in most of the tumors. Only a few tumors lost their fluorescence.

Tumor growth kinetics is displayed by tumor area over time graphs. The changes of the body weight are not presented, because no significant loss of weight was observed.

The in vivo morphology of the tumors was routinely observed by the Masson-Goldner staining of paraffin sections. All tumors were very rich in cells, and the cells were held together as bundles by the connective tissue. The nuclei were pleomorphic and in part possessed multiple prominent nucleoli. The malignancy of these tumors is indicated by numerous mitoses and an invasive growth into the surrounding tissue. No differences in the histological appearance of the transfected and the wild type tumors were observed.

2.4.5.1 Subcutaneous U-87 MG EGFP tumors

The formation of a tumor after the injection of the U-87 MG EGFP cell suspension took a long period of around three months (Figure 2.27). However, after the transplantation of tumor pieces the tumors grew faster. Within six weeks they were disposed for the next transplantation (Figure 2.28).

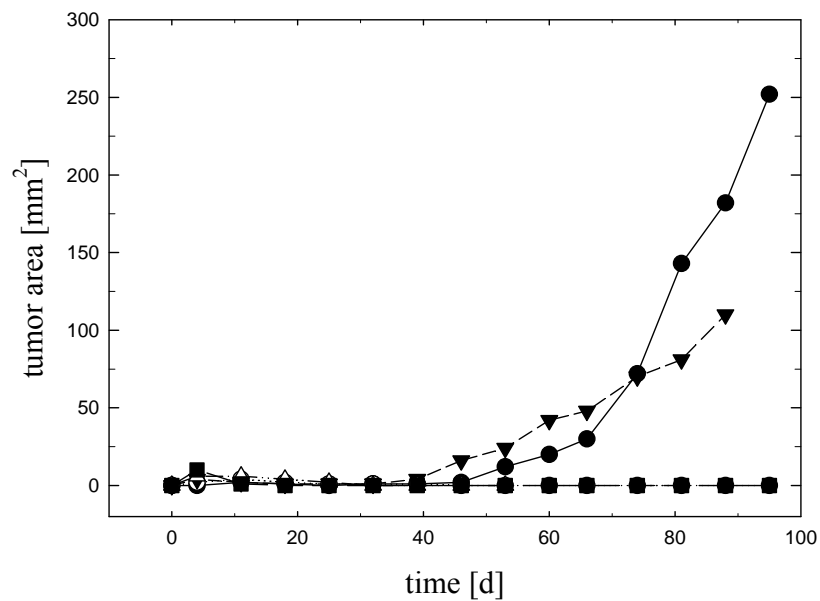


Figure 2.27: Growth of subcutaneous U-87 MG EGFP tumors (passage 0) after the injection of the cell suspension (passage 254 in cell culture).

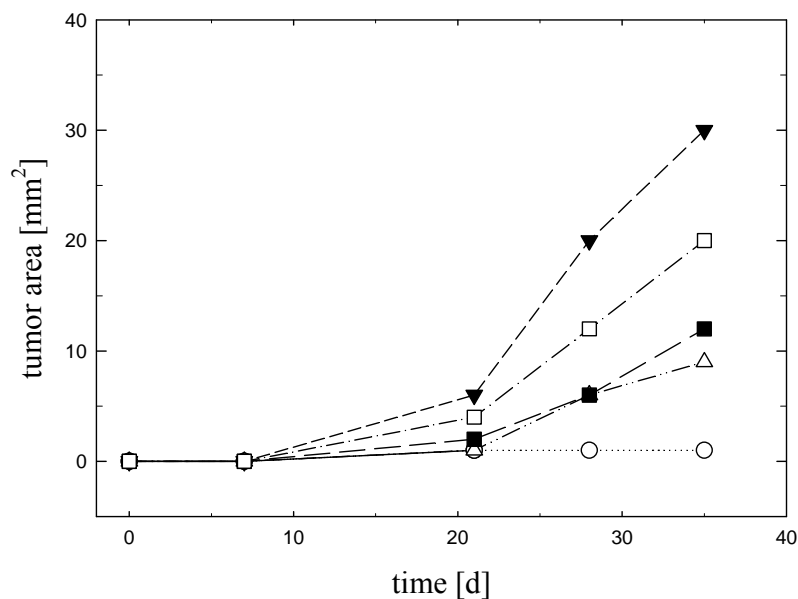


Figure 2.28: Growth of subcutaneous U-87 MG EGFP tumors (passage 1) after the transplantation of the tumor pieces from mouse 359.

2.4.5.2 Subcutaneous U-118 MG EGFP tumors

The formation of a tumor after the injection of the U-118 MG EGFP cell suspension and within the first two passages took a long period of around 3.5 months (Figure 2.29 and Figure 2.30). In passage 0 only one of 6 possible tumors emerged. However, after the transplantation over three passages the tumors grew faster and more evenly. Within five weeks they were disposed for the next transplantation (Figure 2.31 and Figure 2.32).

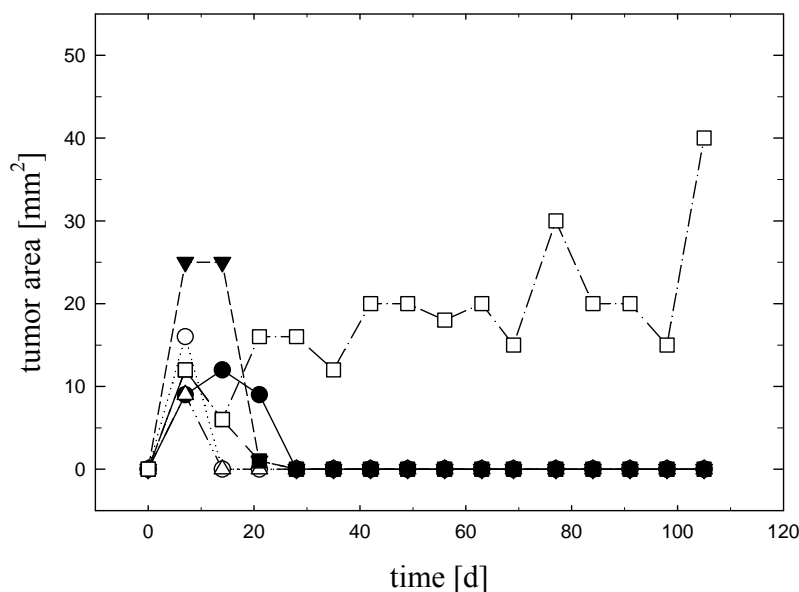


Figure 2.29: Growth of subcutaneous U-118 MG EGFP tumors (passage 0) after the injection of the cell suspension (passage 605 in cell culture). The tumor from mouse 375 was transplanted.

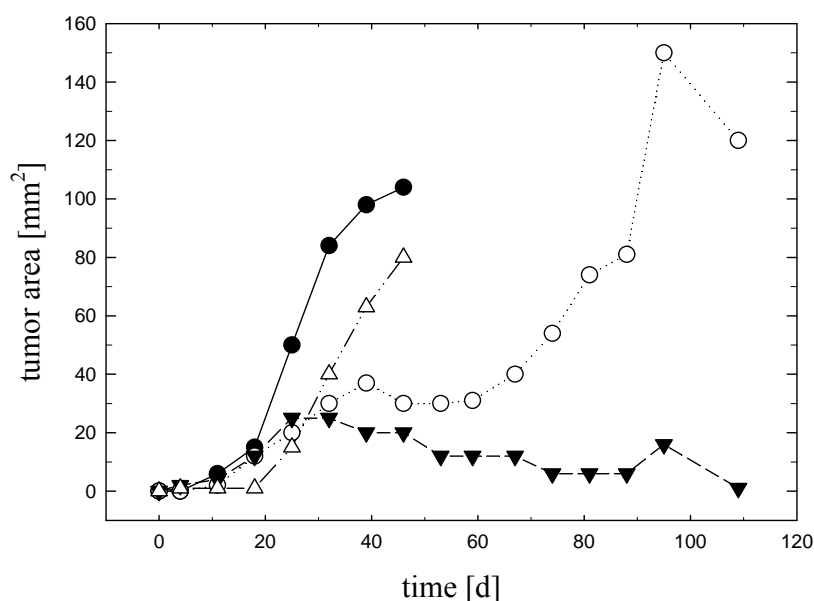


Figure 2.30: Growth of subcutaneous U-118 MG EGFP tumors (passage 2).

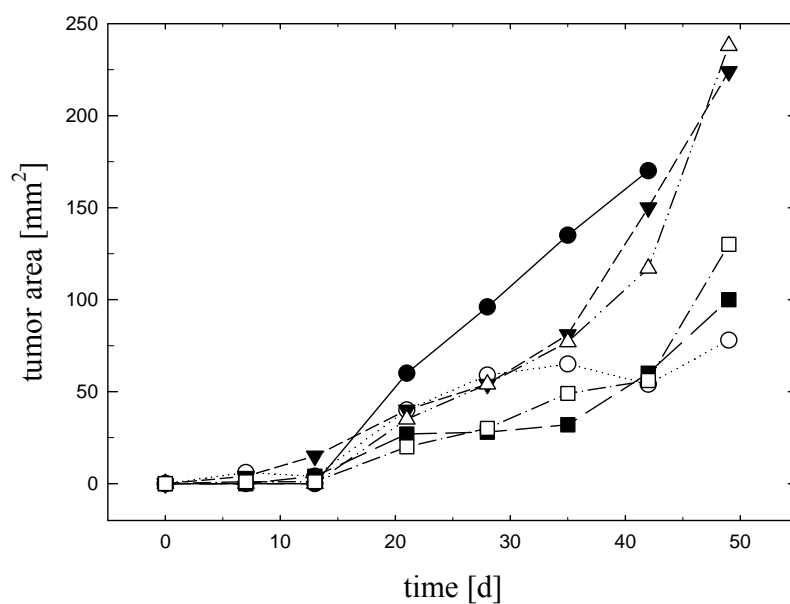


Figure 2.31: Growth of subcutaneous U-118 MG EGFP tumors (passage 3) after the transplantation of the tumor pieces from mouse 367.

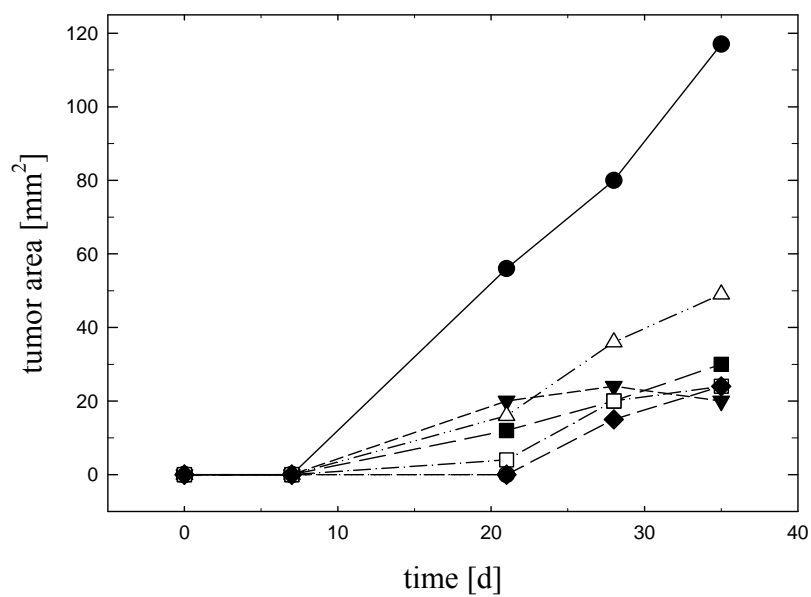


Figure 2.32: Growth of subcutaneous U-118 MG EGFP tumors (passage 4) after the transplantation of the tumor pieces from mouse 501.

2.4.5.3 Subcutaneous U-373 MG EGFP tumors

After the injection of the U-373 MG EGFP cell suspension the tumor formation took a relatively short period of around five weeks (Figure 2.33). However, there was one tumor which lost its fluorescence (mouse 347). After the transplantation of the solid tumor pieces the growth rate was approximately identical to the tumors of passage 0 (Figure 2.34).

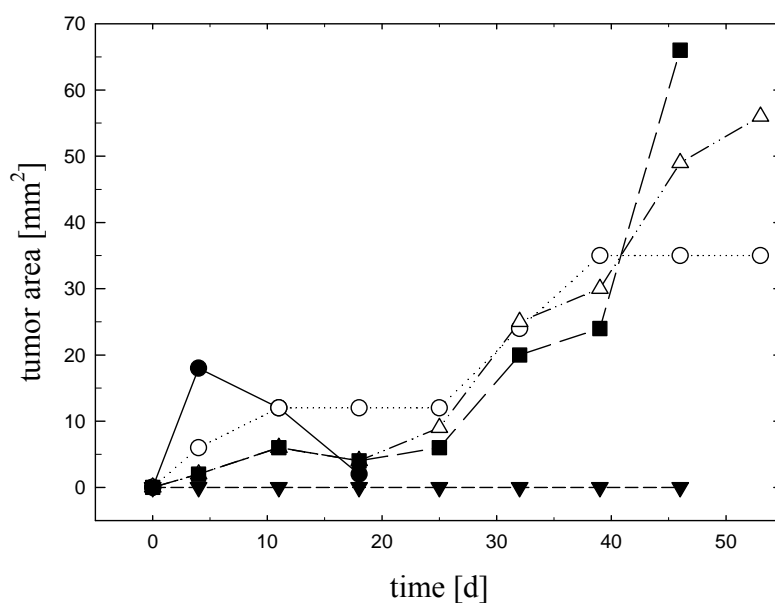


Figure 2.33: Growth of subcutaneous U-373 MG EGFP tumors (passage 0) after the injection of the cell suspension (passage 312 in cell culture).

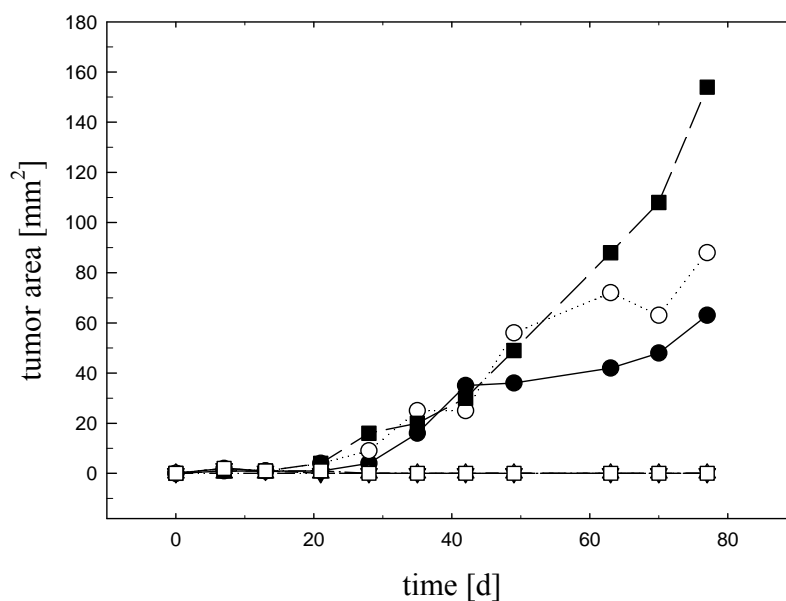


Figure 2.34: Growth of subcutaneous U-373 MG EGFP tumors (passage 1) after the transplantation of the tumor pieces from mouse 345.

2.4.5.4 Subcutaneous DsRed2 expressing glioblastoma

The establishment of subcutaneous DsRed2 expressing tumors was also successful (data not shown). The formation of a tumor after the subcutaneous injection of the cell suspension required a period of around two to four months depending on the cell line. It was comparable to the EGFP expressing tumors. After the transplantation of small pieces of the solid tumors they grew faster and more evenly. Within five to eight weeks they were disposed for the next transplantation.

2.4.6 Quantitation of EGFP in paraffin sections of subcutaneous tumors

Solid tumors were established after subcutaneous injection of EGFP expressing cells into nude mice and quantitation of EGFP was accomplished in histological sections by conventional fluorescence microscopy and confocal laser scanning microscopy.

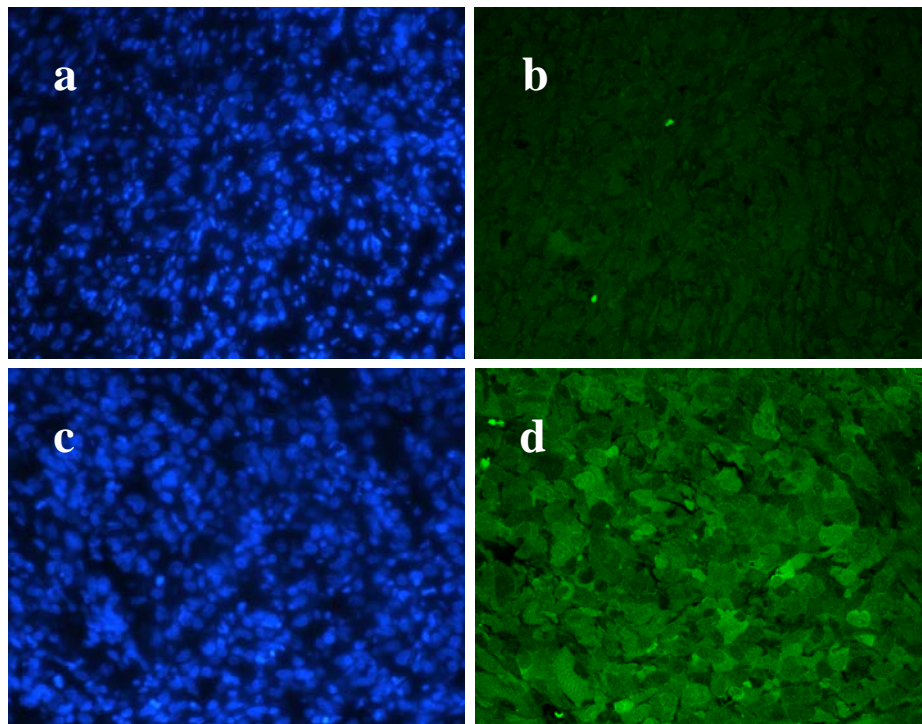


Figure 2.35: a: Fluorescence microscopic image of a U-87 MG s.c. tumor after DAPI staining; b: LSM image of paraffin embedded s.c. U-87 MG tumor with relative fluorescence intensity of 14 (i.e. auto-fluorescence); c: Fluorescence microscopic image of an U- 87 MG EGFP s.c. tumor after DAPI staining; d: LSM image of paraffin embedded U-87 MG EGFP s.c. tumor with relative fluorescence intensity of 66.

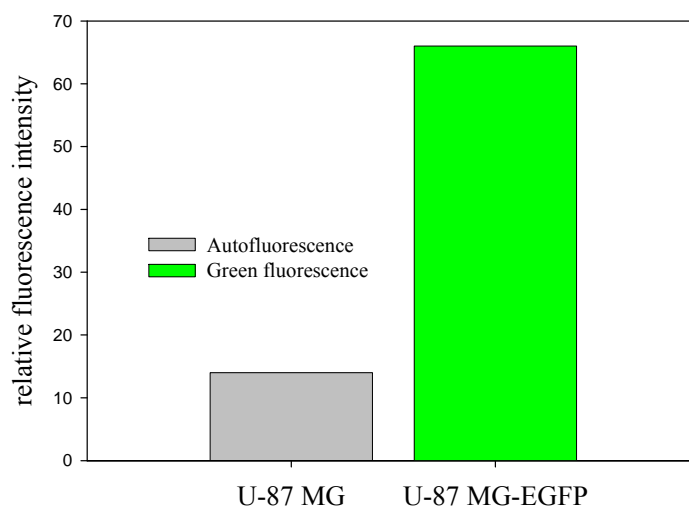


Figure 2.36: Comparison of the relative fluorescence intensity of the s.c. tumor U-87 MG EGFP with the auto-fluorescence of the wild type tumor U-87 MG.

2.4.7 In vivo imaging of subcutaneous U-373 MG EGFP tumors in nude mice

In vivo imaging is a very innovative and favored approach for the detection and quantitation of fluorescent tissues in vivo. This method is non-invasive and the animals can be examined several times during the experiment. In order to gain reliable results in the quantitation of the fluorescence intensity the fluorescent tissues were imaged in three different positions.

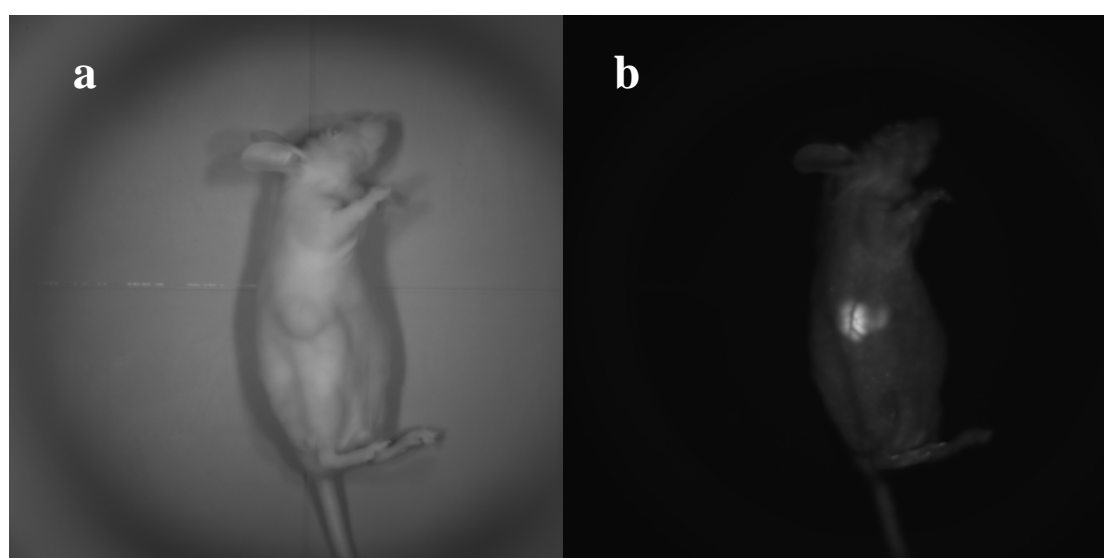


Figure 2.37: Lateral view of a subcutaneous human U-373 MG EGFP glioblastoma. a: transmission light; b: green fluorescence. The fluorescence image shows the vascularization of the tumor.

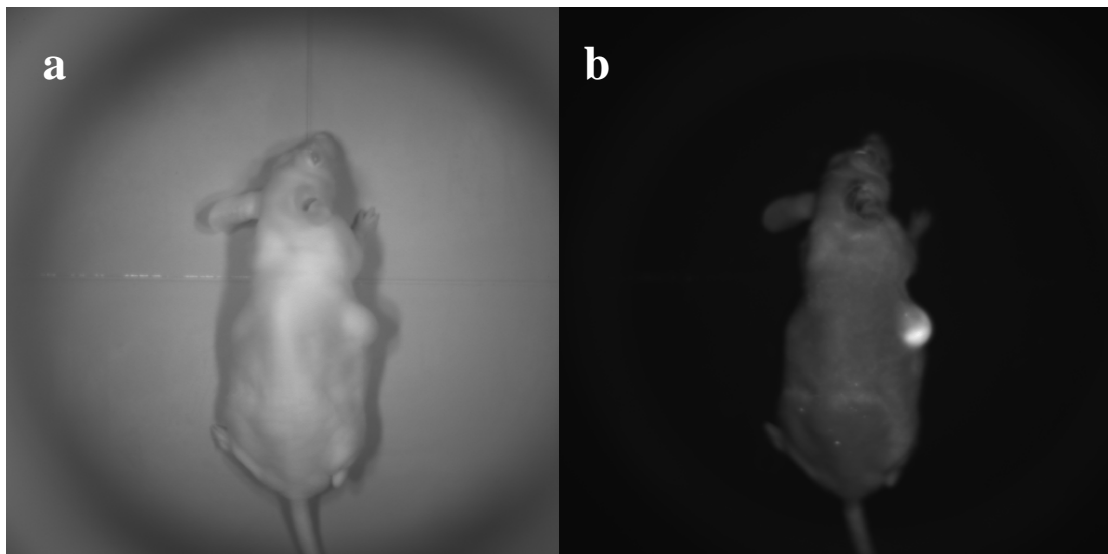


Figure 2.38: Dorsal view of a subcutaneous human U-373 MG EGFP glioblastoma. a: transmission light; b: green fluorescence.

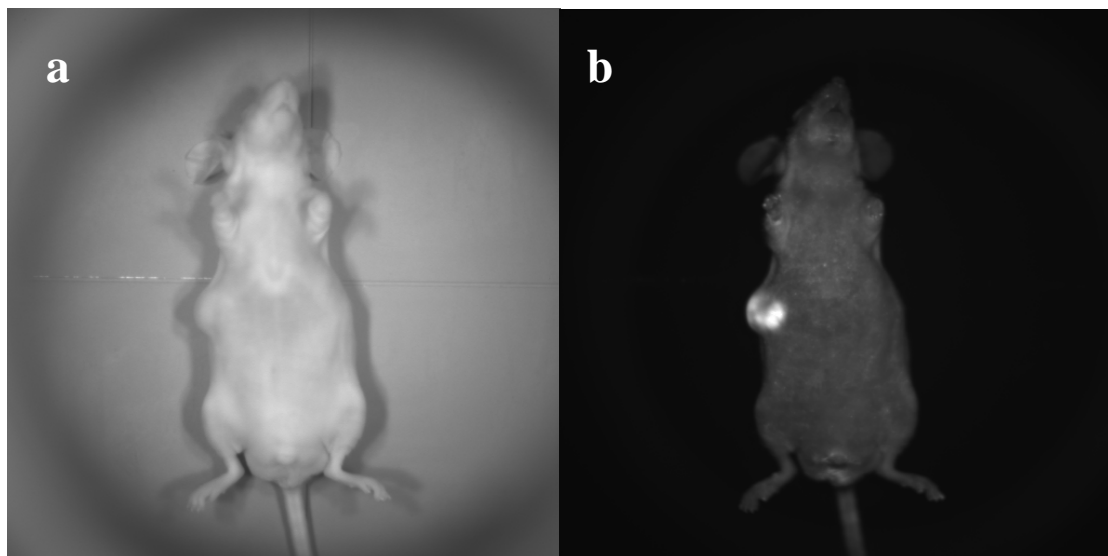


Figure 2.39: Ventral view of a subcutaneous human U-373 MG EGFP glioblastoma a: transmission light; b: green fluorescence.

The quantification of the fluorescence intensity was carried out by the software of the in vivo imaging system with the color palette indicating the fluorescence intensity.

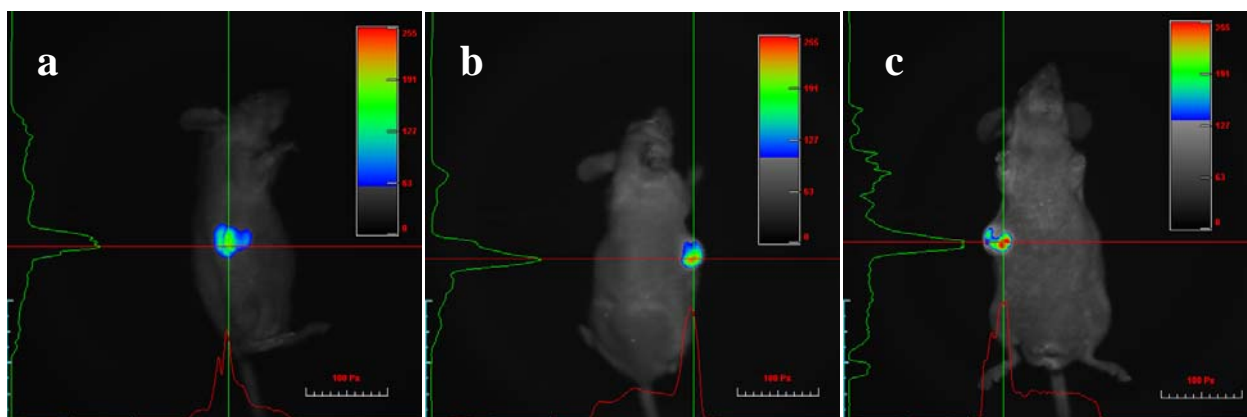


Figure 2.40: Quantification of the fluorescence intensity by a color palette; a: lateral view; b: dorsal view; c: ventral view. The color palette indicates the fluorescence intensity. The auto-fluorescence is displayed in gray scale. The quantification of the fluorescence intensity is carried out by the software of the in vivo imaging system.

2.4.8 Investigations on micro-osmotic pumps

The application of the siRNA-transfection reagent complexes should be carried out by subcutaneous implantation of micro-osmotic pumps to achieve a continuous release of the transfection mixture. For this purpose preliminary in vitro and in vivo studies were accomplished with Evans Blue, a non-toxic dye. The continuous release of the solution was monitored, and the practicability of subcutaneous implanted pumps with an attached catheter was evaluated.

2.4.8.1 Verification of the delivery in vitro

The pumps were filled with 0.9% saline and immersed in PBS. The attached catheters were filled with 0.01% Evans Blue solution. Nearly the complete Evans Blue solution was released after 70 h at 37 °C (Figure 2.41).

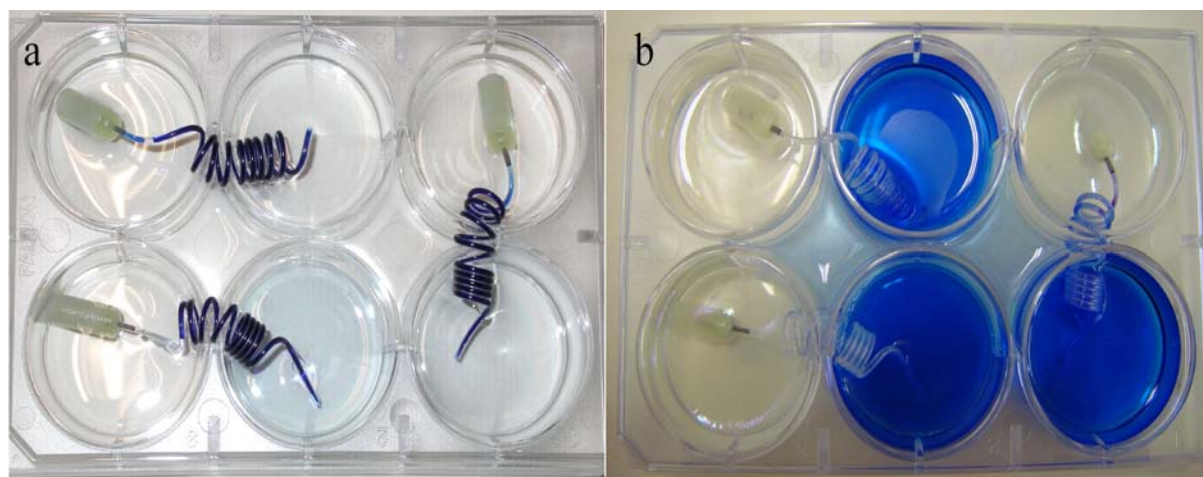


Figure 2.41: Experimental setup of the in vitro experiments with osmotic pumps. a) The pumps directly after the insertion in PBS; b) 70 hours after the insertion of the pumps.

By removing a sample from the reservoir and measuring the absorbance of the blue solution at 600 nm the delivery of the pumps was determined. The steady release and slight variations between the three pumps were demonstrated (Figure 2.42).

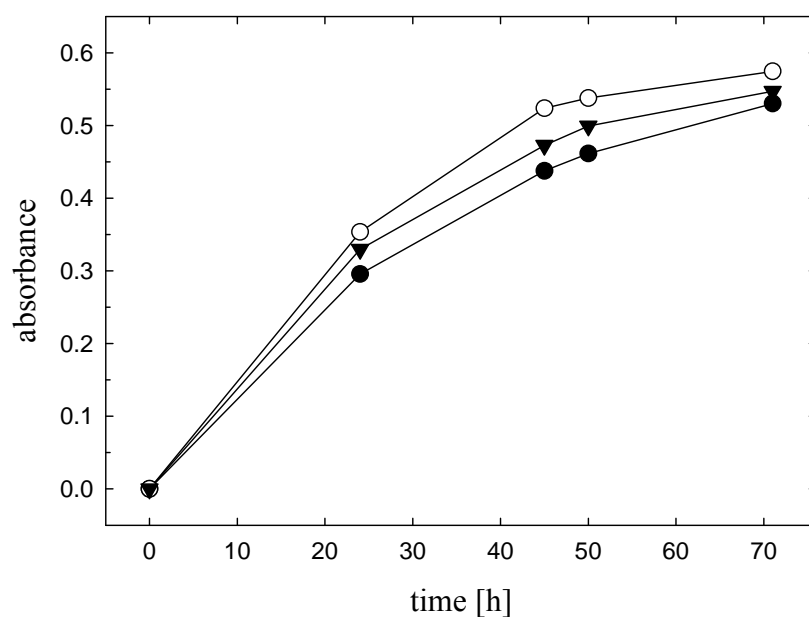


Figure 2.42: Progression of the Evans Blue release from osmotic pumps with attached catheters over 70 hours.

2.4.8.2 Verification of the delivery in vivo

For the implantation of the osmotic pumps 4 nude mice with subcutaneous tumors of comparable size, as shown in Figure 2.43, were selected.

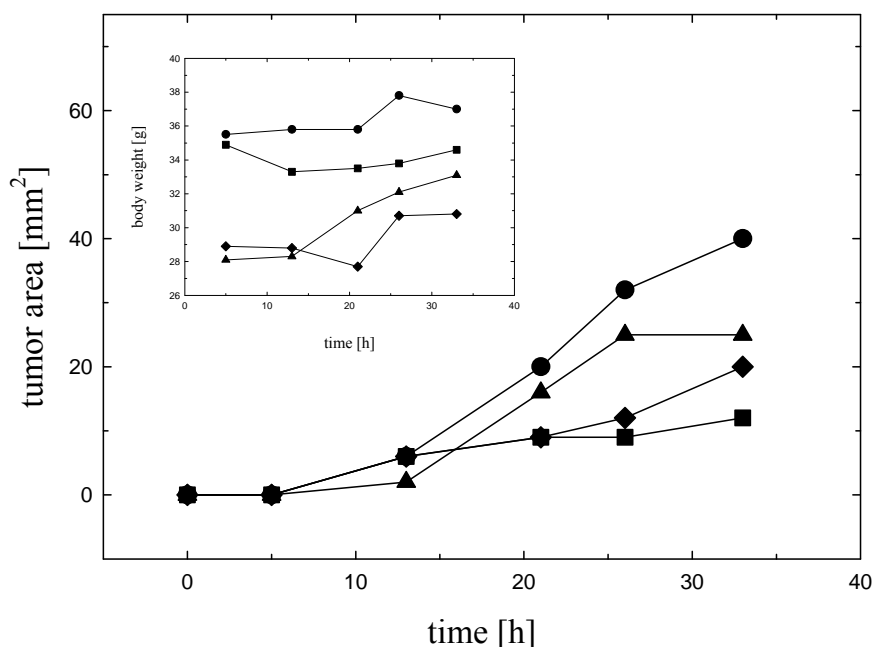


Figure 2.43: Growth of subcutaneous U-118 MG EGFP tumors before the implantation of osmotic pumps. The changes of the body weight of the nude mice are presented as insert.

The pumps were implanted in dorsal position either pointing towards the cranium (Figure 2.44a) or towards the tail (Figure 2.44b).

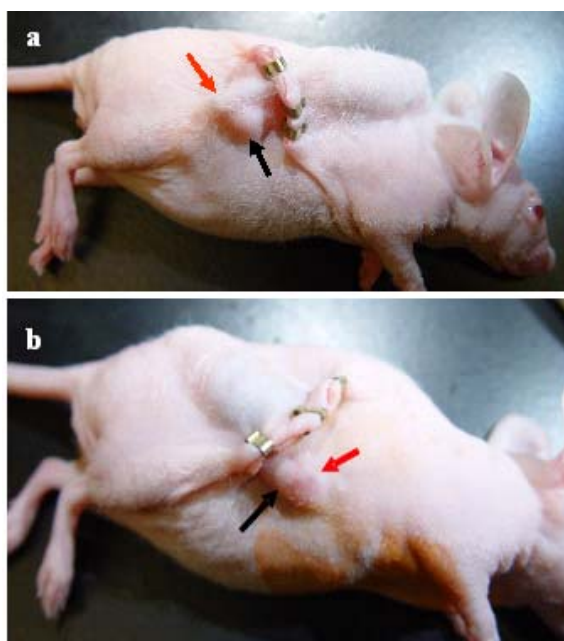


Figure 2.44: Subcutaneous U-118 MG EGFP tumor (black arrow) and placement of the implanted osmotic pumps in situ. The pumps were inserted in such a way that the Evans Blue solution was released directly on the tumor (red arrow).

Before the dissection of osmotic pumps after three days, a distinct blue coloration surrounding the tumor was recognizable (Figure 2.45).

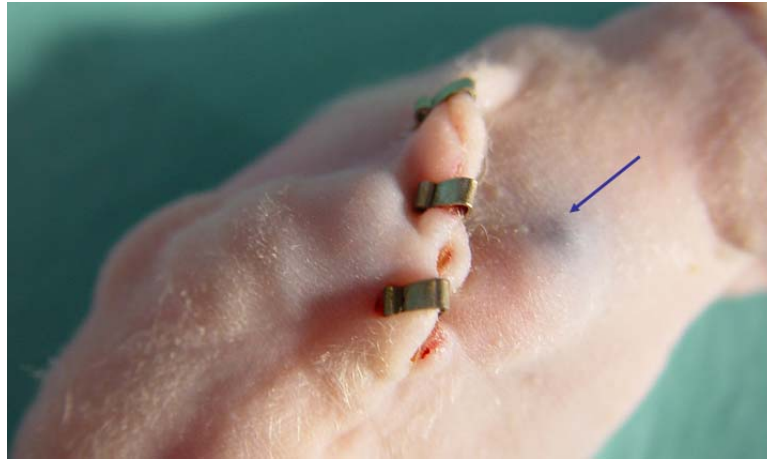


Figure 2.45: Subcutaneous implanted osmotic pump with an attached catheter three days after the application. The outlet of the catheter nearby the tumor is marked with a blue arrow.

After the transection of the skin the position of the osmotic pump and its catheter could be inspected. The positioning of the osmotic pump was not changed and the outlet of the catheter was still placed directly at the well vascularized tumor (Figure 2.46).

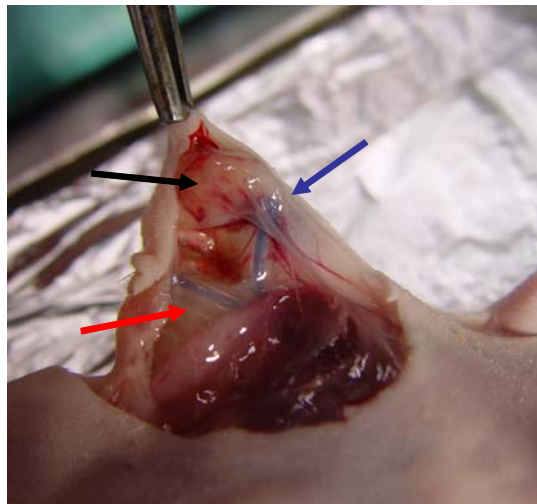


Figure 2.46: Position of an osmotic pump (red arrow) with the outlet of its catheter (blue arrow) close to a subcutaneous U-118 MG EGFP tumor (black arrow).

In order to control the complete release of the Evans Blue solution the osmotic pumps were dissected (Figure 2.47). The ends of the catheters still contained Evans Blue solution, because the catheters were able to take up a volume of 100 μ l, but the used pumps had only an average volume of 88 μ l.



Figure 2.47: The removed osmotic pumps three days after implantation.

2.5 Summary

For the proof of principle of siRNA effects in vitro and in vivo in order to treat brain tumors, the three human glioblastoma cell lines U-87 MG, U-118 MG and U-373 MG were stably transfected with the EGFP and DsRed2 reporter gene, respectively. A large fraction of fluorescent cells is a prerequisite for the quantitative detection of variances in EGFP expression. Hence, the transfectants were selected with the antibiotic G418 and the ratio of fluorescent cells was increased up to 80% by cell sorting with the flow cytometer. Furthermore, in order to assure the similarity of the wild type and the transfected cells we analyzed the growth kinetics. Neither the EGFP expression nor the selection antibiotic G418 affected the cell growth. Moreover, the chemosensitivity of the cell lines against different concentrations of doxorubicin was comparable.

A suitable and convenient in vitro method was established for the quick detection of siRNA effects by using a fluorescence plate reader. Due to the cytotoxicity of cationic lipid or polymer based siRNA transfection reagents resulting in varying cell densities of the test population and consequently in incorrect results, the extent of EGFP or DsRed2 expression was quantified with respect to total cell number. Furthermore, the TmHU did not show any cytotoxic effect up to a very high concentration of 5 μ M.

The validation of this method was performed with specific EGFP-siRNA and nonspecific siRNA. The cationic lipid based siRNA transfection reagent Lipofectamine[®] 2000, the TmHU protein and 1 mM CaCl₂ alone and in combination were compared. Although the TmHU protein showed very promising effects in the transfection of plasmid DNA (Esser et al., 2000), neither the TmHU protein nor the combination of the TmHU with CaCl₂ together with the specific EGFP-siRNA showed a down-regulating effect on the EGFP expression. Also numerous variations in the performance of the assay concerning the concentration ratios of transfection reagent and siRNA and the incubation time of the transfection mixture did not improve the effects. Claudia Immisch from ACGT ProGenomics AG (Halle, Germany) tested further conditions and could show that the combination of TmHU with the endosomolytic chloroquine was efficient (Immisch, 2006). But chloroquine is inappropriate for in vivo studies. Thus, the TmHU protein does not fulfill the requirements of a transfection reagent for siRNAs.

In order to develop a method to study siRNA effects *in vivo*, solid subcutaneous tumors were established after subcutaneous injection of EGFP and DsRed2 expressing glioblastoma cells, respectively, into nude mice. The formation of a tumor after the subcutaneous injection of the cell suspension required a long period of around two to four months depending on the cell line. However, after the transplantation of small pieces of the solid tumors they grew faster and more evenly. Within five to eight weeks they could be disposed for the next transplantation.

Paraffin embedding with the low melting Paraplast X-tra of the subcutaneous tumors enabled the quantitation of the fluorescence intensity in histological sections by conventional fluorescence microscopy and confocal laser scanning microscopy. These fundamental techniques for the determination of siRNA activity provide the basis for the detailed investigation on the effects of siRNA transfection reagents *in vitro* and *in vivo*. However, this morphometric procedure is based on serial sections, very complex and extremely time-consuming. Moreover, the animals were killed and therefore only an end point measurement was possible. Due to this difficulty an *in vivo* imaging system for the quantitation of the fluorescence intensity of the tumors was tested. In order to perform the intended preclinical studies on RNA interference it was shown that *in vivo* imaging offers the appropriate method with reliable results in the quantitation of the fluorescence intensity, particularly with regard to the possibility to take multiple images during the experiment.

Micro-osmotic pumps with an attached catheter will allow a continuous release of the siRNA transfection mixture *in vivo*. This was verified with preliminary *in vitro* and *in vivo* tests by loading the osmotic pumps with a solution of the non-toxic dye Evans Blue. The continuous release of the solution was monitored and the practicability of subcutaneous implantation of the pumps was assured. The position of the implanted osmotic pumps with their catheters did not change and the outlet of the catheter was still placed directly at tumor. Moreover, the required volume of the Evans Blue solution was delivered within the targeted period of time.

The established *in vivo* methods could not be used for the intended investigations on the TmHU protein because numerous *in vitro* experiments with TmHU did not show any effect on siRNA transfection. Nevertheless, these methods are useful and recommendable for the investigation of more promising siRNA transfection reagents for *in vivo* use.

References

- Agrawal, S., Tan, W., Cai, Q., Xie, X. and Zhang, R. (1997) In vivo pharmacokinetics of phosphorothioate oligonucleotides containing contiguous guanosine. *Antisense Nucleic Acid Drug Dev.* 7(3):245-249.
- Alvarado, A. S. and Newmark, P. A. (1999) Double-stranded RNA specifically disrupts gene expression during planarian regeneration. *Proc. Natl. Acad. Sci. U. S. A.* 96(9):5049–5054.
- Balandina, A., Kamashev, D. and Rouviere-Yaniv, J. (2002) The Bacterial Histone-like Protein HU Specifically Recognizes Similar Structures in All Nucleic Acids. DNA, RNA, AND THEIR HYBRIDS. *J. Biol. Chem.* 277(31):27622-27628.
- Baulcombe, D. C. (1999) Gene silencing: RNA makes RNA makes no protein. *Curr. Biol.* 9(16):R599-R601.
- Beckman, G., Beckman, L., Ponten, J. and Westermarck, B. (1971) G-6-PD and PGM phenotypes of 16 continuous human tumor cell lines. Evidence against cross-contamination and contamination by HeLa cells. *Human Heredity* 21(3):238-241.
- Behr, J. (1994) Gene transfer with synthetic cationic amphiphiles: prospects for gene therapy. *Bioconjug. Chem.* 5(5):382-389.
- Behr, J.-P., Demeneix, B., Löffler, J.-P. and Perez-Mutul, J. (1989) Efficient Gene Transfer into Mammalian Primary Endocrine Cells with Lipopolyamine-Coated DNA. *Proc. Natl. Acad. Sci. U. S. A.* 86(18):6982-6986.
- Bernhardt, G., Reile, H., Birnböck, H., Spruss, T. and Schönenberger, H. (1992) Standardized kinetic microassay to quantify differential chemosensitivity on the basis of proliferative activity. *J. Cancer Res. Clin. Oncol.* V118(1):35-43.
- Bernstein, E., Caudy, A. A., Hammond, S. M. and Hannon, G. J. (2001) Role for a bidentate ribonuclease in the initiation step of RNA interference. *Nature* 409(6818):363-366.
- Bonnefoy, E. and Rouviere-Yaniv, J. (1991) HU and IHF, two homologous histone-like proteins of *Escherichia coli*, form different protein-DNA complexes with short DNA fragments. *EMBO J.* 10(3):687-696.
- Borchard, G. (2001) Chitosans for gene delivery. *Adv. Drug Deliv. Rev.* 52(2):145-150.
- Boubrik, F., Bonnefoy, E. and Rouviere-Yaniv, J. (1991) HU and IHF: similarities and differences. In *Escherichia coli*, the lack of HU is not compensated for by IHF. *Res. Microbiol.* 142(2-3):239-247.
- Breunig, M., Lungwitz, U., Klar, J., Kurtz, A., Blunk, T. and Göpferich, A. (2004) Polyplexes of polyethylenimine and per-N-methylated polyethylenimine-cytotoxicity and transfection efficiency. *J. Nanosci. Nanotechnol.* 4(5):512-520.

- Breunig, M., Lungwitz, U., Liebl, R., Fontanari, C., Klar, J., Kurtz, A., Blunk, T. and Göpferich, A. (2005) Gene delivery with low molecular weight linear polyethylenimines. *J. Gene Med.* 7(10):1287-1298.
- Breunig, M., Lungwitz, U., Liebl, R. and Göpferich, A. (2006) Fluorescence resonance energy transfer: Evaluation of the intracellular stability of polyplexes. *Eur. J. Pharm. Biopharm.* 63(2):156-165.
- Breunig, M., Lungwitz, U., Liebl, R., Klar, J., Obermayer, B., Blunk, T. and Göpferich, A. (2007) Mechanistic insights into linear polyethylenimine-mediated gene transfer. *Biochim. Biophys. Acta - Gen. Subj.* 1770(2):196-205.
- Caplen, N. J., Parrish, S., Imani, F., Fire, A. and Morgan, R. A. (2001) Specific inhibition of gene expression by small double-stranded RNAs in invertebrate and vertebrate systems. *Proc. Natl. Acad. Sci. U. S. A.* 98(17):9742-9747.
- Caplen, N. J., Zheng, Z., Falgout, B. and Morgan, R. A. (2002) Inhibition of Viral Gene Expression and Replication in Mosquito Cells by dsRNA-Triggered RNA Interference. *Mol. Ther.* 6(2):243-251.
- Carlisle, R. C., Etrych, T., Briggs, S. S., Preece, J. A., Ulbrich, K. and Seymour, L. W. (2004) Polymer-coated polyethylenimine/DNA complexes designed for triggered activation by intracellular reduction. *J. Gene Med.* 6(3):337-344.
- Carmichael, G. G. (2005) *RNA Silencing - Methods and Protocols*. Humana Press, Totowa, New Jersey.
- Cattel, L., M, C. and F, D. (2003) From conventional to stealth liposomes: a new frontier in cancer chemotherapy. *Tumori* 89(3):237-249.
- Cheng, J. C., Moore, T. B. and Sakamoto, K. M. (2003) RNA interference and human disease. *Mol. Genet. Metab.* 80(1-2):121-128.
- Choi, J. S., Lee, E. J., Jang, H. S. and Park, J. S. (2001) New Cationic Liposomes for Gene Transfer into Mammalian Cells with High Efficiency and Low Toxicity. *Bioconjugate Chem.* 12(1):108-113.
- Christodoulou, E. and Vorgias, C. E. (2002) The thermostability of DNA-binding protein HU from mesophilic, thermophilic, and extreme thermophilic bacteria. *Extremophiles* 6(1):21-31.
- Dass, C. R. (2002) Biochemical and biophysical characteristics of lipoplexes pertinent to solid tumour gene therapy. *Int. J. Pharm.* 241(1):1-25.
- Dokka, S., Toledo, D., Shi, X., Castranova, V. and Rojanasakul, Y. (2000) Oxygen Radical-Mediated Pulmonary Toxicity Induced by Some Cationic Liposomes. *Pharm. Res.* 17(5):521-525.
- Dorsett, Y. and Tuschl, T. (2004) siRNAs: Applications in functional genomics and potential as therapeutics. *Nat. Rev. Drug Discov.* 3(3):318-329.
- Drlica, K. and Rouviere-Yaniv, J. (1987) Histone-like proteins of bacteria. *Microbiol. Mol. Biol. Rev.* 51(3):301-319.

- Dykxhoorn, D. M., Novina, C. D. and Sharp, P. A. (2003) Killing the messenger: short RNAs that silence gene expression. *Nat. Rev. Mol. Cell Biol.* 4(6):457-467.
- Elbashir, S. M., Harborth, J., Lendeckel, W., Yalcin, A., Weber, K. and Tuschl, T. (2001a) Duplexes of 21-nucleotide RNAs mediate RNA interference in cultured mammalian cells. *Nature* 411(6836):494-498.
- Elbashir, S. M., Lendeckel, W. and Tuschl, T. (2001b) RNA interference is mediated by 21- and 22-nucleotide RNAs. *Genes Dev.* 15(2):188-200.
- Elbashir, S. M., Martinez, J., Patkaniowska, A., Lendeckel, W. and Tuschl, T. (2001c) Functional anatomy of siRNAs for mediating efficient RNAi in *Drosophila melanogaster* embryo lysate. *EMBO J.* 20(23):6877-6888.
- Elbashir, S. M., Harborth, J., Weber, K. and Tuschl, T. (2002) Analysis of gene function in somatic mammalian cells using small interfering RNAs. *Methods* 26(2):199-213.
- Ellenberger, T. and Landy, A. (1997) A good turn for DNA: the structure of integration host factor bound to DNA. *Structure* 5(2):153-157.
- Esser, D., Rudolph, R., Jänicke, R. and Böhm, G. (1999) The HU protein from *Thermotoga maritima*: recombinant expression, purification and physicochemical characterization of an extremely hyperthermophilic DNA-binding protein. *J. Mol. Biol.* 291(5):1135-1146.
- Esser, D., Amanuma, H., Yoshiki, A., Kusakabe, M., Rudolph, R. and Böhm, G. (2000) A hyperthermostable bacterial histone-like protein as an efficient mediator for transfection of eukaryotic cells. *Nat. Biotechnol.* 18(11):1211-1213.
- Felgner, J., Kumar, R., Sridhar, C., Wheeler, C., Tsai, Y., Border, R., Ramsey, P., Martin, M. and Felgner, P. (1994) Enhanced gene delivery and mechanism studies with a novel series of cationic lipid formulations. *J. Biol. Chem.* 269(4):2550-2561.
- Felgner, P. L., Gadek, T. R., Holm, M., Roman, R., Chan, H. W., Wenz, M., Northrop, J. P., Ringold, G. M. and Danielsen, M. (1987) Lipofection: A Highly Efficient, Lipid-Mediated DNA-Transfection Procedure. *Proc. Natl. Acad. Sci. U. S. A.* 84(21):7413-7417.
- Filion, M. C. and Phillips, N. C. (1997) Toxicity and immunomodulatory activity of liposomal vectors formulated with cationic lipids toward immune effector cells. *Biochim. Biophys. Acta - Biomembr.* 1329(2):345-356.
- Fillion, P., Desjardins, A., Sayasith, K. and Lagace, J. (2001) Encapsulation of DNA in negatively charged liposomes and inhibition of bacterial gene expression with fluid liposome-encapsulated antisense oligonucleotides. *Biochim. Biophys. Acta - Biomembr.* 1515(1):44-54.
- Fischer, D., Bieber, T., Li, Y., Elsässer, H.-P. and Kissel, T. (1999) A Novel Non-Viral Vector for DNA Delivery Based on Low Molecular Weight, Branched Polyethylenimine: Effect of Molecular Weight on Transfection Efficiency and Cytotoxicity. *Pharm. Res.* 16(8):1273-1279.

- Forrest, M. L. and Pack, D. W. (2002) On the Kinetics of Polyplex Endocytic Trafficking: Implications for Gene Delivery Vector Design. *Mol. Ther.* 6(1):57-66.
- Gaucheron, J., Santaella, C. and Vierling, P. (2001) Improved *in vitro* gene transfer mediated by fluorinated lipoplexes in the presence of a bile salt surfactant. *J. Gene Med.* 3(4):338-344.
- Gehl, J. (2003) Electroporation: theory and methods, perspectives for drug delivery, gene therapy and research. *Acta Physiol. Scand.* 177(4):437-447.
- Godbey, W. T. and Mikos, A. G. (2001) Recent progress in gene delivery using non-viral transfer complexes. *J. Controlled Release* 72(1-3):115-125.
- Goshima, N., Inagaki, Y., Otaki, H., Tanaka, H., Hayashi, N., Imamoto, F. and Kano, Y. (1992) Chimeric HU-IHF proteins that alter DNA-binding ability. *Gene* 118(1):97-102.
- Grayson, A. C. R., Doody, A. M. and Putnam, D. (2006) Biophysical and Structural Characterization of Polyethylenimine-Mediated siRNA Delivery in Vitro. *Pharm. Res.* 23(8):1868-1876.
- Guo, W., Gosselin, M. A. and Lee, R. J. (2002) Characterization of a novel diolein-based LPDII vector for gene delivery. *J. Controlled Release* 83(1):121-132.
- Haerd, T., Sayre, M. H., Geiduschek, E. P. and Kearns, D. R. (1989) A type II DNA-binding protein genetically engineered for fluorescence spectroscopy: the "arm" of transcription factor 1 binds in the DNA grooves. *Biochemistry* 28(7):2813-2819.
- Haley, B. and Zamore, P. D. (2004) Kinetic analysis of the RNAi enzyme complex. *Nat. Struct. Mol. Biol.* 11(7):599-606.
- Hammond, S. M., Bernstein, E., Beach, D. and Hannon, G. J. (2000) An RNA-directed nuclease mediates post-transcriptional gene silencing in *Drosophila* cells. *Nature* 404(6775):293-296.
- Hassani, Z., Lemkine, G. F., Erbacher, P., Palmier, K., Alfama, G., Giovannangeli, C., Behr, J.-P. and Demeneix, B. A. (2005) Lipid-mediated siRNA delivery down-regulates exogenous gene expression in the mouse brain at picomolar levels. *J. Gene Med.* 7(2):198-207.
- Hay, R. J. (1988) The seed stock concept and quality control for cell lines. *Anal. Biochem.* 171(2):225-237.
- Heidenreich, O. (2004) Oncogene suppression by small interfering RNAs. *Curr. Pharm. Biotechnol.* 5(4):349-354.
- Hemann, M. T., Fridman, J. S., Zilfou, J. T., Hernando, E., Paddison, P. J., Cordon-Cardo, C., Hannon, G. J. and Lowe, S. W. (2003) An epi-allelic series of p53 hypomorphs created by stable RNAi produces distinct tumor phenotypes in vivo. *Nat. Genet.* 33(3):396-400.

- Hofland, H. E., Shephard, L. and Sullivan, S. M. (1996) Formation of stable cationic lipid/DNA complexes for gene transfer. *Proc. Natl. Acad. Sci. U. S. A.* 93(14):7305–7309.
- Holen, T., Amarzguioui, M., Wiiger, M. T., Babaie, E. and Prydz, H. (2002) Positional effects of short interfering RNAs targeting the human coagulation trigger Tissue Factor. *Nucleic Acids Res.* 30(8):1757–1766.
- Hwang, D. and Kornberg, A. (1992) Opening of the replication origin of *Escherichia coli* by DnaA protein with protein HU or IHF. *J. Biol. Chem.* 267(32):23083–23086.
- Hwang, S. and Davis, M. (2001) Cationic polymers for gene delivery: designs for overcoming barriers to systemic administration. *Curr. Opin. Mol. Ther.* 3(2):183–191.
- Jaenicke, R., Schurig, H., Beaucamp, N. and Ostendorp, R. (1996) Structure and stability of hyperstable proteins: glycolytic enzymes from hyperthermophilic bacterium *Thermotoga maritima*. *Adv. Protein Chem.* 48(1):181–269.
- Jaenicke, R. and Böhm, G. (1998) The stability of proteins in extreme environments. *Curr. Opin. Struct. Biol.* 8(6):738–748.
- Kamashev, D. and Rouviere-Yaniv, J. (2000) The histone-like protein HU binds specifically to DNA recombination and repair intermediates. *EMBO J.* 19(23):6527–6535.
- Kawasaki, H. and Taira, K. (2003) Short hairpin type of dsRNAs that are controlled by tRNA^{Val} promoter significantly induce RNAi-mediated gene silencing in the cytoplasm of human cells. *Nucleic Acids Res.* 31(2):700–707.
- Ketting, R. F., Fischer, S. E. J., Bernstein, E., Sijen, T., Hannon, G. J. and Plasterk, R. H. A. (2001) Dicer functions in RNA interference and in synthesis of small RNA involved in developmental timing in *C. elegans*. *Genes Dev.* 15(20):2654–2659.
- Kircheis, R., Schüller, S., Brunner, S., Ogris, M., Heider, K.-H., Zauner, W. and Wagner, E. (1999) Polycation-based DNA complexes for tumor-targeted gene delivery *in vivo*. *J. Gene Med.* 1(2):111–120.
- Kircheis, R., Wightman, L., Schreiber, A., Robitza, B., Rössler, V., Kurs, M. and Wagner, E. (2001) Polyethylenimine/DNA complexes shielded by transferrin target gene expression to tumors after systemic application. *Gene Ther.* 8(1):28–40.
- Kontermann, R. (2006) Immunoliposomes for cancer therapy. *Curr. Opin. Mol. Ther.* 8(1):39–45.
- Kunath, K., von Harpe, A., Fischer, D., Petersen, H., Bickel, U., Voigt, K. and Kissel, T. (2003) Low-molecular-weight polyethylenimine as a non-viral vector for DNA delivery: comparison of physicochemical properties, transfection efficiency and *in vivo* distribution with high-molecular-weight polyethylenimine. *J. Controlled Release* 89(1):113–125.
- Lakkaraju, A., Dubinsky, J. M., Low, W. C. and Rahman, Y.-E. (2001) Neurons Are Protected from Excitotoxic Death by p53 Antisense Oligonucleotides Delivered in Anionic Liposomes. *J. Biol. Chem.* 276(34):32000–32007.

- Lappalainen, K., Jaaskeinen, I., Syrjanen, K., Urtti, A. and Syrjanen, S. (1994) Comparison of Cell Proliferation and Toxicity Assays Using Two Cationic Liposomes. *Pharm. Res.* 11(8):1127-1131.
- Lasic, D. D. (1997) *Liposomes in gene delivery*. CRC Press, Boca Raton.
- Lavoie, B. and Chaconas, G. (1994) A second high affinity HU binding site in the phage Mu transpososome. *J. Biol. Chem.* 269(22):15571-15576.
- Lee, R. and Huang, L. (1997) Lipidic vector systems for gene transfer. *Crit. Rev. Ther. Drug Carrier Syst.* 14(2):173-206.
- Lemkine, G. and Demeneix, B. (2001) Polyethylenimines for in vivo gene delivery. *Curr. Opin. Mol. Ther.* 3(2):178-182.
- Lohmann, J. U., Endl, I. and Bosch, T. C. G. (1999) Silencing of Developmental Genes in *Hydra*. *Dev. Biol.* 214(1):211-214.
- Lollo, C., Banaszczyk, M., Mullen, P., Coffin, C., Wu, D., Carlo, A., Bassett, D., Gouveia, E. and Carlo, D. (2002) Poly-L-lysine-based gene delivery systems. Synthesis, purification, and application. *Methods Mol. Med.* 69(1):1-13.
- Lungwitz, U., Breunig, M., Blunk, T. and Göpferich, A. (2005) Polyethylenimine-based non-viral gene delivery systems. *Eur. J. Pharm. Biopharm.* 60(2):247-266.
- Luo, D. and Saltzman, W. M. (2000) Synthetic DNA delivery systems. *Nat. Biotechnol.* 18(1):33-37.
- Luo, J. and Redies, C. (2004) Overexpression of genes in Purkinje cells in the embryonic chicken cerebellum by in vivo electroporation. *J. Neurosci. Methods* 139(2):241-245.
- Mamot, C., Drummond, D. C., Hong, K., Kirpotin, D. B. and Park, J. W. (2003) Liposome-based approaches to overcome anticancer drug resistance. *Drug Resist. Updat.* 6(5):271-279.
- Mao, S., Neu, M., Germershaus, O., Merkel, O., Sitterberg, J., Bakowsky, U. and Kissel, T. (2006) Influence of Polyethylene Glycol Chain Length on the Physicochemical and Biological Properties of Poly(ethylene imine)-*graft*-Poly(ethylene glycol) Block Copolymer/SiRNA Polyplexes. *Bioconjugate Chem.* 17(5):1209-1218.
- Martinez, J., Patkaniowska, A., Urlaub, H., Luhrmann, R. and Tuschl, T. (2002) Single-Stranded Antisense siRNAs Guide Target RNA Cleavage in RNAi. *Cell* 110(5):563-574.
- Merdan, T., Kopecek, J. and Kissel, T. (2002) Prospects for cationic polymers in gene and oligonucleotide therapy against cancer. *Adv. Drug Deliv. Rev.* 54(5):715-758.
- Misquitta, L. and M., P. B. (1999) Targeted disruption of gene function in *Drosophila* by RNA interference (RNA-i): A role for *nautilus* in embryonic somatic muscle formation. *Proc. Natl. Acad. Sci. U. S. A.* 96(4):1451-1456.
- Mitrus, I., Missol-Kolka, E., Plucienniczak, A. and Szala, S. (2005) Tumour therapy with genes encoding apoptin and E4orf4. *Anticancer Res.* 25(2A):1087-1090.

- Miyagishi, M. and Taira, K. (2002) U6 promoter-driven siRNAs with four uridine 3[prime] overhangs efficiently suppress targeted gene expression in mammalian cells. *Nat. Biotechnol.* 20(5):497-500.
- Murphy, L. D. and Zimmerman, S. B. (1994) Macromolecular crowding effects on the interaction of DNA with *Escherichia coli* DNA-binding proteins: A model for bacterial nucleoid stabilization. *Biochim. Biophys. Acta - Gene Struct. Expr.* 1219(2):277-284.
- Nakamura, K., Yahagi, S.-i., Yamazaki, T. and Yamane, K. (1999) *Bacillus subtilis* Histone-like Protein, HBSu, Is an Integral Component of a SRP-like Particle That Can Bind the Alu Domain of Small Cytoplasmic RNA. *J. Biol. Chem.* 274(19):13569-13576.
- Ngô, H., Tschudi, C., Gull, K. and Ullu, E. (1998) Double-stranded RNA induces mRNA degradation in *Trypanosoma brucei*. *Proc. Natl. Acad. Sci. U. S. A.* 95(25):14687-14692.
- Nguyen, H.-K., Lemieux, P., Vinogradov, S. V., Gebhart, C. L., Guérin, N., Paradis, G., Bronich, T. K., Alakhov, V. Y. and Kabanov, A. V. (2000) Evaluation of polyether-polyethyleneimine graft copolymers as gene transfer agents. *Gene Ther.* 7(2):126-138.
- Novina, C. D., Murray, M. F., Dykxhoorn, D. M., Beresford, P. J., Riess, J., Lee, S.-K., Collman, R. G., Lieberman, J., Shankar, P. and Sharp, P. A. (2002) siRNA-directed inhibition of HIV-1 infection. *Nat. Med.* 8(7):681-686.
- Nykänen, A., Haley, B. and Zamore, P. D. (2001) ATP Requirements and Small Interfering RNA Structure in the RNA Interference Pathway. *Cell* 107(3):309-321.
- Oberto, J. and Rouviere-Yaniv, J. (1996) *Serratia marcescens* contains a heterodimeric HU protein like *Escherichia coli* and *Salmonella typhimurium*. *J. Bacteriol.* 178(1):293-297.
- Ochietti, B., Lemieux, P., Kabanov, A. V., Vinogradov, S., St-Pierre, Y. and Alakhov, V. (2002) Inducing neutrophil recruitment in the liver of ICAM-1-deficient mice using polyethyleneimine grafted with Pluronic P123 as an organ-specific carrier for transgenic ICAM-1. *Gene Ther.* 9(14):939-945.
- Oupicky, D., Ogris, M., Howard, K., Dash, P., Ulbrich, K. and Seymour, L. (2002) Importance of Lateral and Steric Stabilization of Polyelectrolyte Gene Delivery Vectors for Extended Systemic Circulation. *Mol. Ther.* 5(4):463-472.
- Paddison, P. J. and Hannon, G. J. (2002) RNA interference: the new somatic cell genetics? *Cancer Cell* 2(1):17-23.
- Patil, S., Rhodes, D. and Burgess, D. (2004) Anionic liposomal delivery system for DNA transfection. *AAPS J.* 6(4):e29.
- Patil, S., Rhodes, D. and Burgess, D. (2005a) DNA-based Therapeutics and DNA Delivery Systems: A Comprehensive Review. *AAPS J.* 7(1):E61-E77.
- Patil, S. D. and Rhodes, D. G. (2000) Influence of divalent cations on the conformation of phosphorothioate oligodeoxynucleotides: a circular dichroism study. *Nucleic Acids Res* 28(12):2439-2445.

- Patil, S. D., Rhodes, D. G. and Burgess, D. J. (2005b) Biophysical characterization of anionic lipoplexes. *Biochim. Biophys. Acta - Biomembr.* 1711(1):1-11.
- Paull, T., Haykinson, M. and Johnson, R. (1993) The nonspecific DNA-binding and -bending proteins HMG1 and HMG2 promote the assembly of complex nucleoprotein structures. *Genes Dev.* 7(8):1521-1534.
- Pavselj, N. and Preat, V. (2005) DNA electrotransfer into the skin using a combination of one high- and one low-voltage pulse. *J. Controlled Release* 106(3):407-415.
- Petersen, H., Fechner, P. M., Martin, A. L., Kunath, K., Stolnik, S., Roberts, C. J., Fischer, D., Davies, M. C. and Kissel, T. (2002) Polyethylenimine-graft-Poly(ethylene glycol) Copolymers: Influence of Copolymer Block Structure on DNA Complexation and Biological Activities as Gene Delivery System. *Bioconjugate Chem.* 13(4):845-854.
- Rambabu, K. M., Rao, S. H. and Rao, N. M. (2005) Efficient expression of transgenes in adult zebrafish by electroporation. *BMC Biotechnology* 5(1):29.
- Rhaese, S., von Briesen, H., Rubsamen-Waigmann, H., Kreuter, J. and Langer, K. (2003) Human serum albumin-polyethylenimine nanoparticles for gene delivery. *J. Controlled Release* 92(1-2):199-208.
- Santel, A., Aleku, M., Keil, O., Endruschat, J., Esche, V., Durieux, B., Löffler, K., Fechtner, M., Röhl, T., Fisch, G., Dames, S., Arnold, W., Giese, K., Klippel, A. and Kaufmann, J. (2006a) RNA interference in the mouse vascular endothelium by systemic administration of siRNA-lipoplexes for cancer therapy. *Gene Ther.* 13(18):1360-1370.
- Santel, A., Aleku, M., Keil, O., Endruschat, J., Esche, V., Fisch, G., Dames, S., Löffler, K., Fechtner, M., Arnold, W., Giese, K., Klippel, A. and Kaufmann, J. (2006b) A novel siRNA-lipoplex technology for RNA interference in the mouse vascular endothelium. *Gene Ther.* 13(16):1222-1234.
- Schwarz, D. S., Hutvagner, G., Haley, B. and Zamore, P. D. (2002) Evidence that siRNAs Function as Guides, Not Primers, in the Drosophila and Human RNAi Pathways. *Mol. Cell* 10(3):537-548.
- Shigekawa, K. and Dower, W. J. (1988) Electroporation of Eukaryotes and Prokaryotes: A General Approach to the Introduction of Macromolecules into Cells. *Biotechniques* 8(6):742-751.
- Shimizu, M., Miyake, M., Kanke, F., Matsumoto, U. and Shindo, H. (1995) Characterization of the binding of HU and IHF, homologous histone-like proteins of Escherichia coli, to curved and uncurved DNA. *Biochim. Biophys. Acta* 1264(3):330-336.
- Simoes, S., Moreira, J., Fonseca, C., Duzgunes, N. and de Lima, M. (2004) On the formulation of pH-sensitive liposomes with long circulation times. *Adv. Drug Deliv. Rev.* 56(7):947-965.
- Stark, G. R., Kerr, I. M., Williams, B. R. G., Silverman, R. H. and Schreiber, R. D. (1998) How cells respond to interferones. *Annu. Rev. Biochem.* 67(1):227-264.

- Svoboda, P., Stein, P., Hayashi, H. and Schultz, R. (2000) Selective reduction of dormant maternal mRNAs in mouse oocytes by RNA interference. *Development* 127(19):4147-4156.
- Tagami, T., Barichello, J. M., Kikuchi, H., Ishida, T. and Kiwada, H. (2007) The gene-silencing effect of siRNA in cationic lipoplexes is enhanced by incorporating pDNA in the complex. *Int. J. Pharm.* 333(1-2):62-69.
- Thanaketpaisarn, O., Nishikawa, M., Yamashita, F. and Hashida, M. (2005) Tissue-Specific Characteristics of in Vivo Electric Gene: Transfer by Tissue and Intravenous Injection of Plasmid DNA. *Pharm. Res.* 22(6):883-891.
- Tiyaboonchai, W., Woiszwilllo, J. and Middaugh, C. R. (2003) Formulation and characterization of DNA-polyethylenimine-dextran sulfate nanoparticles. *Eur. J. Pharm. Sci.* 19(4):191-202.
- Trubetskoy, V. S., Wong, S. C., Subbotin, V., Budker, V. G., Loomis, A., Hagstrom, J. E. and Wolff, J. A. (2003) Recharging cationic DNA complexes with highly charged polyanions for in vitro and in vivo gene delivery. *Gene Ther.* 10(3):
- Tseng, W.-C. and Jong, C.-M. (2003) Improved Stability of Polycationic Vector by Dextran-Grafted Branched Polyethylenimine. *Biomacromolecules* 4(5):1277-1284.
- Tupin, E., Poirier, B., Bureau, M., Khallou-Laschet, J., Vranckx, R., Caligiuri, G., Gaston, A., Duong Van Huyen, J., Scherman, D., Bariety, J., Michel, J. and Nicoletti, A. (2003) Non-viral gene transfer of murine spleen cells achieved by in vivo electroporation. *Gene Ther.* 10(7):569-579.
- Tuschl, T., Zamore, P. D., Lehmann, R., Bartel, D. P. and Sharp, P. A. (1999) Targeted mRNA degradation by double-stranded RNA in vitro. *Genes Dev.* 13(24):3191-3197.
- Venugopalan, P., Jain, S., Sankar, S., Singh, P., Rawat, A. and Vyas, S. (2002) pH-sensitive liposomes: mechanism of triggered release to drug and gene delivery prospects. *Pharmazie* 57(10):659-671.
- Vickers, T. A., Koo, S., Bennett, C. F., Crooke, S. T., Dean, N. M. and Baker, B. F. (2003) Efficient Reduction of Target RNAs by Small Interfering RNA and RNase H-dependent Antisense Agents. A COMPARATIVE ANALYSIS. *J. Biol. Chem.* 278(9):7108-7118.
- Vis, H., Mariani, M., Vorgias, C. E., Wilson, K. S., Kaptein, R. and Boelens, R. (1995) Solution Structure of the HU Protein from *Bacillus stearothermophilus*. *J. Mol. Biol.* 254(4):692-703.
- von Harpe, A., Petersen, H., Li, Y. and Kissel, T. (2000) Characterization of commercially available and synthesized polyethylenimines for gene delivery. *J. Controlled Release* 69(2):309-322.
- Walter, I., Fleischmann, M., Klein, D., Müller, M., Salmons, B., Günzburg, W. H., Renner, M. and Gelbmann, W. (2000) Rapid and Sensitive Detection of Enhanced Green Fluorescent Protein Expression in Paraffin Sections by Confocal Laser Scanning Microscopy. *Histochem. J.* V32(2):99-103.

- Walters, D. K. and Jelinek, D. F. (2002) The Effectiveness of Double-Stranded Short Inhibitory RNAs (siRNAs) May Depend on the Method of Transfection. *Antisense Nucleic Acid Drug Dev.* 12(6):411-418.
- White, S. W., Appelt, K., Wilson, K. S. and Tanaka, I. (1989) A protein structural motif that bends DNA. *Proteins: Struct., Funct., Genet.* 5(4):281-288.
- Wianny, F. and Zernicka-Goetz, M. (2000) Specific interference with gene function by double-stranded RNA in early mouse development. *Nature Cell Biol.* 2(2):70-75.
- Wightman, L., Kircheis, R., Rössler, V., Carotta, S., Ruzicka, R., Kurs, M. and Wagner, E. (2001) Different behavior of branched and linear polyethylenimine for gene delivery *in vitro* and *in vivo*. *J. Gene Med.* 3(4):362-372.
- Wiseman, J. W., Goddard, C. A., McLelland, D. and Colledge, W. H. (2003) A comparison of linear and branched polyethylenimine (PEI) with DCChol/DOPE liposomes for gene delivery to epithelial cells *in vitro* and *in vivo*. *Gene Ther.* 10(19):1654-1662.
- Wong, T.-K. and Neumann, E. (1982) Electric field mediated gene transfer. *Biochem. Biophys. Res. Commun.* 107(2):584-587.
- Wyman, T. B., Nicol, F., Zelphati, O., Scaria, P. V., Plank, C. and Szoka, F. C. (1997) Design, Synthesis, and Characterization of a Cationic Peptide That Binds to Nucleic Acids and Permeabilizes Bilayers. *Biochemistry* 36(10):3008-3017.
- Zaitsev, S. V., Haberland, A., Otto, A., Vorob'ev, V. I., Haller, H. and Böttger, M. (1997) H1 and HMGI7 extracted from calf thymus nuclei are efficient DNA carriers in gene transfer. *Gene Ther.* 4(6):586-592.
- Zelphati, O. and Szoka, F. C. (1996) Liposomes as a carrier for intracellular delivery of antisense oligonucleotides: a real or magic bullet? *J. Controlled Release* 41(1-2):99-119.
- Zeng, Y. and Cullen, B. R. (2002) RNA interference in human cells is restricted to the cytoplasm. *RNA* 8(7):855-860.
- Zhdanov, R. I., Podobed, O. V. and Vlassov, V. V. (2002) Cationic lipid-DNA complexes--lipoplexes--for gene transfer and therapy. *Bioelectrochemistry* 58(1):53-64.
- Zou, S.-M., Erbacher, P., Remy, J.-S. and Behr, J.-P. (2000) Systemic linear polyethylenimine (L-PEI)-mediated gene delivery in the mouse. *J. Gene Med.* 2(2):128-134.

Chapter 3

Inhibitors of kinesin Eg5:

antiproliferative activity of monastrol analogs

against human glioblastoma cells

3.1 Introduction

3.1.1 The mitotic spindle as a target in cancer chemotherapy

Mitosis is an ordered series of fundamentally mechanical events in which identical copies of the genome are moved to two discrete locations within the dividing cell (Figure 3.1). The chromosome segregation during mitosis occurs on a bipolar spindle that consists of dynamic structures, the microtubules, and of associated proteins, contributing to the assembly and functionality of the whole spindle complex. For decades the mitotic spindle was identified as an important target in cancer chemotherapy because of its crucial role in cell division.

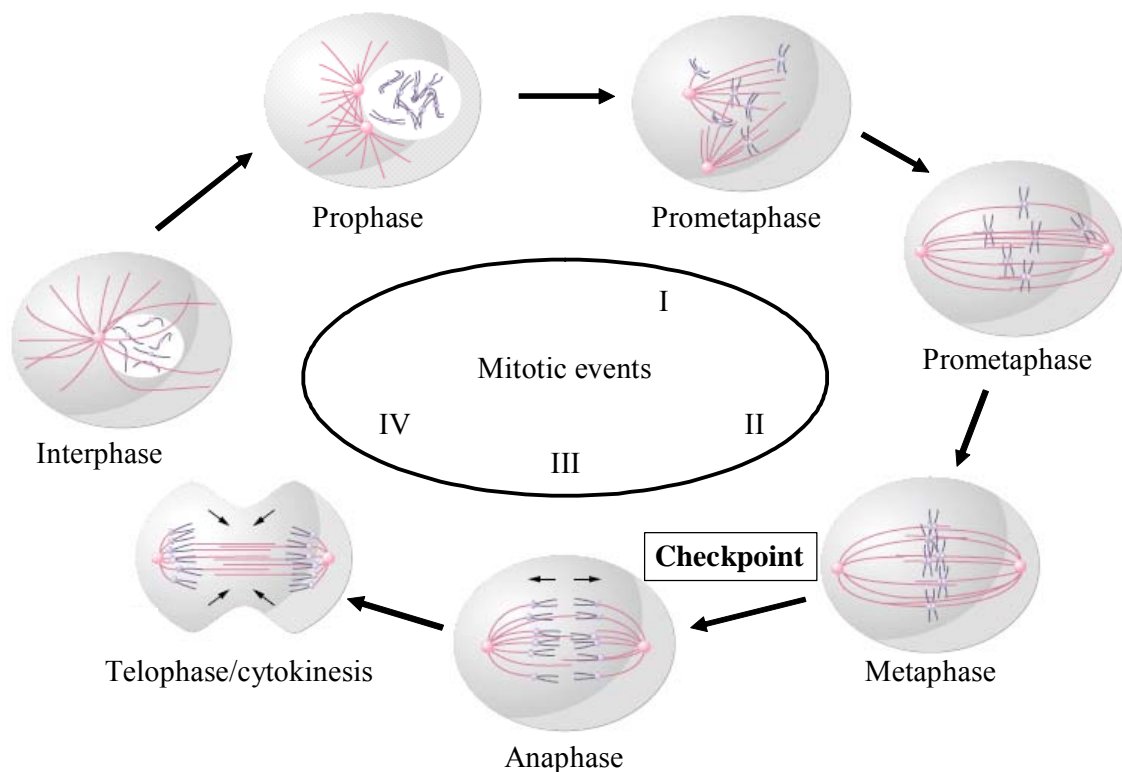


Figure 3.1: Mitosis is a series of ordered mechanical events (I-IV): (I) microtubule capture and spindle pole separation; (II) chromosome alignment; (III) anaphase chromosome movement; (IV) telophase and cytokinesis. A parallel network of kinase-dependent signaling cascades monitors these mechanical events and regulates transition from one stage to another (Wood et al., 2001).

3.1.1.1 The role of microtubules in the mitotic spindle

The hollow cylindrical structure of microtubules is made up of 13 parallel protofilaments, which are composed of alternating α - and β -tubulin units aligned along the longitudinal axis of the microtubule. Microtubules are polar polymers with distinct plus (+) and minus (-) ends. The structural polarity is created by the regular, parallel orientation of their subunits. The process of polymerization uses the energy provided by GTP hydrolysis and shows different dynamics at both ends of the microtubules. The plus (+) end is able to grow rapidly and is kinetically more dynamic than the minus (-) end, which tends to lose subunits if not stabilized. Although both ends grow and shorten alternately by polymerization and depolymerization, net growing occurs at the plus end and net shortening at the minus end (Walker et al., 1988).

Figure 3.2 illustrates the role of microtubules in mitosis. During mitosis, all microtubules are associated at their minus ends with the microtubule organizing centers, the centrosomes, from which they are nucleated (Bailly and Bornens, 1992). Three major classes of microtubules are found in the mitotic spindle, serving different functions. During the prometaphase the duplicated chromosomes attach to some microtubules, the kinetochore microtubules, through their kinetochore. In the following metaphase the kinetochore microtubules attach the sister chromatids to opposite poles of the mitotic spindle, and the chromosomes are aligned at the equator of the spindle. The daughter chromosomes start to get separated polewards at the early anaphase by a shortening of the kinetochore microtubules and by a contributing effect of motor proteins. This process leads to the synchronic separation of the sister chromatids to form two daughter chromosomes. In the later anaphase the spindle poles move apart from each other by the action of motor proteins, which connect and couple the polar or overlapping microtubules at the equator of the mitotic spindle. Furthermore, astral microtubules radiate in all directions from the centrosomes and stabilize the position of the spindle in the mitotic cell by contributing to the separation of the poles.

Destabilization of microtubules, e.g. by microtubule-interfering agents, leads to free kinetochore sites, which activate the mitotic spindle assembly checkpoint. Consequently, the transition to the anaphase is blocked by inhibition of the anaphase-promoting complex. On the other hand, microtubule-stabilizing agents block the formation of spindle fibers even before mitosis is started. When cells are already in mitosis, these agents stabilize the spindle, finally preventing cytokinesis and cell cycle progression.

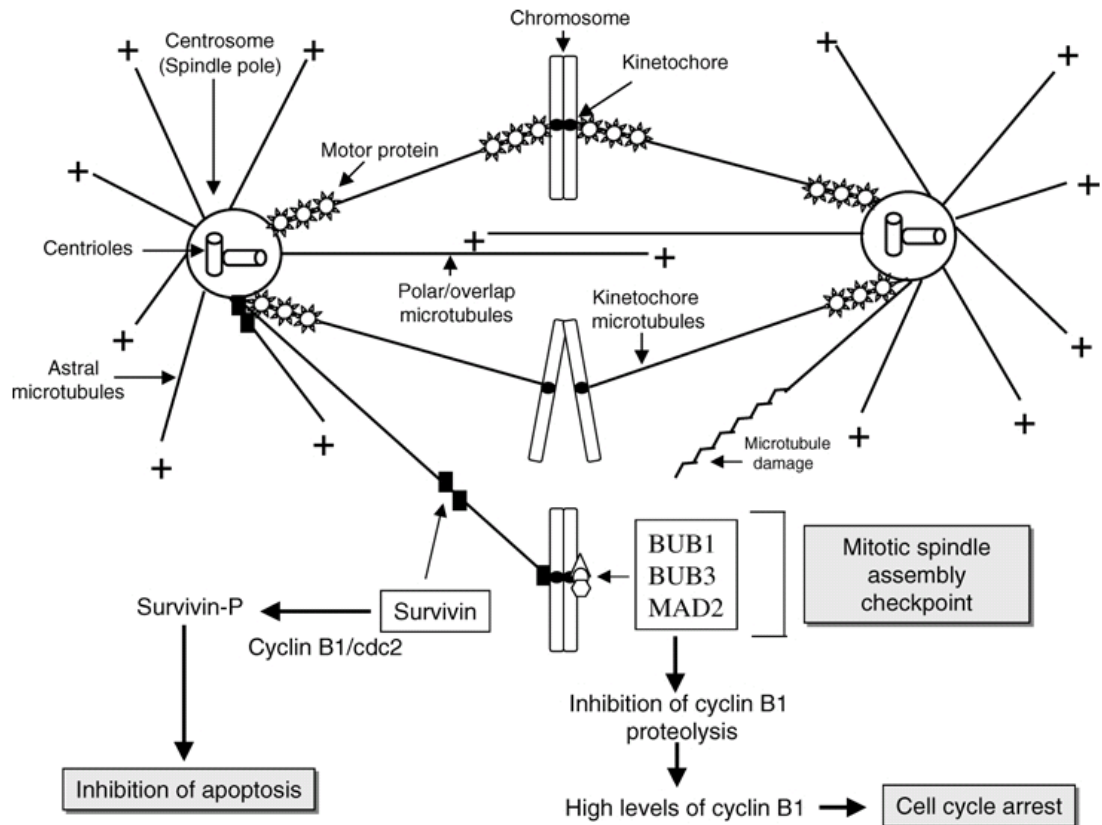


Figure 3.2: Schematic drawing of the mitotic spindle (Mollinedo and Gajate, 2003). Microtubules are organized by the spindle poles or centrosomes, containing a pair of centrioles each, with the microtubule plus ends projecting away from the centrosomes. Three classes of microtubules are distinguished in the mitotic spindle serving different functions during mitosis. Kinetochore microtubules bind to the kinetochores and play a key role in attaching the chromosomes to the spindle and in mediating chromosome movement. Polar or overlap microtubules interdigitate at the equator of the spindle, provide the symmetrical and bipolar shape of the spindle, and mediate spindle separation in anaphase. Astral microtubules radiate away in all directions from the centrosomes and contribute to position the spindle in the cell and to the forces that separate the poles. The roles of the types of microtubules differ due to the binding of different protein complexes that control their respective properties and dynamics. Chromosome movement is mediated by both microtubule dynamics and by the action of motor proteins. Anaphase ensues only when all the kinetochores of each pair of sister chromatids are bound to microtubules (upper chromosome), and a tension is exerted on kinetochores by pulling them through the kinetochore microtubules to opposite directions (middle chromosome). A free kinetochore (lower right chromatid) activates the mitotic spindle assembly checkpoint, which inhibits the anaphase-promoting complex, leading to a blockage in cyclin B1 proteolysis, and thereby to an increased cyclin B1 level and cell cycle arrest at the M phase. Survivin, located in microtubules and kinetochores, seems to play a key role in preserving microtubule integrity and in inhibiting apoptosis during normal cell cycle, and may circumvent checkpoint mechanisms of growth arrest. Only microtubule-bound survivin associates with cdc2 and prevents apoptosis during normal mitosis through a cyclin B1/cdc2-mediated phosphorylation (lower left chromatid). BUB: budding uninhibited by benzimidazole; MAD: mitosis arrest deficient.

3.1.1.2 Microtubule interfering agents

Microtubules are a valuable target for cancer chemotherapy due to their crucial role in vital cellular functions for tumor cells, including mitosis, motility and cell-cell contacts. A large number of chemically diverse compounds are capable to bind tubulin or microtubules leading to the disruption of the mitotic spindle and the inhibition of cell proliferation.

The alkaloid colchicine from *Colchicum autumnale* L. is one of the first compounds identified as “mitotic spindle poisons” (Levan, 1938). However, colchicine is not in use as a cytostatic drug due to its small therapeutic index, defined as the ratio of maximum tolerated dose/minimum effective dose. Two decades later, alkaloids from *Vinca rosea* L. were described as agents arresting cells in mitosis with aberrant mitotic spindles (Palmer et al., 1960). Subsequently, vincristine and vinblastine were introduced into clinical practice in the 1960s. They are still in use as important chemotherapeutic drugs in combinative treatment regimen, e.g. for the curative therapy of testicular cancer, Hodgkin disease, and acute lymphatic leukemia, or for the palliative therapy of solid tumors. In 1986, paclitaxel, isolated from *Taxus brevifolia* L., entered into clinical trials. Paclitaxel has proven to be one of the most broadly effective anticancer agents. Due to its effectiveness against a broad spectrum of tumors and its therapeutic success, the interest in microtubules as a pharmacological target structure increased dramatically and led to extensive efforts put in the development of further, more potent and better tolerated inhibitors of microtubule function (Attard et al., 2006). Naturally derived compounds, such as epothilones, which are secondary metabolites from myxobacteria (Altmann et al., 2000), and coral-derived eleutherobin derivatives (Hamel et al., 1999; McDaid et al., 1999) were evaluated in preclinical investigations. Also many new taxanes, paclitaxel prodrugs, and new formulations of classical microtubule-interfering agents have been in clinical development (Wood et al., 2001).

The microtubule function is maintained in a dynamic state of polymerization and depolymerization (Mitchison, 1984; Desai, 1997). The vinca alkaloids and colchicine promote destabilization of microtubules, leading to depolymerization, whereas paclitaxel and other taxanes stabilize microtubules by blocking depolymerization (Schiff, 1979; Schiff, 1980). Both attacks to the equilibrium between polymerization and depolymerization lead to the disruption of this dynamic process and thus to a breakdown of the integrative function of polymeric tubulin. In this way it can be explained that both types of microtubule interfering agents share the common principle of suppressing microtubule dynamics and thereby microtubule functions, although these compounds have opposite effects on microtubules, (Jordan, 1998).

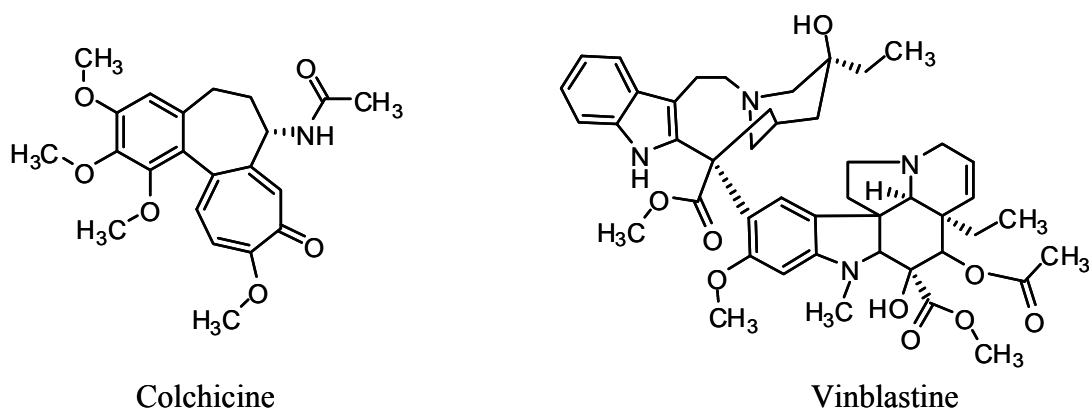


Figure 3.3: Chemical structures of compounds leading to microtubule depolymerization.

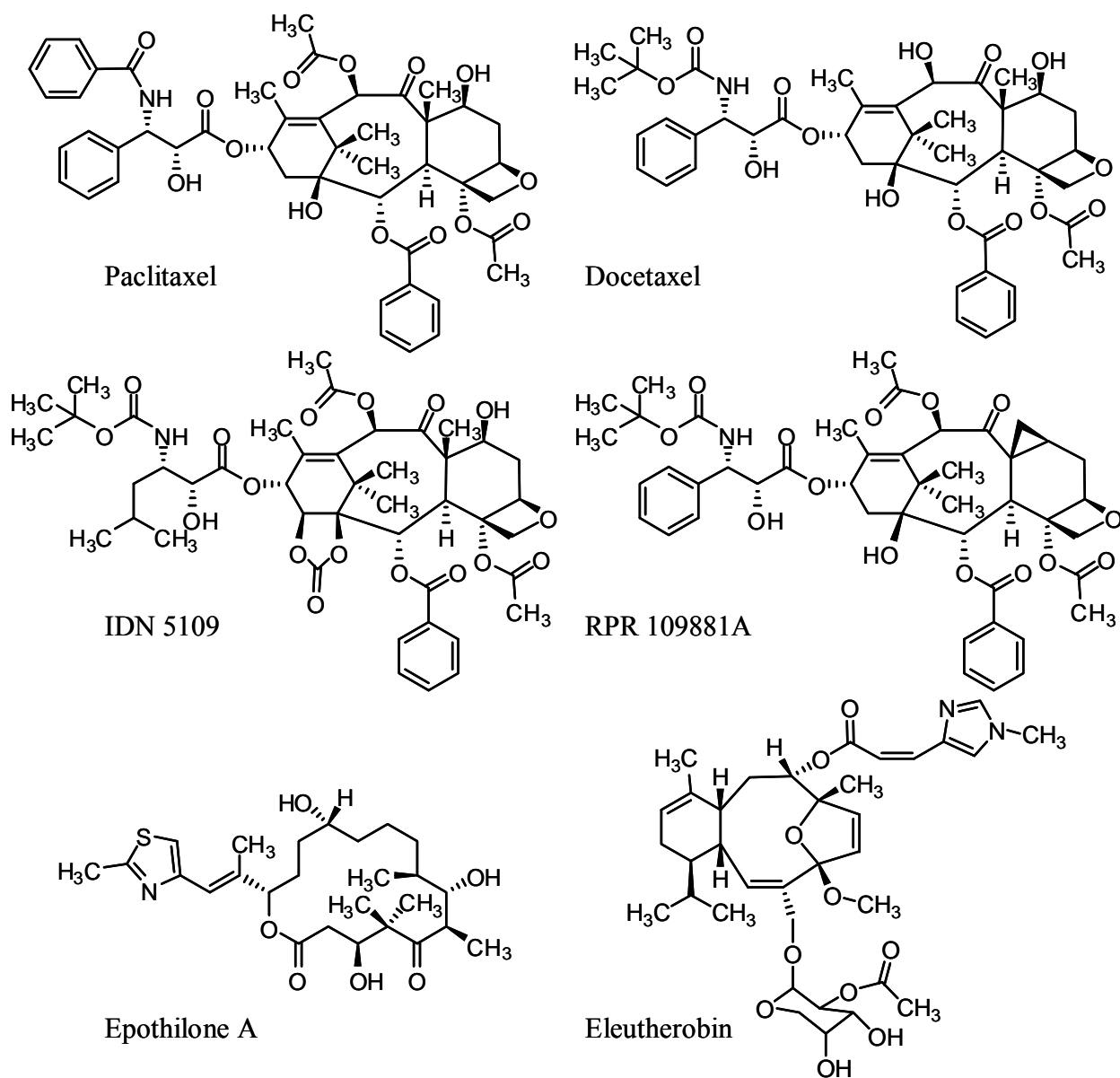


Figure 3.4: Inhibitors of microtubule depolymerization. The cellular target of paclitaxel, docetaxel, RPR 109881A, IDN 5109 and epothilone A is the β -tubulin in the microtubule polymer. The exact binding site for eleutherobin is not known yet (Mollinedo and Gajate, 2003).

Figure 3.3 and Figure 3.4 show the chemical structures of microtubule-interfering agents, inhibiting microtubule polymerization and depolymerization, respectively. Moreover, microtubule interfering agents can be classified into three major categories based on their respective tubulin binding domains, which include the “colchicine” domain, the “vinca alkaloid” domain, and the “paclitaxel” domain (Mollinedo and Gajate, 2003).

Because microtubules are also involved in a large number of other cellular functions, including chemotaxis, membrane and cellular scaffolding, intracellular transport, secretory processes and transmission of receptor signaling, microtubule interfering agents may affect malignant and nonmalignant cells in interphase, in addition to the mitotic phases of the cell cycle. This lack of selectivity towards tumor cells leads to a number of toxic side effects, variable and unpredictable pharmacology and dose-limiting toxicities. Severe peripheral neuropathy occurs in as many as 30 % of patients treated with taxanes (Lee and Swain, 2006). A major problem in the clinical use of tubulin-binding agents is the development of resistance in the tumor tissue. The vinca alkaloids and the taxanes are both substrates of the ABCB1 transporter (p-glycoprotein 170, MDR1) (Kohno et al., 1988; Hunter et al., 1991; Zacherl et al., 1994), and it has been shown that ABCB1 expression causes resistance and reduced sensitivity to those compounds in vitro (Izquierdo et al., 1996; Loe et al., 1996). The new compounds IDN 5109 (Bayer, Leverkusen, Germany) and RPR 109881A (Aventis, Strasbourg, France) are expected to circumvent the ABCB1 mediated multidrug resistance in vivo, and have shown promising effects, when applied to ABCB1 overexpressing tumor cell lines (Polizzi et al., 1999; Gelmon et al., 2000).

Despite the ongoing development of novel microtubule-interfering compounds the occurrence of the same side effects is probable. Thus, other targets providing a similar mechanism of action with greater specificity were explored. In the past few years, more information about the components involved in mitosis and their relationship to each other and to mitotic events was obtained. Although the understanding of these processes is incomplete, several key regulators were identified. The most prominent regulatory molecules involved in the progression through mitosis include members of several kinase families. They play important roles in the proper ordering of events within mitosis. It has become clear that although tubulin is the most abundant protein within the mitotic spindle, many additional proteins play critical roles in the mechanics of mitosis. Most prominent among these are members of the kinesin family of microtubule motor proteins. Previous studies have demonstrated a role for the mitotic kinesin Eg5 in establishment of spindle bipolarity in mammalian cells (Blangy et al., 1995).

3.1.2 Mitotic spindle assembly

Two motile processes are involved in the assembly and disassembly of microtubules and in segregation of chromosomes. The first is the polymerization and depolymerization of microtubules (Figure 3.5) physiologically regulated by a balance of microtubule stabilizing and destabilizing proteins, binding along the microtubules (Andersen, 2000).

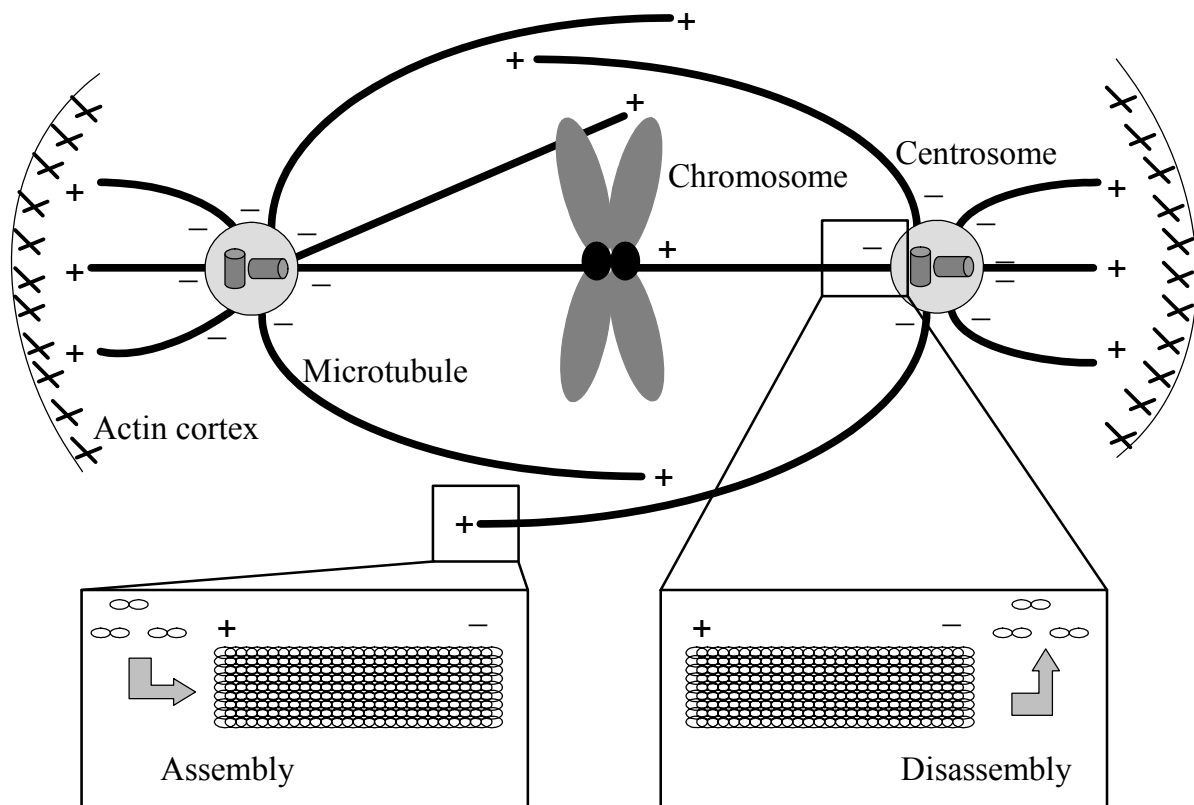


Figure 3.5: Structure and polarity patterns of microtubules in the metaphase spindle. Microtubule assembly occurs at the fast growing plus end by tubulin polymerization and disassembly at the minus end by depolymerization (from Sharp et al., 2000, modified).

Stabilizing proteins include the large group of the so-called microtubule-associated proteins (MAPs) (Mandelkow, 1995). These MAPs are substrates of the cyclin-dependent kinase 1 (CDK1), and, depending on their phosphorylation state, they control the microtubule dynamic properties in the transition from the G2 to the M phase of the cell cycle. During mitosis an increased degree of phosphorylation reduces the affinity of the MAPs to microtubules, and thereby their promoting effect on tubulin-polymerization (Drechsel, 1992; Masson, 1995; Ookata, 1995).

Oncoprotein 18/stathmin and katanin are destabilizing factors promoting microtubule depolymerization (McNally, 1993; Larsson, 1997; Ahmad et al., 1999; Andersen, 2000). The *Xenopus* kinesin central motor 1 (XKCM1), a kinesin-related protein, particularly contributes to microtubule depolymerization during mitotic spindle assembly (Walczak et al., 1996).

The second motile process is the ATP-dependent sliding of microtubule-binding motor proteins along the walls of microtubules. These motor proteins can be subdivided into two superfamilies of ATP-dependent force-generating enzymes, the kinesins and the dyneins (Vale and Fletterick, 1997). They move continuously along the microtubules, and thereby can carry various membrane-enclosed organelles to their destination within the cytoplasm or rearrange filament networks. Moreover, they serve important functions in the mitosis phase, e.g. movement of cytoskeletal filaments against each other, which is an indispensable process too. The N-terminal kinesins play a crucial role in mitotic spindle formation and in chromosome separation and transport. They move towards the plus end of the microtubules (Mandelkow, 1999). However, another kinesin subfamily, the C-terminal motor domain type kinesins move towards the minus end (Noda et al., 2001; Xu et al., 2002). The dyneins are also minus end directed motor proteins, contributing to vesicular trafficking, and to the positioning of cell organelles.

During mitosis, the chronology of the interplay between microtubule-dynamics and motor proteins is controlled by several regulatory molecules such as Bub and Mad kinases. Those are essential components of the mitotic spindle assembly check point (Sorger et al., 1997; Skoufias et al., 2001), which monitors that all chromosomes are bivalently attached to microtubules via kinetochores, before mitosis is moving from the metaphase to the anaphase (Li and Benezra, 1996; Rudner and Murray, 1996; Sorger et al., 1997).

Other regulatory proteins, such as the Aurora B family kinases, play an essential role in chromosome segregation and subsequent cytokinesis, the cytoplasmic division of the cell in the end of mitosis. They are also required for the orientation, condensation and cohesion of chromosomes, and they are involved in microtubular dynamics (Shannon, 2002).

3.1.3 Microtubule-based motor proteins

Two superfamilies of microtubule-based motor proteins have been discovered, the kinesins and the dyneins. Beside tubulin, the kinesins are the most prominent proteins contributing to the proper functionality of the mitotic spindle. The general structural features of the kinesin motors are similar throughout the whole protein superfamily (Vale and Fletterick, 1997). The

force-producing motor domain is divided into two major parts: one part is the globular catalytic core, which is conserved throughout the superfamily. The second part, the neck region, with a length of around 40 amino acids, is either adjacent at the N or C terminus of the catalytic core. Many kinesin proteins contain a long α -helical coiled-coil domain, the “stalk”, which is often connected to an additional globular domain at its end. The latter domain, the “tail”, is thought to target the motor to a particular cargo within the cell.

The kinesins hydrolyze ATP and travel unidirectionally along the microtubule surface. The N-terminal kinesins are plus end directed, and the C-terminal kinesins are minus end directed. In mitosis, the N-terminal kinesins produce an outward-directed force, whereas the C-terminal kinesins act vice versa. A further minus end directed force is exerted by the motor proteins of the dynein superfamily. The specific movement of the mitotic spindle is not driven by the exclusive action of one type of motor protein, but by the simultaneous work of multiple, complementary and antagonistic motors (Sharp et al., 2000). During interphase and prophase, the duplicated centrosomes and slightly interdigitating microtubules between the two future poles of the spindle are formed. This initial spindle assembly is balanced by dynein on the actin cortex at the cell membrane pulling the poles apart (outward-directed force), and C-terminal kinesins in the spindle midzone pulling the poles together (inward-directed force). The C-terminal kinesin force is limited due to the low extent of microtubule overlap in the midzone. However, with the continuous growth of the interdigitating microtubules, the kinesin force gradually increases until a steady state between the dynein and the kinesin forces is reached. After the degradation of the nuclear envelope in the prometaphase, another steady state is achieved. The length of the astral microtubules is decreased and the position of the bipolar spindle is determined and maintained by the action of the C-terminal kinesins and the bipolar kinesins (e.g. Eg5 kinesin). The bipolar kinesins are also located in the spindle midzone and generate an outward-directed force. The poles move further apart due to cortical dynein plus bipolar kinesin activity, overwhelming the inward directed forces generated by the C-terminal kinesin and tipping the balance of forces in the outward direction (Figure 3.6). At the onset of anaphase, the elongation of the spindle results in the “metaphase spindle steady state structure” with tension between the spindle poles, generated by antagonistic “inward” and “outward” forces. After passing the metaphase-anaphase checkpoint (mitotic spindle assembly checkpoint) the tension is released by inactivation of the C-terminal kinesins. Just before the disassembly of the spindle, the final steady state is achieved in the telophase.

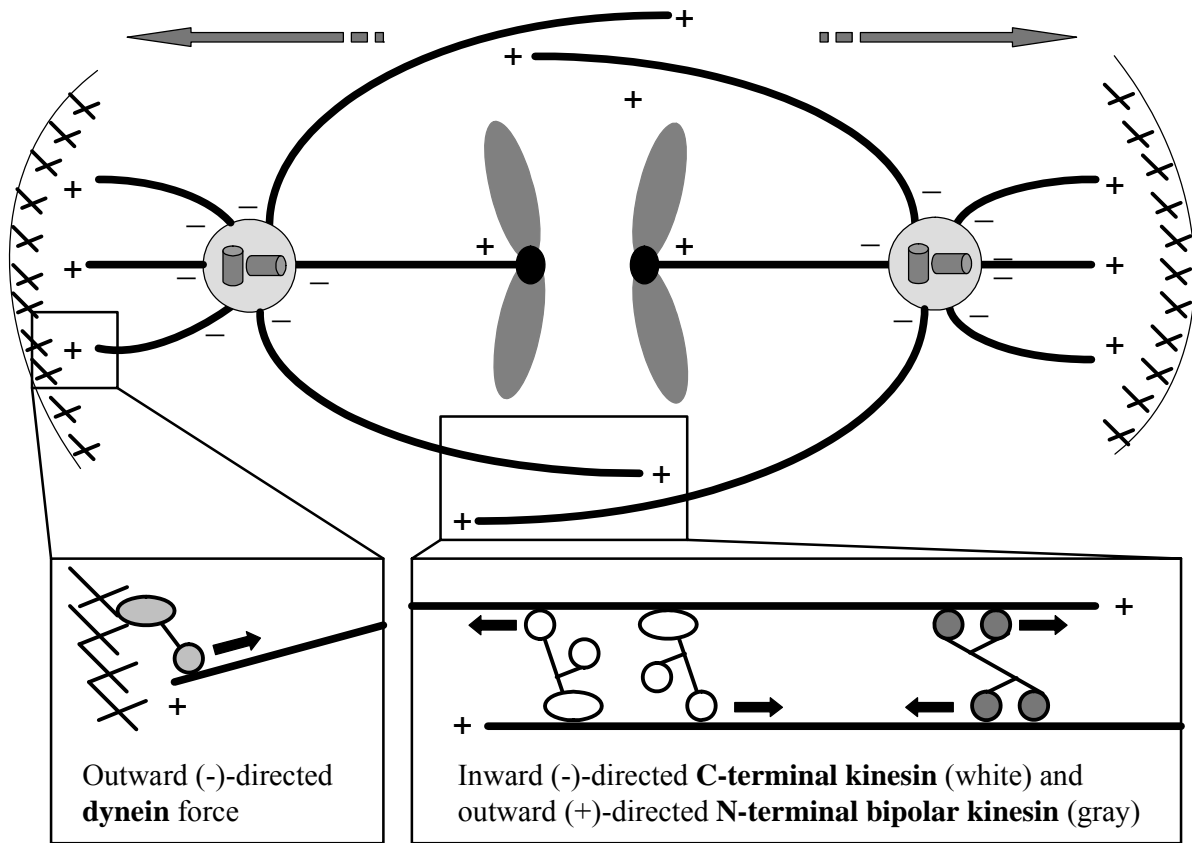


Figure 3.6: Schematic drawing of the prometaphase-metaphase transition. The spindle poles move apart from each other, due to the overweight of outward directed forces. Dynein mediates the interaction between astral microtubules and the actin cortex (dynactin). The major contribution to the outward directed forces is given by the bipolar kinesins, which enforce anti-parallel sliding of the interdigitating microtubules of the spindle midzone. Together, these two forces overcome the inward directed force, produced by C-terminal kinesins, also located at the spindle midzone. The short arrows indicate the moving direction of the motor proteins along the microtubules, which is opposite to the direction of the produced force.

It has been suggested that the expression of certain subtypes is restricted to proliferating tissues, and crucial for mitosis progression due to the cell cycle-dependent degradation of several kinesins (Brown, 1994; Funabiki, 2000; Hill, 2000). Furthermore, these mitotic kinesins have been shown to play essential roles during discrete phases of mitosis (Table 3.1). Dysfunction of certain members of this protein family has been shown to result in mitotic arrest. For example, the kinesin CENP-E has been shown to be an essential component of the mitotic spindle assembly checkpoint *in vitro* (Abrieu et al., 2000). It connects the checkpoint complex to free kinetochores of microtubule-attached chromosomes (Schaar et al., 1997; Yao et al., 2000) and interacts with different kinetochore proteins (Chan et al., 1998). Playing a

vital role in mitosis, this and other kinesins have been considered as potential new pharmacological targets for the treatment of malignancies.

Table 3.1: Role of various mitotic kinesins in mitosis (Wood et al., 2001).

Mammalian kinesin ⁽¹⁾	Functional role	Experimental validation ⁽²⁾	Mitotic arrest ⁽³⁾
Eg5	Spindle pole separation	Human cells	+
HSFT	Microtubule anchorage at the spindle poles	Human cells	-
MKLP1	Microtubule organization in metaphase spindle midzone	Human cells	+
	Late mitotic spindle microtubule organization and cytokinesis	<i>Drosophila</i> , <i>Caenorhabditis elegans</i>	
Kif4	Metaphase chromosome alignment	<i>Xenopus</i> egg extracts and embryos	n. d.
CENP-E	Metaphase chromosome alignment	Human cells	+
Kid	Metaphase chromosome alignment	<i>Xenopus</i> egg extracts	n. d.
MCAK	Anaphase chromosome alignment	Human cells	-
RabK6	Cytokinesis	Human cells	-

- (1) In cases where validation has been performed in non-mammalian systems, the mammalian ortholog of the validated kinesin is indicated.
- (2) Non-mammalian systems are noted only for those kinesins where a mitotic role has not been demonstrated in mammalian cells.
- (3) Dysfunction in kinesin causes mitotic arrest (+), dysfunction does not cause mitotic arrest (-); effect not determined (n. d.).

3.1.4 Mitotic arrest through Eg5 kinesin inhibition

Eg5 is a plus end directed motor protein and belongs to the bipolar kinesin family (Sawin et al., 1992). It has been shown to be tetrameric, with pairs of motor domains at opposite ends of the molecule (Kashina et al., 1996). Due to its tetrameric, bipolar structure, kinesin Eg5 could function in two ways to promote spindle formation. Firstly, Eg5 promotes the formation of a spindle axis by cross-linking two microtubules, which are in the same orientation and moving towards their plus ends. Secondly, microtubules in opposite orientations are pushed apart by Eg5 and are thereby sorted into an antiparallel array (Walczak et al., 1998). The inhibition of Eg5 kinesin causes spindle pole defects and results in “rosette” structures with unseparated centrosomes in the center and microtubules extending radially to surrounding chromosomes (Sawin et al., 1992).

This characteristic spindle morphology with a monoastral spindle is termed “monoaster spindle” (Figure 3.7). The monoaster spindle is probably caused by an imbalance between the outward and inward directed forces, generated by dyneins and C- and N-terminal kinesins.

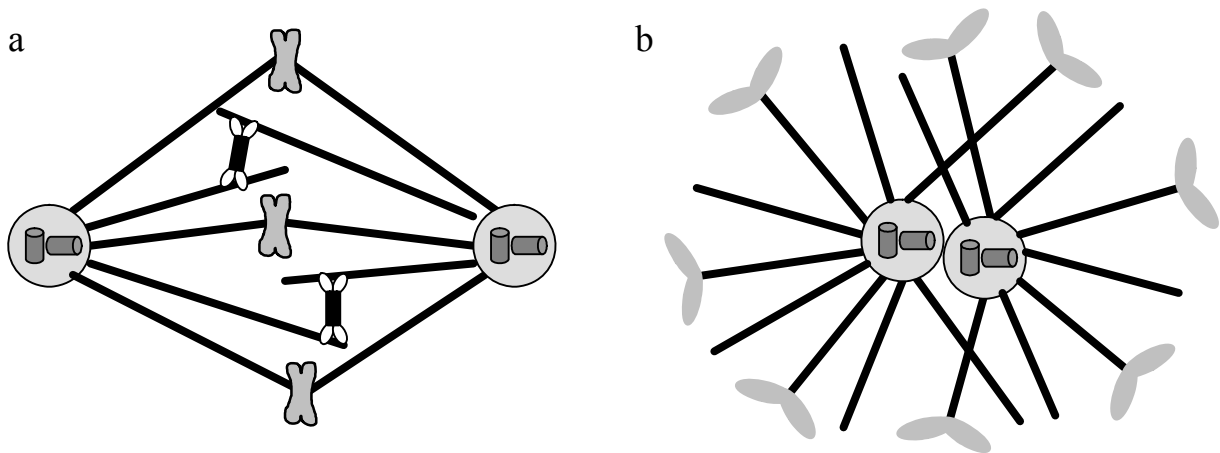


Figure 3.7: (a) Model of spindle bipolarity. Plus end directed kinesins, such as Eg5, are involved in the separation of centrosomes and the establishment of a symmetric spindle axis. Microtubules are shown in black, chromosomes in gray and Eg5 in white as a homotetramer (Walczak et al., 1998). (b) The inhibition of bipolar Eg5 kinesin leads to an overweight of the inward-directed force of the C-terminal kinesins and thus results in the formation of monoastral spindles (Sawin et al., 1992; Blangy et al., 1995).

After the monoaster spindle has completely formed, several free kinetochores of chromosomes are only partially connected to microtubules. As a consequence, mitotic arrest occurs because the mitotic spindle assembly checkpoint cannot be satisfied and the transition from the metaphase to the anaphase is blocked. The inhibition of the mitotic kinesin Eg5 leaves other essential cellular processes, which involve non-mitotic kinesins, unaffected. Due to this major difference to the classical microtubule-interfering agents, specific Eg5 kinesin inhibitors are considered a very promising approach to the development of a new class of anticancer agents with minimal side effects on resting cells.

3.1.5 Eg5 kinesin inhibitors

Sakowicz et al. screened a panel of natural compounds for selective inhibition of kinesin in vitro and identified the first kinesin inhibitor, adociasulfate-2, which competitively inhibits the interaction of the kinesin motor domain with microtubules (Sakowicz et al., 1998). However, this first kinesin inhibitor did not show any selectivity between the three kinesin subtypes. Since only the kinesin Eg5 is known to cause mitotic arrest with the formation of a monopolar mitotic spindle, the monoaster spindle was used as an indicator in the search for specific Eg5 inhibitors. Using a mitotic spindle phenotype-based screening method, Mayer et al. identified monastrol as the first specific kinesin Eg5 inhibitor (Mayer et al., 1999). This compound, a 4-aryl-3,4-dihydropyrimidine-2(1*H*)-thione, led to a reversible mitotic arrest by the formation of a monopolar spindle, and did not affect the transition from the G2 cell cycle phase to mitosis. Moreover, monastrol did not inhibit the motor activity of conventional kinesin heavy chain, and therefore, had no effect on cellular processes involving other kinesins (Mayer et al., 1999; Kapoor et al., 2000). These results provide the first evidence that the concept of the specific Eg5 kinesin inhibition as a new approach in cancer chemotherapy is feasible. However, racemic monastrol and its eutomer, (*S*)-monastrol, were determined to be only moderately potent allosteric inhibitors of Eg5 (Gartner et al., 2005) with IC₅₀ values of 34 μ M and 14 μ M, respectively, determined in the microtubule-stimulated ATPase activity assay (Maliga, 2002). Therefore, new monastrol analogs were synthesized (Gartner et al., 2005; Sarli et al., 2005) in order to obtain more potent Eg5 kinesin inhibitors. Hotha et al. reported on the tetrahydro- β -carboline compound HR22C16, which selectively inhibited Eg5 kinesin with an IC₅₀ value of 800 nM (Hotha et al., 2003). A derivative of HR22C16 showed an IC₅₀ value of 90 nM, which is about one order of magnitude more potent than HR22C16. After the screening of a series of 60 β -carboline derivatives for Eg5 inhibitory activity, the most potent compound showed an IC₅₀ value of 650 nM (Sunder-Plassmann et al., 2005). Further lead structures are currently considered as potent and specific kinesin Eg5 inhibitors. Among them are terpendole E (IC₅₀ = 23 μ M) (Nakazawa, 2003), CK0106023 with a K_i value of 12 nM (Sakowicz, 2004), and KSP-IA, a compound derived from a dihydropyrazole lead structure (IC₅₀ = 10 nM (Tao et al., 2005)). In a high-throughput screening effort, Tarby et al. identified a series of tetrahydroisoquinolines as inhibitors of human Eg5 including a screening hit with an IC₅₀ value of 9.7 μ M (ATPase assay) (Tarby et al., 2006). A medicinal chemistry optimization effort led to the identification of “compound 32a” as a potent Eg5 inhibitor with an IC₅₀ value of 104 nM (Figure 3.8).

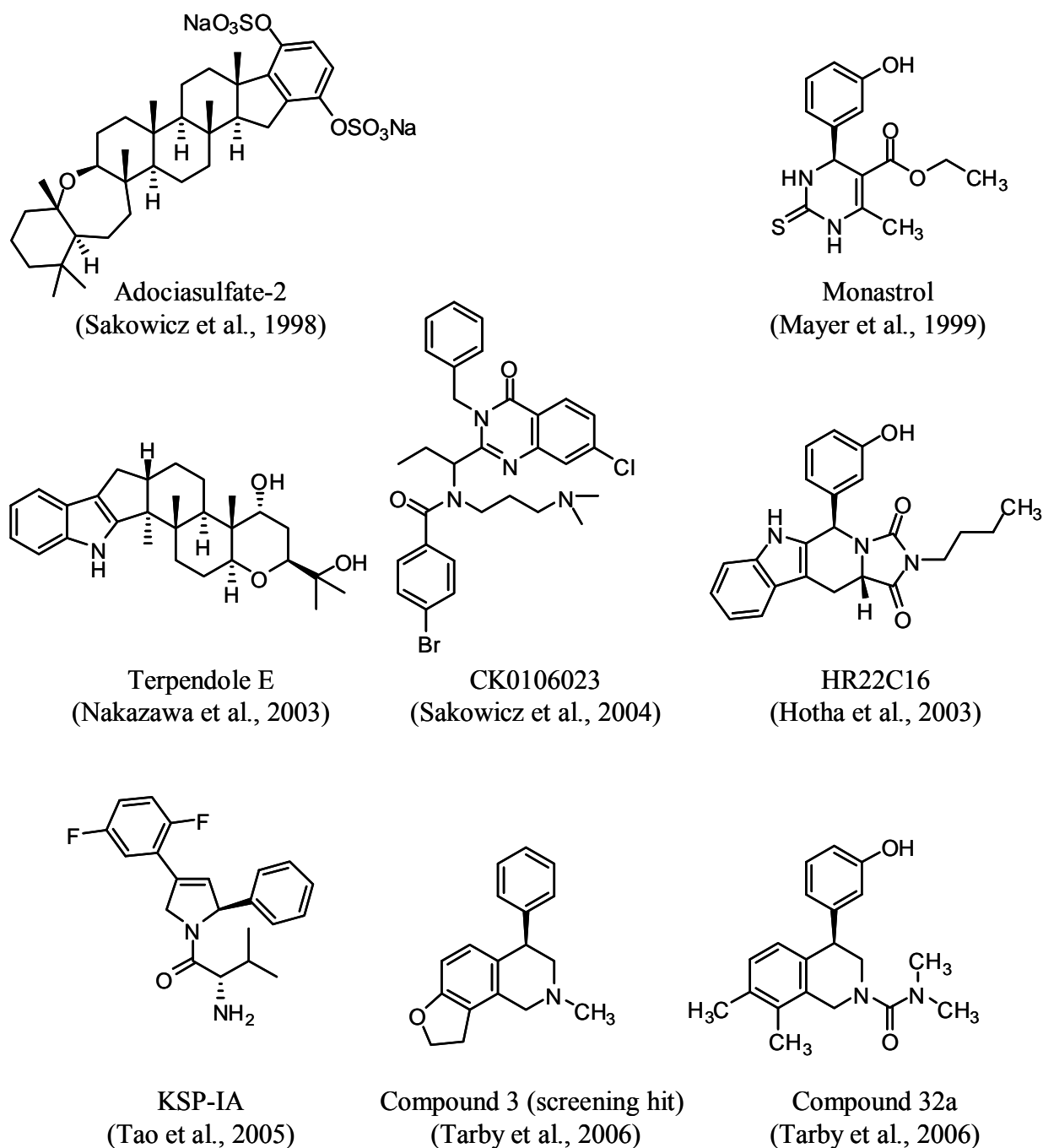


Figure 3.8: Chemical structures of various kinesin inhibitors. Adociasulfate-2, was isolated from a marine sponge, the genus *Haliclona* (also known as *Adocia*) (Sakowicz et al., 1998). The identification of the first specific Eg5 kinesin inhibitor monastrol (Mayer et al., 1999) initiated the development and the preclinical evaluation of further, more potent Eg5 inhibitors as potential new anticancer agents. Among the other lead compounds, structural resemblance to monastrol is only observed for the β -carboline derivative HR22C16 (Hotha et al., 2003). Terpendole E inhibits Eg5 kinesin specifically (Nakazawa, 2003), but with an even lower potency than monastrol. Based on CK0106023 (Sakowicz, 2004), a series of new 2-(aminomethyl)quinazolinone derivatives has been synthesized, of which one is in clinical phase II evaluation. The KSP-IA is the most potent specific Eg5 kinesin inhibitor by now (Tao et al., 2005). A medicinal chemistry optimization effort of a high-throughput screening hit (compound 3) led to the identification of R-4-(3-hydroxyphenyl)-N,N-7,8-tetramethyl-3,4-dihydroisoquinoline-2(1H)-carboxamide named compound 32a (Tarby et al., 2006).

3.2 Objective

The inhibition of kinesin Eg5 by small molecules, such as monastrol, is currently evaluated as an approach to develop a novel class of antiproliferative drugs for the treatment of malignant tumors (Wood et al., 2001). Due to the moderate inhibitory activity of the lead compound monastrol, new monastrol analogs were synthesized by Giannis and coworkers at the University of Leipzig (Gartner et al., 2005; Sarli et al., 2005), in order to obtain more potent Eg5 kinesin inhibitors. Experiments by means of confocal laser scanning microscopy demonstrated that the antiproliferative activity of the new compounds is caused by monoaster formation and subsequent mitotic arrest of the treated cells (Gross, 2006). The common clinical side effects of classical microtubule interfering agents are ascribed to the damage of the microtubule cytoskeleton (Quasthoff and Hartung, 2002). Thus, Dietmar Gross showed that the arrangement of β -actin and tubulin, vital components of the cytoskeleton of mitotic and quiescent cells, were not affected by the new compounds. The effects of the monastrol analogs were compared to the classical tubulin depolymerising agent vinblastine.

With respect to the treatment of primary and secondary CNS tumors, the objective of this work was to investigate the antiproliferative effect of the new monastrol analogs on human glioblastoma cell variants, using the crystal violet chemosensitivity assay (Bernhardt et al., 1992). This project comprises the determination of the antiproliferative activity after the pre-incubation of the compounds in culture medium to consider potential inactivation of the compounds by esterases or binding to serum proteins. The incubation of the cells for 1, 3 and 6 hours with the Eg5 inhibitors was intended to identify the required duration of drug exposure. Furthermore, confluent cells should be treated with Eg5 inhibitors to compare their effects with those of anti-tubulin drugs like paclitaxel against resting cells. Due to the necessity of overcoming the blood-brain barrier in the treatment of brain tumors, we planned to investigate if the Eg5 inhibitors are modulators of the ABCB1 transporter (p-glycoprotein 170) at effective antiproliferative concentrations, using the calcein-AM assay (Homolya et al., 1993; Hollo et al., 1994; Homolya et al., 1996).

The results have been published in part (Müller et al., 2007).

3.3 Materials and methods

3.3.1 Kinesin Eg5 inhibitors

Monastrol and the new monastrol analogs dimethylenastron, enastron, were synthesized and characterized as described (Gartner et al., 2005; Sarli et al., 2005). The 3,4-dihydro-4-(3'-hydroxyphenyl)quinazoline-2(1*H*)-thiones, the vasastrols, VS-12, VS-17, VS-38, VS-42, VS-48, VS-54, VS-83 as well as the 3,4-dihydrophenylquinazoline-2(1*H*)-thiones VS-1, VS-43 and VS-46 were synthesized and characterized as described (Sarli et al., 2005). These compounds and another substance, G-72, were provided by the workgroup of Prof. Giannis (University of Leipzig, Germany). S-Trityl-L-cysteine (Brier et al., 2004) was purchased from MP BIOMEDICALS (Eschwege, Germany) (Figure 3.9). 10 mM stock solutions were prepared in DMSO and stored at -20 °C.

3.3.2 Cell lines and culture conditions

Human U-87 MG (HTB 14), U-118 MG (HTB 15), and U-373 MG (HTB 17) glioblastoma/astrocytoma cell lines were obtained from ATCC (Rockville, MD, USA). Cell banking and quality control were performed according to the "seed stock concept" (Hay, 1988). U-87 MG and U-373 MG cells were grown in Eagle's minimum essential medium containing L-glutamine, 2.2 g/L NaHCO₃, 110 mg/l sodium pyruvate and 5 % fetal calf serum (FCS), whereas the U-118 MG cells were maintained in Dulbecco's minimal essential medium supplemented with 5 % FCS. Kb-V1 cells, a ABCB1 (p-gp 170) overexpressing subclone (Kohno et al., 1988; Hubensack, 2005) of Kb cells (ATCC CCL-17), were maintained in Dulbecco's modified Eagle's medium supplemented with 10 % FCS and 300 ng/ml vinblastine (SIGMA, Munich, Germany). All cell types were maintained in water saturated atmosphere (95 % air/5 % carbon dioxide) at 37 °C in 75-cm² culture flasks (NUNC, Wiesbaden, Germany) and were serially passaged following trypsinization using 0.05 % trypsin/0.02 % EDTA (Roche Diagnostics, Mannheim, Germany). Mycoplasma contamination was routinely monitored by PCR (Venor® GeM, Minerva Biolabs GmbH, Berlin, Germany), and only *Mycoplasma* free cultures were used.

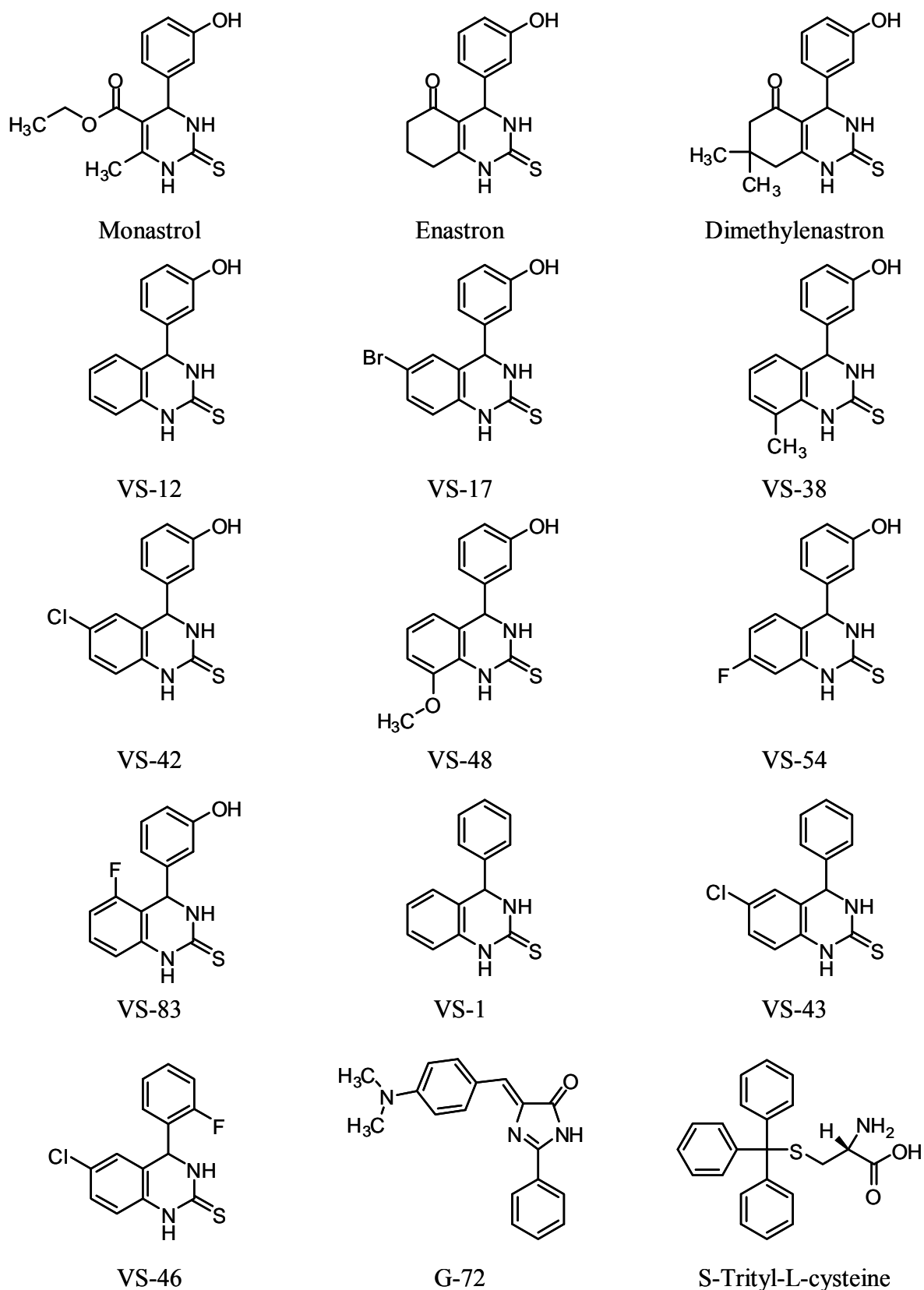


Figure 3.9: Chemical structures of the selective Eg5 inhibitor monastrol, the new monastrol analogs enastron and dimethylenastron, the 3,4-dihydro-4-(3'-hydroxyphenyl)quinazoline-(1H)-thiones VS-12, VS-17, VS-38, VS-42, VS-48, VS-54, VS-83, the 3,4-dihydrophenylquinazoline-2(1H)-thiones VS-1, VS-43 and VS-46, the Eg5 inhibitor G-72 and the non-specific kinesin inhibitor S-trityl-L-cysteine.

3.3.3 Chemosensitivity assay

The assays were performed as described previously (Bernhardt et al., 1992). In brief, tumor cell suspensions (100 μ l/well) were seeded into 96-well flat-bottomed microtitration plates (GREINER, Frickenhausen, Germany) at a density of ca. 15 cells/microscopic field (magnification 320-fold). After 2–3 days, the culture medium was removed by suction and replaced by fresh medium (200 μ l/well) containing varying drug concentrations or vehicle (DMSO). Drugs were added as 1,000-fold concentrated feed solutions. On every plate 16 wells served as controls and 16 wells were used per drug concentration. After various times of incubation the cells were fixed with glutardialdehyde (Merck, Darmstadt, Germany) and stored at 4 °C. At the end of the experiment, all plates were processed simultaneously [staining with 0.02 % aqueous crystal violet (SERVA, Heidelberg, Germany) solution (100 μ l/well)]. Excess dye was removed by rinsing the trays with water for 20 min. The stain bound by the cells was re-dissolved in 70 % ethanol (180 μ l/well) while shaking the microplates for about 3 h. Absorbance at 578 nm (a parameter proportional to cell mass) was measured using a BIOTEK 309 Autoreader (TECNOMARA, Fernwald, Germany). Drug effects were expressed as corrected T/C-values for each group according to

$$T/C_{\text{corr}} = \frac{T - C_0}{C - C_0} \cdot 100 [\%] \quad (\text{eq. 3.1}),$$

where T is the mean absorbance of the treated cells, C the mean absorbance of the controls and C_0 the mean absorbance of the cells at the time ($t = 0$) when drug was added.

When the absorbance of treated cells T is less than that of the culture at $t = 0$ (C_0), the extent of cell killing was calculated as

$$\text{cytotoxic effect } [\%] = \frac{C_0 - T}{C_0} \cdot 100 \quad (\text{eq. 3.2}).$$

3.3.4 Flow cytometric calcein-AM efflux assay

In Kb-V1 cells, calcein-AM is extruded by ABCB1 (p-gp) before esterases can cleave the ester bonds, and calcein is not accumulated (Homolya et al., 1993). Therefore, modulators of the ABCB1 function can easily be recognized by flow cytometric measurement of the change in the calcein-AM efflux.

Calcein-AM (Molecular Probes Eugene, OR, USA) was dissolved in DMSO (MERCK, Darmstadt, Germany) to achieve a final concentration of 1 mM and aliquoted into stock solutions that were stored at -20 °C. Elacridar, a 3rd generation ABCB1 inhibitor (kindly provided by GlaxoSmithKline, NC, USA) served as a positive control for the inhibition of calcein-AM efflux.

Kb-V1 cells were trypsinized 3 or 4 days after the passaging and washed with PBS at 25 °C. To 0.75 ml cell suspension containing $1 \cdot 10^6$ cells in loading buffer (120 mM NaCl, 5 mM KCl, 2 mM $\text{MgCl}_2 \cdot 6 \text{H}_2\text{O}$, 1.5 mM, $\text{CaCl}_2 \cdot 2 \text{H}_2\text{O}$, 25 mM HEPES, 10 mM glucose, pH 7.4) 0.25 ml loading suspension (loading buffer, 20 mg/ml BSA, 5 $\mu\text{l/ml}$ of Pluronic[®] F127 [Molecular Probes, Eugene, OR, USA, 20 % stock in DMSO]) was added. The samples were mixed with different concentrations of test compounds and vortexed. After 15 min, calcein-AM solution was added to achieve a concentration of 1 μM . After incubation for 10 min at 37 °C/5 % CO_2 the supernatant was discarded after centrifugation for 7 min at 4 °C and 1,100 rpm. The cell pellet was rinsed once with ice-cold PBS and resuspended in 0.5 ml of loading buffer per $1 \cdot 10^6$ cells. Calcein fluorescence was measured by a FACS Calibur[®] (Becton Dickinson, Heidelberg, Germany) flow cytometer in the FL1-H channel. In each measurement 30,000 gated events were evaluated. The photomultiplier settings were as follows: E-1 for FSC, 270 for SSC and 300 for FL1-H. Data were analyzed by the WinMDI 2.8 software.

3.3.5 Confocal laser-scanning microscopy

All investigations performed by confocal laser-scanning microscopy were done by Dietmar Gross. For details see his doctoral thesis (Gross, 2006).

3.3.5.1 Treatment of the cells

Cells were seeded into 8-well Lab-Tek Chamber Slides (NUNC, Wiesbaden, Germany). At 75 % confluency, the culture medium was replaced with medium containing 50 μ M monastrol, 1 μ M S-trityl-L-cysteine or 10 nM vinblastine. The concentrations of the new monastrol analogs were selected on the basis of chemosensitivity data, obtained by the kinetic crystal violet assay. Cells were incubated at 37 °C for 2 h.

3.3.5.2 Fixation and permeabilization of the glioblastoma cells

After the incubation with drugs, the medium was carefully removed, and the cells were fixed with 4 % paraformaldehyde solution in phosphate buffered saline (PBS) for 20 min at room temperature. Thereafter, each well was washed three times with PBS containing 0.5 % bovine serum albumin (BSA, SERVA, Heidelberg, Germany). Cells were permeabilized by incubation with PBS containing 0.5 % BSA and 1 % Triton-X 100 (SERVA, Heidelberg, Germany) for 10 min at room temperature, followed by three washing steps with PBS 0.5 % BSA.

3.3.5.3 Staining and immunofluorescence

Chromosomes were stained with SYTOXGreen[®] nucleic acid staining dye (Molecular Probes, Eugene, OR, USA). Microtubules were stained using mouse anti-human α -tubulin primary antibody (Dianova, Hamburg, Germany) and Alexa Fluor[®] 546 conjugated goat anti-mouse secondary antibody (Molecular Probes). All antibodies were used in a 1:200 dilution in PBS, containing 0.5 % BSA. β -Actin was stained with Alexa Fluor[®] 647 phalloidin (Molecular Probes). Microscopic images were acquired with a Carl Zeiss Axiovert 200M LSM510 confocal laser scanning microscope. Multi-fluorescence image acquisition was performed in multitrack acquisition mode using the following parameters: SYTOXGreen[®], 488 nm Argon laser, 505 nm longpass filter, Alexa Fluor[®] 546, 543 nm HeNe laser, 560–615 nm bandpass filter, Alexa Fluor[®] 647, 633 nm HeNe laser, 650 nm longpass filter.

3.3.5.4 Image processing

False colors were used for β -actin (red), tubulin (green) and DNA (blue). Images (Figure 3.18a) were processed with the AutoDeBlur[®] deconvolution software.

3.4 Results

3.4.1 Drug exposure and chemosensitivity

48 h after seeding glioblastoma cells were treated with monastrol, enastron, dimethylenastron, vasastrol VS-12, VS-17, VS-38, VS-42, VS-48, VS-54, VS-83, with VS-1, VS-43, VS-46 and G-72 at various concentrations up to 10 μM . In these experiments, the drug (and vehicle) containing culture media were not exchanged during the whole incubation period. The results are exemplarily summarized for U-373 MG cells in Figure 3.10, Figure 3.11, Figure 3.12 and Figure 3.13. In these plots of T/Ccorr versus time of incubation $t = 0$ indicates the time when drug was added. According to eq. 4.1, any growth curve of a drug treated cell population can be reconstructed from the T/Ccorr values and the data from the growth curve of the corresponding control (Bernhardt et al., 1992).

For enastron a cytotoxic effect was observed at a concentration of 5 μM (Figure 3.10b), whereas monastrol was less effective even at 50 μM (Figure 3.10a). A cytostatic effect (0 % T/Ccorr towards the end of the incubation period, i.e., 100 % inhibition of net cell proliferation) was observed at 1 μM of dimethylenastron (Figure 3.10c). Compared to monastrol, the two new compounds showed an at least one order of magnitude higher antiproliferative activity against the glioblastoma cells.

The vasastrols VS-12, VS-38 and VS-42 showed no relevant cytotoxic effect up to a concentration of 10 μM (Figure 3.11a, c, d). A cytotoxic effect was observed for VS-17 (Figure 3.11b) and VS-48 (Figure 3.12a) at a concentration of 10 μM . The vasastrols VS-54 and VS-83 showed a strong cytostatic effect at a concentration of 10 μM and 5 μM , respectively. Compared to monastrol, VS-83 showed an at least one order of magnitude higher antiproliferative activity against the glioblastoma cells.

Even at a high concentration of 10 μM , all 3,4-dihydrophenylquinazoline-2(1*H*)-thiones, VS-1, VS-43 and VS-46 (Figure 3.13a, b, c), were ineffective. However, the (Z)-4-(4-(dimethylamino)benzylidene)-2-phenyl-1*H*-imidazol-5(4*H*)-one, G-72, showed cytotoxic and cytostatic effects at a concentration of 1 μM and 10 μM , respectively (Figure 3.13d).

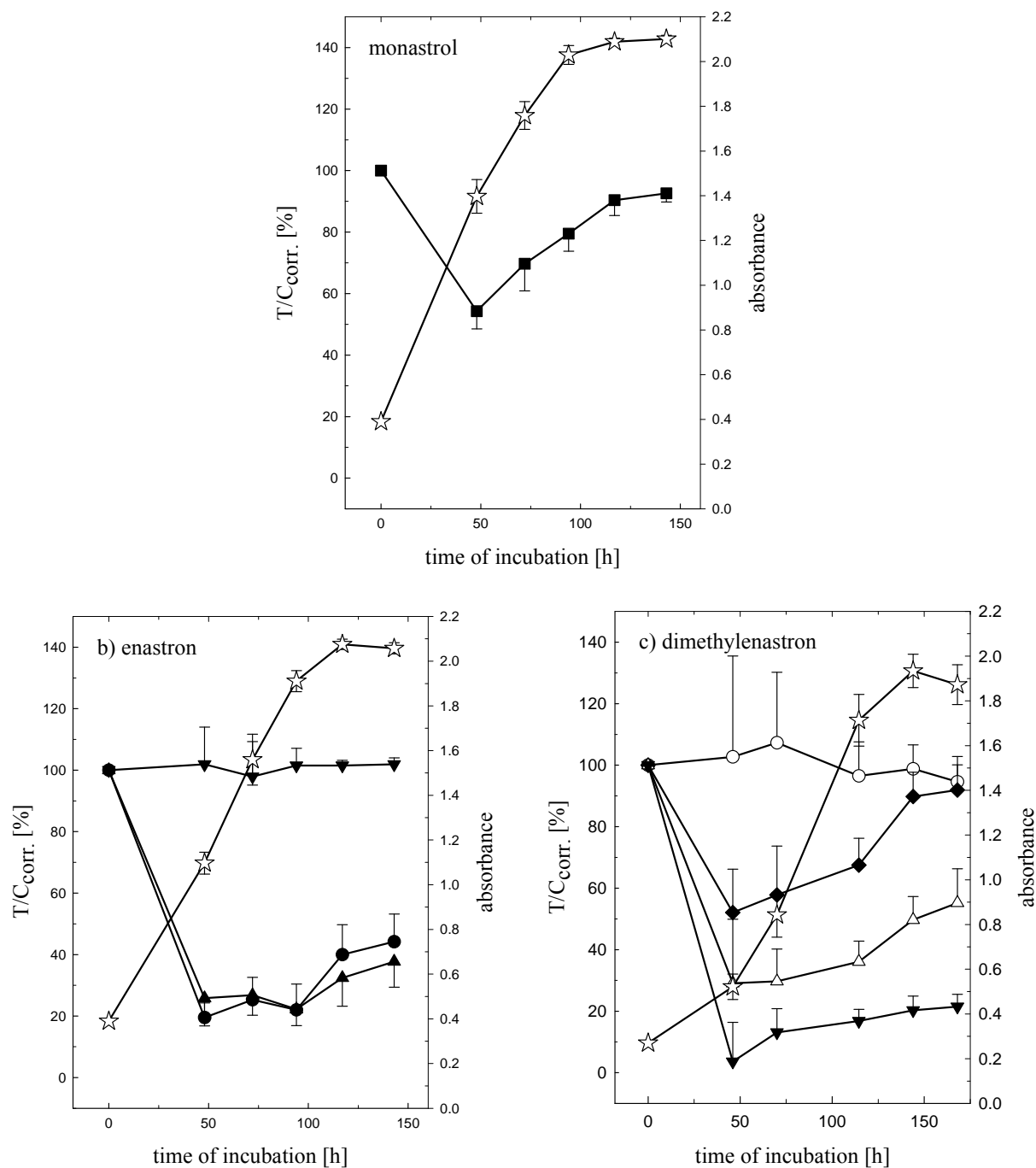


Figure 3.10: Proliferation kinetics of U-373 MG cells (passage 317) during permanent incubation with monastrol (a), the new monastrol analogs enastron (b) and dimethylenastron (c). *Open stars* vehicle (DMSO), *open circles* 0.25 μ M, *filled diamond* 0.5 μ M, *filled inverted triangles* 1 μ M, *filled circles* 5 μ M, *filled triangles* 10 μ M and *filled squares* 50 μ M.

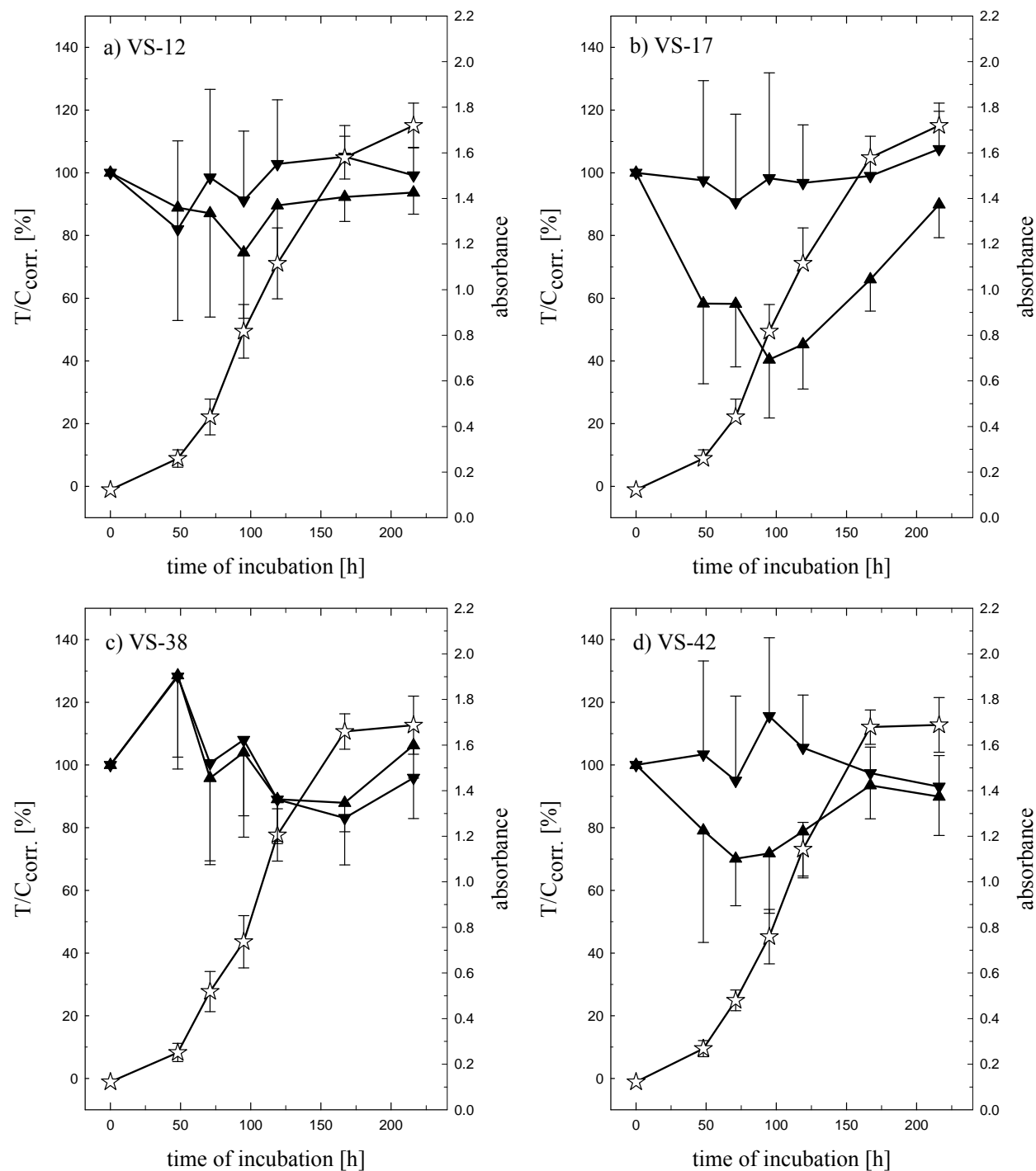


Figure 3.11: Proliferation kinetics of U-373 MG cells (passage 317) during permanent incubation with the vasastrols VS-12 (a), VS-17 (b), VS-38 (c) and VS-42 (d). *Open stars* vehicle (DMSO), *filled inverted triangles* 1 μ M and *filled triangles* 10 μ M.

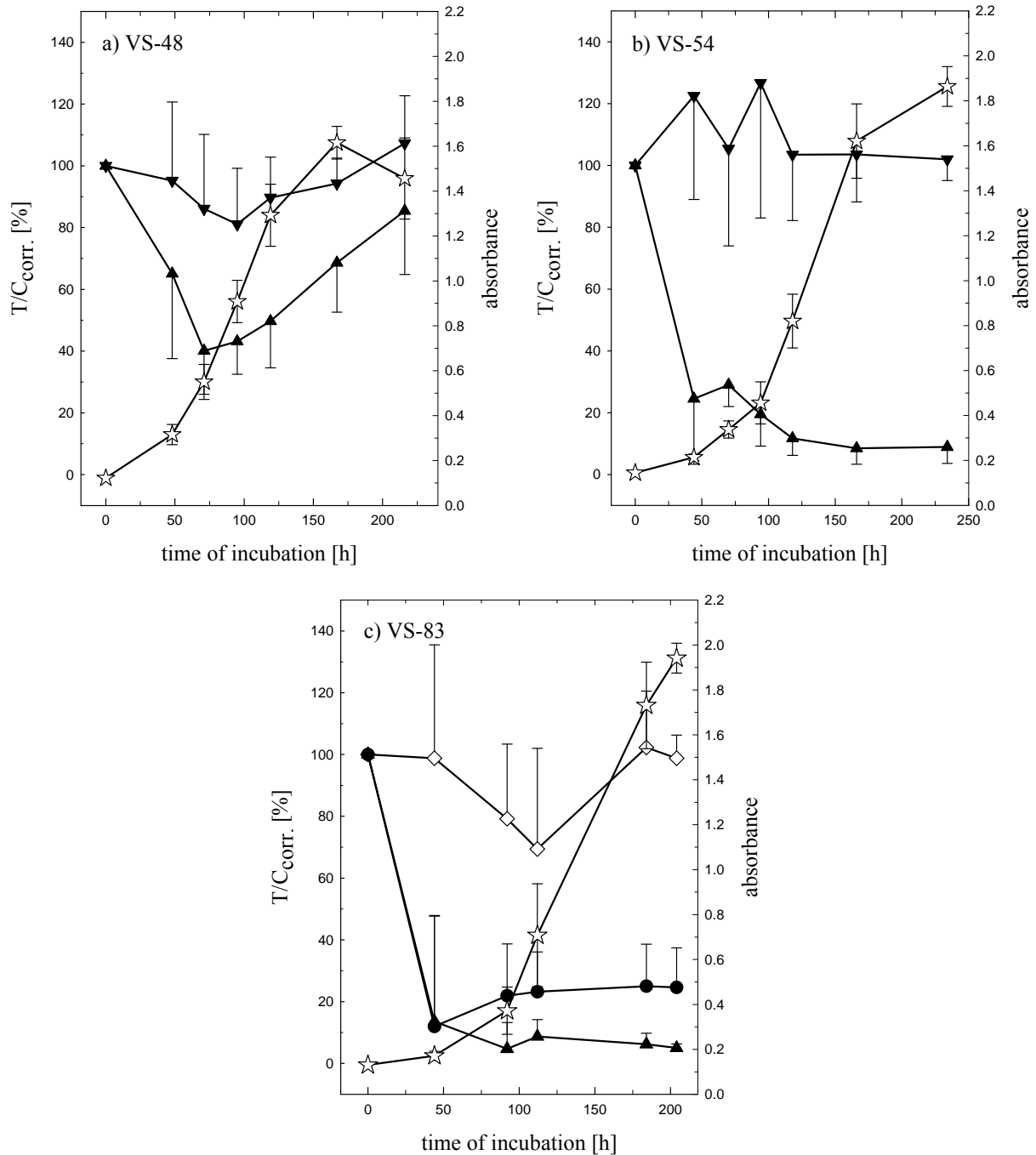


Figure 3.12: Proliferation kinetics of U-373 MG cells (passage 317) during permanent incubation with the vasastrols VS-48 (a), VS-54 (b) and VS-83 (c). *Open stars* vehicle (DMSO), *filled inverted triangles* 1 μ M, *open diamonds* 3 μ M, *filled circles* 5 μ M and *filled triangles* 10 μ M.

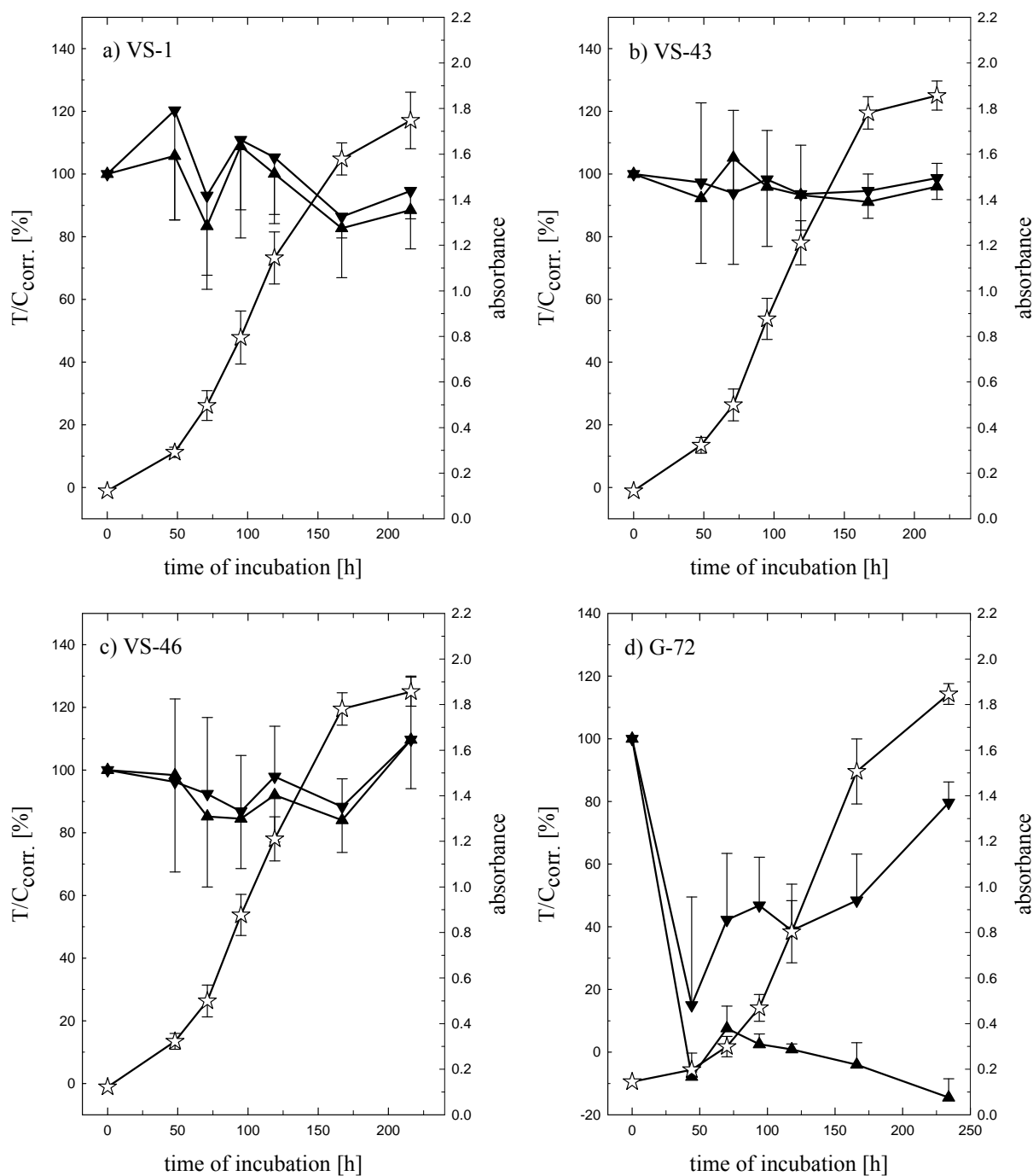


Figure 3.13: Proliferation kinetics of U-373 MG cells (passage 317) during permanent incubation with the 3,4-dihydrophenylquinazoline-2(1*H*)-thiones VS-1 (a), VS-43 (b), VS-46 (c) and the (*Z*)-4-(4-(dimethylamino)benzylidene)-2-phenyl-1*H*-imidazol-5(4*H*)-one G-72 (d). Open stars vehicle (DMSO), filled inverted triangles 1 μ M and filled triangles 10 μ M.

3.4.2 Incubation of glioblastoma cells after pre-incubation of new Eg5 inhibitors in culture medium

To consider potential inactivation of the compounds by esterases or binding to serum proteins, we pre-incubated monastrol (50 μM), enastron (5 μM), dimethylenastron (1 μM) and G-72 (10 μM) in culture medium for 1, 3 (data not shown) and 6 h. Then, the cells (U-87 MG, U-118 MG, and U-373 MG) were continuously incubated with culture medium containing the pre-incubated compounds. As shown for U-373 MG cells in Figure 3.14, the antiproliferative effects of monastrol, enastron, dimethylenastron and G-72 were retained compared to permanent drug exposure of the cells (Figure 3.10a, b, c and Figure 3.13d), indicating that the compounds were neither inactivated by hydrolysis nor by binding to serum proteins.

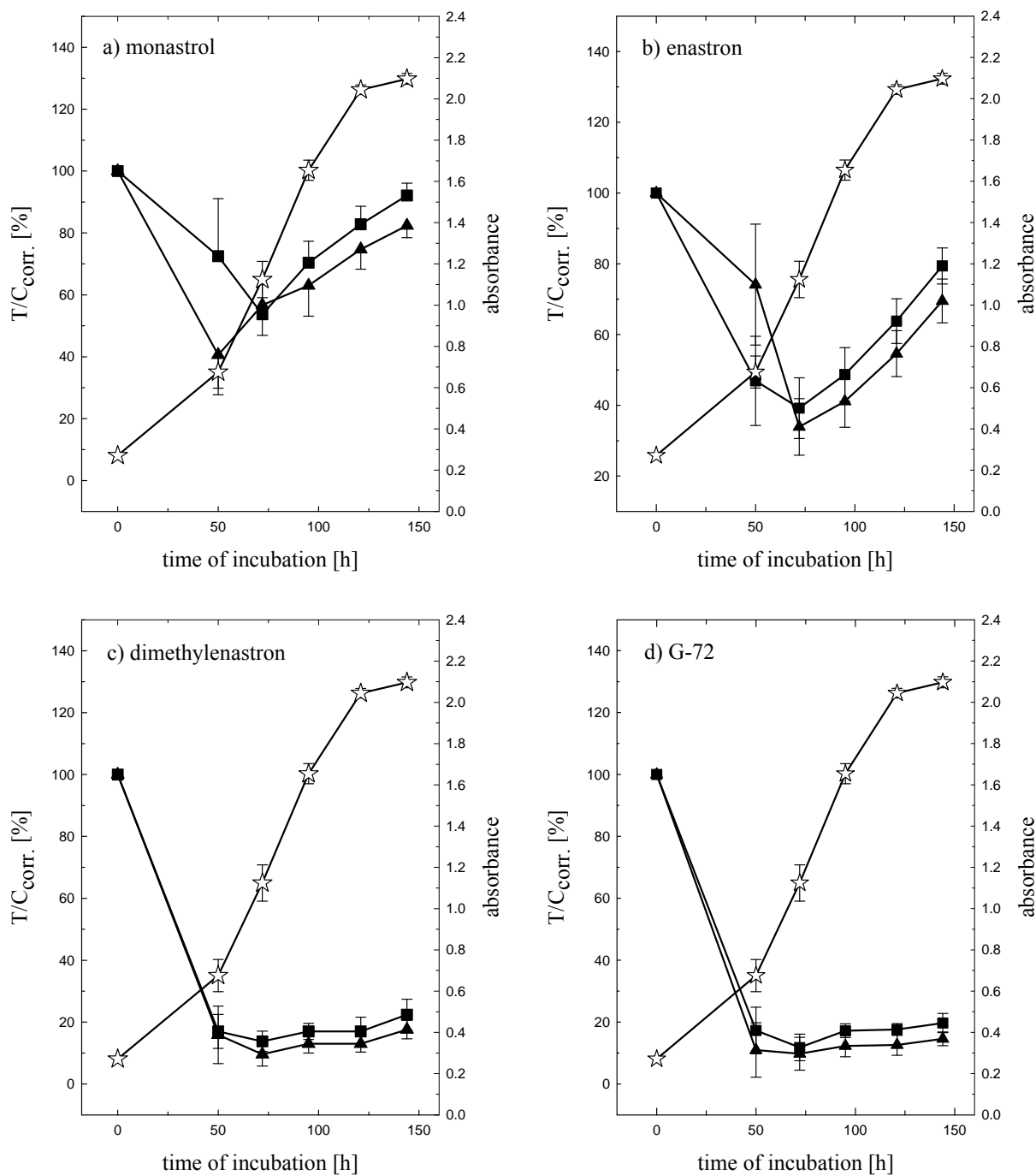


Figure 3.14: Incubation of U-373 MG cells (passage 310) after pre-incubation of 50 μM monastrol (a), 5 μM enastron (b), 1 μM dimethylenastron (c) and 10 μM G-72 (d) in culture medium. *Open stars* vehicle (DMSO), *filled squares* 1 h and *filled triangles* 6 h pre-incubation period.

3.4.3 Effect of new Eg5 inhibitors after incubation times of 1, 3 and 6 h

To explore the necessary drug residence time to reach a sufficient antiproliferative effect, the cells were incubated for 1, 3 (data not shown) and 6 hours with 10 μM of dimethylnastron and G-72 (Figure 3.15). Drug exposure for 1, 3 or 6 hours caused a significant reduction of the cytostatic effect compared to continuous incubation. However, this short incubation period of only 1 hour was sufficient to achieve a significant cytotoxic effect.

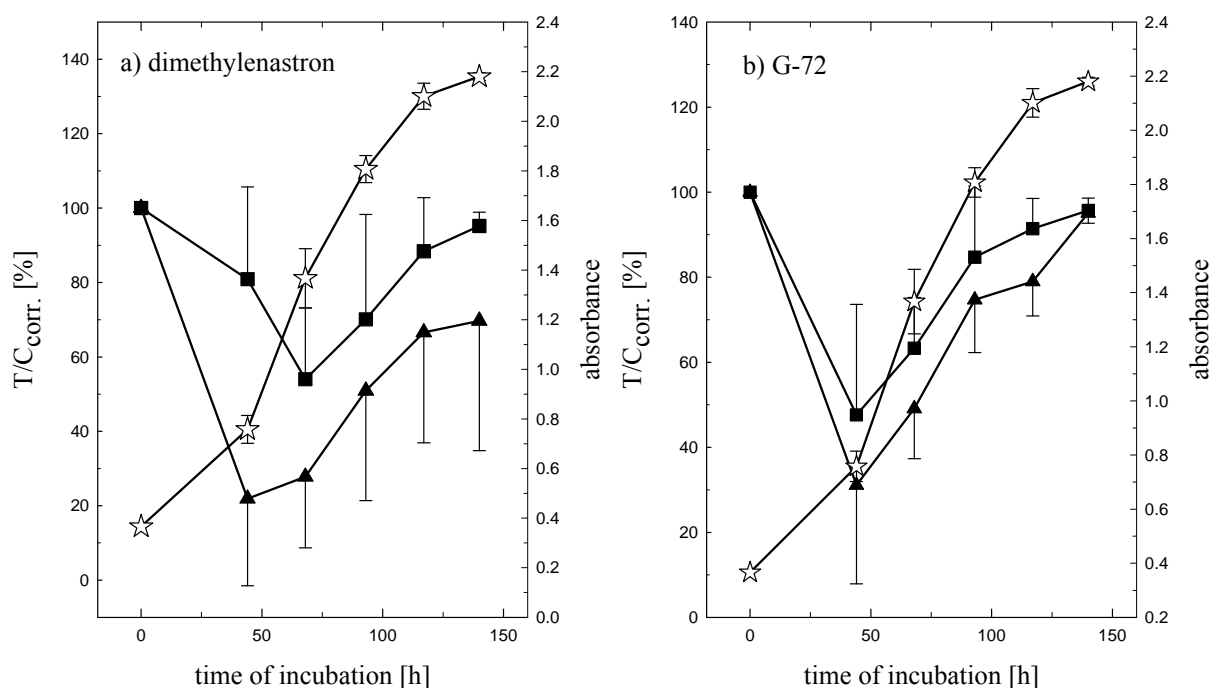


Figure 3.15: Drug exposure of U-373 MG cells with 10 μM of dimethylnastron (a) and G-72 (b) for a time period of 1 and 6 h. *Open stars* vehicle (DMSO), *filled squares* 1 h and *filled triangles* 6.

3.4.4 Effect of new monastrol analogs on quiescent cells

Confluent cells were treated with Eg5 inhibitors to compare their effects against resting cells with those of anti-tubulin drugs like paclitaxel. Rotenone, an ubiquinon reductase inhibitor blocking ATP synthesis, served as a positive control for maximum cytotoxic effect. The results are shown in Figure 3.16. Cell death (see eq. 4.2) was observed as expected for the rotenone treated cells. In contrast to paclitaxel, all tested Eg5 inhibitors had no effect on resting cells. All results described above were qualitatively and quantitatively similar for human U-118 MG glioblastoma/astrocytoma cells (results not shown).

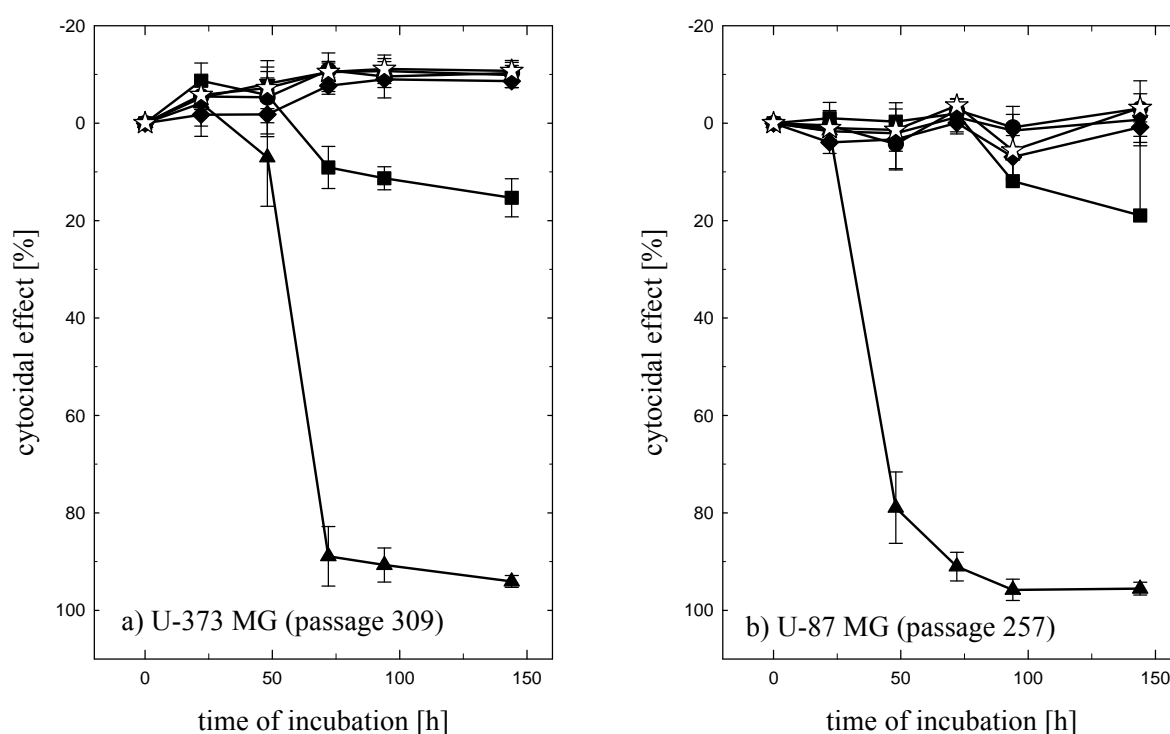


Figure 3.16: Incubation of resting U-373 MG (a) and U-87 MG cells (b) with paclitaxel, rotenone, the new monastrol analogs and G-72. *Open stars* vehicle (DMSO), *filled squares* paclitaxel (10 nM), *filled triangles* rotenone (500 nM), *filled circles* enastron (20 μM), *filled diamonds* dimethylenastron (20 μM) and *filled inverted triangles* G-72 (20 μM).

3.4.5 Flow cytometric calcein-AM efflux assay (ABCB1 assay)

We used the 3rd generation ABCB1 inhibitor elacridar (Kemper, 2003) as positive control. The new kinesin Eg5 inhibitors dimethylenastron and vasastrol VS-83 did not inhibit ABCB1 activity up to a concentration of 20 μ M (Figure 3.17).

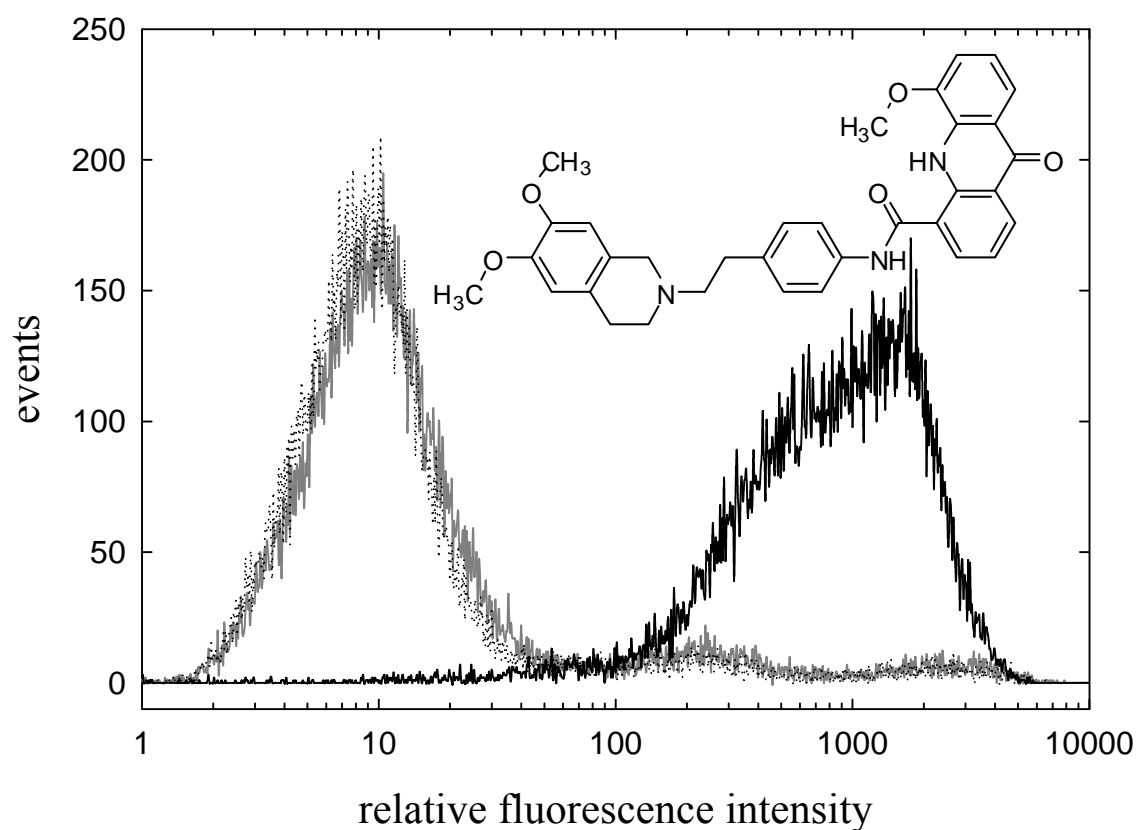


Figure 3.17: Calcein-AM efflux from Kb-V1 cells after incubation with vehicle (dotted), 50 nM elacridar (black) and 20 μ M dimethylenastron (grey). Overlay histograms of gated Kb-V1 cells using fluorescence 1 (BP/30 nm). Structural formula: elacridar.

3.4.6 Effect of the new monastrol analogs on the spindle apparatus and on the cytoskeleton of resting cells

According to the results of the chemosensitivity tests, human U-87 MG cells were incubated with 5 μ M enastron, 1 μ M dimethylenastron and 5 μ M vasastrol VS-83 for 2 h. As shown in Figure 3.18a, the compounds enastron and dimethylenastron produced the same characteristic effect on the formation of the mitotic spindle as the selective Eg5 kinesin inhibitor monastrol. However, the new compounds induced monoasters at lower concentrations, confirming the observations of monoaster formation in other cell types (Gartner et al., 2005). A different monoaster phenotype was observed after incubation with VS-83, similar to monoaster formation induced by the non-selective kinesin inhibitor S-trityl-L-cysteine (Figure 3.18a).

While vinblastine treatment resulted in the disruption of the tubulin assembly in resting cells, the new monastrol analogs showed no effect on microtubular structures (Figure 3.18b). Neither was the β -actin cytoskeleton affected by the new compounds, exemplarily shown for dimethylenastron (Figure 3.18d). No differences to the morphology of the untreated cells (Figure 3.18c) were observed.

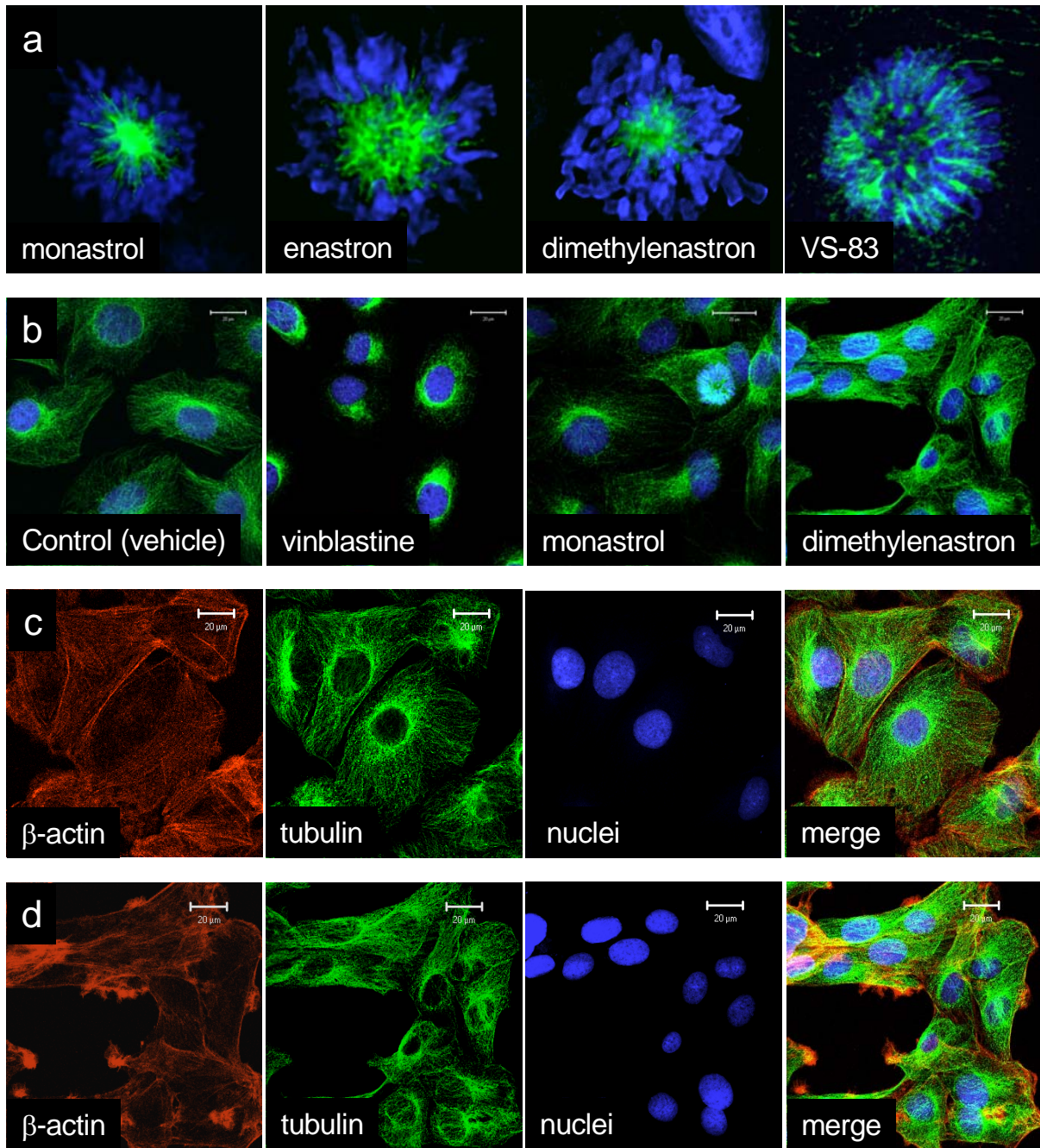


Figure 3.18: a) Formation of monoastrol spindles in human U-87 MG cells after incubation with monastrol (50 μM), the new monastrol analogs enastron (1 μM), dimethylenastron (1 μM), vasaastrol VS-83 (5 μM), and S-trityl-L-cysteine (1 μM); merged images of stained spindle and chromosomes. b) Human U-87 MG glioblastoma cells, incubation with 10 nM vinblastine, 1 μM S-trityl-L-cysteine and dimethylenastron (1 μM). c) Resting U-87 MG cells after incubation with 1 μM dimethylenastron and d) untreated cells. In quiescent cells, the microtubular and the β-actin cytoskeleton are not affected by the kinesin inhibiting compound.

3.5 Discussion

In the present study we demonstrated that, compared to the first selective small molecule Eg5 kinesin inhibitor monastrol, the newly synthesized monastrol analogs enastron, dimethylenastron and vasastron VS-83 exhibit higher antiproliferative activity against human glioblastoma cells. Enastron and vasastron VS-83 showed cytotoxic effects at a concentration of 5 μ M, whereas monastrol was less effective even at 50 μ M. For dimethylenastron, even higher antiproliferative potency was observed. The latter monastrol analogue was identified as the most potent compound with an approximately 100-fold higher antiproliferative efficacy compared to monastrol.

The vasastron VS-83 represents the most potent Eg5 inhibitor of the 3,4-dihydro-4-(3'-hydroxyphenyl)quinazoline-2(1*H*)-thiones with higher antiproliferative activity compared to VS-12, VS-17, VS-38, VS-42, VS-48 and VS-54. The 3,4-dihydrophenylquinazoline-2(1*H*)-thiones VS-1, VS-43 and VS-46 were ineffective up to a concentration of 10 μ M, indicating that the 3'-hydroxyl group is essential for the Eg5 inhibitory activity.

The antiproliferative activity of all tested monastrol derivatives and G-72 was not reduced by the pre-incubation in serum supplemented culture medium, indicating that the compounds were not inactivated by esterase cleavage or by binding to serum proteins.

By analogy to the results of the chemosensitivity experiments, the microscopic studies showed that the new monastrol analogues give rise to mitotic arrest in human glioblastoma cells by inducing the formation of monoasters, the characteristic effect of the Eg5 kinesin inhibition. This effect was observed after 2 h of drug exposure. In contrast to the work of Sarli et al. (Sarli et al., 2005), reporting on similar effects of monastrol and VS-83, in our studies the incubation with VS-83 led to a different monoaster phenotype, which was also observed after incubation with S-trityl-L-cysteine. However, Sarli et al. (Sarli et al., 2005) applied 100 μ M monastrol and 25 μ M VS-83 to synchronized simian BSC-1 cells. In addition, the BSC-1 cells were incubated for 10 h, whereas the human U-87 MG glioblastoma cells were treated with monastrol (50 mM) and VS-83 (5 μ M) for 2 h.

In contrast to the antimicrotubular agent paclitaxel, none of the investigated Eg5 inhibitors had a cytotoxic effect on resting cells. These results were supported by microscopic studies on the effect of the new monastrol analogs on the microtubules and the β -actin (cytoskeleton) of resting cells. Thus, these compounds are supposed to be less neurotoxic anticancer drugs in comparison to classical tubulin inhibitors.

Since the ABCB1 efflux pump, located at the blood–brain barrier, is suggested to be the major reason for multidrug resistance of brain tumors against numerous anticancer agents (Fellner et al., 2002), the effect of the new Eg5 kinesin inhibitors on the ABCB1 function was investigated using the flow cytometric calcein-AM efflux assay. While the 3rd generation p-gp inhibitor elacridar showed a high ABCB1 inhibition and consequently a strong calcein accumulation in Kb-V1 cells, no difference between the vehicle control and the tested Eg5 inhibitors was observed.

This demonstrates that the new compounds are neither modulators nor substrates of the ABCB1 transporter up to 20 μ M, a concentration much higher than required for monoaster formation and the inhibition of cell proliferation, respectively. From a therapeutic point of view, ABCB1 inhibition at higher concentrations (f2 value of 113 μ M), as recently described for monastrol (Peters, 2006), seems to be of minor relevance.

Taken together the new monastrol analogs enastron and its derivative dimethylenastron as well as the vasastrol VS-83 represent an interesting class of potential anticancer drugs, whereas dimethylenastron (ATPase IC₅₀ 200 nM) is considered as a promising lead structure for the development of further new derivatives with even higher potency for the inhibition of the Eg5 kinesin. This is supported by the report of Tarby et al. (Tarby et al., 2006), who developed a potent Eg5 inhibitor, derived from the 4-phenyl-tetrahydroisoquinoline lead series. The compound showed an IC₅₀ value of 104 nM in an ATPase assay and induced the characteristic monoastral spindles in PtK2 cells.

Enastron, dimethylenastron and VS-83 were ineffective against resting cells so that these compounds should be less neurotoxic in comparison to classical tubulin inhibitors. As the monastrol analogs are neither substrates nor modulators of ABCB1, these Eg5 inhibitors may be promising new agents for further preclinical studies aiming at the treatment of primary and secondary CNS tumors.

References

- Abrieu, A., Kahana, J. A., Wood, K. W. and Cleveland, D. W. (2000) CENP-E as an essential component of the mitotic checkpoint in vitro. *Cell* 102(6):817-826.
- Ahmad, F. J., Yu, W., McNally, F. J. and Baas, P. W. (1999) An Essential Role for Katanin in Severing Microtubules in the Neuron. *J. Cell Biol.* 145(2):305-315.
- Altmann, K.-H., Wartmann, M. and O'Reilly, T. (2000) Etoposides and related structures - a new class of microtubule inhibitors with potent in vivo antitumor activity. *Biochim. Biophys. Acta* 1470(3):M79-M91.
- Andersen, S. S. (2000) Spindle assembly and the art of regulating microtubule dynamics by MAPs and Stathmin/Op18. *Trends Cell Biol.* 10(7):261-267.
- Attard, G., Greystoke, A., Kaye, S. and De Bono, J. (2006) Update on tubulin-binding agents. *Pathol. Biol.* 54(2):72-84.
- Bailly, E. and Bornens, M. (1992) Cell biology. Centrosome and cell division. *Nature* 355(6358):300-301.
- Bernhardt, G., Reile, H., Birnböck, H., Spruss, T. and Schönenberger, H. (1992) Standardized kinetic microassay to quantify differential chemosensitivity on the basis of proliferative activity. *J. Cancer Res. Clin. Oncol.* V118(1):35-43.
- Blangy, A., Lane, H. A., d'Herin, P., Harper, M., Kress, M. and Nigg, E. A. (1995) Phosphorylation by p34cdc2 regulates spindle association of human Eg5, a kinesin-related motor essential for bipolar spindle formation in vivo. *Cell* 83(7):1159-1169.
- Brier, S., Lemaire, D., DeBonis, S., Forest, E. and Kozielski, F. (2004) Identification of the Protein Binding Region of S-Trityl-L-cysteine, a New Potent Inhibitor of the Mitotic Kinesin Eg5. *Biochemistry* 43(41):13072-13082.
- Brown, K. D. C., R M; Yen, T J; Cleveland, D W (1994) Cyclin-like accumulation and loss of the putative kinetochore motor CENP-E results from coupling continuous synthesis with specific degradation at the end of mitosis. *J. Cell Biol.* 125(6):1303-1312.
- Chan, G. K. T., Schaar, B. T. and Yen, T. J. (1998) Characterization of the Kinetochore Binding Domain of CENP-E Reveals Interactions with the Kinetochore Proteins CENP-F and hBUBR1. *J. Cell Biol.* 143(1):49-63.
- Desai, A. M., T J (1997) Microtubule polymerization dynamics. *Annu. Rev. Cell Dev. Biol.* 13(83-117).
- Drechsel, D. N. H., A. A.; Cobb, M. H.; Kirschner, M. W. (1992) Modulation of the dynamic instability of tubulin assembly by the microtubule-associated protein Tau. *Mol. Biol. Cell* 3(10):1141-1154.

- Fellner, S., Bauer, B., Miller, D. S., Schaffrik, M., Fankhänel, M., Spruss, T., Bernhardt, G., Gräff, C., Färber, L., Gschaidmeier, H., Buschauer, A. and Fricker, G. (2002) Transport of paclitaxel (Taxol) across the blood-brain barrier in vitro and in vivo. *J. Clin. Invest.* 110(9):1309-1318.
- Funabiki, H. M., A W (2000) The *Xenopus* chromokinesin Xkid is essential for metaphase chromosome alignment and must be degraded to allow anaphase chromosome movement. *Cell* 102(4):411-424.
- Gartner, M., Sunder-Plassmann, N., Seiler, J., Utz, M., Vernos, I., Surrey, T. and Giannis, A. (2005) Development and Biological Evaluation of Potent and Specific Inhibitors of Mitotic Kinesin Eg5. *ChemBioChem* 6(7):1173-1177.
- Gelmon, K. A., Latreille, J., Tolcher, A., Genier, L., Fisher, B., Forand, D., D'Aloisio, S., Vernillet, L., Daigneault, L., Lebecq, A., Besenval, M. and Eisenhauer, E. (2000) Phase I Dose-Finding Study of a New Taxane, RPR 109881A, Administered as a One-Hour Intravenous Infusion Days 1 and 8 to Patients With Advanced Solid Tumors. *J. Clin. Oncol.* 18(24):4098-4108.
- Hamel, E., Sackett, D. L., Vourloumis, D. and Nicolaou, K. C. (1999) The Coral-Derived Natural Products Eleutherobin and Sarcodictyins A and B: Effects on the Assembly of Purified Tubulin with and without Microtubule-Associated Proteins and Binding at the Polymer Taxoid Site. *Biochemistry* 38(17):5490-5498.
- Hay, R. J. (1988) The seed stock concept and quality control for cell lines. *Anal. Biochem.* 171(2):225-237.
- Hill, E. C., Mairi; Barr, Francis A (2000) The Rab6-binding kinesin, Rab6-KIFL, is required for cytokinesis. *EMBO J.* 19(21):5711-5719.
- Hollo, Z., Homolya, L., Davis, C. W. and Sarkadi, B. (1994) Calcein accumulation as a fluorometric functional assay of the multidrug transporter. *Biochim. Biophys. Acta* 1191(2):384-388.
- Homolya, L., Hollo, Z., Germann, U., Pastan, I., Gottesman, M. and Sarkadi, B. (1993) Fluorescent cellular indicators are extruded by the multidrug resistance protein. *J. Biol. Chem.* 268(29):21493-21496.
- Homolya, L., Hollo, Z., Muller, M., Mechetner, E. B. and Sarkadi, B. (1996) A new method for quantitative assessment of p-glycoprotein-related multidrug resistance in tumor cells. *Br. J. Cancer* 73(7):849-855.
- Hotha, S., Yarrow, J. C., Yang, J. G., Garrett, S., Renduchintala, K. V., Mayer, T. U. and Kapoor, T. M. (2003) HR22C16: A Potent Small-Molecule Probe for the Dynamics of Cell Division. *Angew. Chem. Int. Ed. Engl.* 42(21):2379-2382.
- Hunter, J., Hirst, B. H. and Simmons, N. L. (1991) Epithelial secretion of vinblastine by human intestinal adenocarcinoma cell (HCT-8 and T84) layers expressing P-glycoprotein. *Br. J. Cancer* 64(3):437-444.
- Izquierdo, M. A., Scheffer, G. L., Flens, M. J., Schroeijers, A. B., Van Der Valk, P. and Scheper, R. J. (1996) Major vault protein LRP-related multidrug resistance. *Eur. J. Cancer* 32A(6):979-984.

- Jordan, M. A. W., L (1998) Microtubules and actin filaments: dynamic targets for cancer chemotherapy. *Curr. Opin. Cell Biol.* 10(1):123-130.
- Kapoor, T. M., Mayer, T. U., Coughlin, M. L. and Mitchison, T. J. (2000) Probing Spindle Assembly Mechanisms with Monastrol, a Small Molecule Inhibitor of the Mitotic Kinesin, Eg5. *J. Cell Biol.* 150(5):975-988.
- Kashina, A. S., Baskin, R. J., Cole, D. G., Wedaman, K. P., Saxton, W. M. and Scholey, J. M. (1996) A bipolar kinesin. *Nature* 379(6562):270-272.
- Kemper, E. M. v. Z., A. Erik; Cleypool, Cindy; Mos, Henk A.; Boogerd, Willem; Beijnen, Jos H.; van Tellingen, Olaf (2003) Increased penetration of paclitaxel into the brain by inhibition of P-glycoprotein. *Clin. Cancer Res.* 9(7):2849-2855.
- Kohno, K., Kikuchi, J., Sato, S., Takano, H., Saburi, Y., Asoh, K. and Kuwano, M. (1988) Vincristine-resistant human cancer KB cell line and increased expression of multidrug-resistance gene. *Jpn. J. Cancer Res.* 79(11):1238-1246.
- Larsson, N. M., Ulrica; Gradin, Helena Melander; Brattsand, Goran; Gullberg, Martin (1997) Control of microtubule dynamics by oncoprotein 18: dissection of the regulatory role of multisite phosphorylation during mitosis. *Mol. Cell. Biol.* 17(9):5530-5539.
- Lee, J. J. and Swain, S. M. (2006) Peripheral Neuropathy Induced by Microtubule-Stabilizing Agents. *J. Clin. Oncol.* 24(10):1633-1642.
- Levan, A. (1938) The effect of colchicine on root mitosis in *Allium*. *Hereditas* 24(471-486.
- Li, Y. and Benezra, R. (1996) Identification of a Human Mitotic Checkpoint Gene: hsMAD2. *Science* 274(5285):246-248.
- Loe, D. W., Deeley, R. G. and Cole, S. P. C. (1996) Biology of the multidrug resistance-associated protein, MRP. *Eur. J. Cancer* 32A(6):945-957.
- Maliga, Z. K., Tarun M.; Mitchison, Timothy J (2002) Evidence that Monastrol Is an Allosteric Inhibitor of the Mitotic Kinesin Eg5. *Chem. Biol.* 9(9):989-996.
- Mandelkow, E. H., Andreas (1999) Structures of kinesin and kinesin-microtubule interactions. *Curr. Opin. Cell Biol.* 11(1):34-44.
- Mandelkow, E. M., Eva-Maria (1995) Microtubules and microtubule-associated proteins. *Curr. Opin. Cell Biol.* 7(1):72-81.
- Masson, D. K., Thomas E (1995) Binding of E-MAP-115 to microtubules is regulated by cell cycle-dependent phosphorylation. *J. Cell Biol.* 131(4):1015-1024.
- Mayer, T. U., Kapoor, T. M., Haggarty, S. J., King, R. W., Schreiber, S. L. and Mitchison, T. J. (1999) Small molecule inhibitor of mitotic spindle bipolarity identified in a phenotype-based screen. *Science* 286(5441):971-974.
- McDaid, H. M., Bhattacharya, S. K., Chen, X.-T., He, L., Shen, H.-J., Gutteridge, C. E., Horwitz, S. B. and Danishefsky, S. J. (1999) Structure-activity profiles of eleutherobin analogs and their cross-resistance in Taxol-resistant cell lines. *Cancer Chemother. Pharmacol.* V44(2):131-137.

- McNally, F. J. V., R D (1993) Identification of katanin, an ATPase that severs and disassembles stable microtubules. *Cell* 75(3):419-429.
- Mitchison, T. K., Marc (1984) Dynamic instability of microtubule growth. *Nature* 312(5991):237-422.
- Mollinedo, F. and Gajate, C. (2003) Microtubules, microtubule-interfering agents and apoptosis. *Apoptosis* V8(5):413-450.
- Müller, C., Gross, D., Sarli, V., Gartner, M., Giannis, A., Bernhardt, G. and Buschauer, A. (2007) Inhibitors of kinesin Eg5: antiproliferative activity of monastrol analogues against human glioblastoma cells. *Cancer Chemother. Pharmacol.* V59(2):157-164.
- Nakazawa, J. Y., Junichiro; Usui, Takeo; Ueki, Masashi; Takatsuki, Akira; Imoto, Masaya; Toyoshima, Yoko Y.; Osada, Hiroyuki (2003) A Novel Action of Terpendole E on the Motor Activity of Mitotic Kinesin Eg5. *Chem. Biol.* 10(2):131-137.
- Noda, Y., Okada, Y., Saito, N., Setou, M., Xu, Y., Zhang, Z. and Hirokawa, N. (2001) KIFC3, a microtubule minus end-directed motor for the apical transport of annexin XIIIb-associated Triton-insoluble membranes. *J. Cell Biol.* 155(1):77-88.
- Ookata, K. H., Shin-ichi; Bulinski, Jeannette Chloe; Murofushi, Hiromu; Aizawa, Hiroyuki; Itoh, Tomohiko J.; Hotani, Hirokazu; Okumura, Eiichi; Tachibana, Kazunori; Kishimoto, Takeo (1995) Cyclin B interaction with microtubule-associated protein 4 (MAP4) targets p34cdc2 kinase to microtubules and is a potential regulator of M-phase microtubule dynamics. *J. Cell Biol.* 128(5):849-862.
- Palmer, C. G., Livengood, D., Warren, A. K., Simpson, P. J. and Johnson, I. S. (1960) The action of the vincalcolastine on mitosis in vitro. *Exp. Cell Res.* 198-201(0014-4827).
- Peters, T. L., Heike; Häfeli, Walter E.; Weiss, Johanna (2006) Interaction of the mitotic kinesin Eg5 inhibitor monastrol with P-glycoprotein. *Naunyn-Schmiedeberg's Arch. Pharmacol.* 372(4):291-299.
- Polizzi, D., Pratesi, G., Tortoreto, M., Supino, R., Riva, A., Bombardelli, E. and Zunino, F. (1999) A novel taxane with improved tolerability and therapeutic activity in a panel of human tumor xenografts. *Cancer Res.* 59(5):1036-1040.
- Quasthoff, S. and Hartung, H. P. (2002) Chemotherapy-induced peripheral neuropathy. *J. Neurol.* V249(1):9-17.
- Rudner, A. D. and Murray, A. W. (1996) The spindle assembly checkpoint. *Curr. Opin. Cell Biol.* 8(6):773-780.
- Sakowicz, R., Berdelis, M. S., Ray, K., Blackburn, C. L., Hopmann, C., Faulkner, D. J. and Goldstein, L. S. B. (1998) A marine natural product inhibitor of Kinesin motors. *Science* 280(5361):292-295.
- Sakowicz, R. F., Jeffrey T.; Beraud, Christophe; Crompton, Anne; Lewis, Evan; Fritsch, Alex; Lee, Yan; Mak, John; Moody, Robert; Turincio, Rebecca; Chabala, John C.; Gonzales, Paul; Roth, Stephanie; Weitman, Steve; Wood, Kenneth W. (2004) Antitumor Activity of a Kinesin Inhibitor. *Cancer Res.* 64(9):3276-3280.

- Sarli, V., Hümmer, S., Sunder-Plassmann, N., Mayer, T. and Giannis, A. (2005) Synthesis and Biological Evaluation of Novel Eg5 Inhibitors. *ChemBioChem* 6(11):2005-2013.
- Sawin, K. E., LeGuellec, K., Philippe, M. and Mitchison, T. J. (1992) Mitotic spindle organization by a plus-end-directed microtubule motor. *Nature* 359(6395):540-543.
- Schaar, B. T., Chan, G. K. T., Maddox, P., Salmon, E. D. and Yen, T. J. (1997) CENP-E Function at Kinetochores Is Essential for Chromosome Alignment. *J. Cell Biol.* 139(6):1373-1382.
- Schiff, P. B. F., J; Horwitz, S B (1979) Promotion of microtubule assembly in vitro by taxol. *Nature* 277(5698):665-667.
- Schiff, P. B. H., Susan Band (1980) Taxol stabilizes microtubules in mouse fibroblast cells. *Proc. Natl. Acad. Sci. U. S. A.* 77(3):1561-1565.
- Shannon, K. B. S., E. D. (2002) Chromosome Dynamics: New Light on Aurora B Kinase Function. *Curr. Biol.* 12(13):R458-R460.
- Sharp, D. J., Rogers, G. C. and Scholey, J. M. (2000) Microtubule motors in mitosis. *Nature* 407(6800):41-47.
- Skoufias, D. A., Andreassen, P. R., Lacroix, F. B., Wilson, L. and Margolis, R. L. (2001) Mammalian mad2 and bub1/bubR1 recognize distinct spindle-attachment and kinetochore-tension checkpoints. *Proc. Natl. Acad. Sci. U. S. A.* 98(8):4492-4497.
- Sorger, P. K., Dobles, M., Tournebize, R. and Hyman, A. A. (1997) Coupling cell division and cell death to microtubule dynamics. *Curr. Opin. Cell Biol.* 9(6):807-814.
- Sunder-Plassmann, N., Sarli, V., Gartner, M., Utz, M., Seiler, J., Hümmer, S., Mayer, T. U., Surrey, T. and Giannis, A. (2005) Synthesis and biological evaluation of new tetrahydro-beta-carbolines as inhibitors of the mitotic kinesin Eg5. *Bioorg. Med. Chem.* 13(22):6094-6111.
- Tao, W., South, V. J., Zhang, Y., Davide, J. P., Farrell, L., Kohl, N. E., Sepp-Lorenzino, L. and Lobell, R. B. (2005) Induction of apoptosis by an inhibitor of the mitotic kinesin KSP requires both activation of the spindle assembly checkpoint and mitotic slippage. *Cancer Cell* 8(1):49-59.
- Tarby, C. M., Kaltenbach, R. F., Huynh, T., Pudzianowski, A., Shen, H., Ortega-Nanos, M., Sheriff, S., Newitt, J. A., McDonnell, P. A., Burford, N., Fairchild, C. R., Vaccaro, W., Chen, Z., Borzilleri, R. M., Naglich, J., Lombardo, L. J., Gottardis, M., Trainor, G. L. and Roussel, D. L. (2006) Inhibitors of human mitotic kinesin Eg5: Characterization of the 4-phenyl-tetrahydroisoquinoline lead series. *Bioorg. Med. Chem. Lett.* 16(8):2095-2100.
- Vale, R. D. and Fletterick, R. J. (1997) The design plan of kinesin motors. *Annu. Rev. Cell Dev. Biol.* 13(1):745-777.
- Walczak, C. E., Mitchison, T. J. and Desai, A. (1996) XKCM1: A Xenopus Kinesin-Related Protein That Regulates Microtubule Dynamics during Mitotic Spindle Assembly. *Cell* 84(1):37-47.

- Walczak, C. E., Vernos, I., Mitchison, T. J., Karsenti, E. and Heald, R. (1998) A model for the proposed roles of different microtubule-based motor proteins in establishing spindle bipolarity. *Curr. Biol.* 8(16):903-913.
- Walker, R., O'Brien, E., Pryer, N., Soboeiro, M., Voter, W., Erickson, H. and Salmon, E. (1988) Dynamic instability of individual microtubules analyzed by video light microscopy: rate constants and transition frequencies. *J. Cell Biol.* 107(4):1437-1448.
- Wood, K. W., Cornwell, W. D. and Jackson, J. R. (2001) Past and future of the mitotic spindle as an oncology target. *Curr. Opin. Pharmacol.* 1(4):370-377.
- Xu, Y., Takeda, S., Nakata, T., Noda, Y., Tanaka, Y. and Hirokawa, N. (2002) Role of KIFC3 motor protein in Golgi positioning and integration. *J. Cell Biol.* 158(2):293-303.
- Yao, X., Abrieu, A., Zheng, Y., Sullivan, K. F. and Cleveland, D. W. (2000) CENP-E forms a link between attachment of spindle microtubules to kinetochores and the mitotic checkpoint. *Nat. Cell Biol.* 2(8):484-491.
- Zacherl, J., Hamilton, G., Thalhammer, T., Riegler, M., Cosentini, E. P., Ellinger, A., Bischof, G., Schweitzer, M., Teleky, B., Koperna, T. and Wenzl, E. (1994) Inhibition of P-glycoprotein-mediated vinblastine transport across HCT-8 intestinal carcinoma monolayers by verapamil, cyclosporine A and SDZ PSC 833 in dependence on extracellular pH. *Cancer Chemother. Pharmacol.* V34(2):125-132.

Chapter 4

Tariquidar analogs as
ABCB1 and ABCG2 inhibitors

4.1 Introduction

The chemotherapy of brain tumor often fails due to extremely low drug concentrations reached in the brain, although the administered cytostatics should be able to penetrate across the blood brain barrier (BBB) because of their physicochemical properties (Loeschner and Potschka, 2005). This can be explained by the high affinity of these compounds to efflux transporters (Johnson, 2002), localized at the luminal membrane of the brain capillary endothelial cells (Bendayan et al., 2002). These efflux transport proteins belong to the ABC superfamily including ABCB1 (P-glycoprotein 170) and ABCG2 (breast cancer resistance protein) (Dean and Allikmets, 2001) and are also responsible for the classical multiple drug resistance (MDR) and atypical multiple drug resistance of cancer cells (Bosch and Croop, 1996; Doyle and Ross, 2003; Glavinas et al., 2004).

An attractive strategy to overcome the BBB is the administration of an efflux pump inhibitor in combination with a cytostatic (Breedveld et al., 2006). The study by Fellner et al. with the 2nd generation ABCB1 inhibitor valspodar (SDZ PSC-833) and the anticancer drug paclitaxel, an ABCB1 substrate, has proven this concept (Fellner et al., 2002). This combination led to increased brain levels of paclitaxel in nude mice by a factor of 6-8 compared to paclitaxel monotherapy. Moreover, in nude mice with intracerebral human U-118 MG glioblastoma the co-administration of valspodar and paclitaxel reduced the tumor volume by 90 %, whereas paclitaxel alone was ineffective. However, due to the modulation of ABCB1 in liver, kidneys and bone marrow by valspodar, the paclitaxel blood level increased and paclitaxel toxicity became dose-limiting with valspodar. Another reason for increased plasma concentrations of paclitaxel is the fact that valspodar inhibits the cytochrome P450 3A4-mediated metabolism of paclitaxel (Fischer et al., 1998).

To overcome the limitations of the 2nd generation ABCB1 modulators, 3rd generation inhibitors, purported to specifically and potently inhibit ABCB1 function have been developed (Krishna and Mayer, 2000). These agents do not affect cytochrome P450 3A4 at relevant concentrations (Dantzig et al., 1999; Wandel et al., 1999). One of the most promising 3rd generation ABCB1 inhibitors is tariquidar, which is supposed to selectively modulate the ABCB1 transporter (Thomas and Coley, 2003). This assumption is supported by investigations on the effect of tariquidar on the tissue distribution of paclitaxel (Fankhänel et al., 2005). The co-administration of tariquidar (p.o.) and paclitaxel (i.v.) led to high

brain/plasma ratios of paclitaxel (ratio 1.5 – 4.5) indicating that ABCB1 inhibition by tariquidar did lead to a specific accumulation of paclitaxel in the brain of nude mice. In contrast, the co-administration of valspodar resulted in 2- to 15-fold lower brain/plasma ratios of paclitaxel compared to tariquidar. But, tariquidar was not able to induce the same increase in the concentration of paclitaxel in the brain of nude mice as that achieved by valpodar administration (6- to 8-fold), although tariquidar showed higher inhibitory activity in vitro. Despite very high tariquidar concentrations in the brain, co-application of tariquidar led only to an increase in paclitaxel brain concentrations by a factor of 2.5- to 6.7. As an explanation it can be speculated that the highly lipophilic tariquidar is trapped in the lipid compartment of the brain.

To investigate this hypothesis more hydrophilic tariquidar analogs with improved pharmacokinetic properties were synthesized. The compounds were investigated for inhibition of ABCB1 and ABCG2. Surprisingly, minimal structural changes at the aromatic core of tariquidar yielded very potent and selective ABCG2 inhibitors. The use of ABCG2 inhibitors might also be of interest for improvement of CNS penetration of ABCG2 substrates (Breedveld et al., 2006). Due to the relatively recent discovery of the ABCG2 transporter in 1998 (Allikmets et al., 1998; Doyle et al., 1998) only a few ABCG2 inhibitors have been reported so far (Ahmed-Belkacem et al., 2006). Fumitremorgin C (FTC), a mycotoxin from *Aspergillus fumigatus*, was reported first (Rabindran et al., 2000), but its neurotoxicity precluded its use in in vivo experiments. One of the most potent ABCG2 inhibitors is elacridar (GF120918), which is also known to be a very potent ABCB1 inhibitor (Hyafil, 1993). But it is not known, whether for cancer treatment a dual ABCB1 and ABCG2 inhibitor is superior to a selective inhibitor (Breedveld et al., 2006). This probably depends on the affinity of the cytostatic to the ABCB1 or ABCG2 transporter. The most potent ABCG2 inhibitor known so far is the FTC analog Ko143 with an EC₉₀ value of 23 nM determined by the fluorescence based measurement of increased mitoxantrone accumulation in drug-resistant mouse MEF3.8/T6400 cells and in human IGROV/T8 cells (Allen et al., 2002). Its low cytotoxicity, with an IC₅₀ value of 100- to 1000-fold higher than for ABCG2 inhibition, made it promising for in vivo studies. Ko143 was non-toxic in mice at 10-50 mg/kg oral doses, and it increased the bioavailability of orally administered topotecan compared to elacridar (Allen et al., 2002).

However, in order to use the ABCG2 inhibitors for the treatment of tumors, compounds with specific cytotoxicity might be advantageous with regard to the concept that every type of cancer contains cancer stem cells. This cancer stem cell model considers malignant tumors as abnormal organs initiated by cancer stem cells. The cancer stem cells might play a decisive role in tumor initiation and progression because they have the ability to self-renew and to give rise to new tissues (Reya et al., 2001). Furthermore, they tend to be more resistant to chemotherapeutics than other cell types from the same tissue due to the expression of the ABCG2 transporter.

4.2 Objective

The efflux of cytostatics due to (over)expression of ABC transporters such as ABCB1 (P-glycoprotein 170) and ABCG2 (breast cancer resistance protein, BCRP) is a major limitation in cancer chemotherapy (Johnson, 2002). Inhibition of the transporters is an effective approach to the treatment of glioblastoma by overcoming the blood brain barrier as proven by the study of Fellner et al. with a combination of valspodar and paclitaxel (Fellner et al., 2002). Using the more potent ABCB1 inhibitor tariquidar, a higher brain/plasma ratio of paclitaxel was detected in mice (Fankhänel et al., 2005). However, despite of high tariquidar concentrations in the brain, paclitaxel brain levels did not increase compared to the valspodar group (Fankhänel et al., 2005). As an explanation it can be speculate that the highly lipophilic tariquidar is trapped in the lipid compartment of the brain. To investigate this hypothesis we started a project to develop more hydrophilic tariquidar analogs with improved pharmacokinetic properties. The new tariquidar analogs were synthesized and characterized by Michael Egger and Xuqin Li from the workgroup of Prof. König at the Institute for Organic Chemistry, University of Regensburg.

The objective of this work was to investigate the new tariquidar analogs for inhibition of ABCB1 and ABCG2 in order to determine the potency and the selectivity. Therefore, the IC_{50} values of the compounds were determined in two different flow cytometric fluorescence-based assays. The inhibitory activity at the ABCB1 transporter was examined with the calcein-AM efflux assay and at the ABCG2 transporter with the mitoxantrone efflux assay, respectively. An alternative for the determination of the inhibitory activity is to investigate the potential of the compounds to overcome the multidrug resistance of ABCB1 or ABCG2 expressing cells. Therefore, ABCB1 positive Kb-V1 cells and ABCG2 positive MCF-7/Topo cells, respectively, were treated with different concentrations of tariquidar analogs alone and in combination with non-toxic topotecan concentrations.

With respect to the treatment of brain tumors the antiproliferative effect of the new tariquidar analogs was investigated on human glioblastoma U-373 MG cells, using the crystal violet chemosensitivity assay. Furthermore, confluent U-373 MG cells should be treated with tariquidar analogs to compare their effects with those of anti-tubulin drugs like paclitaxel against resting cells.

The results have been published in part (Egger et al., 2007)

4.3 Materials and methods

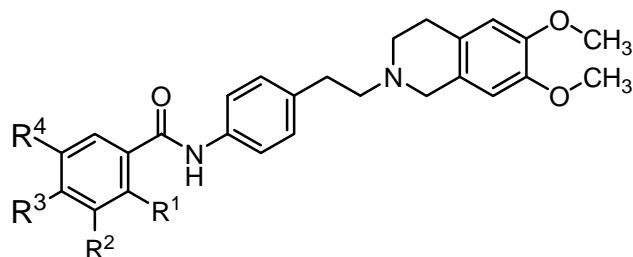
4.3.1 Drugs and chemicals

Tariquidar (free base) was synthesized according to Dodic et al. (1995), Roe et al. (1999) and Sharp et al. (1998) with slight modifications (Hubensack, 2005). Calcein-AM, purchased from Biotrend (Köln, Germany), was dissolved in DMSO (Merck, Darmstadt, Germany) to achieve a final concentration of 1 mM. The aliquoted stock solutions were stored at -20 °C. Mitoxantrone stocks were obtained by diluting Novantron® (Wyeth Pharma, Münster, Germany) in 70 % ethanol to a concentration of 2 mM. The 1 mM stock solutions of vinblastine (Vinblastine sulfate, Sigma, Munich, Germany) and paclitaxel (Sigma) were made in 70 % ethanol. All stocks were stored at -20 °C. Topotecan stocks were obtained by diluting Hycamtin® (GlaxoSmithKline, München, Germany) in 70 % ethanol to a concentration of 0.1 mM and stored at 4 °C.

4.3.2 Tariquidar analogs

All tariquidar analogs were synthesized, characterized and provided by the workgroup of Prof. König (University of Regensburg, Germany). 10 mM stock solutions were prepared in DMSO and stored at -20 °C. According to the substitution pattern the tariquidar analogs can be subdivided in three series of compounds. The general structure of the tariquidar analogs with residues R^1 , R^2 , R^3 and R^4 and the corresponding compounds are listed in Table 4.1, Table 4.2 and Table 4.3.

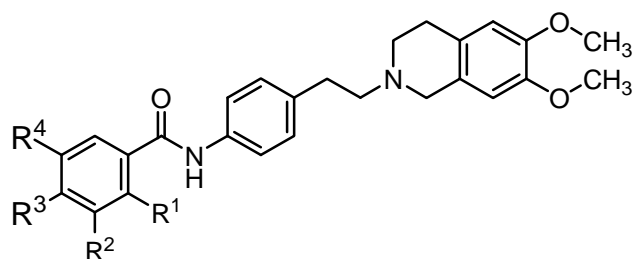
Table 4.1: Structures of tariquidar, tariquidar analogs and intermediates with variations in residue R³ and R⁴.



Compound (lab code)	R ¹	R ²	R ³	R ⁴
tariquidar		H	OCH ₃	OCH ₃
1 (ME5-5)	NH ₂	H	SO ₂ NH ₂	H
2 (ME5-7)		H	SO ₂ NH ₂	H
3* (ME27-1)	NHBoc	H	H	Br
4* (ME27-2)	NH ₂	H	H	Br
5* (ME27-3)		H	H	Br
6* (ME27-4)		H	H	H ₃ CO(CH ₂) ₂ O(CH ₂) ₂ NH-
7* (ME30-1)		H	H	morpholino
8* (ME33-1)		H	H	H ₅ C ₂ O(CH ₂) ₂ O-

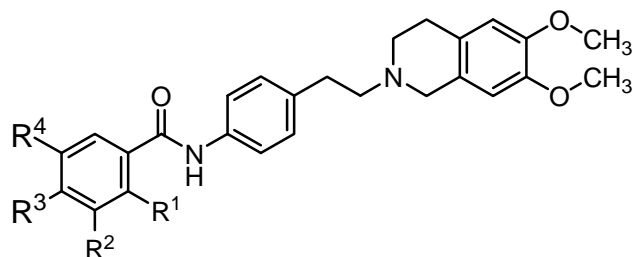
*) Synthesis of these compounds has already been published (Egger et al., 2007)

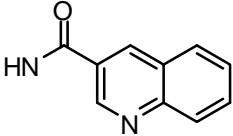
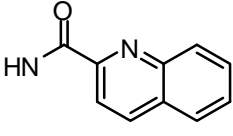
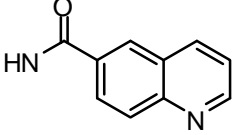
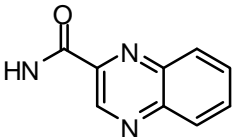
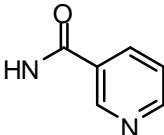
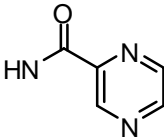
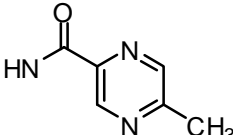
Table 4.2: Structures of tariquidar and tariquidar analogs with quinoline-3-carboxamido as R² and variations of R³ and R⁴.



Compound (lab code)	R ¹	R ²	R ³	R ⁴
tariquidar		H	OCH ₃	OCH ₃
9 (ME24-5)	H		H	OCH ₃
10 (ME25-3)	H		OCH ₃	OCH ₃
11 (ME18-3)	H		OCH ₃	H
12 (ME17-3)	H		CH ₃	H

Table 4.3: Structures of tariquidar analogs and intermediates with a methoxycarbonyl group as R³.



Compound (lab code)	R ¹	R ²	R ³	R ⁴
13 (ME1-2)	H	NO ₂	COOCH ₃	H
14 (ME1-3)	H	NH ₂	COOCH ₃	H
15 (ME1-4)	H		COOCH ₃	H
16 (ME22-1)	H		COOCH ₃	H
17 (ME19-2)	H		COOCH ₃	H
18 (ME11-1)	H		COOCH ₃	H
19 (ME12-1)	H		COOCH ₃	H
20 (ME14-1)	H		COOCH ₃	H
21 (ME21-1)	H		COOCH ₃	H

4.3.3 Cell lines and culture conditions

Kb-V1 cells, an ABCB1 overexpressing subclone (Kohno et al., 1988) of HeLa derived human Kb cells (ATCC CCL-17), were obtained by adding increasing amounts of vinblastine after subculturing to achieve a final concentration of 300 ng/ml culture medium within a period of about 90 days. The culture medium was Dulbecco's modified Eagle's medium (Sigma, Deisenhofen, Germany) supplemented with 10 % FCS (Biochrom, Berlin, Germany) and 300 ng/ml vinblastine. After 3 passages the chemoresistant cells expressed sufficient quantities of the ABCB1 transporter. New cells were thawed after Kb-V1 cells were cultivated for about 15 weeks (Hubensack, 2005).

MCF-7/Topo cells, an ABCG2 overexpressing subclone of MCF-7 breast adenocarcinoma cells (ATCC HTB-22), were obtained by adding increasing volumes of a topotecan solution within a period of about 40 days to achieve a final concentration of 500 ng/ml culture medium. After three passages in Eagle's minimum essential medium (Sigma, Deisenhofen, Germany) supplemented with 5 % FCS and 500 ng/ml topotecan, the treated cells expressed sufficient quantities of ABCG2 (Hubensack, 2005). All cell types were maintained in a water saturated atmosphere (95 % air/5 % carbondioxide) at 37 °C in 75-cm² culture flasks (NUNC, Wiesbaden, Germany) and were serially passaged following trypsinization using 0.05 % trypsin/0.02 % EDTA (Roche Diagnostics, Mannheim, Germany). Mycoplasma contamination was routinely monitored by PCR (Venor® GeM, Minerva Biolabs GmbH, Berlin), and only *Mycoplasma* free cultures were used.

4.3.4 Flow cytometric calcein-AM efflux assay

In Kb-V1 cells calcein-AM is extruded by ABCB1 before esterases can cleave the ester bonds, and calcein is not accumulated (Homolya et al., 1993). Therefore, p-gp modulators can easily be recognized by flow cytometry. Depending on the modulator concentration the change in the calcein-AM efflux or rather in the relative fluorescence intensity of the cells is measured (see Chapter 4). The assay was performed according to Müller et al (Müller et al., 2007).

4.3.5 Flow cytometric mitoxantrone efflux assay

The assay was performed according to the cited literature (Lee et al., 1994; de Bruin et al., 1999; Maliepaard et al., 1999; Robey et al., 2001) with modified assay conditions. ABCG2 expressing MCF-7/Topo cells were passaged 3 or 4 days before the assay was carried out, trypsinized, washed with PBS at 25 °C, and adjusted to a number of $1 \cdot 10^6$ cells per ml with culture medium. Mitoxantrone was added to the cell suspension to achieve a concentration of 20 μ M (10 μ l of 2 mM stock solution in 70 % ethanol). Different concentrations of the test compound, solvent and fumitremorgin C (10 μ M) were added, respectively. After a short vortexing step the cell suspensions were incubated for 30 min at 37 °C/5 % CO₂, which is a sufficient incubation period for maximal mitoxantrone uptake into the cells, according to the literature. Subsequently, the cells were washed with ice cold PBS at 4 °C. For the determination of the 100 % mitoxantrone uptake the cells of the fumitremorgin C sample were resuspended in ice cold PBS and placed on ice in the dark until measurement to avoid mitoxantrone efflux. All other samples were resuspended in culture medium. After an incubation period of 1 h at 37 °C/5 % CO₂ an equilibrium of mitoxantrone had developed between the cytoplasm of the cells and the surrounding medium. After the medium was removed by centrifugation, the cell pellet was rinsed once with ice cold PBS, resuspended in 0.5 ml of PBS per $1 \cdot 10^6$ cells. A FACS Calibur™ (Becton Dickinson, Heidelberg, Germany) was used to analyze the fluorescence intensity of the cells. A minimum of 20,000 events was collected per sample and the events were gated according to forward scatter and sideward scatter to exclude clumps and debris. The photomultiplier settings were as follows: E-1 for FSC, 200 for SSC, 450 for FL1-H and 700 for FL4-H. FL4-H histograms were analyzed by the WinMDI 2.8 software.

4.3.6 Chemosensitivity assay

The assays were performed as described previously (Bernhardt et al., 1992). In brief: tumor cell suspensions (100 μ l/well) were seeded into 96-well flat bottomed microtitration plates (Greiner, Frickenhausen, Germany) at a density of ca. 15 cells/microscopic field (magnification 320-fold). After 2-3 days the culture medium was removed by suction and replaced by fresh medium (200 μ l/well) containing varying drug concentrations or vehicle. Drugs were added as 1000-fold concentrated feed solutions. On every plate 16 wells served as controls and 16 wells were used per drug concentration. After various times of incubation the cells were fixed with glutardialdehyde (Merck, Darmstadt, Germany) and stored in a refrigerator. At the end of the experiment all plates were processed simultaneously (staining with 0.02 % aqueous crystal violet (SERVA, Heidelberg, Germany) solution (100 μ l/well)). Excess dye was removed by rinsing the trays with water for 20 min. The stain bound by the cells was redissolved in 70 % ethanol (180 μ l/well) while shaking the microplates for about 3 hours. Absorbance (a parameter proportional to cell mass) was measured at 578 nm using a BIOTEK 309 Autoreader (TECNOMARA, Fernwald, Germany).

Drug effects were expressed as corrected T/C-values for each group according to

$$T/C_{\text{corr}} = \frac{T - C_0}{C - C_0} \cdot 100 [\%] \quad (\text{eq. 4.1}),$$

where T is the mean absorbance of the treated cells, C the mean absorbance of the controls and C_0 the mean absorbance of the cells at the time ($t = 0$) when drug was added.

When the absorbance of treated cells T is less than that of the culture at $t = 0$ (C_0), the extent of cell killing was calculated as

$$\text{cytotoxic effect } [\%] = \frac{C_0 - T}{C_0} \cdot 100 \quad (\text{eq. 4.2}).$$

4.3.7 Cell cycle analysis

Cell cycle analysis was performed with the new tariquidar analogs at a concentration of 10 μ M. In order to obtain a sufficient number of cells the incubation was carried out in 75 cm² culture flasks (NUNC, Wiesbaden, Germany) with 20 ml of culture medium. For each concentration of the test compounds U-373 MG cells were seeded in one culture flask, respectively, and grown to 70-80 % confluence. 20 μ l of the stock solutions were added to the culture medium to achieve the final concentration of the test compounds and afterwards the cells were incubated for 24 h in a water saturated atmosphere (95 % air/5 % carbondioxide) at 37 °C. The culture medium was removed, the cells were trypsinized, washed with PBS and adjusted to number of $1 \cdot 10^6$ cells per ml with PBS. 5 ml of this cell suspension ($5 \cdot 10^6$ cells) was pipetted in a 12 ml Falcon[®] tube (BD Biosciences, Heidelberg, Germany) and centrifuged at 1200 rpm for 10 min. The supernatant was discarded, the cell pellet was resuspended with 1 ml of PBS and the cells were separated by pipetting.

The fixation of the cells was assured by adding 9 ml ice cold 70 % ethanol and incubated at 4 °C for 1 h. After centrifugation the supernatant was discarded, cells were separated by pipetting with 1 ml of PBS and finally 9 ml of PBS were added. The cell suspension was centrifuged again, the supernatant was discarded, the cell pellet was resuspended with 0.5 ml of PBS and 0.5 ml of DNA extraction buffer (192 ml of 0.2 M Na₂HPO₄ and 8 ml of 0.1 M citric acid, pH 7.8) were added. After an incubation period of 5 min at room temperature the cell suspension was centrifuged, the supernatant was discarded and 1 ml DNA staining solution (20 mg/l propidium iodide (SIGMA) and 200 mg/l RNase (SIGMA) in PBS) was added. All samples were incubated as exactly as possible for 30 min in the dark (Jaroszeski et al., 1998). A FACS Calibur[™] (Becton Dickinson, Heidelberg, Germany) and CellQuest software was used to analyze the fluorescence intensity of the cells. A minimum of 30,000 events was collected per sample and the events were gated according to forward scatter and sideward scatter to exclude clumps and debris. The photomultiplier settings were as follows: E-1 for FSC (log), 150 for SSC (log) and 375 for FL3-H (linear). The amplifier gain for FL3-H, FL3-A and FL3-W were 2.00, 1.85 and 1.00, respectively. The FL3-A versus FL3-W dot plots and the corresponding FL3-H histograms were analyzed by the software "MultiCycle for Windows" (Phoenix Flow Systems, San Diego, CA, USA) at the Institute of Pathology (University of Regensburg)

4.4 Results

The Kb-V1 and the MCF-7/Topo cell variants, respectively, were used to investigate the inhibitory activity and selectivity of new tariquidar analogs at the ABCB1 and ABCG2 transporter. The tariquidar analogs were examined in two different test series. Firstly, the inhibitory activity and selectivity was investigated with the flow cytometric calcein-AM efflux assay and mitoxantrone efflux assay, respectively. Secondly, the ability of the modulators to potentiate the cytotoxicity of the cytostatic topotecan was evaluated in the chemosensitivity assay.

Furthermore, the antiproliferative effect of the compounds on human glioblastoma U-373 MG cells was determined in the chemosensitivity assay during permanent incubation. In order to proof whether the cytotoxic effect of the compounds is caused by specific interference during cell cycle, quiescent U-373 MG cells were incubated with the tariquidar analogs.

4.4.1 Inhibitory activity and selectivity

The ABCB1 inhibitory activity (IC_{50} values) of the new tariquidar analogs was determined in the calcein-AM efflux assay. In order to obtain information about the selectivity of the modulators the inhibitory activity at the ABCG2 transporter was tested in the mitoxantrone assay. The test compounds were used at different concentrations with respect to the construction of concentration response curves. A sample incubated without test compounds (with DMSO as vehicle) served as negative control and represented 0 % inhibition. The value for 100 % inhibition was determined with tariquidar (1 μ M) in case of the calcein-AM efflux assay and with fumitremorgin C (10 μ M) in case of the mitoxantrone efflux assay. The geometric means were calculated from the fluorescence intensity histograms, related to the controls and plotted against the test compound concentration. Addition of increasing modulator concentrations led to sigmoidal concentration response curves. The IC_{50} values were calculated using Hill equation. The results of the calcein-AM efflux assay (a) and of the mitoxantrone efflux assay (b) of the tariquidar analogs are shown in Figure 4.1, Figure 4.2, Figure 4.3 and Figure 4.4.

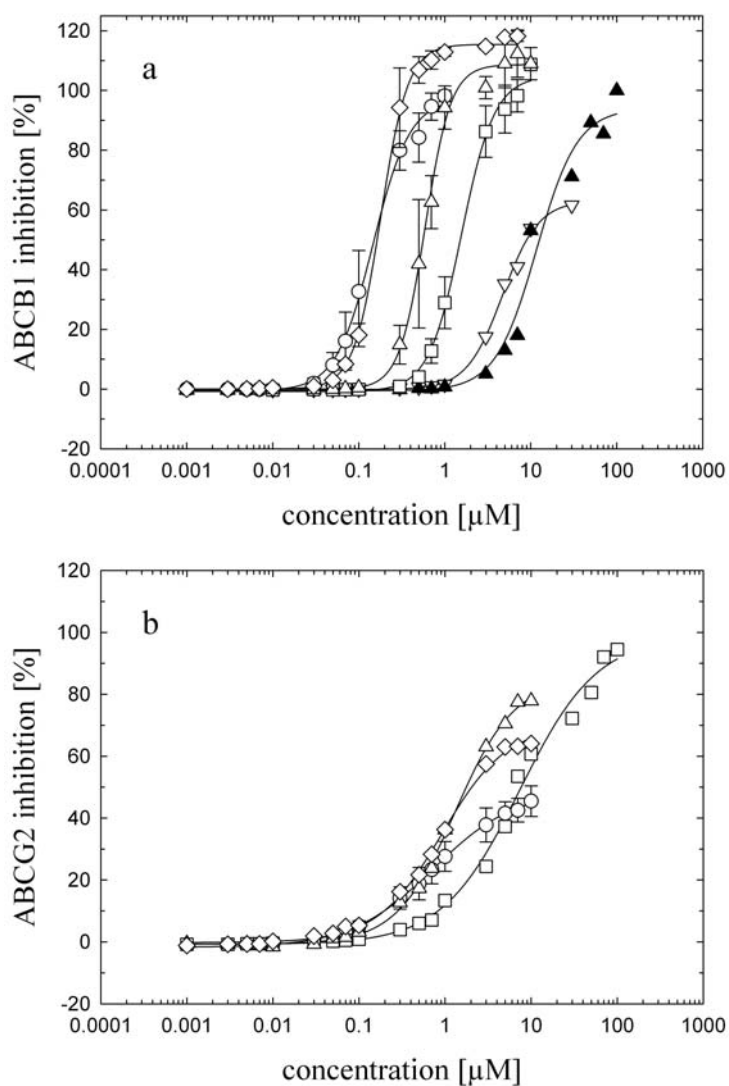


Figure 4.1: a) ABCB1 inhibition and b) ABCG2 inhibition by tariquidar and new tariquidar analogs in dependence of their concentrations. Compound **3** (*open inverted triangle*), **4** (*filled triangle*), **5** (*open circle*), **6** (*open square*), **7** (*open triangle*) and **8** (*open diamond*). The inhibitory activity of the compounds **3** and **4** has not been tested so far.

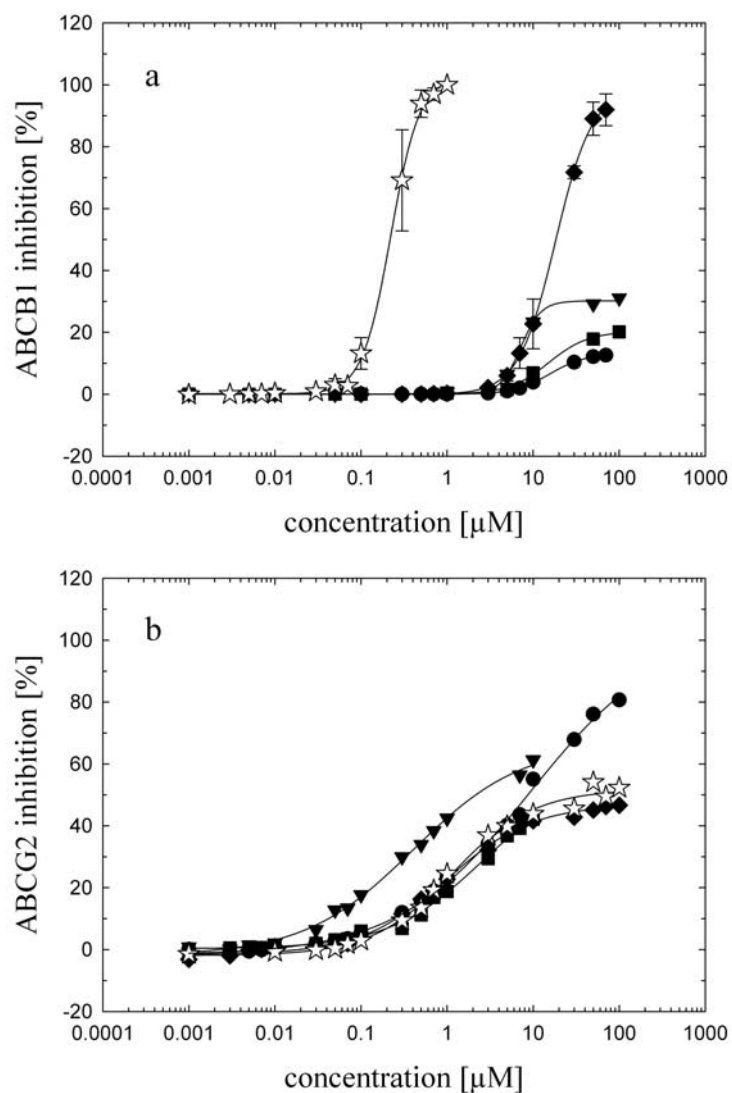


Figure 4.2: a) ABCB1 inhibition and b) ABCG2 inhibition by tariquidar and new tariquidar analogs in dependence of their concentrations. Tariquidar (*open stars*), compound **9** (*filled circle*), **10** (*filled diamond*), **11** (*filled inverted triangle*) and **12** (*filled square*).

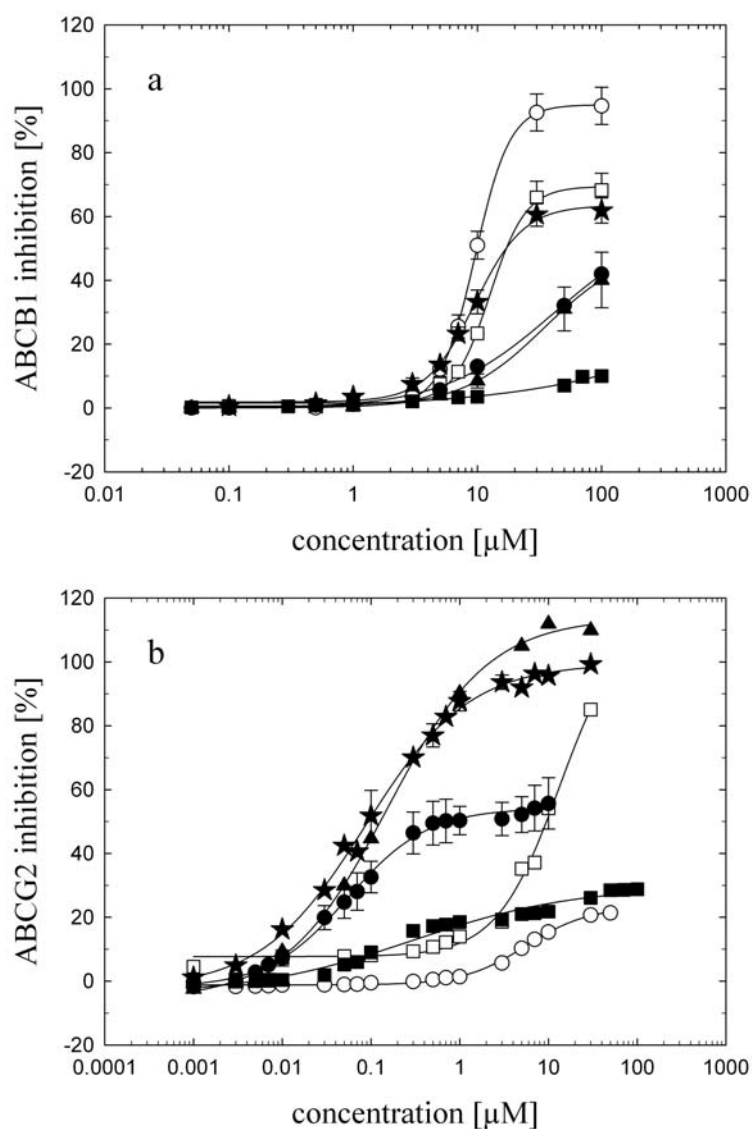


Figure 4.3: a) ABCB1 inhibition and b) ABCG2 inhibition by tariquidar and new tariquidar analogs in dependence of their concentrations. Compound **13** (*open circle*), **14** (*open square*), **15** (*filled star*), **16** (*filled circle*), **17** (*filled square*) and **18** (*filled triangle*).

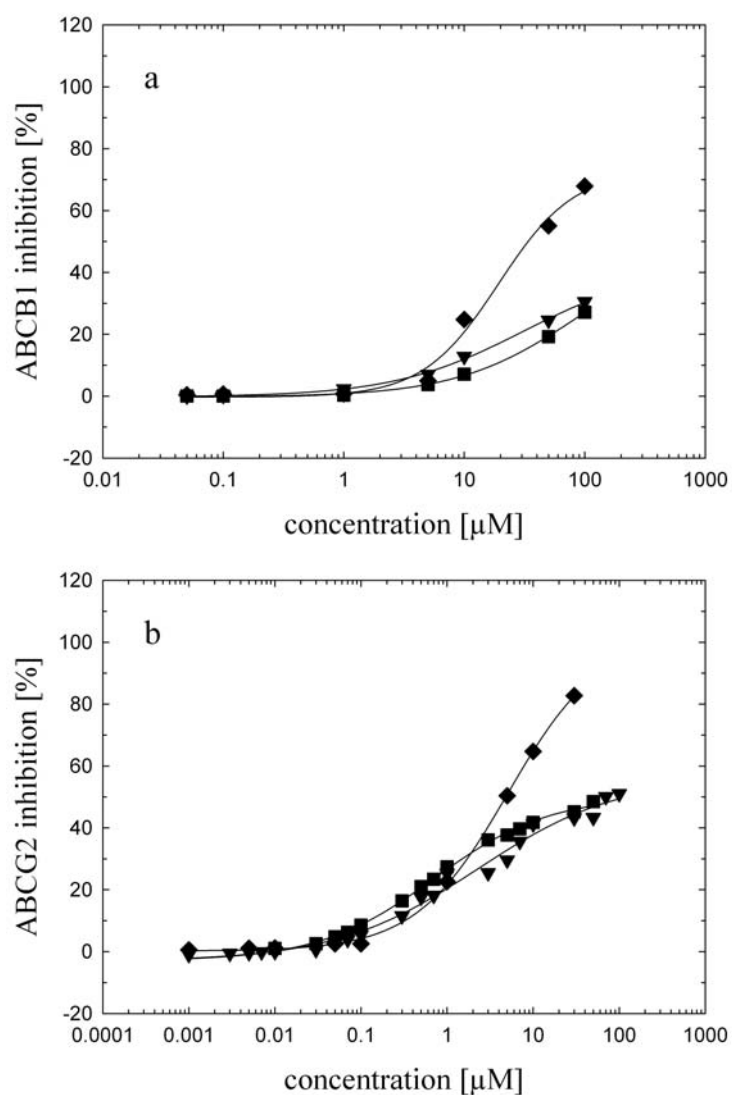


Figure 4.4: a) ABCB1 inhibition and b) ABCG2 inhibition by tariquidar and new tariquidar analogs in dependence of their concentrations. Compound **19** (*filled diamond*), **20** (*filled inverted triangle*) and **21** (*filled square*).

The results of the concentration-response curves of the tariquidar analogs are summarized as IC_{50} values, efficacies and Hill coefficients in Table 4.4.

Table 4.4: Inhibitory activity (IC₅₀ values), efficacy and Hill coefficients of tariquidar and tariquidar analogs at the ABCB1 and ABCG2 transporter, respectively.

Compd.	IC ₅₀ [nM] ABCB1	efficacy [%]	Hill coeff.	n	IC ₅₀ [nM] ABCG2	efficacy [%]	Hill coeff.	n
tariquidar	223 ± 8	102	2.6	5	1,176 ± 123	52	0.9	1
1	no effect	–	–	2	no effect	–	–	2
2	no effect	–	–	2	no effect	–	–	2
3	4,720 ± 169	63	2.1	1	n. d.			
4	11,700 ± 1,510	94	1.8	1	n. d.			
5*	145 ± 12	98	1.9	3	711 ± 62	49	0.9	2
6*	1,575 ± 98	105	2.3	3	7,375 ± 1,000	99	1.0	1
7*	593 ± 21	109	2.9	3	1,320 ± 83	85	1.3	1
8*	181 ± 6	116	2.7	3	920 ± 64	70	1.2	1
9	15,840 ± 2,500	13	2.1	2	9,333 ± 1,970	104	0.7	1
10	17,950 ± 4,200	98	2.2	2	988 ± 64	47	0.9	1
11	7,175 ± 190	30	3.7	1	393 ± 59	66	0.7	1
12	15,100 ± 1,550	20	1.9	1	1,990 ± 355	52	0.9	1
13	9,600 ± 85	95	3.1	3	5,564 ± 323	23	1.2	1
14	12,570 ± 502	70	2.9	3	13,300 ± 4,300	114	1.2	1
15	9,450 ± 417	64	2.1	3	100 ± 8	100	0.7	2
16	38,570 ± 8,840	59	1.0	1	55 ± 4	54	1.0	3
17	~ 30,000	~ 10	0.5	1	290 ± 110	30	0.5	1
18	34,660 ± 183	50	1.3	2	154 ± 15	114	0.8	1
19	19,300 ± 5,180	73	0.9	1	6,310 ± 1,106	111	1.2	1
20	29,100 ± 8,430	41	0.8	1	2,270 ± 760	57	0.5	1
21	84,170 ± 26,690	50	0.9	1	709 ± 63	50	0.7	1

*) ABCB1 inhibitory activity has already been published (Egger et al., 2007)

4.4.2 Effect of tariquidar analogs on the chemosensitivity of Kb-V1 cells against topotecan

Over the whole incubation period of up to 150 h Kb-V1 cells were exposed to the cytostatic drug topotecan, which is a known ABCB1 substrate. Topotecan was used at a low concentration of 50 nM that did not affect the growth of Kb-V1 cells. Additionally, the cells were incubated with combinations of topotecan and 4 different concentrations of the tariquidar analogs. The ability of the tariquidar analogs to reverse resistance of the Kb-V1 cells to topotecan is shown in Figure 4.5, Figure 4.6, Figure 4.7, Figure 4.8 and Figure 4.9. To consider that this effect results from ABCB1 inhibition, the effect of the tariquidar analogs alone on Kb-V1 cells was tested as well.

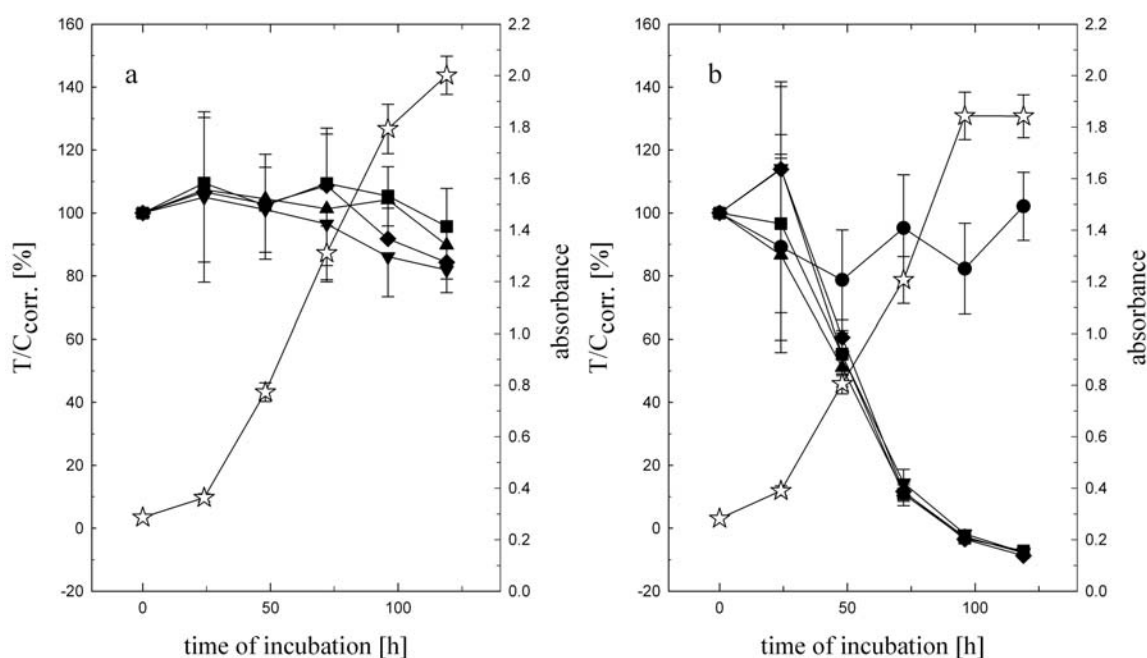


Figure 4.5: a) Effect of compound **5** on proliferating Kb-V1 cells (passage 46) during permanent incubation. b) Effect of compound **5** in combination with 50 nM topotecan. Vehicle (*open star*), 50 nM topotecan (*filled circle*) and compound **5** at different concentrations: 50 nM (*filled square*), 100 nM (*filled triangle*), 500 nM (*filled diamond*) and 1 μM (*filled inverted triangle*).

The resistance of Kb-V1 cells to topotecan was completely reversed by the addition of compound **5** (Figure 4.5) and **7** (Figure 4.6), respectively, at a concentration of 50 nM, whereas these tariquidar analogs alone had no cytotoxic effect. Compound **13** (Figure 4.7) showed a weak cytotoxic effect at a concentration of 10 μM. But the same effect could be observed by the addition of compound **13** at a concentration of 1 μM to topotecan and the completely reversed resistance was determined at a concentration of 10 μM.

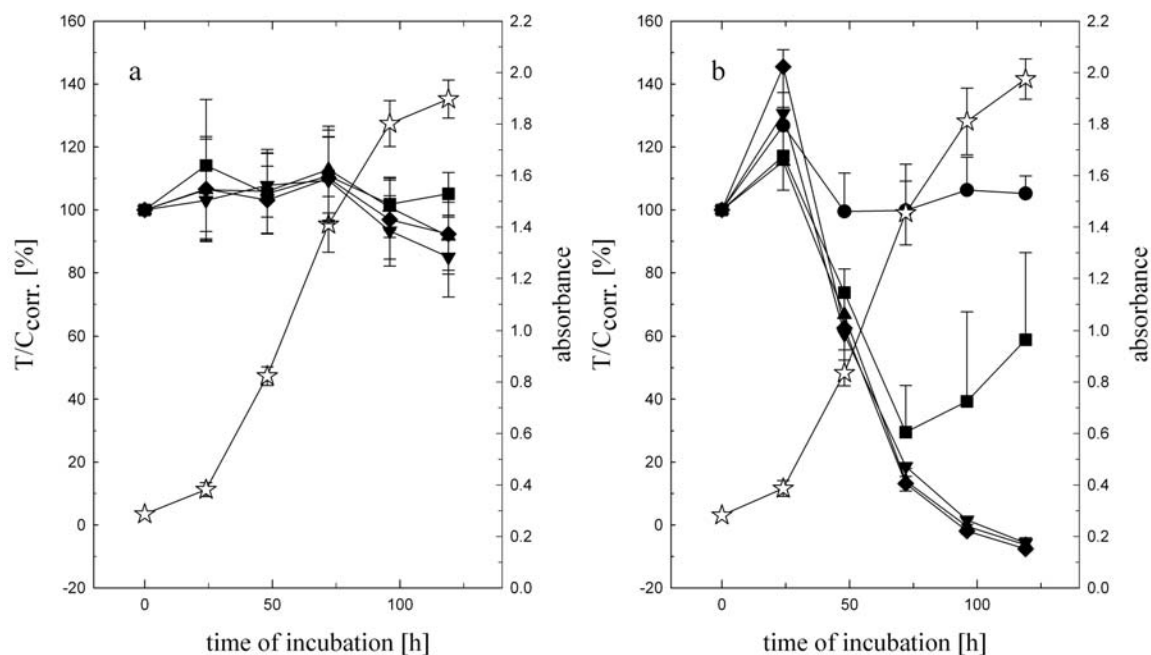


Figure 4.6: a) Effect of compound **7** on proliferating Kb-V1 cells (passage 46) during permanent incubation. b) Effect of compound **7** in combination with 50 nM topotecan. Vehicle (*open star*), 50 nM topotecan (*filled circle*) and compound **7** at different concentrations: 50 nM (*filled square*), 100 nM (*filled triangle*), 500 nM (*filled diamond*) and 1 μ M (*filled inverted triangle*).

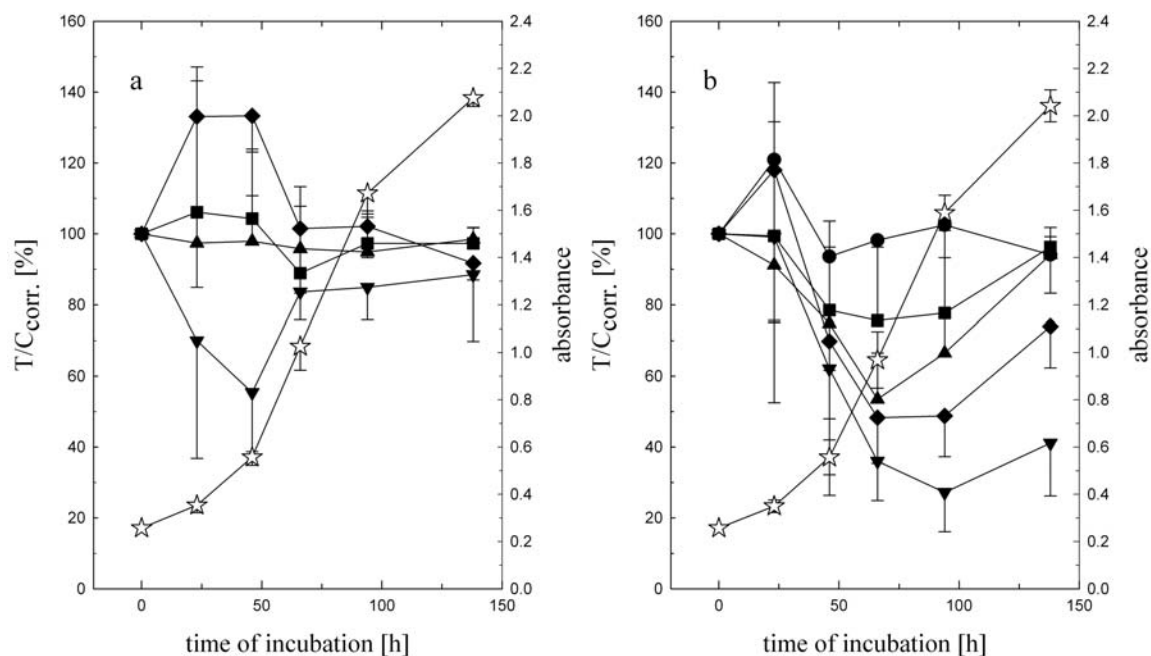


Figure 4.7: a) Effect of compound **13** on proliferating Kb-V1 cells (passage 29) during permanent incubation. b) Effect of compound **13** in combination with 50 nM topotecan. Vehicle (*open star*), 50 nM topotecan (*filled circle*) and compound **13** at different concentrations: 0.5 μ M (*filled square*), 1 μ M (*filled triangle*), 3 μ M (*filled diamond*) and 10 μ M (*filled inverted triangle*).

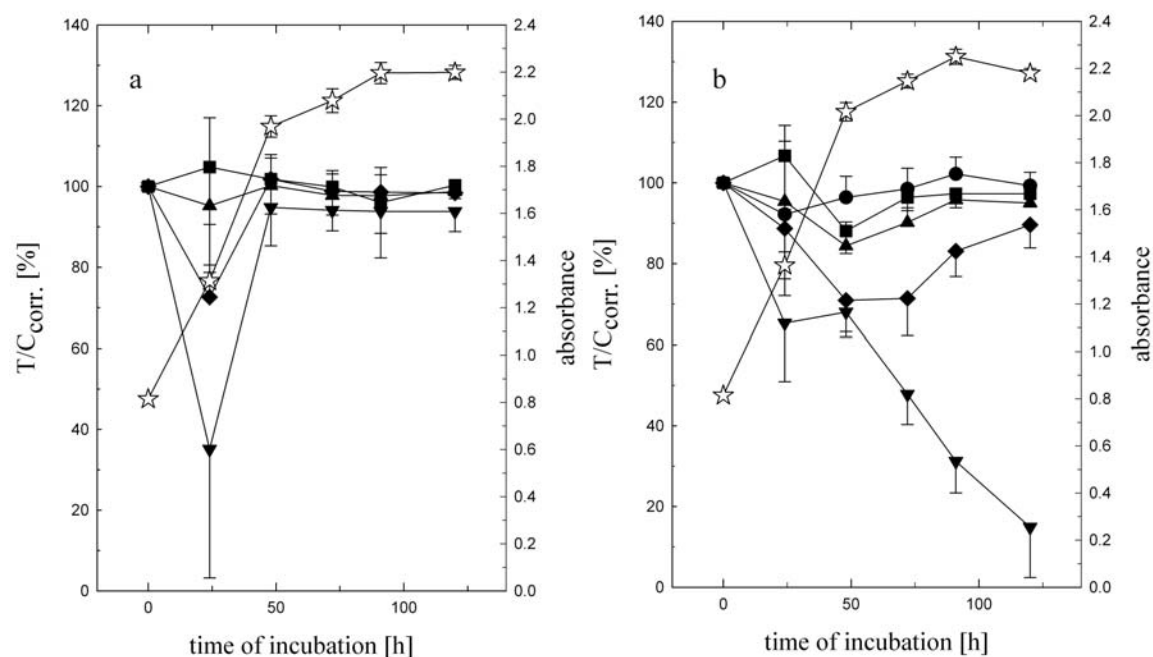


Figure 4.8: a) Effect of compound **14** on proliferating Kb-V1 cells (passage 38) during permanent incubation. b) Effect of compound **14** in combination with 50 nM topotecan. Vehicle (*open star*), 50 nM topotecan (*filled circle*) and compound **14** at different concentrations: 0.5 μM (*filled square*), 1 μM (*filled triangle*), 3 μM (*filled diamond*) and 10 μM (*filled inverted triangle*).

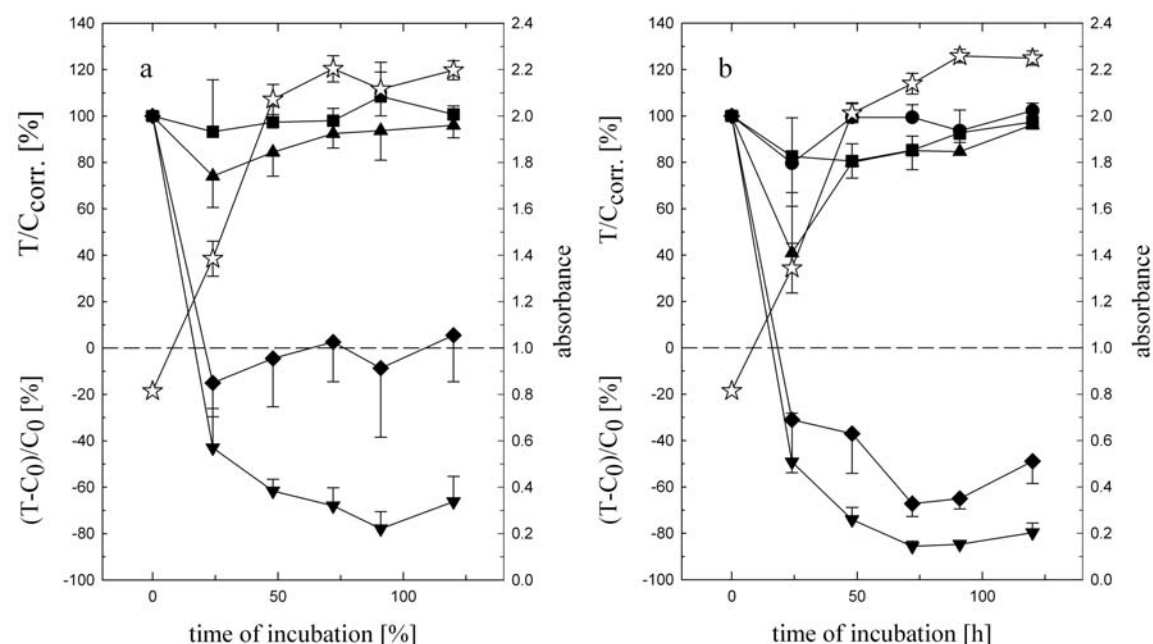


Figure 4.9: a) Effect of compound **15** on proliferating Kb-V1 cells (passage 38) during permanent incubation. b) Effect of compound **15** in combination with 50 nM topotecan. Vehicle (*open star*), 50 nM topotecan (*filled circle*) and compound **15** at different concentrations: 0.5 μM (*filled square*), 1 μM (*filled triangle*), 3 μM (*filled diamond*) and 10 μM (*filled inverted triangle*).

Compound **14** (Figure 4.8) showed a cytotoxic effect at a concentration of 10 μ M. The combination of topotecan with **14** at this concentration resulted in a strong cytostatic effect. However, concentrations above 1 μ M are very high and not relevant for in vivo applications. The combination of topotecan with compound **15** (Figure 4.9) at a concentration of 3 μ M resulted in a cytotoxic effect indicating the reversion of the topotecan resistance. But at this concentration compound **15** alone had a cytostatic effect, and incubation with 10 μ M of compound **15** led to a cytotoxic effect.

4.4.3 Effect of tariquidar analogs on the chemosensitivity of MCF-7/Topo cells against topotecan

Over the whole incubation period of up to 170 h MCF-7/Topo cells were exposed to the cytostatic drug topotecan which is not only a known ABCB1 but also an ABCG2 substrate. Topotecan was used at a low concentration of 100 nM that did not affect the growth of MCF-7/Topo cells. Additionally, the cells were incubated with combinations of topotecan and 4 different concentrations of the tariquidar analogs. The ability of the tariquidar analogs to reverse resistance of the MCF-7/Topo cells to topotecan is shown in Figure 4.10, Figure 4.11, Figure 4.12, Figure 4.13, Figure 4.14, Figure 4.15 and Figure 4.16. To consider that this effect results from ABCG2 inhibition, the effect of the tariquidar analogs alone on MCF-7/Topo cells was tested.

The resistance of MCF-7/Topo cells to topotecan was completely reversed by the addition of compound **11** (Figure 4.10) at a concentration of 100 nM, whereas these tariquidar analog alone had no cytotoxic effect at this concentration. Only at a concentration of 500 nM this analog showed a cytostatic effect.

Compound **12** (Figure 4.11) alone had no cytotoxic effect on MCF-7/Topo cells at all. But the combination of **12** at a concentration of 500 nM with topotecan caused a cytostatic effect.

Compound **13** (Figure 4.12) and **14** (Figure 4.13) exhibited very similar antiproliferative effects. The incubation of MCF-7/Topo cells with 30 μ M of the tariquidar analogs alone and in combination with topotecan resulted both in a cytotoxic effect. However, at a concentration of 10 μ M a difference became obvious: the tariquidar analog alone had only a cytotoxic effect whereas the combination with topotecan led to a cytostatic effect.

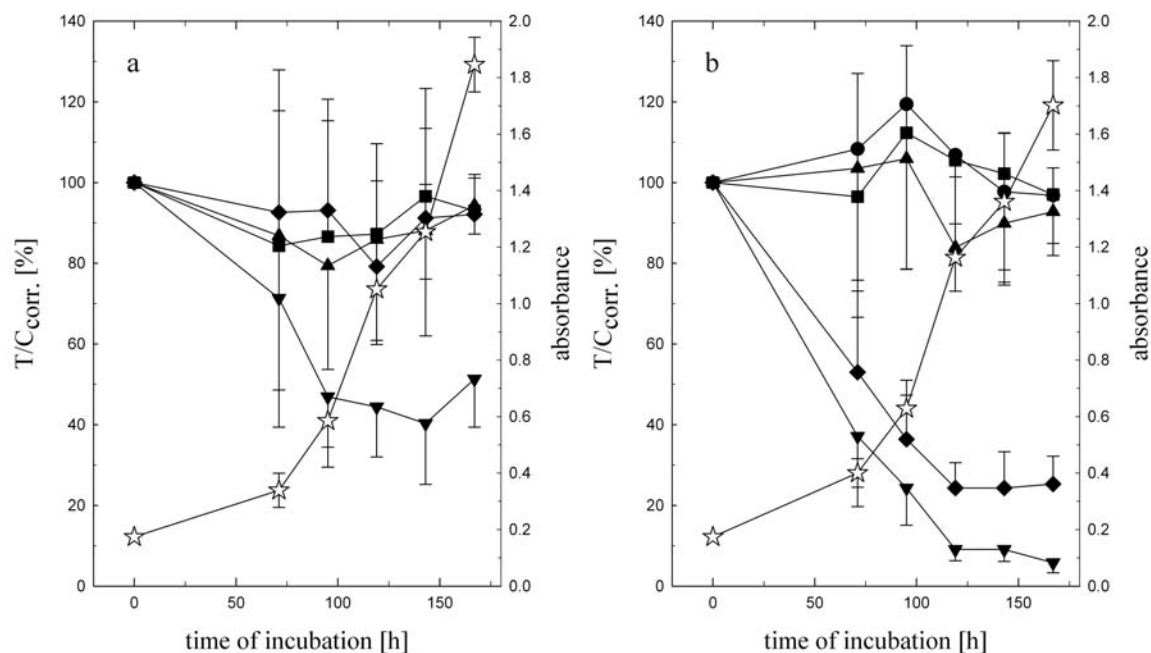


Figure 4.10: a) Effect of compound **11** on proliferating MCF-7/Topo cells (passage 94) during permanent incubation. b) Effect of compound **11** in combination with 100 nM topotecan. Vehicle (*open star*), 100 nM topotecan (*filled circle*) and compound **11** at different concentrations: 1 nM (*filled square*), 10 nM (*filled triangle*), 100 nM (*filled diamond*) and 500 nM (*filled inverted triangle*).

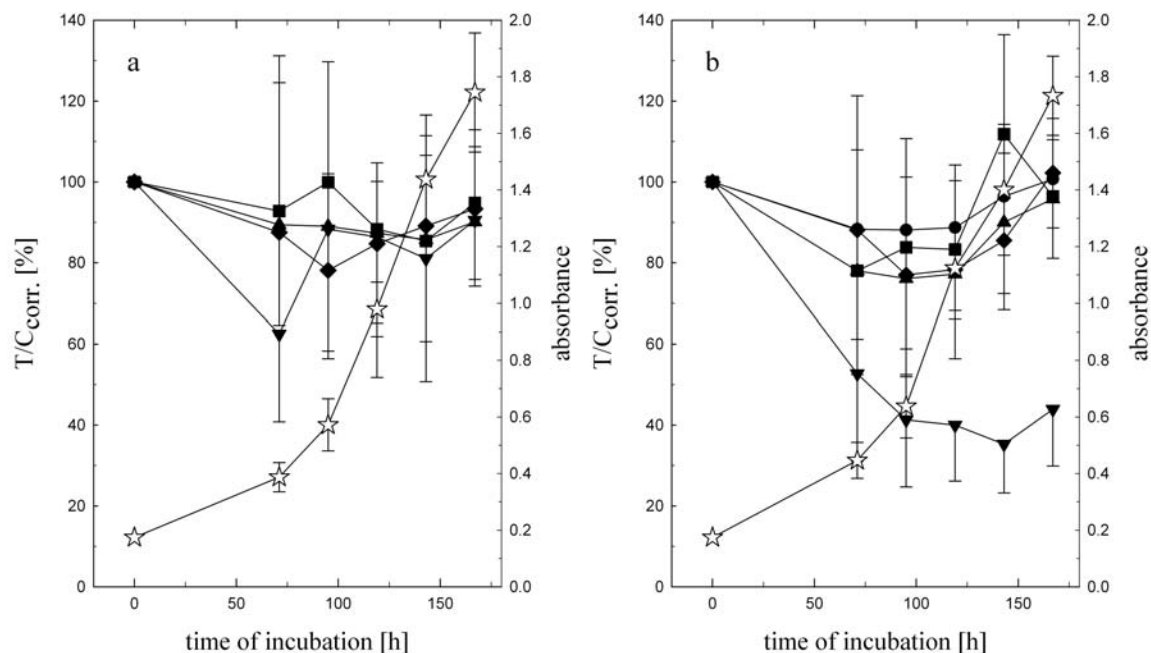


Figure 4.11: a) Effect of compound **12** on proliferating MCF-7/Topo cells (passage 94) during permanent incubation. b) Effect of compound **12** in combination with 100 nM topotecan. Vehicle (*open star*), 100 nM topotecan (*filled circle*) and compound **12** at different concentrations: 1 nM (*filled square*), 10 nM (*filled triangle*), 100 nM (*filled diamond*) and 500 nM (*filled inverted triangle*).

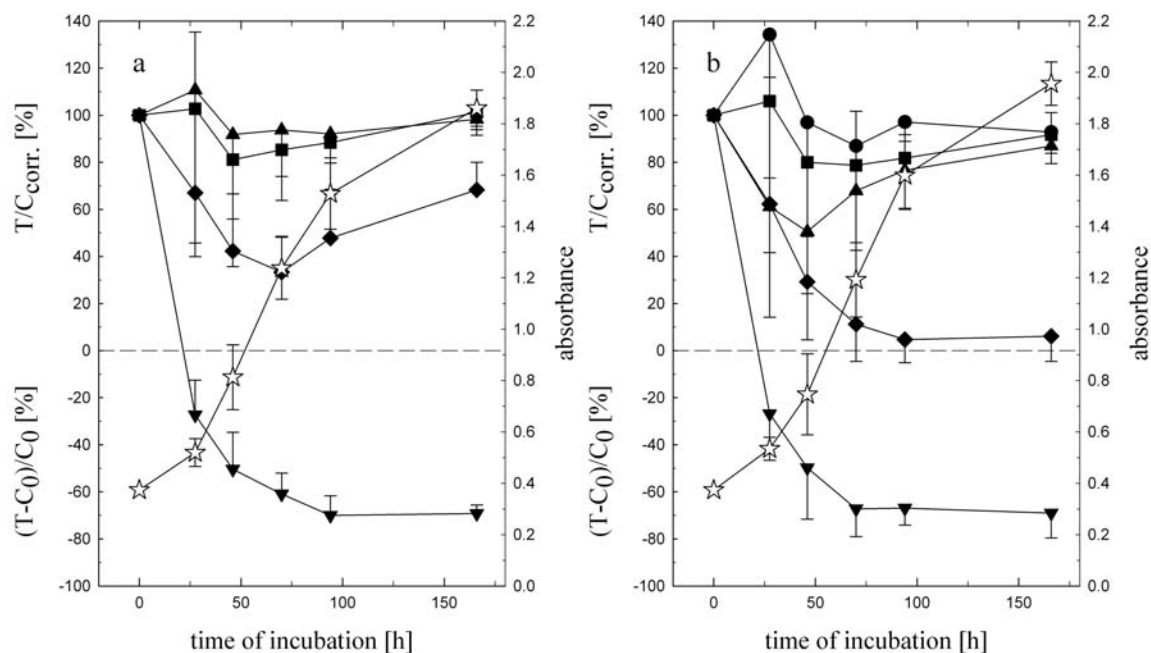


Figure 4.12: a) Effect of compound **13** on proliferating MCF-7/Topo cells (passage 90) during permanent incubation. b) Effect of compound **13** in combination with 100 nM topotecan. Vehicle (*open star*), 100 nM topotecan (*filled circle*) and compound **13** at different concentrations: 1 μM (*filled square*), 3 μM (*filled triangle*), 10 μM (*filled diamond*) and 30 μM (*filled inverted triangle*).

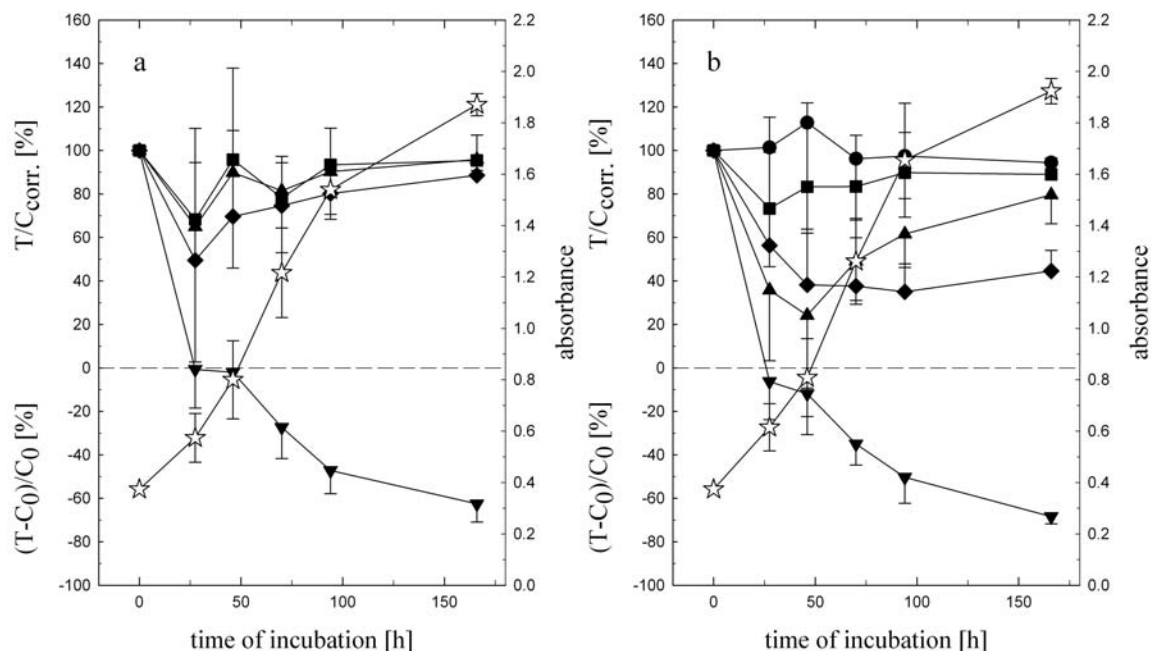


Figure 4.13: a) Effect of compound **14** on proliferating MCF-7/Topo cells (passage 90) during permanent incubation. b) Effect of compound **14** in combination with 100 nM topotecan. Vehicle (*open star*), 100 nM topotecan (*filled circle*) and compound **14** at different concentrations: 1 μM (*filled square*), 3 μM (*filled triangle*), 10 μM (*filled diamond*) and 30 μM (*filled inverted triangle*).

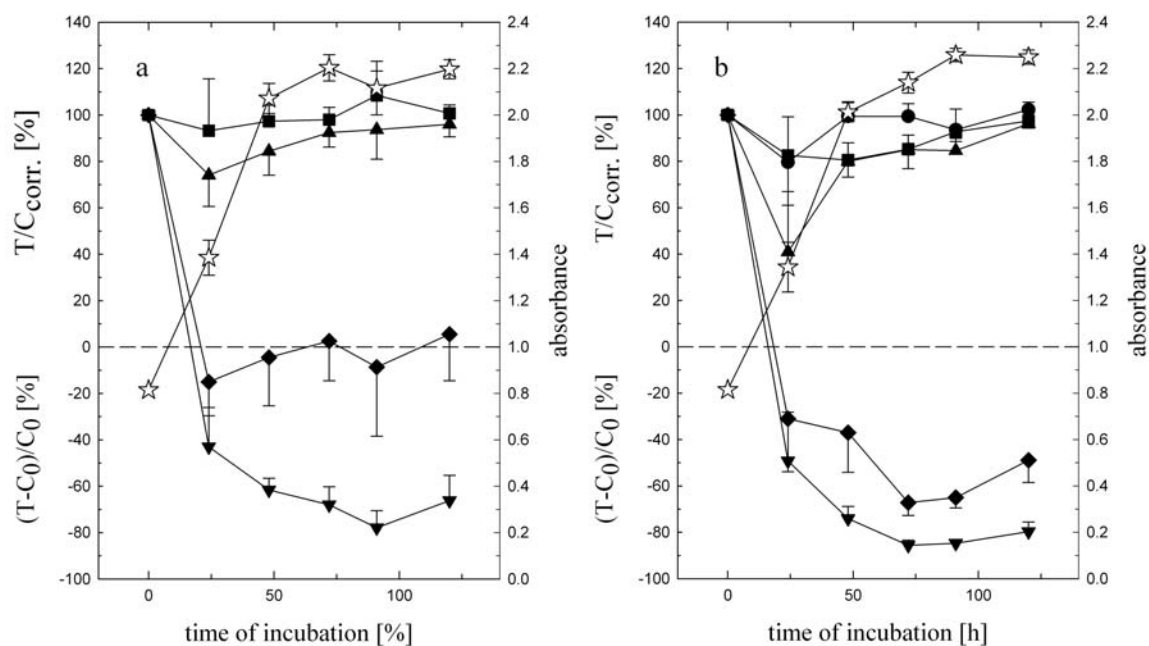


Figure 4.14: a) Effect of compound **15** on proliferating MCF-7/Topo cells (passage 49) during permanent incubation. b) Effect of compound **15** in combination with 100 nM topotecan. Vehicle (*open star*), 100 nM topotecan (*filled circle*) and compound **15** at different concentrations: 1 nM (*filled square*), 10 nM (*filled triangle*), 100 nM (*filled diamond*) and 500 nM (*filled inverted triangle*).

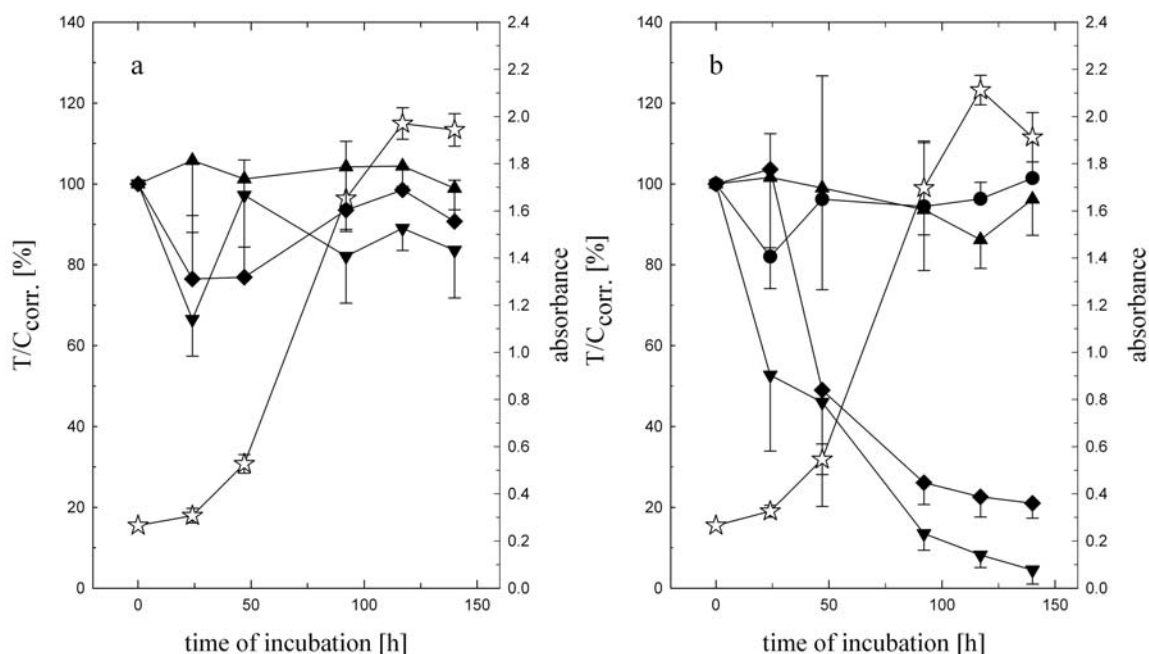


Figure 4.15: a) Effect of compound **16** on proliferating MCF-7/Topo cells (passage 110) during permanent incubation. b) Effect of compound **16** in combination with 100 nM topotecan. Vehicle (*open star*), 100 nM topotecan (*filled circle*) and compound **16** at different concentrations: 10 nM (*filled triangle*), 100 nM (*filled diamond*) and 500 nM (*filled inverted triangle*).

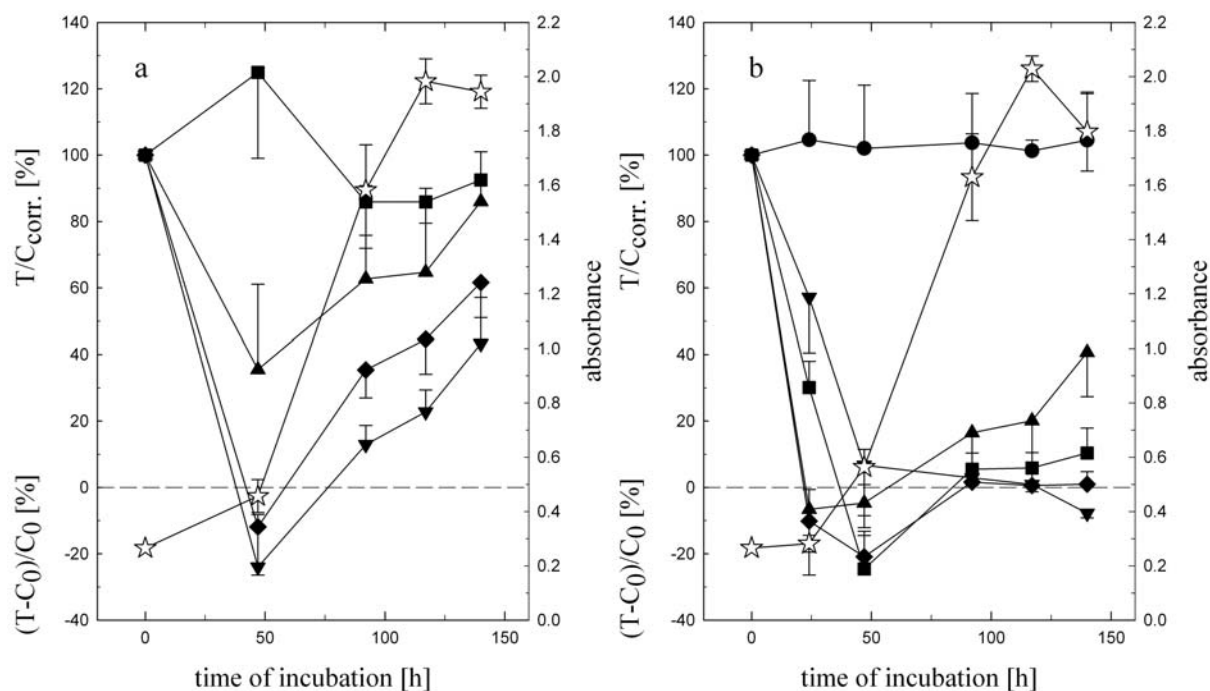


Figure 4.16: a) Effect of compound **18** on proliferating MCF-7/Topo cells (passage 110) during permanent incubation. b) Effect of compound **18** in combination with 100 nM topotecan. Vehicle (*open star*), 100 nM topotecan (*filled circle*) and compound **18** at different concentrations: 1 nM (*filled square*), 10 nM (*filled triangle*), 100 nM (*filled diamond*) and 500 nM (*filled inverted triangle*).

Compound **15** (Figure 4.14) alone had such a pronounced cytostatic effect on MCF-7/Topo cells at a concentration of 100 nM that only a slight enhancement of the effect caused by the combination with topotecan was detectable. At a concentration of 500 nM no difference between the treatment of the cells with **15** alone and in combination with topotecan was measured at all.

Incubation of MCF-7/Topo cells with compound **16** (Figure 4.15) alone resulted in weak cytotoxic effects at concentrations of 100 nM and 500 nM. However, the same concentrations of **16** resulted in cytostatic effects when the compound was combined with topotecan indicating that the topotecan resistance of the cells was completely reversed.

Strong cytostatic effects were observed incubating MCF-7/Topo cells with compound **18** (Figure 4.16) at concentrations of 10 nM, 100 nM and 500 nM. However, the combination of topotecan and compound **18** at a very low concentration of 1 nM resulted in a complete reversion of the multidrug resistance of the cells and a cytostatic effect. The use of higher concentrations of **18** also yielded a cytostatic effect, thus providing no benefit.

4.4.4 Effect of tariquidar analogs on proliferating U-373 MG cells

Incubating Kb-V1 or MCF-7/Topo cells, respectively, with the new tariquidar derivatives alone, some of the compounds showed cytotoxic, cytostatic or cytocidal effects. In order to proof whether these effects resulted from the inhibition of the ABC transporters or not, the chemosensitivity of ABCB1 and ABCG2 negative human glioblastoma U-373 MG cells was investigated (Figure 4.17 to Figure 4.21). Antiproliferative effects of the tariquidar derivatives on U-373 MG cells would point out that the cytotoxicity of the compound is independent of their inhibitory activity at the ABCB1 or ABCG2 transporter, respectively.

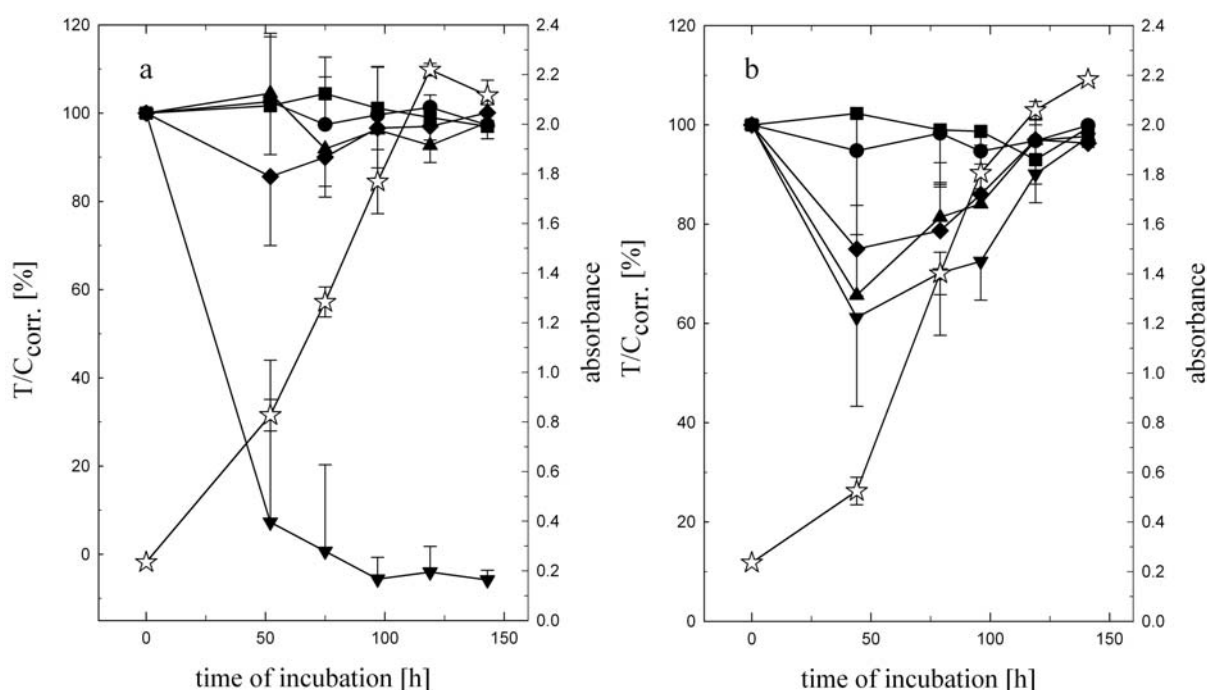


Figure 4.17: Effect of compound **11** (a) and compound **12** (b) on proliferating U-373 MG cells (passage 362) during permanent incubation; vehicle (*open star*), 0.1 μM (*filled circle*), 0.5 μM (*filled square*), 1 μM (*filled triangle*), 3 μM (*filled diamond*) and 10 μM (*filled inverted triangle*).

On proliferating U-373 MG cells compound **11** showed a cytostatic effect at a concentration of 10 μM indicating that the cytotoxic effect on proliferating MCF-7/Topo was independent of ABCG2 inhibition. Compound **12** had a very weak cytotoxic effect on MCF-7/Topo cells and also the effect on U-373 MG cells was very weak even at very high concentrations of 3 and 10 μM. On Kb-V1 and MCF-7/Topo cells compounds **13** and **14** exerted nearly the same cytotoxic effect at 10 μM and cytostatic effect at 30 μM, respectively. On U-373 MG cells both compounds had a strong cytostatic effect at a concentration of 10 μM.

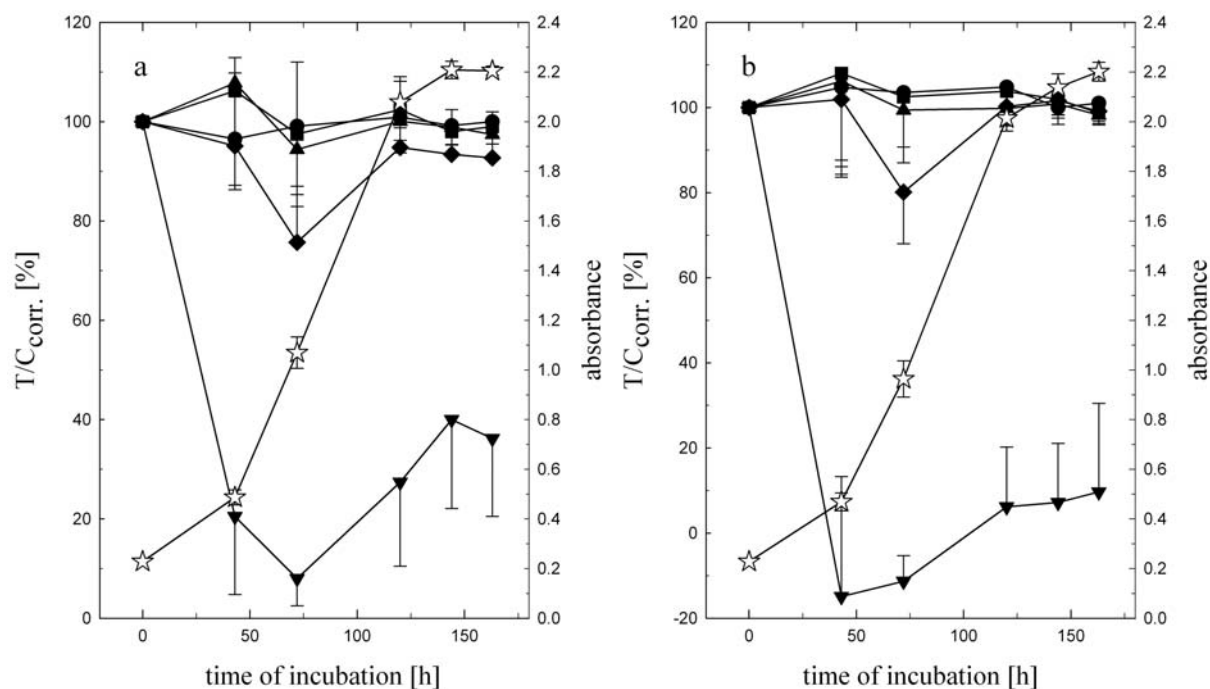


Figure 4.18: Effect of compound **13** (a) and compound **14** (b) on proliferating U-373 MG cells (passage 359) during permanent incubation; vehicle (*open star*), 0.1 μ M (*filled circle*), 0.5 μ M (*filled square*), 1 μ M (*filled triangle*), 3 μ M (*filled diamond*) and 10 μ M (*filled inverted triangle*).

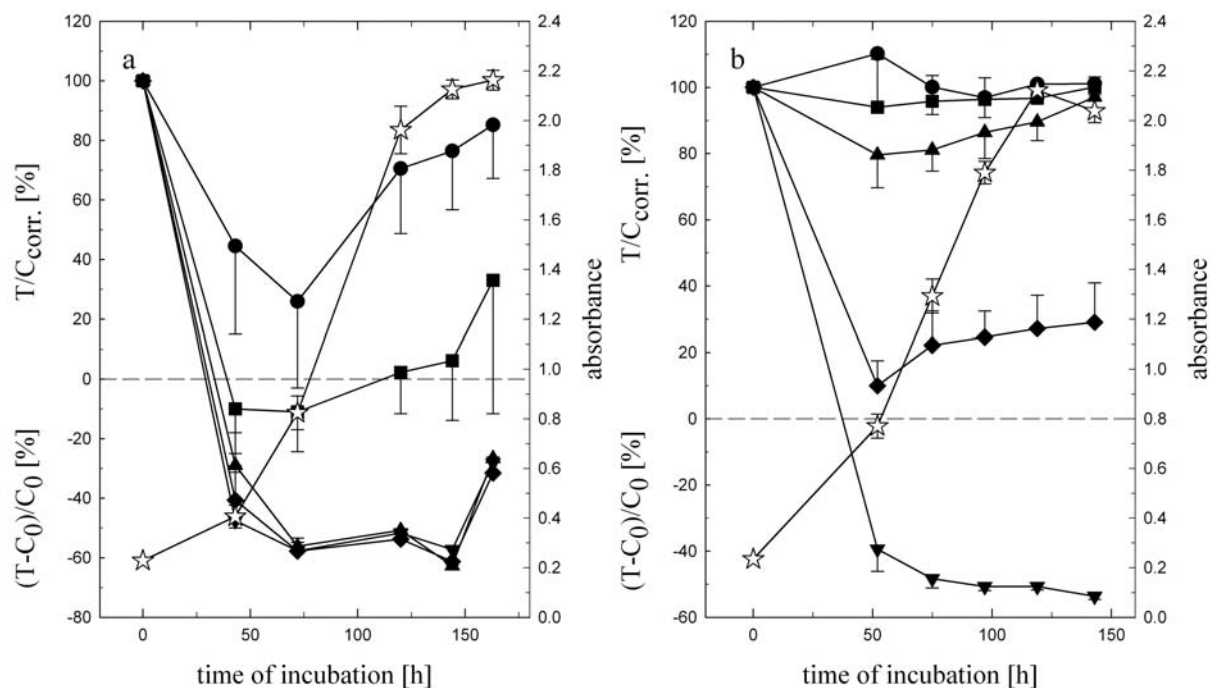


Figure 4.19: Effect of compound **15** (a) and compound **16** (b) on proliferating U-373 MG cells (passage 359 and 362, respectively) during permanent incubation; vehicle (*open star*), 0.1 μ M (*filled circle*), 0.5 μ M (*filled square*), 1 μ M (*filled triangle*), 3 μ M (*filled diamond*) and 10 μ M (*filled inverted triangle*).

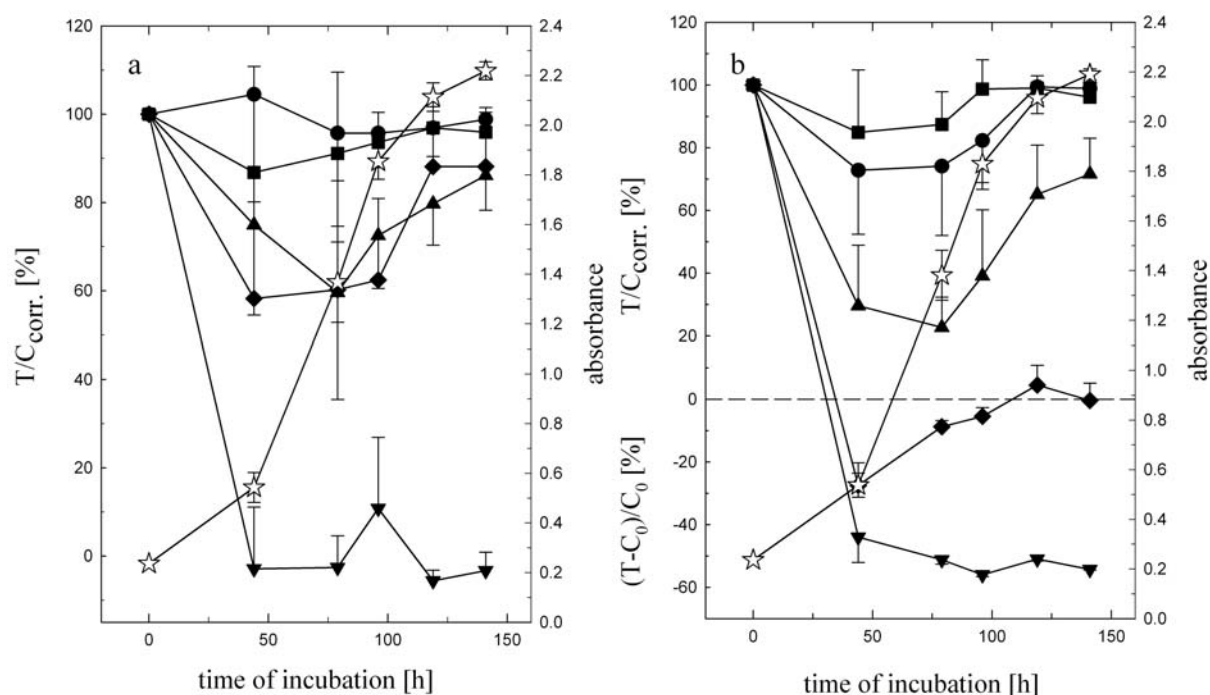


Figure 4.20: Effect of compound **18** (a) and compound **20** (b) on proliferating U-373 MG cells (passage 362) during permanent incubation; vehicle (*open star*), 0.1 μ M (*filled circle*), 0.5 μ M (*filled square*), 1 μ M (*filled triangle*), 3 μ M (*filled diamond*) and 10 μ M (*filled inverted triangle*).

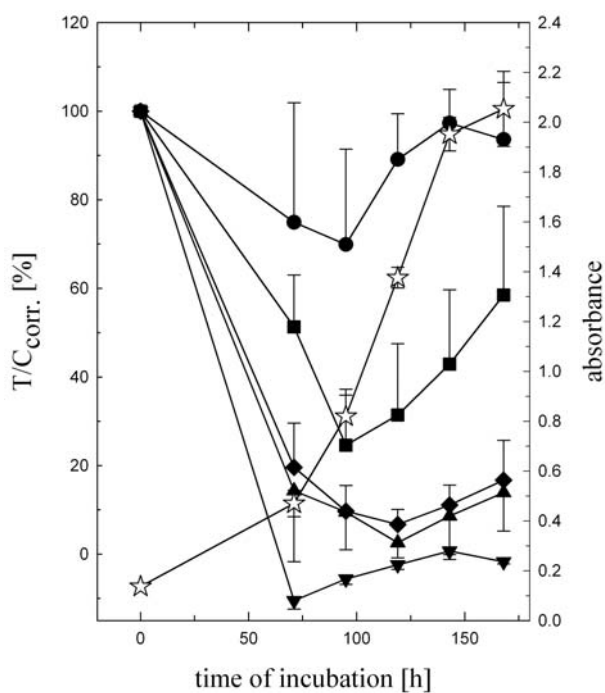


Figure 4.21: Effect of compound **21** on proliferating U-373 MG cells (passage 363) during permanent incubation; vehicle (*open star*), 0.01 μ M (*filled circle*), 0.05 μ M (*filled square*), 0.1 μ M (*filled triangle*), 1 μ M (*filled diamond*) and 10 μ M (*filled inverted triangle*).

On Kb-V1 and on MCF-7/Topo cells compound **15** had a cytostatic effect at a concentration of 3 μ M and 100 nM, respectively. On proliferating U-373 MG cells compound **15** showed a cytotoxic effect at a concentration of 100 nM and a cytostatic effect at 500 nM indicating that its cytotoxicity is independent of the ABCB1 or ABCG2 inhibition. The incubation of U-373 MG cells with compound **16** led to a cytostatic effect at a concentration of 3 μ M and to a cytocidal effect at 10 μ M. On proliferating U-373 MG cells compound **18** had a cytostatic effect at a concentration of 10 μ M indicating that the cytotoxic effect on proliferating MCF-7/Topo cells was independent of the inhibitory activity at the ABCG2 transporter. Compound **20** exerted a cytotoxic effect on proliferating U-373 MG cells at a concentration of 1 μ M, a cytostatic effect at 3 μ M and a cytocidal effect at 10 μ M. The strongest cytotoxicity exhibited compound **21** with a cytostatic effect at a very low concentration of 50 nM and a cytostatic effect at 100 nM.

4.4.5 Effect of tariquidar analogs on quiescent U-373 MG cells

It was shown that some of the new tariquidar analogs exhibited cytotoxic effects on proliferating Kb-V1, on MCF-7/Topo and on U-373 MG cells. In order to compare their effects with those of tubulin inhibitors like paclitaxel against resting cells, confluent cells were treated with the tariquidar analogs at a very high concentration of 10 μ M. Rotenone, an ubiquinon reductase inhibitor, blocking ATP synthesis, served as a positive control for maximum cytotoxic effect. The results are shown in Figure 4.22 and Figure 4.23.

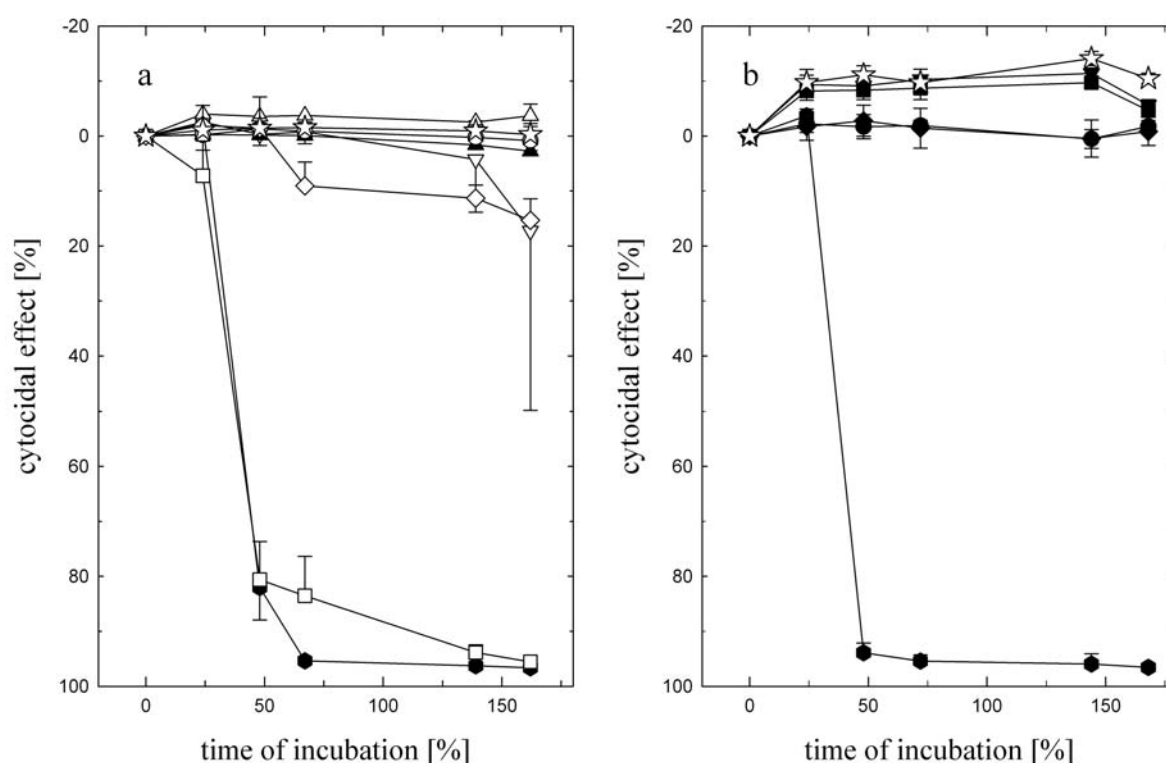


Figure 4.22: Incubation of resting U-373 MG cells with rotenone (500 nM), paclitaxel (10 nM) and new tariquidar analogs (20 μ M); vehicle (*open star*), rotenone (*filled hexagon*). a) Paclitaxel (*open diamond*) and series 1 with compound **3** (*open inverted triangle*), **4** (*filled triangle*), **5** (*open circle*), **6** (*open square*), **7** (*open triangle*) and b) series 2 with compound **9** (*filled circle*), **10** (*filled diamond*), **11** (*filled inverted triangle*) and **12** (*filled square*).

After 48 h, the positive control rotenone had a very strong cytotoxic effect as expected. Compound **6** produced nearly the same effect as rotenone. The cytostatic paclitaxel exerted a very weak cytotoxic effect after 3 days and compound **3** showed this effect after 6 days. The tariquidar analogs **4**, **5**, **7** of series 1 and **9**, **10**, **11**, **12** of series 2 had no effect on resting cells.

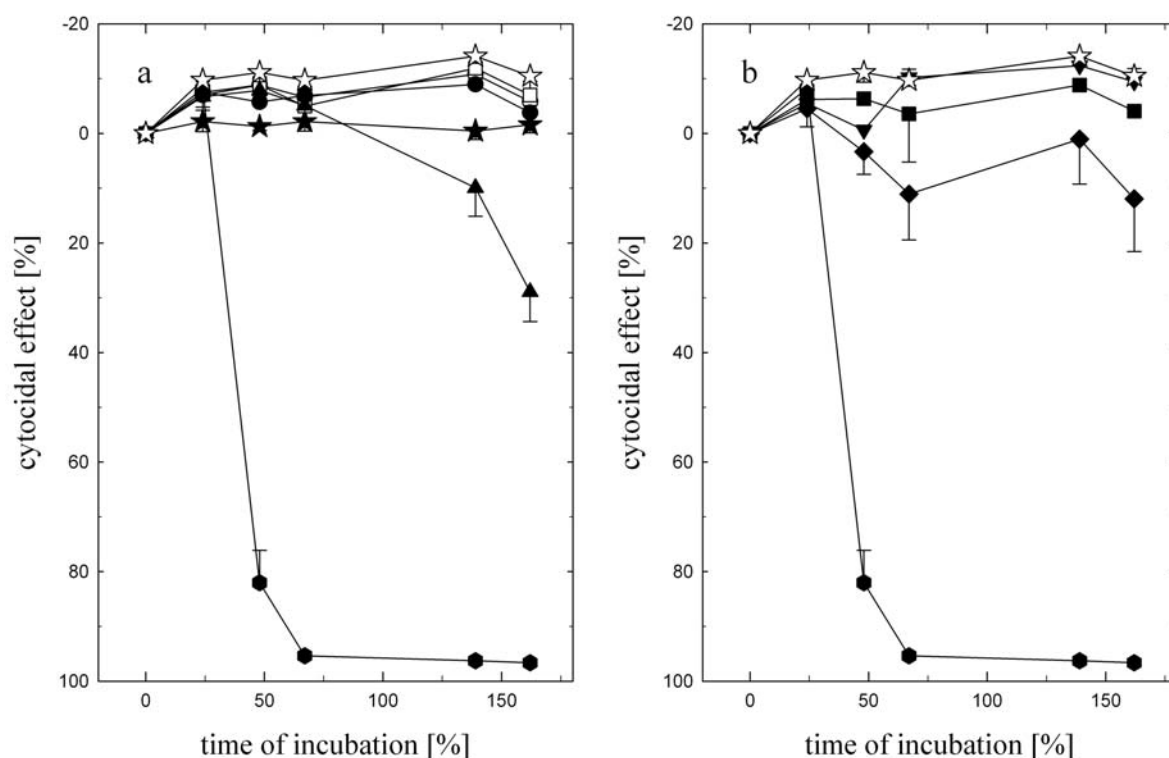


Figure 4.23: Incubation of resting U-373 MG cells with rotenone (500 nM) and new tariquidar analogs (20 μ M); vehicle (*open star*), rotenone (*filled hexagon*). a) Series 3 with compound **13** (*open circle*), **14** (*open square*), **15** (*filled star*), **16** (*filled circle*), **18** (*filled triangle*) and b) series 4 with compound **19** (*filled diamond*), **20** (*filled inverted triangle*) and **21** (*filled square*).

The tariquidar analogs **13**, **14**, **15**, **16**, **20** and **21** had no effect on resting cells. Compounds **18** and **19** produced a cytotoxic effect after 6 and 3 days, respectively. The results demonstrate that the cytotoxic effect of the tariquidar analogs on proliferating cells resulted from a specific interference of the compounds during the cell cycle. Only compound **6** showed a very strong cytotoxic effect caused by an unspecific effect on the cells indicating that this tariquidar analog is not suitable for in vivo studies.

4.4.6 Cell cycle analysis of tariquidar analogs

In order to gain information about the mechanism of cytotoxicity cell cycle analyses were performed with the new tariquidar analogs. As positive control for the cell cycle arrest during mitosis (G2/M phase) the microtubule interfering agent vinblastine was used (Figure 4.24c). Topotecan, an inhibitor of the DNA topoisomerase I leading to cell arrest during DNA synthesis (S phase), served as the second positive control (Figure 4.24d).

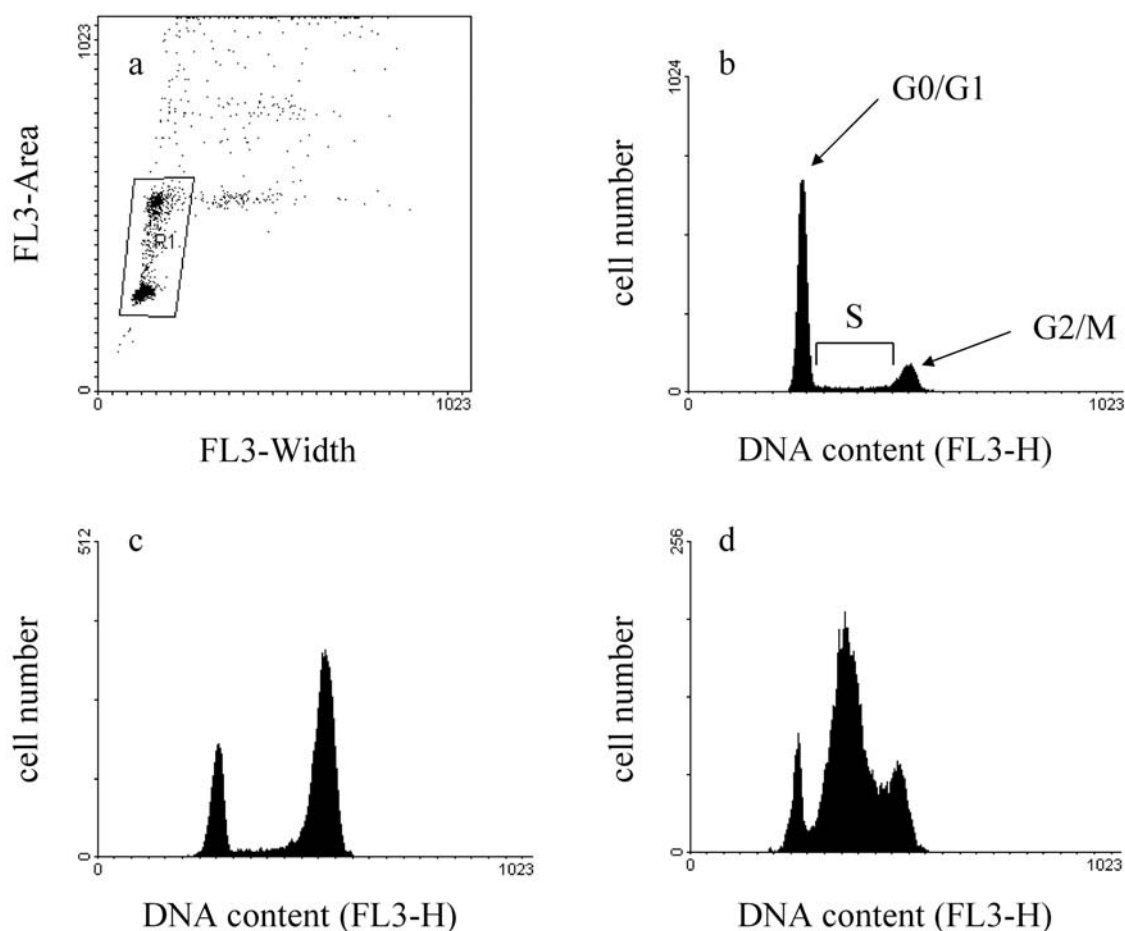


Figure 4.24: Cell cycle analysis of U-373 MG cells. a) FL3-Area versus FL3-Width dot plot of the DMSO control showing a singlet gate R1, which excludes aggregates. b) Cells gated in region R1 displayed in the FL3-H histogram representing the DNA distribution of untreated cells. c) FL3-H Histogram representing the DNA content of U-373 MG cells incubated with vinblastine (50 nM) and d) with topotecan (100 nM).

The fractions of U-373 MG cells in the G1/G0 phase, in the S phase and in the G2/M phase after the incubation with the cytostatic drugs and the tariquidar analogs, respectively, were calculated and are summarized in Table 4.5. Compared to the cells incubated with the solvent DMSO, the treatment of the cells with vinblastine resulted in a very strong increase in the percentage of M/G2 phase cells and a decrease in the portion of cells in G1/G0 phase.

Table 4.5: Effect of DMSO, vinblastine, topotecan and the tariquidar analogs on the portion of U-373 MG cells in G1/G0 phase, S phase and G2/M phase.

Compound	Concentration [μ M]	G1/G0 phase [%]	S phase [%]	G2/M phase [%]
DMSO		72.3	13.2	14.5
vinblastine	0.01	24.0	12.6	63.4
vinblastine	0.05	10.4	16.0	73.6
topotecan	0.1	12.2	70.8	17.0
3	10	72.2	13.0	14.8
4	10	72.1	11.8	16.1
5	10	74.6	9.9	15.5
6	10	53.6	23.0	23.4
7	10	70.4	10.1	19.5
8	10	75.5	11.0	13.5
9	10	70.2	11.2	18.6
10	10	71.9	9.9	18.2
11	10	75.1	11.4	12.9
12	10	70.6	10.5	18.9
13	10	62.8	11.3	26.0
14	10	69.3	9.1	21.5
15	3	73.4	12.7	13.8
16	10	70.3	13.1	16.6
17	10	67.5	11.5	21.0
18	10	67.1	12.8	20.1
19	10	58.9	28.6	12.5
20	10	69.8	12.6	17.6
21	10	65.9	17.7	16.4

As expected, topotecan led to an increased ratio of cells arrested during S phase. Compound **6**, **13** and **19** led to a slightly increased portion of the cells in S phase or G2/M phase, respectively. But these results are not definitely and allow no statement about the mechanism of the cytotoxic effect of the compounds. Moreover, the cell cycle analysis of all other tariquidar analogs showed about the same percental distribution of the cells like the control sample indicating that the toxicity of the compounds is caused by an effect on the cell cycle during the G1/G0 phase.

4.5 Discussion

Aiming at tariquidar analogs with improved solubility and pharmacokinetics more hydrophilic analogs were synthesized. The new compounds were investigated for their inhibitory activity and their selectivity on ABCB1 overexpressing Kb-V1 cells (Müller et al., 2007) and ABCG2 overexpressing MCF-7/Topo cells. The IC₅₀ values of the compounds were determined with the calcein-AM efflux assay at the ABCB1 transporter and with the mitoxantrone efflux assay at the ABCG2 transporter, respectively. The ABCB1 inhibitory activity was retained in the series of tariquidar analogs bearing more hydrophilic substituents and having the quinolinecarboxamide moiety in the same position as in tariquidar (compounds **5**, **6**, **7** and **8** of series 1). Compared to tariquidar with an IC₅₀ value of 223 nM, the compounds **5** and **8** were even more potent with IC₅₀ values of 181 nM and 145 nM, respectively. These results demonstrate that structural changes in the chosen position are indeed tolerated without considerable decrease in activity. Regarding the clog P values of the compounds **5**, **6**, **7** and **8** with 7.1, 4.3, 5.1 and 6.0, respectively, a correlation between the lipophilicity of the compounds and the inhibitory activity was observed (Egger et al., 2007). In the same order, as clog P rises, the activity against ABCB1 increases. In the literature it is still a matter of debate whether high lipophilicity is an important criterion (amongst others) for the inhibition of ABC transporters (Wiese and Pajeva, 2001). The results obtained from this small series are in accordance with this hypothesis, assuming that the newly introduced side chains only affect physicochemical parameters. As the lipophilicity of the compounds ranges from clog P values of 7 to 4, this series of new ABCB1 modulators is well suited to test in vivo if the more lipophilic analogs accumulate to a higher extent in the lipid compartment of the brain or not. These compounds are also ABCG2 inhibitors but with a clear selectivity to the ABCB1 transporter.

Further tariquidar analogs with the carboxamide residue shifted to the neighbor position were synthesized. Surprisingly, this structural modification resulted in ABCG2-selective inhibitors. For three derivatives, compound **16**, **15** and **18**, IC₅₀ values of 55, 100, and 154 nM were determined. With the mitoxantrone efflux assay an IC₅₀ value of 225 nM for Ko143, the most potent ABCG2 inhibitor reported so far (Allen et al., 2002), was measured. Hence, the new tariquidar analogs **16**, **15** and **18** are more potent than Ko143. Moreover, compound **16** had only a very weak effect on ABCB1, thus representing the most potent and a very selective ABCG2 inhibitor.

Furthermore, the comparison of the Hill coefficients at the ABCB1 and ABCG2 transporters is informative. The Hill coefficients at the ABCG2 transporter range from 0.5 to 1.3 pointing out that the ABCG2 transporter comprises only one binding site. However, the investigations on the tariquidar analogs at the ABCB1 transporter resulted in very variable Hill coefficients between 0.5 and 3.7, indicating that the ABCB1 transporter includes up to four binding sites with positive cooperativeness.

The potential of the compounds to overcome the multidrug resistance mediated by ABC transporters was observed in the kinetic chemosensitivity assay. Therefore, ABCB1 positive Kb-V1 cells and ABCG2 positive MCF-7/Topo cells, respectively, were incubated with different concentrations of the tariquidar analogs alone and in combination with non-toxic topotecan concentrations. All tested tariquidar analogs were able to overcome the topotecan resistance of the cells, and concentrations far below the IC_{50} value of the respective compounds led to cytostatic effects. In addition, the incubation of Kb-V1 or MCF-7/Topo cells, respectively, with the tariquidar analogs alone resulted in some cases in cytotoxic, cytostatic or cytocidal effects. The investigation of these compounds on ABCB1 and ABCG2 negative human glioblastoma U-373 MG cells revealed that the toxicity of the compounds is independent of their inhibitory activity at the ABC transporters. Furthermore, confluent U-373 MG cells were treated with the cytotoxic tariquidar analogs in order to proof if the antiproliferative effect is caused by a specific interference during the cell cycle or not. Only compound **6** induced a very strong cytocidal effect caused by an unspecific interference with the cells. All other tariquidar analogs had no relevant cytocidal effect on quiescent cells and are therefore suitable for in vivo investigations.

In summary, potent and more hydrophilic ABCB1 inhibitors derived from tariquidar were obtained. These new P-glycoprotein inhibitors are promising candidates for future preclinical investigations to compare their accumulation in the brain of nude mice with that of the parent compound and to study the antitumor activity-enhancing effect in combination with cytostatic drugs. Furthermore, very potent and selective ABCG2 inhibitors were identified which should be useful pharmacological tools for in vitro and in vivo investigations. With respect to the treatment of brain tumors and regarding the tumor stem cell concept, the ABCG2 inhibitors with cytotoxic effects are possibly very effective cytostatic drugs.

References

- Ahmed-Belkacem, A., Pozza, A., Macalou, S., Pérez-Victoria, J. M., Boumendjel, A. and Di Pietro, A. (2006) Inhibitors of cancer cell multidrug resistance mediated by breast cancer resistance protein (BCRP/ABCG2). *Anticancer Drugs* 17(3):239-243.
- Allen, J. D., van Loevezijn, A., Lakhai, J. M., van der Valk, M., van Tellingen, O., Reid, G., Schellens, J. H. M., Koomen, G.-J. and Schinkel, A. H. (2002) Potent and Specific Inhibition of the Breast Cancer Resistance Protein Multidrug Transporter in Vitro and in Mouse Intestine by a Novel Analogue of Fumitremorgin C. *Mol. Cancer Ther.* 1(6):417-425.
- Allikmets, R., Schriml, L. M., Hutchinson, A., Romano-Spica, V. and Dean, M. (1998) A Human Placenta-specific ATP-Binding Cassette Gene (ABCP) on Chromosome 4q22 That Is Involved in Multidrug Resistance. *Cancer Res.* 58(23):5337-5339.
- Bendayan, R., Lee, G. and Bendayan, M. (2002) Functional expression and localization of P-glycoprotein at the blood brain barrier. *Microsc. Res. Tech.* 57(5):365-380.
- Bernhardt, G., Reile, H., Birnböck, H., Spruss, T. and Schönenberger, H. (1992) Standardized kinetic microassay to quantify differential chemosensitivity on the basis of proliferative activity. *J. Cancer Res. Clin. Oncol.* 118(1):35-41.
- Bosch, I. and Croop, J. (1996) P-glycoprotein multidrug resistance and cancer. *Biochim. Biophys. Acta* 1288(2):F37-F54.
- Breedveld, P., Beijnen, J. H. and Schellens, J. H. M. (2006) Use of P-glycoprotein and BCRP inhibitors to improve oral bioavailability and CNS penetration of anticancer drugs. *Trends Pharmacol. Sci.* 27(1):17-24.
- Dantzig, A. H., Shepard, R. L., Law, K. L., Tabas, L., Pratt, S., Gillespie, J. S., Binkley, S. N., Kuhfeld, M. T., Starling, J. J. and Wrighton, S. A. (1999) Selectivity of the Multidrug Resistance Modulator, LY335979, for P-Glycoprotein and Effect on Cytochrome P-450 Activities. *J. Pharmacol. Exp. Ther.* 290(2):854-862.
- de Bruin, M., Miyake, K., Litman, T., Robey, R. and Bates, S. E. (1999) Reversal of resistance by GF120918 in cell lines expressing the ABC half-transporter, MXR. *Cancer Lett.* 146(2):117-126.
- Dean, M. and Allikmets, R. (2001) Complete Characterization of the Human ABC Gene Family. *J. Bioenerg. Biomembr.* 33(6):475-479.
- Doyle, L. and Ross, D. (2003) Multidrug resistance mediated by the breast cancer resistance protein BCRP (ABCG2). *Oncogene* 22(47):7340-7358.

- Doyle, L. A., Yang, W., Abruzzo, L. V., Krogmann, T., Gao, Y., Rishi, A. K. and Ross, D. D. (1998) A multidrug resistance transporter from human MCF-7 breast cancer cells. *Proc. Natl. Acad. Sci. U. S. A.* 95(26):15665–15670.
- Egger, M., Li, X., Müller, C., Bernhardt, G., Buschauer, A. and König, B. (2007) Tariquidar Analogues: Synthesis by Cu^I-Catalysed N/O-Aryl Coupling and Inhibitory Activity against the ABCB1 transporter. *Eur. J. Org. Chem.* DOI: 10.1002/ejoc.200700142
- Fankhänel, M., Fellner, S., Spruss, T., Bernhardt, G. and Buschauer, A. (2005) Report of the European High Grade Glioma Group Meeting, February 25-26, Regensburg, Germany - The p-gp modulators elacridar and tariquidar enhance the paclitaxel concentration in the brain of nude mice. *Turk J Cancer* 35(1):41.
- Fellner, S., Bauer, B., Miller, D. S., Schaffrik, M., Fankhänel, M., Spruss, T., Bernhardt, G., Gräff, C., Färber, L., Gschaidmeier, H., Buschauer, A. and Fricker, G. (2002) Transport of paclitaxel (Taxol) across the blood-brain barrier in vitro and in vivo. *J. Clin. Invest.* 110(9):1309-1318.
- Fischer, V., Rodriguez-Gascon, A., Heitz, F., Tynes, R., Hauck, C., Cohen, D. and Vickers, A. E. M. (1998) The Multidrug Resistance Modulator Valspodar (PSC 833) Is Metabolized by Human Cytochrome P450 3A. Implications for Drug-Drug Interactions and Pharmacological Activity of the Main Metabolite. *Drug Metab. Dispos.* 26(8):802-811.
- Glavinas, H., Krajcsi, P., Cserepes, J. and Sarkadi, B. (2004) The role of ABC transporters in drug resistance, metabolism, and toxicity. *Curr. Drug Deliv.* 1(1):27-42.
- Homolya, L., Hollo, Z., Germann, U., Pastan, I., Gottesman, M. and Sarkadi, B. (1993) Fluorescent cellular indicators are extruded by the multidrug resistance protein. *J. Biol. Chem.* 268(29):21493-21496.
- Hyafil, F., Vergely, C., Du Vignaud, P., Grand-Perret, T. (1993) In vitro and in vivo reversal of multidrug resistance by GF120918, an acridonecarboxamide derivative. *Cancer Res.* 53(19):4595-4602.
- Jarozeski, M., Gilbert, R. and Heller, R. (1998) Flow cytometric detection and quantitation of cell-cell electrofusion products. *Methods Mol. Biol.* 91(1):149-156.
- Johnson, W. W. (2002) P-glycoprotein-mediated efflux as a major factor in the variance of absorption and distribution of drugs: modulation of chemotherapy resistance. *Methods Find. Exp. Clin. Pharmacol.* 24(8):501-514.
- Kohno, K., Kikuchi, J., Sato, S., Takano, H., Saburi, Y., Asoh, K. and Kuwano, M. (1988) Vincristine-resistant human cancer KB cell line and increased expression of multidrug-resistance gene. *Jpn. J. Cancer Res.* 79(11):1238-1246.

- Krishna, R. and Mayer, L. D. (2000) Multidrug resistance (MDR) in cancer: Mechanisms, reversal using modulators of MDR and the role of MDR modulators in influencing the pharmacokinetics of anticancer drugs. *Eur. J. Pharm. Sci.* 11(4):265-283.
- Lee, J., Paull, K., Alvarez, M., Hose, C., Monks, A., Grever, M., Fojo, A. and Bates, S. (1994) Rhodamine efflux patterns predict P-glycoprotein substrates in the National Cancer Institute drug screen. *Mol. Pharmacol.* 46(4):627-638.
- Loescher, W. and Potschka, H. (2005) Drug resistance in brain diseases and the role of drug efflux transporters. *Nature Rev. Neurosc.* 6(8):591-602.
- Maliepaard, M., van Gastelen, M. A., de Jong, L. A., Pluim, D., van Waardenburg, R. C. A. M., Ruevekamp-Helmers, M. C., Floom, B. G. J. and Schellens, J. H. M. (1999) Overexpression of the BCRP/MXR/ABCP Gene in a Topotecan-selected Ovarian Tumor Cell Line. *Cancer Res.* 59(18):4559-4563.
- Müller, C., Gross, D., Sarli, V., Gartner, M., Giannis, A., Bernhardt, G. and Buschauer, A. (2007) Inhibitors of kinesin Eg5: antiproliferative activity of monastrol analogues against human glioblastoma cells. *Cancer Chemother. Pharmacol.* 59(2):157-164.
- Rabindran, S. K., Ross, D. D., Doyle, L. A., Yang, W. and Greenberger, L. M. (2000) Fumitremorgin C Reverses Multidrug Resistance in Cells Transfected with the Breast Cancer Resistance Protein. *Cancer Res.* 60(1):47-50.
- Reya, T., Morrison, S. J., Clarke, M. F. and Weissman, I. L. (2001) Stem cells, cancer, and cancer stem cells. *414(6859):105-111.*
- Robey, R. W., Honjo, Y., van de Laar, A., Miyake, K., Regis, J. T., Litman, T. and Bates, S. E. (2001) A functional assay for detection of the mitoxantrone resistance protein, MXR (ABCG2). *Biochimica et Biophysica Acta (BBA) - Biomembranes* 1512(2):171-182.
- Thomas, H. and Coley, H. M. (2003) Overcoming multidrug resistance in cancer: an update on the clinical strategy of inhibiting p-glycoprotein. *Cancer Control* 10(2):159-165.
- Wandel, C., Kim, R. B., Kajiji, S., Guengerich, F. P., Wilkinson, G. R. and Wood, A. J. (1999) P-Glycoprotein and Cytochrome P-450 3A Inhibition: Dissociation of Inhibitory Potencies. *Cancer Res.* 59(16):3944-3948.
- Wiese, M. and Pajeva, I. K. (2001) Structure-Activity Relationships of Multidrug Resistance Reversers. *Curr. Med. Chem.* 8(6):685-713.

Chapter 5

Summary

No effective chemotherapy for the treatment of malignant brain tumors, especially glioblastoma, exists so far. Despite the progress in surgical techniques and advances in the irradiation treatment, the concomitant chemotherapy is essential for the prevention of relapse and of major importance for patient outcome. The introduction of temozolomide combined with radiation in clinical practice led to slightly improved long-term survival, but malignant gliomas remain resistant to cancer chemotherapy. Thus, new strategies for the treatment of brain tumors are still needed. Objectives of this work were the evaluation of the TmHU protein as siRNA transfection reagent (Chapter 2), investigations on new kinesin Eg5 inhibitors, which specifically inhibit cell division during mitosis (Chapter 3), and the exploration of new tariquidar analogs as ABCB1 and ABCG2 inhibitors (Chapter 4).

Due to the selective down-regulation of oncogene expression by small interfering RNA, siRNAs are considered as promising anticancer agents allowing the selective killing of tumor cells. The suitability of the non-toxic TmHU protein as siRNA transfection reagent was explored *in vitro* and *in vivo* in order to investigate the down-regulation of gene expression in human glioblastoma cells. The efficient transfection of the cancer cells is a prerequisite for this new concept, and, therefore, reliable *in vitro* and *in vivo* models were developed for the proof of principle. A suitable and convenient *in vitro* method was established for the quick detection of siRNA effects on the EGFP or DsRed2 expression, respectively, with respect to total cell number by using a fluorescence plate reader. In order to study siRNA effects *in vivo* subcutaneous tumor models were established in nude mice and two fluorescence detection methods were evaluated. The fluorescence intensity was quantified by confocal laser scanning microscopy of paraffin embedded tumor sections and by *in vivo* imaging. In preliminary tests with micro-osmotic pumps the continuous release of a suspension and the practicability of subcutaneous implantation were assured. Unfortunately, the established *in vivo* methods could not be used for the intended investigations on TmHU because this protein was not suitable for siRNA transfection. Nevertheless, these methods are recommendable for the investigation of promising *in vivo* transfection reagents.

The inhibition of kinesin Eg5 by small molecules such as monastrol is currently evaluated as an approach to develop a novel class of antiproliferative drugs for the treatment of malignant tumors. Therefore, the effects of new monastrol analogs on the proliferation of human U-87 MG, U-118 MG, and U-373 MG glioblastoma cells were investigated. Compared to monastrol, the new cell cycle specific compounds showed an at least one order of magnitude higher antiproliferative activity. The compounds were neither inactivated by hydrolysis nor by binding to serum proteins. Due to the necessity of overcoming the blood–brain barrier (BBB)

in the treatment of brain tumors, it was investigated if the new monastrol analogues are modulators or substrates of the ABCB1 transporter by a flow cytometric calcein-AM efflux assay. The tested compounds showed no modulating effects on the ABCB1 function. With respect to the treatment of primary and secondary CNS tumors, the results suggest that the new monastrol analogs represent an interesting class of potential anticancer drugs, predicted to be less neurotoxic in comparison to classical tubulin inhibitors.

The efflux of cytostatics due to expression of ABC transporters such as ABCB1 and ABCG2 at the BBB leads to extremely low drug concentrations in the brain and is therefore a major limitation in cancer chemotherapy. A strategy to overcome the BBB is the administration of an efflux inhibitor in combination with a cytostatic. The 3rd generation inhibitor tariquidar led to better brain/plasma ratios of paclitaxel but could not increase the paclitaxel brain levels compared to co-administration of the 2nd generation inhibitor valspodar. The very high tariquidar brain levels indicate that the very lipophilic tariquidar is trapped in the lipid compartment of the brain. Aiming at tariquidar analogs with improved solubility and pharmacokinetics, more hydrophilic analogs were synthesized. The compounds were investigated on ABCB1 overexpressing Kb-V1 and ABCG2 overexpressing MCF-7/Topo cells for inhibitory activity and for cytotoxicity, alone and in combination with cytostatics. Surprisingly, slight structural modifications resulted in ABCG2 selective inhibitors. Three analogs have IC₅₀ values of 55, 100, and 154 nM, comparable with the most potent reported ABCG2 inhibitor Ko143. Some ABCG2 inhibitors showed specific toxicity which could be advantageous regarding the treatment of brain tumors. These very potent and selective ABCG2 inhibitors should be useful pharmacological tools for in vitro and in vivo investigations.